On Compliant Underactuated Robotic Fingers

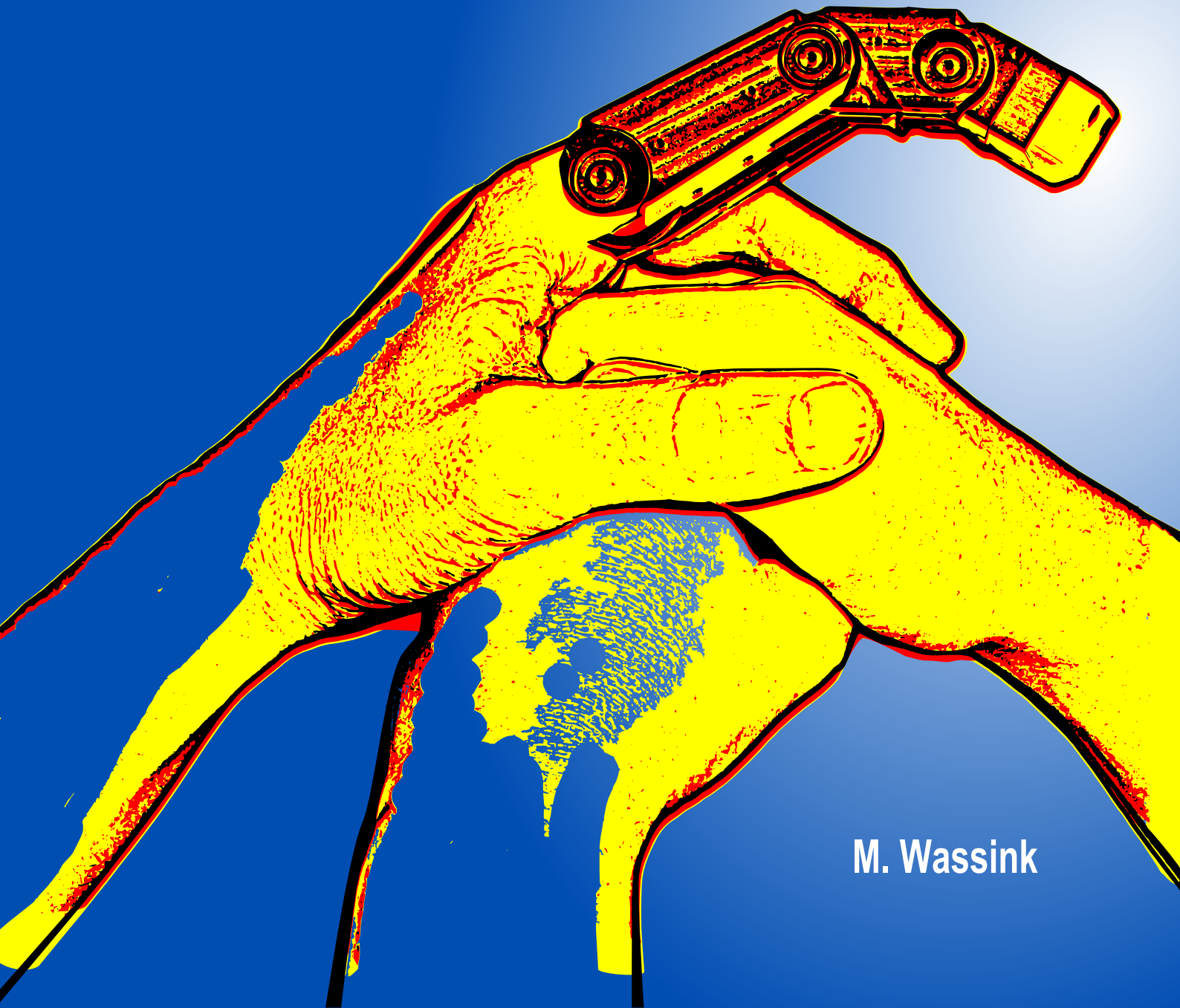

M. Wassink

On Compliant Underactuated Robotic Fingers

The work described in this thesis has been carried out as part of the FALCON project under the responsibility of the Embedded Systems Institute with Vanderlande Industries as the industrial partner. This project is partially supported by the Netherlands Ministry of Economic Affairs under the Embedded Systems Institute (BSIK03021) program.

Graduation committee

Chairman & Secretary	prof. dr. ir. A.J. Mouthaan	Univ. Twente, EWI
Acting Chairman	prof. dr. P.J. Gellings	
Promotor (Supervisor)	prof. dr. ir. S. Stramigioli	Univ. Twente, EWI
Ass. Promotor (Ass. Supervisor)	dr. R. Carloni	Univ. Twente, EWI
Members	prof. dr. ir. B. Haverkort	Univ. Twente, EWI
	prof. dr. ir. J. Herder	Univ. Twente, CTW
	prof. dr. C. Melchiorri	University of Bologna
	prof. dr. ir. P.P. Jonker	TU Eindhoven
	prof. dr. ir. J. van Amerongen	Univ. Twente, EWI

ISBN 978-90-365-3154-2
DOI 10.3990/1.9789036531542

Cover picture: "Joint efforts determine the future of robotics"

E-mail: m.wassink-1@alumnus.utwente.nl

Printed by Asbreuk drukkerij, Enschede, The Netherlands

ON COMPLIANT UNDERACTUATED ROBOTIC FINGERS

PROEFSCHRIFT

ter verkrijging van
de graad van doctor aan de Universiteit Twente,
op gezag van de rector magnificus,
prof. dr. H. Brinksma,
volgens besluit van het College voor Promoties
in het openbaar te verdedigen
op donderdag 3 maart 2011 om 14.45 uur

door

Martin Wassink
geboren op 5 september 1981
te Alkmaar, Nederland

Dit proefschrift is goedgekeurd door:

Prof. dr. ir. S. Stramigioli (promotor)	Universiteit Twente
dr. R. Carloni (assistent promotor)	Universiteit Twente

Summary

Driven by societal trends, such as aging, and by a desire to drive economic growth and enhance commercial competitiveness, researchers have tried to move robots from structured manufacturing tasks to unstructured professional and personal service applications.

As announced in the Falcon project, an example of a possible unstructured professional service task for future robots is found in package-handling tasks in warehouses (distribution centers). The Falcon project aimed to design a new system architecture for a fully automated distribution center and to define, within this architecture, specific critical robotic components, which were then targeted to be researched. The author observed some inherent challenges in following such an application driven research approach. Chapter 2 presents the author's reflections on the tensions between top-down systems engineering approaches and the classical bottom-up approach for doing research.

Rather than targeting one specific robotic service application, several general technological challenges were identified that require resolution to let robots move from structured to unstructured applications. One such general technological challenge is to develop versatile robotic end-effectors which are able to execute a diverse set of unstructured human-like service tasks, either being professional or personal tasks. Various approaches can be taken to develop these versatile end-effectors. This thesis focuses on contributing in the development of human-like dexterous robotic hands. The thesis presents a study on a novel robotic finger concept (aimed to be used in dexterous robotic hands), the control thereof and an accompanying theoretic treaty on natural pseudo-inverses.

Inspired by human hand studies, Chapter 3 describes the desired functions for a dexterous robotic hand, being dexterous grasping, dexterous manipulation, free motion and interactive motion. Following a brief review of the current status of dexterous robotic hand technology, Chapter 3 formulates design considerations and a research direction for further developments and innovations in dexterous robotic hand technology. Variable mechanical compliance and underactuated actuation methods are marked as important design features to support robust, reliable, low weight, human dimensional and affordable technologies for dexterous robotic hands. Benefits of using actuation methods with variable compliance for grasping are presented separately in Chapter 4. Several simple grasp scenarios are used to show that different scenarios have different preferred compliance settings, which highlights the advantages of using variable compliance.

Chapter 5 gives insights on natural space decompositions for the pseudo-inverse of physical maps in models of physical systems, such as the actuation Jacobian (also called transmission matrix) in a kinematic model of a drive-train of an underactuated robotic finger. Multiple mathematical view-points are used to explain the importance of choosing proper metrics on vector spaces, especially when the elements of the vector spaces represent physical quantities of a physical system. For the case of damped linear motions, a time-dependent physically equivalent metric is derived, which defines the natural decomposition of spaces for the studied case.

These insights are used for compliance analysis of a novel variable compliant underactuated robotic finger concept. The concept is introduced in Chapter 6. It implements minimal actuation, variable mechanical compliance and dexterous manipulability by utilizing the well-known underactuated 'soft-gripper' concept, combined with switched locks on the joints and antagonistic non-linear series elastic actuation. This combination of features allows for a minimal actuation design, while reducing control complexity and still providing dexterity and grasping capabilities. The conceptual properties (such as variable compliance) are extensively studied in a port-Hamiltonian framework and by applying the natural space decompositions.

Chapter 7 presents a low-level controller for the novel robotic finger concept. It enables full utilization of the features of the robotic finger concept by controlling the finger compliance and the states of the locks. The conceptual design of the controller also illustrates usage of the insights from natural space decompositions (Chapter 5). Simulation results validate the concepts and present usage of the low-level controller by demonstrating execution of various task scenarios of the robotic finger concept (tip-grasping, power-grasping and dexterous finger manipulation).

Samenvatting

Gedreven door maatschappelijke trends - zoals vergrijzing - en door de wens om economische groei te stimuleren en de commerciële concurrentieposities van bedrijven te versterken, zijn onderzoekers al jaren bezig om de inzet van robots uit te breiden. Niet alleen wil men de inzet richten op gestructureerde productie taken, maar ook op ongestructureerde professionele en persoonlijke service toepassingen.

Een voorbeeld van een mogelijke ongestructureerde professionele service toepassing voor toekomstige robots is te vinden in de afhandeling van goederen in magazijnen (distributiecentra). Deze mogelijkheid is onderzocht in het Falcon project. Het doel van het Falcon project was om een nieuwe systeemarchitectuur voor een volledig geautomatiseerd distributiecentrum te ontwerpen en om binnen deze architectuur specifieke robotcomponenten aan te wijzen als onderzoeksobjecten. De auteur observeerde een aantal inherente uitdagingen in een dergelijke applicatiegedreven onderzoeksaanpak. Hoofdstuk 2 presenteert de reflecties van de auteur over de spanningen tussen een 'top-down systems engineering' benadering en de klassieke 'bottom-up' benadering voor het doen van onderzoek.

In tegenstelling tot het zoeken naar robot technologiën voor één specifieke service toepassing, is een aantal generieke technologische uitdagingen geïdentificeerd, waarvoor oplossingen nodig zijn om de verschuiving van robots van gestructureerde naar ongestructureerde toepassingen mogelijk te maken. Eén zo'n technologische uitdaging is het ontwikkelen van veelzijdige robotische eind-effectoren, die in staat zijn om een gevarieerde set van ongestructureerde menselijke service taken uit te voeren, hetzij professionele taken, hetzij persoonlijke taken. Voor de ontwikkeling van deze veelzijdige eind-effectoren zijn verschillende benaderingen mogelijk. Een mogelijke benadering is de ontwikkeling van mensachtige robothanden. Dit proefschrift richt zich op een bijdrage in de ontwikkeling van behendige mensachtige robotische handen. Het proefschrift presenteert een studie naar een nieuw concept voor een behendige robotvinger (bedoeld om te worden gebruikt voor de vervaardiging van behendige mensachtige robothanden), de bijbehorende regelaar en een begeleidende theoretische verhandeling over natuurlijke pseudo-inversies.

Op basis van studies naar de menselijke hand beschrijft hoofdstuk 3 de gewenste functies voor een behendige robothand: behendig grijpen, behendig manipuleren, vrije beweging en interactieve beweging. Na een kort overzicht van de huidige status van de ontwikkeling van behendige robothand technologiën, formuleert hoofdstuk 3 de ontwerpoverwegingen en een onderzoeksrichting voor verdere ontwikkelingen en innovaties voor de toepassing van behendige robothand technologiën. Variabele mechanische compliantie en ondergeactuateerde actuatiemethoden zijn beiden geïdentificeerd als belangrijke ontwerpaspecten voor de ontwikkeling van robuuste, betrouwbare, lichte, menselijk geproportioneerde en betaalbare behendige robothand technologiën. Voordelen van het gebruik van actuatiemethoden met variabele compliantie voor het grijpen van objecten worden apart behandeld in hoofdstuk 4. Enkele eenvoudige grijpscenario's worden gebruikt om aan te tonen dat verschillende scenario's andere compliantie instellingen behoeven, waarmee de voordelen van het gebruik van variabele compliantie worden

gemarkeerd.

Hoofdstuk 5 beschrijft inzichten over natuurlijke decomposities van vectorruimtes voor de pseudo-inverse van functies in modellen van fysische systemen, zoals bijvoorbeeld de actuatie Jacobiaan (ook wel bekend als de transmissie-matrix) in een kinematisch model van de aandrijving van een ondergeactueerde robotvinger. Verschillende wiskundige beschrijvingen worden gebruikt om het belang van het kiezen van de juiste metriek op vectorruimtes uit te leggen en in het bijzonder voor situaties waarin de elementen van de vectorruimtes fysieke toestanden van een fysisch systeem voorstellen. Voor het geval van gedempte lineaire bewegingen is een tijdafhankelijke fysiek equivalente metriek afgeleid, die voor de gegeven set van bestudeerde casussen de natuurlijke decompositie van vectorruimtes definieert.

Deze inzichten worden gebruikt voor de analyse van de compliantie eigenschappen van een nieuw robotvinger concept met variabele compliantie. Dit nieuwe concept wordt geïntroduceerd in hoofdstuk 6. Het implementeert minimale actuatie, variabele mechanische compliantie en de mogelijkheid tot behendige manipulatie. Hierbij wordt gebruik gemaakt van het bekende ondergeactuateerde 'soft-gripper' concept in combinatie met in- en uitschakelbare mechanische vergrendelingen op de gewrichten en een antagonistische aandrijving door middel van zogenaamde pezen, die in serie zijn geschakeld met niet-lineaire elastische elementen. Deze combinatie van functies zorgt voor een ontwerp met minimale actuatie en een afname in complexiteit voor de te ontwerpen regelaar, terwijl de gewenste vingerbehendigheid en grijpmogelijkheden behouden blijven. De conceptuele eigenschappen (zoals variabele compliantie) worden uitgebreid bestudeerd in een poort-Hamiltoniaans modeleringsraamwerk en door toepassing van natuurlijke decomposities van vectorruimtes, zoals inzichtelijk gemaakt in hoofdstuk 5.

Hoofdstuk 7 presenteert een basis ("low-level") regelaar voor het nieuwe robotvinger concept. Het maakt volledige benutting van de kenmerken van het robotvinger concept mogelijk door het regelen van de compliantie van de vinger en het aansturen van de toestanden van de mechanische vergrendelingen. Het conceptuele ontwerp van de regelaar illustreert ook het gebruik van de inzichten over de natuurlijke decompositie van vectorruimtes (hoofdstuk 5). Simulatieresultaten valideren de concepten en presenteren het gebruik van de basis regelaar door het demonstreren van diverse taakscenario's van het robotvinger concept (pincet grijpen, volledig grijpen en behendige vinger manipulatie).

Symbols and Abbreviations

Symbols

$\dim \mathcal{X}$	Dimension of (sub)space $\mathcal{X}$ (p. 92)
$\dot{\epsilon}_i \in \mathbb{R}^{n_{ci} \times 1}$	Velocity vector of transmitted velocities of contact i (p. 66)
$\dot{\epsilon} \in \mathcal{E}_c$	Consolidated vector containing all n_t transmittable contact velocity components of the grasp system (p. 84)
$\operatorname{im} a$	Image of map a; $\operatorname{im} a = \{u \in \mathcal{U} \mid u = a(x), x \in \mathcal{X}\}$, where $a : \mathcal{X} \mapsto \mathcal{U}$ (p. 79)
$\ker a$	Kernel of map a; $\ker a = \{x \in \mathcal{X} \mid a(x) = 0\}$, where $a : \mathcal{X} \mapsto \mathcal{U}$. (p. 81)
$\mathcal{C}$	[-] Controller (p. 62)
$\mathcal{F}_c$	Space of transmittable contact forces, $\dim \mathcal{F}_c = n_t$ (p. 84)
$\mathcal{H}_i$	Contact model of contact i, defining contact constraints (p. 66)
μ	[-] Friction coefficient (p. 47)
Ψ_k	Reference frame/coordinate system k (p. 65)
$\tilde{x}_o$	[m] expected object position (measured by e.g. vision) (p. 61)
e_o	[m] Object positioning error (p. 61)
$e_{h,max}$	[m] End-effector position tolerance (p. 61)
$f_c \in \mathcal{F}_c$	Consolidated co-vector containing all n_t transmittable contact force components of the grasp system (p. 84)
F_d	[N] External disturbance force at robot-arm (p. 62)
f_g	[N] Gravitation force (p. 60)
f_o	[N] Net force on object along manipulation direction (p. 60)
f_r	[N] Friction force (p. 62)
F_{arm}	[N] Actuation force at robot-arm (p. 60)
$f_{c,max}$	[N] Maximum allowable contact force (p. 59)
$f_{c,min}$	[N] Minimum needed contact force (p. 59)
$f_{ci} \in \mathbb{R}^{1 \times n_{ci}}$	[N] Transmitted contact force(s) co-vector for contact i. Depending on the model of contact i, f_{ci} may have one or more force/torque components. (p. 59)
G	Grasp matrix (p. 84)
k	[N/m] Stiffness of elastic element (e.g. spring) (p. 60)
M	[kg] Total mass of robot-arm and end-effector palm (p. 62)
m_f	[kg] Finger mass (p. 62)
m_o	[kg] Object mass (p. 60)
n_c	Total number of contacts in the grasp system. (p. 67)
n_t	Total number of transmittable contact force components in the grasp system (p. 84)
n_{ci}	Number of transmitted degrees of freedom of contact i (p. 66)
n_{qi}	The number of joints of the finger with finger-tip contact i (p. 68)
$T_i^{k,j}$	[(rad/s,m/s)] Twist of body i w.r.t. body j expressed in coordinates of reference frame Ψ_k (p. 65)
$T_\epsilon \mathcal{E}_c$	Space of transmittable contact velocities, $\dim \mathcal{E}_c = n_t$ (p. 84)

W_i^k	[(Nm,N)] Total wrench on body i expressed in coordinates of reference frame Ψ_k (p. 65)
$W_{i,ci}^k$	[(Nm,N)] Wrench on body i, due to interaction at contact point ci, expressed in coordinates of reference frame Ψ_k (p. 65)
W_o	Total wrench on the object as result of *all* wrenches acting on the object. (p. 84)
W_{co}, F_{co}	Total wrench/force on the object due to contact interactions (p. 83)
x_a	[m] Actuator position (p. 60)
x_f	[m] Finger position (p. 60)
x_h	[m] End-effector position (p. 60)
x_o	[m] Object position on fixed world (p. 59)
x_{hd}	[m] Desired end-effector position (p. 60)
x_{od}	[m] Desired object position on fixed world (for releasing) (p. 59)

Abbreviations

ESI Embedded Systems Institute

TU Delft Delft University of Technology

TU/e Eindhoven University of Technology

UT University of Twente

Falcon Flexible Automated Logistics CONcepts

IFR International Federation of Robotics

EUROP European Robotics Technology Platform

JARA Japan Robot Association

WTEC World Technology Evaluation Center

CCC Computing Community Consortium

CRA Computing Research Association

fte full time equivalent

FODV Functional Order Dependent Variable

LDV Layout Dependent Variable

FTI functions move to items

ITF items move to functions

i/o in- and output

CNS Central Nervous System

DOF degree of freedom

EMC Electromagnetic Compatibility

MTBF mean time between failure

MTBM mean time between maintenance

MTTM mean time to maintain

PwoF point-contact-without-friction

HF hard finger contact

SF soft finger contact

IPC Intrinsically Passive Controller

VIA Variable Impedance Actuator

Contents

Chapter 1

Introduction

Technology changes the world. Robots are coming. Ever since breaking innovations like the Watt steam engine (1763) catalyzed machine-based manufacturing, technology development created new industries and jobs, turned around societies, and brought economic growth and welfare to capitalist economies. It did not only stimulate the automation of production processes, it also paved the way for many products that inevitably changed daily activities of people.

Just think about opportunities that arose from the introduction of electrical power generation ($\sim$1900); many household devices stem from the early 1900's. Or what about the way transportation changed through series of technological advances (e.g. internal combustion engine, battery for electric starter, drum brakes, etc...) that leveraged development of automobiles. Or such a seemingly simple thing as a light bulb, light anywhere, anytime! It is endless; communication and information availability changed completely from telephone, radio, television to pc's, internet and mobile cellphones through enabling innovations like vacuum tubes, transistors and integrated circuits (IC's).

Technology development is a complex process of causal relations between many innovations and discoveries. Novel technologies allow to produce new products and, vice versa, innovative products require new technologies. New products create new ideas, asking for technological breakthroughs, which again induce another technological avalanche of product innovations. Society changes once again and economic activity is ensured.

For the coming decades, robotics is said to be one of these areas in which innovations will bring robotic products to the every day lives of human society. Manipulation and grasping are identified as key-enabling technologies to make these promises come true. Challenges remain to assure robust and versatile manipulation and grasping to execute human-like tasks in human environments. This work presents novel insights and concepts for compliant and versatile dexterous robotic grasping.

1.1 Robots of Tomorrow

Robots started in industrial manufacturing. Today, new opportunities lie on the horizon. This section summarizes trends in robotics and motivates the topic of this work: dexterous grasping.

1.1.1 Robots invented

In industrial manufacturing environments, machines are invented continuously to automate and optimize production processes. From the early 1960's, many of these machines became to be

known as manufacturing robots.

The word 'robot' was introduced by the Czech Karel Čapek in his science fiction play R.U.R. (Rossum's Universal Robots, 1921) in the Czech language. He uses it to refer to 'artificial people'[1], who are supposed to happily work for humans. Today, many definitions of robots go around. Intuitively, people define a robot as a mechanical machine that performs human tasks either pre-programmed, remotely controlled or autonomously operated. For industrial manufacturing robots, a more strict definition is given by ISO 8373:

> *"An automatically controlled, reprogrammable, multipurpose manipulator programmable in three or more axes, which may be either fixed in place or mobile for use in industrial automation applications."*

Reprogrammable implies that the robot's motions and hence its tasks can be altered without physically changing the robot. The axes represent the directions of motion. Several industrial manufacturing robots are shown in Figure 1.1 as an example. Due to the minimal number of three axes and the multipurpose requirement, many industrial manufacturing robots have great resemblance with human arm functionality. This makes them suitable for replacing and optimizing human manipulation tasks.

As suggested by Čapek's robots, industrial manufacturing robots replaced humans to execute repetitive or dangerous manipulation tasks like painting, parts assembly and spot welding in for example automotive industry and electronics industries (e.g. printed circuit board assembly). They brought huge economical benefits to factories through improved throughput and operation times (humans rest and get ill), accuracy, repeatability and constant quality. Furthermore, robots enabled production processes that were not feasible before, allowing to invent and produce new products.

After a period of strong growth in sales and operational stock of industrial manufacturing robots, growth is now stagnating and new trends are signaled by different institutes worldwide, such as the International Federation of Robotics (IFR), the European Robotics Technology Platform (EUROP) and the Japan Robot Association (JARA) [1, 2, 3].

(a) Assembly (FANUC Robot M-1*i*A)

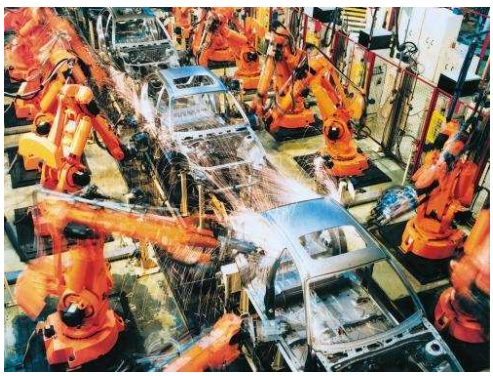

(b) Spot Welding (Kuka Robot Group)

Figure 1.1: Examples of manufacturing robots

1.1.2 Future robotic trends

Service robotics is predicted to form an emerging application field for new robotics technologies to fill future market demands by solving societies' biggest concern; aging populations. The following sections discuss the classification of service robots, which is then used in the remaining sections to summarize future robotic trends and technology demands.

[1] http://en.wikipedia.org/wiki/R.U.R._(Rossum%27s_Universal_Robots)

Service robots Formulating a clear definition for this rising category of so called service robots is not trivial due to its broad application field and variety of appearance forms. Whereas industrial manufacturing robots have been strictly defined by ISO 8373, service robots have no strict internationally accepted definition yet. The IFR adopted a preliminary definition[2]:

> *"A service robot is a robot which operates semi- or fully autonomously to perform services useful to the well-being of humans and equipment, excluding manufacturing operations."*

Clearly the given definition still leaves room for different interpretations, since the word robot itself is not uniquely defined. It even allows a manipulating industrial robot to be regarded as service robot as well, in case it is installed in non-manufacturing operations. This leads to the observation that the actions from a service robot do not add value to any product produced. It is the service itself that is worth value (e.g. entertainment, cleaning) or it assists in adding value (e.g. robot assisted surgery).

Multiple robotic classifications exist that support the above stated and help to clarify the distinction from an application point of view. Van den Brandt combined the IFR and EUROP classifications and identifies two major robotic segments: *industrial manufacturing robots* and *service robots* [4]. The classification is completed by splitting service robotics into two separate application segments: *professional service robotics* and *personal service robotics*. Figure 1.2 presents two currently commercially available examples of both service robot segments.

(a) Personal service: vacuum cleaning (iRobot Roomba ®)

(b) Professional service: robot assisted surgery (Intuitive Surgical, da Vinci® Surgical System)

Figure 1.2: Examples of service robots

Altering the presented segmentation from an added-value (manufacturing or service) versus usage (personal or professional) view to an interaction (structured or unstructured) versus usage view, changes the existing classifications from application oriented to a broader classification that combines both application and technology viewpoint. This is illustrated in Figure 1.3. Not so much the application type (manufacturing or service), but rather the interaction type is the key driver behind robotic technology developments. Structured interaction refers to an interaction between the robot and its environment which is predefined by the developer. Oppositely, unstructured interaction can not be defined by the developer a priori, since the application's operation environment is not fixed or identical for all individual robots and possibly changes continuously.

The presented interaction-usage segmentation in Figure 1.3 shows to encompass the previously discussed classical application classes. Interestingly, two extra application classes are identified; *customized mass production* and *first generation personal service robotics*.

Customized mass production refers to mass customization, which is a trend in professional context for a.o. manufacturing industries. At its core is a tremendous increase in variety and

[2] http://www.ifr.org

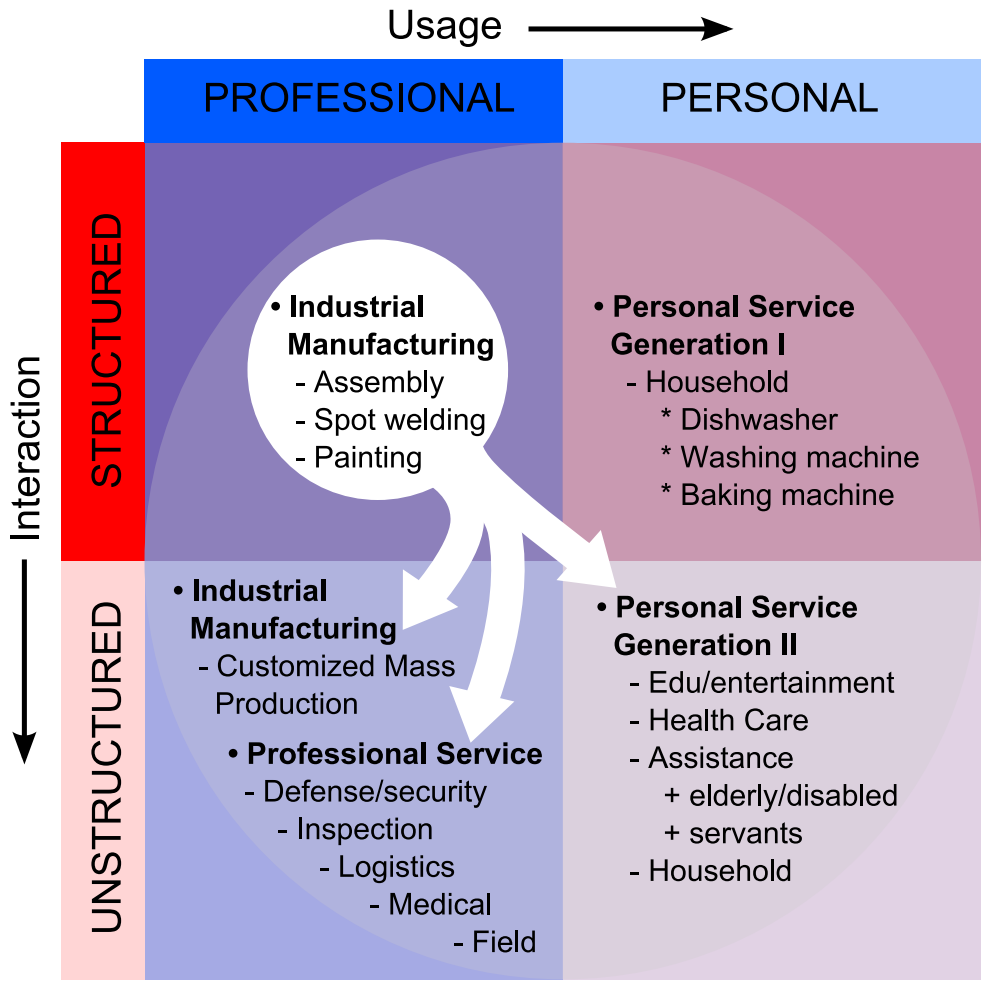

Figure 1.3: Robotic application segmentation; interaction-usage matrix. This interaction versus usage matrix view holds both application classification and technology demands implications. Shifting robotic developments from industrial manufacturing towards service applications implies the requirement to shift from structured to unstructured interaction technologies.

customization of products without a corresponding increase in costs[3]. Interesting pioneering examples are found in customization of apparel by e.g. Levi Strauss & Co., Brooks Brothers and Lands' and in footwear by Nike and Adidas, where customers can actually design clothing themselves. Examples of the first generation personal service robotics are found by recognizing that e.g. dishwashers and washing machines provide personal service by automating human tasks. Remember that devices that automatically perform human tasks were intuitively defined as robots. These examples are rather structured tasks. The interaction with the user and the clothes or dishes is always the same and can be prescribed and controlled by the developer. Hence it is observed that a first generation personal service robots has been around for quite a while.

Thus, when speaking about personal service robots, most of the time people refer to the second generation personal service robots, that have to deal with unstructured interaction. Within professional usage, not only service robots are identified, also trends in manufacturing will require unstructured interaction.

[3] http://en.wikipedia.org/wiki/Mass_customization

Service robotics form next technological revolution All recent studies on trends in robotics from major robotic institutes like IFR, EUROP, JARA, World Technology Evaluation Center (WTEC) and Computing Community Consortium (CCC) & Computing Research Association (CRA) report the same trends; robotics technology will play a key role in worldwide economical and social changes for the coming decades [1, 2, 3, 5, 6].

These predictions are based on future economics, demographics and technology developments. The latter already successfully opened new markets for second generation personal and professional service robots, like the examples in Figure 1.2. Starting from the 1960's until the end of 2008, almost 2 Million industrial manufacturing robots were sold, while in the last decade already 7 million personal service robots (30% entertainment, 70% household (mainly vaccum cleaning & lawn mawing robots)) were sold of which almost 1 million were sold in 2009 alone [1]. These fast growth figures are expected to increase even more for the near future; from 2009 to 2012 the IFR predicts that another 11.4 million personal service robots will be sold. For professional service robots, growth predictions are equally optimistic [1].

Also future economics and demographics will change dramatically. The world is changing. Companies and countries are facing global competition nowadays (induced by shorter transportation times and better means of communication), while new economic centers are on the rise (e.g. China and India) with extensive availability of a relatively cheap workforce. At the same time, Western developed countries face aging populations, which implies declining work forces while more and more people will need health care and assistance in daily live activities. Nevertheless, to sustain economic growth and welfare, production levels need to be maintained.

At the same time, within this changing competitive environment, mass customization requires industry to shift automated production and product handling from standardized to customized, small batch and short life-cycle products [7].

The IFR, EUROP, JARA, WTEC and CCC & CRA all agree that especially service robotics can, will and even must create many opportunities to sustain welfare and quality of life by solving these concerns of Western societies [1, 2, 3, 5, 6]. Hence, service robotics is believed to catalyze the next technological revolution [8, 9, 10].

Figure 1.4: Justin Robot, Inst. of Robotics and Mechatronics, DLR[4]. Example of current state of the art of robotic personal assistants.

Technology demands for 2nd generation service robots Clearly, robotic technology is maturing and at the same time it is needed to be applied for robotic services. This implies, as illustrated in Figure 1.3, that robots shift from industrial manufacturing to personal and professional service applications.

For personal services, single-purpose robots, e.g. autonomous vacuum cleaners and lawn mowers, are now widely available and make up the pioneers of the second generation of personal service robots. The development of full multi-purpose humanoid robots is still ongoing research. These humanoid robots are aimed to have a natural human-like appearance and behavior. The end goal is to have them working in a human environment doing all kinds of different household

[4]Deutsches Zentrum f ur Luft- und Raumfahrt e.V. (DLR), i.e. Germany's national research center for aeronautics and space. Taken from download section on http://www.dlr.de.

chores, like for example the upper body humanoid robot assistants ARMAR [11] and Justin (see Figure 1.4) and the full humanoid Honda Asimo [12]. Such domestic robots are envisioned to release humans from time-consuming tasks and to please by serving and entertaining them. For disabled and elderly people (our aging society demands for labor free solutions), they will assist in their primary needs, see e.g. RI-MAN [13].

For professional service robots, many different applications are on the roll reaching from defense and security (e.g. de-mining and surveillance robots) to logistics and medical applications. Yet another task waiting for the next generation of robots lies in human-robot cooperation, within both the household and industrial environment [11].

Mass customization, see Figure 1.3, is also recognized by robotic researchers as interesting application domain for next generation robots. Urged by heavy global competition, some industries start to shift from classical mass production, i.e. repetitive tasks in structured environments, towards automated production and handling of customized, small batch and short life-cycle products [7].

The interaction-usage matrix in Figure 1.3 clearly shows one major commonality for the envisioned trends. From a technology point of view, shifting towards mass customization and services, implies the necessity to deal with unstructured interaction due to mostly human (i.e. changing) environments, with varying (possibly unknown) objects and circumstances. Therefore, these emerging robotic applications ask for highly versatile robots for both personal and professional usage. As such, all roadmap studies agree on several critical technologies that need to mature to deploy service robotics successfully. Among those are **autonomous perception** and **dexterous manipulation** through versatile end-effectors [1, 2, 3, 5, 6].

Dexterous manipulation From these critical technologies, this work is particularly interested in the study on dexterous manipulation. The human hand is of course very versatile regarding these wide variety of tasks and circumstances. Not to forget, the domestic robots are to operate in an environment suited for humans. Hence, dexterous robot hands that have human hand functionality and dimensions are believed to be the required end-effectors for dexterous manipulation. Such a dexterous robot hand should be able to *grasp*, *hold*, *release* and *manipulate* regular and irregular objects and to *manipulate* fingers[5].

1.1.3 Conclusions on robotic trends

Current trends in society and technology developments show that the robots of 'tomorrow' can and will create a technological revolution. They will provide personal and professional services in unstructured environments which requires them to be versatile. Therefore, proper dexterous human-like robotic hands are of key importance. Developing these robotic hands is not trivial at all and is far from being finished. It brought many researchers to take up the challenge to tackle bits and pieces of dexterous manipulation and grasping. This work strives to contribute in finding solutions for creating human-like dexterous robotic hands.

1.2 Falcon Project: Service Robots in Logistics

As discussed previously, professional service applications for dexterous robot hands are numerous. Possible applications are found in logistics, where transportation, processing, storage and distribution of products make up a significant part of the price of goods sold. Today, only 15 %

[5]Think off pre-shaping, wiping surfaces, pushing buttons, making signs and gesturing with the finger, etc.

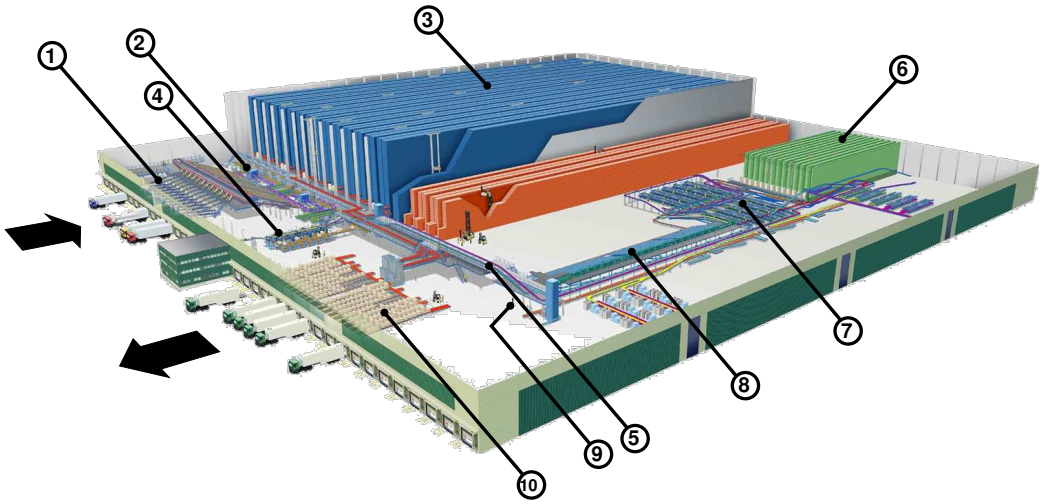

Figure 1.5: Typical large retail distribution center. Usual flow of goods: Products, packed in cardboard boxes, arrive from manufacturers in containers at *goods receiving* (1), continue on conveyor belts to an automated *pallitizer* (2), pallets are stored in automated *pallet bulk storage* (3), pallets move to human-operated *tote fill area* (4), products go from cardboard boxes into *product totes*, product totes move on *conveyor belts* (5) to the *miniload* (automated tote storage, 6), product totes move to human-operated *order picking stations* (7), ordered products are put into order totes and move to buffer lanes, *sorter* (8), order totes move to automatic *dollitizer*, which stacks totes on dollies (9), dollies are dispatched into trucks in *outbound area* (10).

of the end-to-end distribution process is automated [6]. Next generation professional service robots are thought to be capable of providing solutions for automated handling of products.

This work is part of the Flexible Automated Logistics CONcepts (Falcon) project, which originated from the desire to explore automated handling of products for future applications in warehousing. In these environments, although not necessarily dexterous nor robotic, objects need to be manipulated for sure.

This section introduces the Falcon project by giving a very brief introduction to warehousing (Section 1.2.1) and presenting a summary on the consortium of partners and the project goals (Section 1.2.2). Furthermore, the interest for dexterous robot hands within this context is motivated (Section 1.2.3).

1.2.1 Falcon project background: Warehousing

These days, labor intensive industries like warehousing face the challenge of surviving in Western countries. A warehouse is a building for storage of goods in supply chains of manufacturers, and (large) retail organizations. It is a point in the supply chain where a product pauses, however briefly, and is touched [14]. Warehouses are used to match supply with customer demand (buffering), to consolidate products (reduction of transportation) and to provide value-added processing (e.g. light assembly, pricing, labeling).

Several types of warehouses can be distinguished, such as a *retail* distribution center and a *catalog fulfillment* or *e-commerce* distribution center [14, 6]. For the Falcon project, a large retail distribution center served as a reference case. A typical retail distribution center layout is presented in Figure 1.5. It describes the usual flow of goods from receiving products from the manufacturers to dispatching the orders to the retail shops. Of course, there exist many exceptions to this usual flow, like goods returned by customers and oversize products. Figure 1.6 gives an impression of the different stock keeping units.

Retail shops regularly send their orders to the distribution center. Each order comprises

(a) Boxes - hold identical product items

(b) Pallet - holds boxes

(c) Order totes - hold different ordered product items

(d) Dollies - hold order totes

Figure 1.6: Examples of different stock keeping units. Smallest unit is a single product item as it is bought by the end-customer.

many items, consisting of both many different items as well as many items of the same type. The distribution center serves numerous retailers. Also the set of products is large and changes, based on customer demands, seasons and market developments. All-in-all, the distribution center handles huge flows of many different products. Furthermore, both the product flows and the products itself change continuously.

Obviously, the design of warehouses is optimized for a trade-off in *operational costs* and *operational performance*. The operational performance is characterized by throughput times, storage capacity and product flexibility. Costs are mainly determined by building size, equipment (installation and maintenance) and labor demands. Hence, optimization of these parameters depends on the inventory characteristics (number of products, variety of products, sizes, etc) and order statistics (order sizes, order frequencies, shipment rates, product variation, fast/slow movers, etc).

As described in Figure 1.5, labor intensive operations are found in goods receiving (1) and dispatching (10) (unloading and loading of containers/trucks) and in human operated tote filling (4) and order picking (7). The first two operate on consolidated products which results in much higher throughput times (on product level) than can be realized with the latter two, which operate on single products. Hence, human operated tote filling and order picking are bottleneck processes.

1.2.2 Falcon consortium and project goals

Increasing labor costs, tightening labor legislations and human failure rates raise the need for further automating the warehouse operations. Vanderlande Industries B.V.[6], one of the world leading warehouse system integrators, has picked up the challenge to pursue the fully automated warehouse. Together with the Dutch Embedded Systems Institute (ESI)[7] and academic partners from Dutch universities (Delft University of Technology (TU Delft), Eindhoven University of Technology (TU/e) and University of Twente (UT)), the Falcon project was formed to research the challenges involved in further automating the warehouse.

The project embodies a workforce of ca. 20 full time equivalent (fte) employee positions of which 13 fte is reserved for academic research activities (9 phd students, 2 postdocs and supervision). Remaining fte's are reserved for management, administration, general project members, ESI research fellows and engineering work (1.75 fte).

[6]Dutch commercial company, see: http://www.vanderlande.com
[7]http://www.esi.nl

The goal of the Falcon project was formulated as follows:

> *To design a fully automated warehouse as a system of systems based upon research that develops:*
>
> 1. *techniques and tools for the design and implementation of professional systems, including optimization and decomposition of global requirements concerning system performance, reliability, and cost using a model-driven approach.*
> 2. *integrated demonstrators of critical components to prove the feasibility of derived subsystems.*

The first objective starts with high-level system models. System models will be created for different design abstraction levels to analyze and guide the (de-)composition and propagation of design requirements over system components. The second objective strives to create critical evidence of feasibility of derived components and requirements. This work belongs to the planned technology development for demonstrators of critical mechatronic components (second objective).

1.2.3 Dexterous robotic hands for Falcon

Following the top-down-bottom-up application driven analysis method, see details in Chapter 2, it was found that the general global warehouse behavior is built up from six primary functions, like e.g. item storage, singulating product items[8] and composing orders. Item singulation and order composing are both highly versatile functions, due to the wide variety of objects to be handled. These item handling functions are still implemented by human operated work stations. Clearly, current technology does not suffice to automate these functions (in a cost effective way).

Hence, research areas that possibly lead to novel technologies to automate these functions are of major interest. Within these research areas only two basic technology options for composing orders can be identified: either *dropping* or *placing*. And also for singulating items only two basic technology options can be identified: *filtering* or *picking*.

Without having worked-out solutions, it is clear that dropping options endanger product conditions. Furthermore, the item packing density is low due to the inherent inaccurate targeting of item placing positions. For singulating items, filtering technologies would impose many small operations on the items, which is likely to worsen throughput times and may also damage the items. Hence picking and placing technologies are in favor for both singulating items and composing orders.

For both technology options, manipulators and end-effectors are needed. Manipulators such as robotic arms and xyz-stages are widely available. Versatile end-effector technologies suitable to be deployed in singulating and composing functions are far from begin mature. The items to be picked and placed in such logistics environments are typically items designed for human usage. This makes human-like dexterous robotic hands an interesting versatile end-effector technology to be investigated for technology development towards usage in professional logistic service robots.

[8] Singulating product items: refers to separating a batch of product items into single product items.

1.3 Problem Definitions & Thesis Goals

This section motivates the goals of this thesis by identifying some issues to be challenged. One part focuses on the process of formulating and executing application driven research projects. The majority of the thesis deals with enabling technologies and knowledge for dexterous robotic grasping.

1.3.1 Application driven research projects

An application driven research project is a project that aims to develop a working application on a short-term, while addressing the need for research activities that develop enabling technologies for the application.

Falcon project work observations The Falcon project plan (Section 1.2.2) has a clear focus on application driven top-down systems engineering. The top-down approach must lead to (1) new systems engineering insights and to (2) clear evidence of applicable results through building demonstrators by integrating critical components derived from top-down requirements analysis. Naturally, applicability of project results for the application of the industrial carrying partner, Vanderlande Industries B.V., is targeted as central objective.

A component is a sub-system as part of a total system. A component specification defines both the sub-system behavior, its constraints and input/output requirements. To do so, a total system architecture is needed which defines the decomposition of the total system into sub-systems. At the start of the Falcon project, a system architecture was not yet available for the automated warehouse, since it was projected as a research result itself. Hence, critical components to be demonstrated (second objective, see Section 1.2.2) could not be specified at the start of this work.

Instead of pursuing an application driven top-down analysis as a team effort to jointly define each of the necessary sub-systems to be investigated (first objective), project participants individually selected their research topics, without having defined a system architecture. As shown in Chapter 2, also the research goals on dexterous grasping in this thesis work stem from such a bottom-up selection process. The author observed that these individual interest driven bottom-up choices led to divert people from aiming for shared project goals and seemed to hinder interdisciplinary teamwork. The members of the Falcon project have produced research contributions in their fields. However, within the project, the author observed difficulties in aligning these achievements with the overall central system architecture to be developed.

Hence, although the Falcon project pushed forward state-of-the-art research results, it did not achieve all the potential it could have achieved as aimed for in the project plan. Hence, the author observes a mismatch between the Falcon project plan and the actual execution of the plan:

- Non-optimal teamwork: The Falcon project plan clearly has ambitious aims to set up an interdisciplinary project based on teamwork. However, coherence and teamwork between different project partners showed room for improvement.

- Non application centered activities: research activities seem to be bottom-up interest driven, without relating to a commonly shared end-goal.

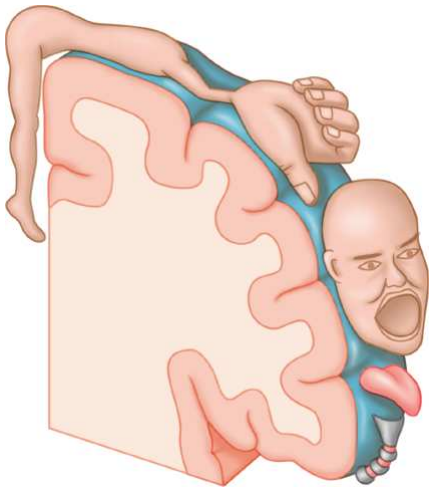

Figure 1.7: Homunculus of Dr. Penfield[9]. The motor homunculus and sensory homonuculus map the motor and senory cortex to body parts. The hand uses a large portion of the cortex (both for sensing and motion). Courtesy of *BrainConnect.com*.

Thesis Goal Current Dutch subsidy and project funding systems for technology disciplines push towards multidisciplinary projects with tense collaborative participations between academia and industry. Governmental organizations try to stimulate high pay-off rates in terms of direct industrial usability of research results. The Falcon project is a good example of this, as well as many other projects.

As discussed above in the Falcon project work observations, such collaborative projects put a clear demand on handling the tension between the inherent interest driven process of doing research and the application driven top-down systems engineering approach in industry. Based upon lessons learned from participating in an application driven research project (i.e. the Falcon project), part of this thesis aims to:

- reflect on causes of the above indicated tensions;
- offer proposed solutions on how to deal with such opposing attitudes;

1.3.2 Dexterous robotic grasping

For dexterous robotic grasping, robotic hands are needed together with appropriate sensory and control systems.

Challenges for dexterous robotic hands To survive in natural (i.e. unstructured) environments, humans are given highly versatile and complex hands, which require complex control as well. Figure 1.7 confirms the control complexity by illustrating that sensing and control processes of the hand occupy a major part in human brains. The complex dexterous abilities of the human hand let humans create complex objects and environments. As pointed out earlier, although highly challenging, it is believed that a multi-purpose robotic solution needs to be human-like to handle human tasks in human-made environments.

Despite many celebrated efforts and breaking research contributions, still the resulting robotic hands are clever but complex designs housing many (fragile) components. Figure 1.8 shows some of those famous examples like Soft gripper [15], Salisbury hand [16], Utah/MIT hand [17], Gifu hand [18], UBHand III [19], Karlsruhe hand [20] and DLR hand [21]. They

(a) Barrett Hand (Barrett Technology Inc.)

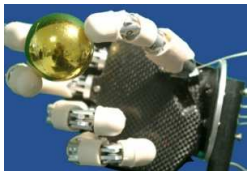

(b) CyberHand.org (ARTS Lab, Italy)

(c) Shadow hand (Shadow Robot Company)

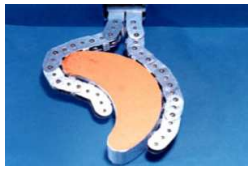

(d) Soft Gripper (Hirose Fukushima Robotics Lab)

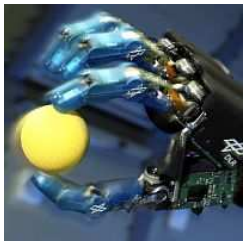

(e) DLR-HIT-Hand (DLR - Institute of Robotics and Mechatronics)

(f) Utah/MIT hand (Artificial Intelligence Laboratory at MIT)

(g) UB Hand III (Lab. of Autom. and Rob., D.E.I.S., University of Bologna)

(h) Gifu hand (Co.,Ltd. Dainichi)

Figure 1.8: Some of the state of art of dexterous robotic hands and grippers.

compromise on dimensions, weights, reliability, functionality and costs. For example, the number of actuators is a clear source of this complexity [7]. Besides, controlling these devices for stable grasping and manipulation remains another challenge.

Decreasing the number of actuators, drastically reduces the number of required components, which reduces the weight and energy usage, while robustness becomes easier to assure and cost price will benefit as well. For the prospected large field of emerging robotic applications, major breakthroughs in this respect are needed to get dexterous robotic hands into practice. In fact the same applies for dexterous prosthetic hands, for which the same design goals and functionalities apply.

Thesis goals In line with these dexterous grasping challenges, this thesis aims to create enabling technologies and knowledge for dexterous grasping by:

1. contributing in development of novel robotic dexterous hands by introducing a novel underactuated robotic finger concept, which features a minimal actuation design and variable compliance[10];

2. presenting and contributing theory on natural vector space decompositions for the analysis of physical systems, which have non-invertible maps in their model representations. One example of these maps is the actuator Jacobian in underactuated robotic fingers. Presented insights are applied for the analysis of the novel robotic finger concept;

[9]Penfield, W. & Rasmussen,T. (1950) The Cerebral Cortex of Man: A clinical study of localization. Boston: Little, Brown and Co.

[10]Stiffness: the resistance (force) of a body against deformation. It is the second derivative of the potential energy with respect to the corresponding deformation (around a certain configuration). It is a linear(ized) property; Compliance is the mathematical inverse of stiffness. Throughout this thesis, both compliance and stiffness will be used.

3. presenting specific low-level controller synthesis to (1) utilize the features of the novel robotic finger concept for executing robotic finger tasks and to (2) demonstrate usage of presented insights on natural vector space decompositions;

1.3.3 Thesis goals summary

The introduction has shown the interest for dexterous robotic hands, both within worldwide trends and in the context of the Falcon project. In the field of dexterous robotic grasping, still many challenges remain to be solved in order to produce reliable useful dexterous grasping technology. Presented thesis goals aim to contribute in further developing dexterous robotic grasping technology and knowledge.

Being still at such a fundamental level, for the Falcon project, application specific knowledge on dexterous robotic grasping for logistics may not be addressed yet. However, every fundamental contribution supports future developments of such logistic applications. Nevertheless, the Falcon project plan was aiming at delivering integrated demonstrations of automated warehousing sub-systems. Another goal of this thesis is to try to reflect on challenges in application driven research projects, such as the Falcon project.

1.4 Thesis Outline

The thesis is organized as follows. Chapter 2 starts with reflections on application driven research projects (see thesis goal in Section 1.3.1). It describes the Falcon project as a case example and it gives a framework to analyze the reflections and to formulate lessons learned.

Then, Chapter 3 presents a brief overview on the current status of dexterous robotic hand technology. The overview is used to formulate design considerations and a research direction for further developments and innovations in dexterous robotic hand technology. Variable compliance and underactuation are marked as important topics. Hence, Chapter 4 presents analysis for simple grasp scenarios to show the importance of variable compliance.

Next, Chapter 5 gives insights on natural space decompositions. Multiple mathematical view-points are used to explain the importance of choosing proper metrics on vector spaces, especially when the elements of the vector spaces represent physical quantities of a physical system. For the case of damped motions, a time-dependent physically equivalent metric is derived, which defines the natural decomposition of spaces for the studied case. These insights are used for the compliance analysis of a novel underactuated robotic finger concept, which is introduced and extensively analyzed in Chapter 6. It encompasses the design considerations as formulated in Chapter 3. Chapter 7 presents a low-level controller for the novel robotic finger concept. It allows to fully utilize the proposed features of the robotic finger and illustrates usage of the insights from Chapter 5. Simulation results are shown to demonstrate execution of various task scenarios of the proposed robotic finger. Finally, Chapter 8 ends this thesis with conclusions and recommendations.

Chapter 2

Application Driven Research Projects

More and more academic research projects shift from being fundamental research to being application driven research projects. An application driven research project is a project that aims to develop a working application on a short-term, while addressing the need for research activities that develop enabling technologies for the application.

The Falcon project plan, see Section 1.2.2, formulates the objective to design a fully automated warehouse. For such a system, for sure novel components are needed. To keep focus on the central application and to maintain coherent interrelated activities between all project partners, the project plan proposed to jointly follow a top-down systems engineering approach to design a novel system architecture. The next project step was to select for each of the project partners different critical components and work packages from this architecture. Ultimately, it was aimed to integrate these components to implement actual demonstrations. However, the formulated approach led to re-think specific approaches for application driven research projects.

Some inherent challenges that arise in application driven research projects were observed in Section 1.3.1. Although the Falcon project pushed forward state-of-the-art research results, to the authors opinion, it did not achieve all the potential it could have achieved as aimed for in the project plan. Hence, the author observed a mismatch between the Falcon project plan and the actual execution of the plan. In this chapter the author aims to discusses these challenges by reflecting on the Falcon project as a case example. Along the discussion, the author builds a framework to model the involved aspects of formulating and executing an application driven research project plan. The framework is also used to reflect on the Falcon project, which allows the author to formulate some lessons learned. The author wishes to share these lessons learned for future application driven research projects.

2.1 Chapter Outline

This chapter is organized as follows. Section 2.2 starts with the top-down systems engineering analysis for the Falcon project. It will be shown that establishing a system architecture is obstructed. Section 2.3 introduces a top-down-bottom-up analysis framework to circumvent this obstruction, without loosing project ties and teamwork between partners. Then, in Section 2.4, the proposed framework is utilized to show how research directions within the Falcon project were established and how they can be related to other project activities and the project goal (i.e. justification). Then the Falcon case is closed and the general framework is used to present aspects and approaches involved in the process of setting up and running application driven research projects (Sections 2.6 and 2.5). Section 2.7 turns back to the Falcon case to use the presented insights to reflect on the Falcon project plan and outcomes. Finally, Section 2.8

draws some conclusions on application driven research projects.

2.2 Critical Component Analysis: Top-down Approach

Systems engineering starts with systems architecting. Systems architecting is the process of executing activities to transform problem and solution know how into a new architecture of a technology intensive product. The system architecture describes at least internal aspects, such as construction and structure of sub-systems (i.e. building blocks) of the new system, i.e. a product. External aspects, such as experience and perception, may be included as well [22].

This approach was advocated in the project plan. As discussed, it starts with a multi-stakeholder viewpoint iterative top-down (i.e. putting desired end-system central) analysis of transforming wishes, visions and requirements into a suitable architecture. An extensive treaty on such systems architecting approach is given in [22].

2.2.1 Black-box view: Top-level desired behavior

In the top-down analysis, the distribution center to be automated is considered a system with certain *system requirements*. The system requirements prescribe the desired system by describing the *desired behavior* and specifying desired values for a set of *requirement parameters*.

For the distribution center, the desired behavior is summarized as follows; it accepts consumer products stored in cardboard boxes from different sources (e.g. containers, trucks), stores products and sends out ordered products in order totes on dollies, whenever requested from a retailer. The requirement parameters encompass for example operational performance (e.g. throughput times, storage capacity and product flexibility) and costs (e.g. ownership costs, operational costs, etc). Giving specific values for these requirement parameter falls beyond the scope of this discussion.

A so called black-box view with given inputs and outputs, allows to be open-minded in composing an optimized automated distribution center architecture, without being hindered by existing components. Note that existing components (like e.g. storage systems and order-picking stations) are useful if they contribute to optimality, but should not be seen as components that need to be replaced with automated solutions in a one-to-one manner. It was acknowledged in the project plan that the success of novel automated components may fail, due to a possibly non-optimal (mis-balanced cost of ownership vs. performance (throughput, error-rates) in comparison to existing non-fully automated solutions) system architecture. Hence, an open-minded view-point was taken, which explicitly aims for a so called green field architecture[1] in order not to exclude or miss powerful (non-existing) technology options.

2.2.2 Primary functions

Several primary functions were identified which together make up the desired total system behavior: **unpack boxes**, **store product items**, **singulate product items**, **check product items**, **compose orders** and **move items**. *Singulating* refers to separating a batch of product items into single product items, *checking* encompasses everything concerning identification, verification, damage detection, etcetera and *composing orders* is defined as transferring items into an order tote to consolidate an order of multiple (different) items. A function can be

[1] Green field architecture: problems without pre-existing architecture, or where existing architectures can be ignored [22].

either implemented into a separate sub-system, or several functions can be taken together into one sub-system implementation.

Top-down systems engineering aims to define sub-systems with clear boundaries and specifications, which together implement the desired system. Specifications for each of the sub-systems define the necessary values of the (sub-system) requirement parameters. They are derived from the desired system behavior and requirement parameter values. This allows to develop and implement sub-systems independently. Moreover, multiple different implementations (i.e. different components with same input/output interfaces) can exist. Designing for sub-systems instead of the total system as a whole enables modularity and a structured problem analysis that may lead to better solutions. Thus, first sub-systems need to be defined, then specifications can be set for each of them.

2.2.3 Sub-system definition

Defining sub-systems implies designing a top level system architecture. The top level system architecture holds two design aspects: a **functional order** and a **layout**. The functional order defines in which sequential order the primary functions are executed, whereas the layout defines which functions are taken together as sub-systems and, if applicable, (like in the case of distribution systems, are placed where.

In systems architecting in an industrial context with classical multi-disciplinary engineering disciplines for software or technology products, choices on the functional order and the layout are a result of optimizing achievable values for the requirement parameters (e.g. performance and costs) and other design goals like e.g. re-usability, transparency and modularity of the design. Optimization and trade-off choices are based on knowledge of available technology options from existing components and known technologies. This knowledge is used to finish the optimization process and settle for a system architecture. Always, even if information is available, determining optimality itself is of course also a complex task. It involves determining behavior and performance of the composition of sub-systems.

In the case of the distribution centers, besides mechatronic engineering disciplines, this also encompasses analyzing and predicting logistic processes, e.g. stochastic queuing processes. This is illustrated with a small example:

> *First unpacking boxes, then singulating and then storing the product items, implies the need for a storage function that can store separate individual product items. This may cost more storage space (larger building costs), but seems to make fast (high throughput) automated composing much easier. However, transportation of single items increases traffic load on the logistics network, which raises the question how, and at what cost (financially and throughput), to design such a network.*

The topic of simulating, analyzing and control of logistic systems is also studied within the Falcon project (TU/e, see e.g. [23]). The goal of these studies was to develop analysis tools, rather than design tools.

The system architecture defines the sub-systems for which then specifications can be set. Next, the sub-systems can be designed and implemented for their given requirements. Of course, more iterations are possible by considering primary functions of one sub-system and again design a sub-system architecture, put requirements on the sub-sub-systems etcetera. Being able to reason (e.g. modeling, simulating) about technologies for optimizing the architecture is typical for engineering. This is in fact what makes engineering different from research, as will become clear later.

However, designing (i.e. optimizing) the top level system architecture for the fully automated distribution center of the Falcon project is found to be non-trivial for one important reason:

Absence of suitable technology
Fully automated solutions do not exist for all primary functions. This brings large uncertainties about both the expected operational costs and operational performance of the technologies to be developed. It complicates or actually obstructs the formation of a (optimized) top level system architecture.

Furthermore, it should be noticed that the actual required suitable technology depends on the definition of sub-systems (taking together primary functions and encompassing functional orders). Moreover, existing automated components may not cover newly defined sub-systems anymore, such that these technologies do not suffice for new architectures. Without such information, reasoning about optimality is useless, independent of the existence or suitable optimization methods.

Conclusively, absence of technology options obstructs the design of an architecture, while the lack of an architecture and hence the lack of sub-system definitions blocks the choice on existing components or selection of new technologies to be explored and developed. Absence of technology options implies the need for research. As such, incorporating research into a project hinders systems architecting and hence asks for another project approach.

2.3 Technology Gap Identification: Bottom-up Analysis

The previous section discussed why, in the context of projects where novel technologies are needed, the formation of a top level architecture fails. A top-down systems engineering approach did not result in sub-system definitions and requirements. Clearly, this did not lead to the identification of critical components to be developed for a fully automated distribution center. Another approach is needed, which is presented in this section as a top-down-bottom-up analysis approach.

2.3.1 Research

Technology development starts with research. Research can be defined as the search for knowledge or any systematic investigation to establish facts[2]. As a result, research may lead to new technologies and new knowledge on its applicability for different purposes and applications. Applicability depends on achievable values for the requirement parameters of an aimed application. However, applicability is not a guaranteed result of research.

2.3.2 Top-down-bottom-up framework

Figure 2.1 shows the proposed top-down-bottom-up framework. It supports to identify interesting research directions within an application driven top-down organized project context, where absence of existing technology obstructs the architectural system design and sub-system formation.

At the top, one recognizes the black box view of the desired top level system behavior, in this case the distribution center. Going down, as previously discussed, a set of primary functions

[2] http://en.wikipedia.org/wiki/Research

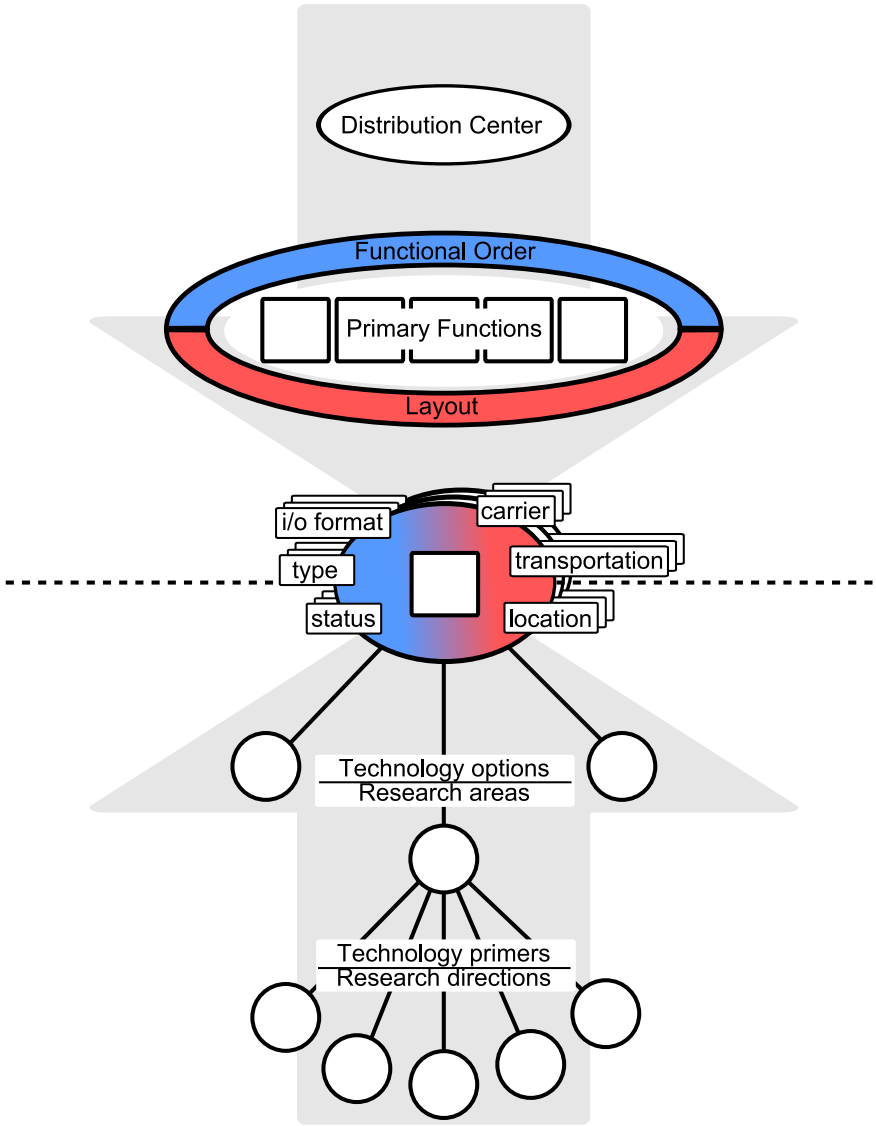

Figure 2.1: Top-down-bottom-up framework for research direction identifications within an application driven top-down organized project context.

is distilled from the top level system behavior. Instead of using these functions to optimize for a system architecture with sub-systems and their derived requirements, only the notion of a system architecture is used. Namely, the fact that the architecture defines a *functional order* and a physical *layout*, which influence a set of architecture variables. These are to be identified. From there, (novel) technology-options and technology primaries are generated. These will be the research directions of interest for the project. Once again, applicability and feasibility are not known a priori.

2.3.3 Architecture variables

The architecture variables are those variables for which requirements (values) are needed to define interfaces between sub-systems and to form a total system architecture. Within this framework two types of architecture variables are distinguished:

1. Functional Order Dependent Variables (FODVs);
2. Layout Dependent Variables (LDVs).

type	architecture variable	value set
FODV	item type	{regular, irregular} × {static, varying}
	i/o format	{single, batched} × {mixed, equal}
	status	{checked, unchecked }
LDV	location	{co-located, separated}
	transportation	{FTI, ITF}
	carrier	{box, pallet, tote or nothing}

Table 2.1: Architecture variables and value sets for distribution center. Acronyms: FTI = functions move to items, ITF = items move to functions, FODV = functional order dependent variables, LDV = layout dependent variables.

Figure 2.2: Human operated order picking workstation

The architecture variables should be identified together with their *value sets*. A value set is a set of values that a variable can accept for different architectures (orders and layouts). It is important to identify the set of possible values, instead of trying to choose specific values, since that would require optimization, which is considered impossible (as discussed).

For the Falcon project, the following architecture variables and sets of possible values can be identified, see also Table 2.1. The functional order determines in- and output (i/o) for each function; the **item type** to be handled or processed can be either *regular* or *irregular* and the set of types can be *static* or *varying*. More detailed value sets (e.g. weight, size, shape classes) are possible here as well. Whereas the **i/o format** can be either single or batched items, mixed or equal, with **status** checked or unchecked. The distribution center layout is composed of; **locations** of functions, being co-located or separated and **transportation**, either functions move to items (FTI) or items move to functions (ITF). The combination of both the functional order and the layout determines the **carrier** of the items, either by box, pallet, tote or nothing.

The following example illustrates how choices on architecture variable values can be traced back from an existing architecture.

Example architecture: Commonly used goods-to-man order picking
Product items, both irregular and regular (item type) are stored in totes (carrier) as batches of equal products (i/o format). When ordered, these products move, carried in their totes, from storage to order-pick work stations (location: separate / transportation, ITF). In these work stations, human order pickers singulate products by picking them from the totes, then they check the single product item (carrier: none) and finally they compose the order by placing the product item into order totes (format: mixed batched items). Because singulating, checking and composing are co-located, they could be implemented as one sub-system, i.e. the human operated order picking workstation, see Figure 2.2.

2.3.4 Selection of research areas

The presented top-down insights resulted in a set of primary functions with an accompanied set of architecture variables and value sets, but lack the coherence of an architecture.

These insights are utilized in a bottom-up strategy to produce (one or more) *technology-options* for each of the primary functions (See Figure 2.1). In this context, a primary function roughly defines **what** needs to be done. A technology-option addresses **how** this could be achieved. Of course, creativity is needed, because unproved approaches are to be generated. Each of such a technology-option corresponds to a (different) *research area*. Of course, refinements are possible; one technology-option (research area) may contain several sub-options (sub-areas).

The identified architecture variables and their value sets are used to reason about the likeliness of *feasibility* of the technology-option for the targeted primary function (Next section, Section 2.4, gives examples for the Falcon project). Furthermore, importantly, the *interest of the people and their affiliation* is of influence here (also reward mechanisms from their affiliation influence interest of people, see Section 2.6.4). Since the technology has still to be researched, qualitative reasoning is guided by the interest of the people involved and leads to decide upon the selection of research areas that will be explored.

2.3.5 Selection of research directions

The identified *technology-options* indicate critical technology-gaps for the future application/system. For each of these technology-options, different elementary technologies, i.e. problem solving approaches, called *technology-primers*, can be generated, investigated, researched, etcetera. Each of these technology primaries leads research into different directions, i.e. *research directions*, within one research area (See Figure 2.1). Refinements are possible.

Again, the choice for a research direction will be the combined result of reasoning about expected achievable results, of current trends in the research area and of the interest of the people and affiliations involved.

Conclusively, *research areas* are chosen that are indicated as technology-gaps for the future application/system. And, *research directions* (i.e. problem solving approaches) are selected based on either expected applicability or curiosity for new approaches or a combination of both. Within the context of a project, research along the chosen directions leads to novel technology-primers. For each novel technology-primer, research should address proofs that present expected achievable values of the requirement parameters for different values from the value sets of the architecture variables.

2.4 Selection of Falcon Research Directions

The previous sections presented a top-down-bottom-up framework (Figure 2.1) to guide the process of selecting interesting research directions for application driven research projects. Although not planned in the project plan, looking back in time, such top-down-bottom-up approach was more or less (implicitly[3]) used by several project partners.

So far, analysis resulted in a set of primary functions accompanied with a set of architecture variables and value sets (Section 2.2.2 and 2.3.3). This section finishes the selection process by summarizing research areas and research directions for some of the project partners. This selection process is projected onto the top-down-bottom-up framework. It is important that,

[3]implicit refers to the fact that such approach was not planned but more or less happened

in this case, this selection process is done by people who fulfill the role of researchers (Ph.D students) affiliated to academic institutes[4].

The purpose of this section is to show how to continue the analysis within the presented framework, to introduce some other Falcon project activities and to show the identified (but not guaranteed) relevance of dexterous grasping for automating distribution centers.

2.4.1 Primary functions

Independent of any functional sequence, *unpacking boxes* and *storing items* are considered relatively trivial to implement with current technology (primers). The other three primary functions have no obvious implementations and current technology does not suffice. Hence, technology development for these functions is critical for successfully automating the distribution center.

2.4.2 Falcon partners' research directions

Check items Some project partners (TU Delft) were interested in contributing in technology and knowledge development for *item checking*. Figure 2.3 shows a brake-down of the primary function check items. The function contains some sub-functions: identification, localization, recognition and diagnose[5]. For each of those, several technology-options were generated from which laser and vision based imaging were selected to be explored. Hence, multiple research areas were selected with a primary focus on computer based imaging techniques.

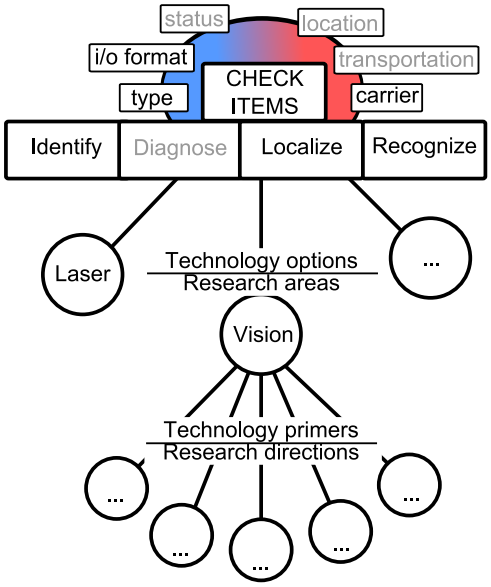

Figure 2.3: Selection of research areas and directions for the primary function: check items. Light-gray colored elements are considered not of importance at this stage of technology exploration.

For each of these areas, several solution approaches were newly generated and identified from literature. These approaches form multiple research directions, such as the work reported in e.g. [24, 25].

As shown in Figure 2.3, from the project context, only the architecture variables *item type*, *i/o format* and *carrier* were considered relevant. Relevant refers to whether or not different values from the value sets may require different solution approaches or influence performance of the investigated novel technology primer. Hence research in the context of the Falcon project should try to address these different combinations of architecture variable values. For example: localization of product items with flat- or rough-surfaces (type) within a batch of mixed or equal products (i/o format) inside a tote or without any carrier (carrier), while knowing that the set of products can vary over time. This will result in knowledge about the applicability of the novel technology primer for different architectures.

Technology variables Of course, also specific *technology variables* exist. These technology variables are independent of the application, but go along with the specific technology to be

[4] As said, the selection process is driven by the interest of the people and affiliations involved. This is discussed more extensively from Section 2.6.4 onwards.

[5] Diagnose: check if item is damaged or not.

researched. In the case of vision based imaging, lightning conditions are commonly known to be very influential on performance. Such technology dependent technology variables are to be explored and understood before even trying to reason about application specific variables. As said before, the technology must be understood before knowing how to reason about applying it (in a system architecture). Hence, technology specific variables are investigated first (fundamental research) and architecture variables are tested next (applied research). Fundamental research seeks to find out which values can be achieved for certain requirement parameters as a function of technology variables. Applied research investigates how different architecture variable values relate to achievable values for the requirement parameters.

Move items Another project partner (TU/e) got interested to contribute in technology development for novel ways to *move items*, i.e. transportation approaches. More flexibility in routing of item displacement (ITF) or in function execution locations (FTI) can be beneficial for maintaining high throughputs for varying product demands (e.g. due to seasonal changes).

Figure 2.4: Kiva Mobile Fulfillment material handling system from Kiva Systems (www.kivasystems.com).

As such, the identified technology-option is to find flexible conveyor belt replacements. An interesting approach can be to use mobile robots. This approach seems promising, as marked by an early commercial successes, illustrated in Figure 2.4. The mobile robots research area contains many sub-areas that address several technology needs. For example robot mechanics, motion control and autonomous navigation. The later research (sub-)area was chosen to be the focus of this project partner.

Within the area of autonomous control and navigation, many different solution approaches may be tried, improved and invented. For the Falcon project, the project partner selected the research direction of swarm control strategies, see e.g. [26].

The navigation task (i.e. calculating and following the correct route) is influenced by some of the identified architecture variables from the project context: *location* and *transportation*. For example, the degree of co-location of functions determines a.o. path lengths and route diversity. And, the selection of transportation (ITF or FTI) determines the required number and speed of movements. Hence, for the Falcon project, it is interesting to investigate how results from the chosen research direction are effected by these architecture variables.

2.4.3 Research direction: Dexterous grasping for Falcon project

Two primary functions are left untouched so far: *item singulation* and *order composing*. Again, the framework is followed to derive useful research directions to develop novel technology primers. Both functions will be treated simultaneously, as it turned out that both functions share equal preferred research areas and directions. This is illustrated in Figure 2.5.

The figure also shows that four architecture variables (item type, item carrier, status and transportation) may influence technology needs and performance. Therefore, selection of research directions is weighted based on interest and expected applicability of the technology primer for the value sets of these variables. Furthermore, applicability with respect to these variables need to be investigated during research and development of the novel technology primer.

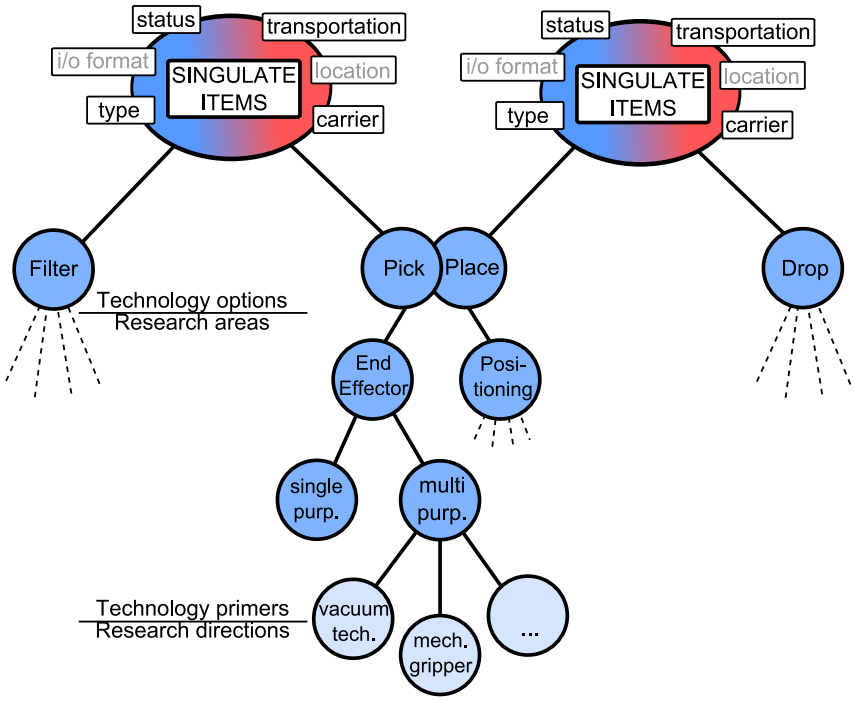

Figure 2.5: Bottom-up analysis and selection of research direction that may lead to useful novel technology primers for the primary functions: singulation and composing.

The i/o format is fixed by nature of the function. The location (co-located or separate) does not change the fundamental technology needs.

Singulation technology-options Independent of any architecture variable, only two basic technology options for singulating items can be identified: *filtering* or *picking*. The input format is a batch of products. Filtering involves multiple 'simple' sequential operations on all batched input items until one item remains to be separated, i.e. singulated. Whereas, picking refers to the direct selecting action on one item surrounded by multiple items.

Although filtering might consist of easier operations, it requires more operations and item specific operations. This makes it possibly time consuming and less scalable for large and changing sets of items. Hence, single picking is considered a favorable technology-option to singulate the items.

Compose technology-options Independent of any architecture variables, only two basic technology options for composing orders can be identified: either *dropping* or *placing*. The input format is singulated products, since composing has to be the last function. Dropping refers to approaches that let items inaccurately land together into a batch of mixed items. Whereas placing involves the direct and accurate action of putting one item onto a specific place in the batch of mixed items.

Although dropping items may be easier, it leads to lower fill-rates[6] in the carrier that holds the batch of mixed items that are ordered. This stems from the fact that, due to dropping, items will more or less randomly find their place in the carrier. The fill-rate is an important cost driver for transportation costs. Costs should be kept low, hence the fill-rate can not be deteriorated. Furthermore, dropping goods will increase undesired damages. Thus, single placing is chosen a favorable technology-option to compose orders.

[6]Fill-rate: ratio of actual volume of products and total carrier volume.

Clearly, if it turns out that the costs of single placing technology exceeds the cost increases due to reduced fill-rates, then this choice should be reassessed on economics. However, this is part of the systems architecting process, which was obstructed by a lack of such information, since the technology (and hence knowledge thereof) does not exist yet. Therefore, qualitative reasoning is used, influenced by the interest of the people and affiliations involved.

Research sub-areas It was established that for singulation, *picking* was identified to the critical area to be researched. For composing orders this became *placing* technologies. Picking and placing belong to the same research area and share the same research sub-areas: *end-effectors technology* and *positioning technology*, see Figure 2.5. In the area of positioning a wide variety of technologies is available, ranging from xyz-stages to full robotic arms.

For end-effectors, two main classes can be distinguished; end-effectors for either *single-* or *multi-purpose* tasks. In single-purpose tasks, always the same objects have to be picked and/or placed by the end-effector. For these tasks current technology suffices. Whereas, in multi-purpose tasks the end-effector has to deal with a wide variety of objects. This makes it a unstructured tasks, since not all objects are known at development time.

In the distribution center, the item types are irregular and vary continuously, which makes it impossible to use single-purpose end-effectors. Hence multi-purpose end-effectors are needed to implement singulation and composing.

Research direction Clearly, technology primers are needed for multi-purpose end-effectors. Several technology primer classes can be generated of which vacuum gripper technologies and mechanical gripper technologies are most obvious, see Figure 2.5.

Lately, two vacuum grippers were developed as technology primers for the singulation and composing tasks in logistic environments. In [27], an innovative vacuum gripper is proposed as multi-purpose gripper, see Figure 2.6(a). Versatility with respect to object shape and orientation is tackled by the shape adaptable vacuum gripper head. It has not been employed in a real distribution environment yet. Inspired by the Falcon project, also Vanderlande Industries BV developed a multipurpose vacuum gripper, see figure 2.6(b). Versatility is achieved by a patented flexible mount. Note that the demonstration setup, as shown in Figure 2.6 shows an actual sub-system built-up. The gripper is used for both singulation and composing function at the same location (co-located), i.e. both functions are implemented as one sub-system.

These trends confirm the interest and need for automating distribution centers and the necessity of multi-purpose end-effectors. However, as primer for end-effectors, vacuum technology has some limitations with respect to the architecture variables:

- *Transportation*: vacuum technology is not suitable to use in FTI architectures, which requires the (relatively) large vacuum source to move along with the gripper.

- *Item type*: The items can be roughly categorized into two main groups. Of all *ordered* items, 65% is found to be regular (box shaped, stackable), while still 35% is highly irregular (deformable, not box shaped, non-stackable). Furthermore, the items have limited dimension and weight (i.e. can be handled by a single human hand) and new items with different shapes are introduced continuously[7]. Vacuum suction-heads have difficulty with irregular objects, e.g. non flat surfaces, non planar surfaces and deformable objects (e.g. products in foil plastic or plastic bags).

[7]Summarized from order statistics of Falcon reference case, i.e. Argos Distribution Center, Great Brittain.

(a) Toroid Gripper; jointly developed by the workgroup material flow systems of the Fraunhofer-Institute (Dortmund) and the chair of materials handling and warehousing at the University of Dortmund.

(b) Vanderlande gripper; flexible vacuum gripper, Vanderlande Industries BV (source: http://www.youtube.com/watch?v=4hjmLYvy5DI). Product items are picked from product tote (red box), singulation, and placed into order tote (blue box), composing.

Figure 2.6: Multi-purpose end-effectors based on vacuum technologies.

- *Carrier*: Product items will have different orientations inside the carrier. Depending on the carrier, the vacuum gripper can only approach the object from a limited set of directions. Hence the suction-head can not always approach the object optimally, leading to misalignments in suction-head orientation and object surface orientation. This misalignment hinders gripping performance for vacuum technologies.

- *Status*: to properly pick the object, status information about the item is needed. For example, location, orientation and dimensions are needed to determine the suction head application point.

Also with respect to several requirement parameters, vacuum technology has some limitations:

- *Labor legislation*: vacuum technology brings along loud noise.

- *Task robustness*[8]: no adaptation mechanism if object slipping tends to occur (e.g. due to smooth surfaces).

Clearly, from a bottom-up technology point of view, current vacuum technology primers leave room to investigate other research directions.

As apposed to vacuum gripper technologies, mechanical robotic grippers with small electrical sources are suitable for both FTI and ITF transportation architectures. Also less noise production is expected and throughput is expected to improve due to faster motions allowed by firmer grips and robustness against variety in object orientation. Furthermore, these robotic technologies could be utilized to circumvent the uncertainties introduced by the highly unstructured character of the item types (irregular, varying over time) and the carrier constraints. As discussed in Section 1.1.2, unstructured tasks require versatile robotic solutions. These considerations led to have another TU Delft project partner investigate performance based design principles for underactuated grippers to contribute in developing technology primers for understanding and building underactuated versatile grippers, see e.g. [28].

Nevertheless, underactuated mechanisms compromise on dexterity, while the objects to be handled, are designed for human (dexterous) usage. Section 1.1.2 illustrated that the

[8]Task robustness: ability to to complete task successfully. In systems engineering quantified by 'yield', i.e. ratio of successful task trials over total task trials.

highest degree of versatility for unstructured tasks of future service robots is found in human-like hands. However, as discussed in Section 1.3.2, current technology and knowledge about dexterous robotic hands does not suffice yet. These insights triggered interest to investigation the research direction of human-like dexterous robotic hands, the topic of this work.

Conclusively, the goal of this work is to contribute in knowledge and technology development of novel technology primers for dexterous robotic hands in future service robots. As presented above, such service robots are expected to be used in logistics as well, like in the singulation and composing functions of distribution centers.

2.5 General Framework Usage - Project Approach

This section considers general application driven projects, separated from the Falcon case. Today, modern application driven projects have adopted a top-down systems engineering approach. It was shown that such a top-down approach relies on existing technology in order to reason about a suitable system architecture. A suitable architecture typically is optimized for the top-level requirement parameters (such as performance, cost (savings, earnings and investments) and usability). Reasoning is usually done in several iterations through modeling, simulation and (if time and money permits) testing with prototypes of several technologies.

2.5.1 Framework summary

However, when technology and knowledge thereof is non-existing, the top-down approach is obstructed in the phase where a architecture needs to be drawn from primitive functions. Therefore, no architecture is decided, hence no sub-systems and no specifications are formulated. Instead, research is needed to develop technology and knowledge. Which technologies are needed is not clear from the non-existing architecture. Nevertheless, research directions can be chosen by following the presented top-down-bottom-up framework (Section 2.3 and Figure 2.1).

Based on the top-level desired functional behavior, the identified primitive functions must be accompanied with requirement parameters, architecture variables and value sets. Without any architecture (no sub-systems, no values for requirement parameters) defined , possible technology options and various technology primers are to be generated for each of the primitive functions for which no technology exists yet. From these technology primers, research directions are chosen. Selections are based upon expected achievable values for the requirement parameters for different values of the architecture variables and guided by research interest of people and affiliations involved.

2.5.2 Framework implications

One important inevitable implication is extracted from the top-down-bottom-up approach: an application driven project, which aims at improving or inventing applications which require novel technologies, must and will shift from being application centered towards technology centered. This implication drives two insights.

Firstly, one can recognize that technology and knowledge development go first and the application follows. Within application driven projects, several distinct *activity types* can be recognized. They are connected to certain *technology abstraction levels* and each of the activities produce different *activity outputs*. The activities are listed below and illustrated in Figure 2.7:

- *Research* Research directions are selected from research areas for each of the critical primary functions under investigation. Research into these selected directions must aim at inventing technology primers accompanied with the creation of knowledge thereof.
  - *Fundamental research: explores technology variables leading to fundamental knowledge.* For each technology primer, specific technology variables exist. These variables are independent of the application. They are to be explored and understood before even trying to reason about application specific variables or applying the technology in a system architecture. Fundamental research seeks to find out which values can be achieved for certain requirement parameters as a function of technology variables.
  - *Applied research: explores architecture variables leading to application specific knowledge.* After having understood the novel technology primer, research can be directed towards a specific application. Applied research investigates how different values of the application specific architecture variables relate to achievable values for the requirement parameters. Applicability of the technology follows from a comparison between the achievable and needed requirement parameter values. Applicability is not guaranteed a priori.
- *Integrating* In a later stage, applications can be built by applying and integrating either newly developed or already pre-existent, knowledge and technology from applied research.
  - *Systems Engineering: utilize application specific knowledge to construct system architecture.* Application development consists of integrating several technology primers into (sub-)systems. The (sub-)systems are defined in an architecture, which is optimized based on application specific knowledge.
  - *Engineering: utilize technology to built (sub-)systems.* Implement (sub-)systems by applying and integrating technology knowledge according to specifications from the architecture.

Secondly, the bottom-up research direction selection procedure is mainly guided by the research interest of the people involved. Hence, one should recognize that such a project shifts from being application centered towards technology and hence people centered.

Figure 2.7 summarizes the above implied relation between activities, people, technology abstraction level and activity outputs.

2.6 General Framework Usage - Project plan

This section considers a general application driven projects, separated from the Falcon case. The author believes that the previously mentioned implications are important to realize for all of the project partners involved in a project.

Project plan for application driven research project In general, a project is guided by a project plan, mutually agreed upon by all project partners. Such plan contains *organizational* content and *administrative* content. The organizational part contains *project objectives*, a *project strategy* and *people* involved (see later in Section 2.6.3). The strategy explains which activities should be executed in which order. This is linked to who is responsible for these activities and deliverables, i.e. people. Whereas, the goal motivates why these activities are projected and to what they must lead.

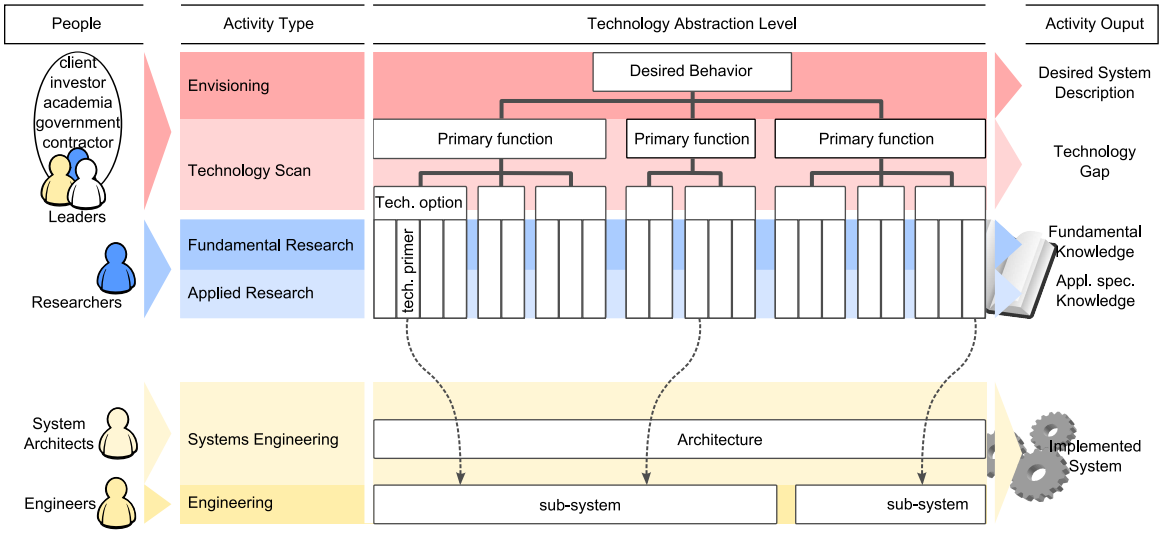

Figure 2.7: Technology-Activities-People-Output diagram for application driven research project. A group of people (e.g. client, government, investors, academics, contractors) develop a desired system description based on envisioning future needs and applications. Typically, a technology scan identifies technology gaps. Thus, current technology does not suffice to implement the system straight away. Research is needed to develop technology, which makes the project an application driven *research* project. Research activities are executed by researchers, who deliver knowledge on (novel) technology primers. System architects run systems engineering activities that utilize knowledge on technology primers to produce an architecture for the system to be implemented. The architecture contains definitions of sub-systems, based on available technology (knowledge). Sub-systems are implemented by engineers, who deliver an implemented system.

The administrative part contains activity scheduling (timing), financial budgeting, etcetera. These aspects are addressed after having established the organizational content in order to facilitate the organizational content to assure that the project achieves objectives. The administrative content of a project plan is not discussed here.

Project expectations As such, the project plan manages expectations of all project partners as to what to expect from each other and from the project as a whole. If realistic and mutually agreed upon, the plan creates shared responsibilities and awareness of the greater end-goal of each of the individual activities.

Due to new insights, the plan can change over time, either refining (adding detail) or adapting objectives and strategies. These changes should be communicated explicitly in order to keep all partners involved, aware and responsible for the end-goals.

The formulation of a project plan for an application driven research project, is a process for which insights gained from the top-down-bottom-up framework can be used. This process is described trough the following three steps. Hereafter, the author addresses how these insights can be reflected in the project plan.

2.6.1 Step 0: Desired system definition

For the type of projects under discussion, the high level end-goal is to work towards the realization of some system or application. Hence, the process of setting up a project plan, starts with the formulation of a *desired system*. This formulation prescribes the functional description of a desired future system or application (i.e. desired behavior), together with some requirements (requirement parameters with or without values), special wishes, requests,

constraints or other circumstances to take into account.

The level of detail should be supporting to the next step (step 1), i.e. the technology scan, not necessarily ready for system architecture design. Supporting implies that crucial and typical requirements/constraints are needed to identify whether technology suffices or not.

Example - Falcon
Desired System: Fully automated distribution center.
Constraints: no human labor, cost effective, increased performance w.r.t. current distribution centers, inputs and outputs remain unchanged.

2.6.2 Step 1: Technology scan

For the desired system, apply the application driven top-down analysis up until a first identification of primary functions[9], architecture variables and according value sets. Furthermore, perform a technology-scan to identify existing technology for the primary functions. Note that only those technology primers should be considered that are expected to be suitable to achieve the values of the requirement parameters and to handle one or more values for each of the architecture variables. See also Section 2.4.

2.6.3 Step 2: Formulate project plan

From the technology scan, two cases can arise:

1. Full technology coverage: all primary functions are covered with one or more existing technology primers. Not necessarily all values from the architecture value sets are covered, but at least one or more architectures are possible.

2. Technology gaps exist: one or more primary functions have no technology primers.

The presented framework addresses projects that have to (or want to) deal with technology gaps while aiming for applications, i.e. application driven *research* projects. Research is needed, because current technology does not suffice to implement the system straight away. Typically, a technology scan identifies technology gaps, i.e. the second case.

Clearly, the first case, full technology coverage, is not part of this discussion, since such a case can follow known top-down systems engineering approaches. In that case, it is important to realize that system architects and engineers must be involved. As shown in Figure 2.7, according to the goals of research people, their output must result in knowledge. Hence, researchers should not be involved in top-down systems engineering projects. Exceptions arise, when the project wishes to 'ignore' existing technology and wants to strive for developing novel technology primers for all or some of the primary functions. In that case, the proposed framework should be followed.

Having established that technology development, i.e. research, is needed to reach the envisioned system, it is time to set up the project plan. Focus must be directed to the organizational content. Both for the project as a whole and for each of the technology gaps (i.e. primary functions that lack technology primers), choices and agreements must be made on the three organizational project elements. For each of these elements, a limited set of basic choices is available. These choices follow from the Technology-Activities-People-Output diagram (Figure 2.7):

[9] During the project this may be refined if desired by project partner. Possibly new primary functions may come up.

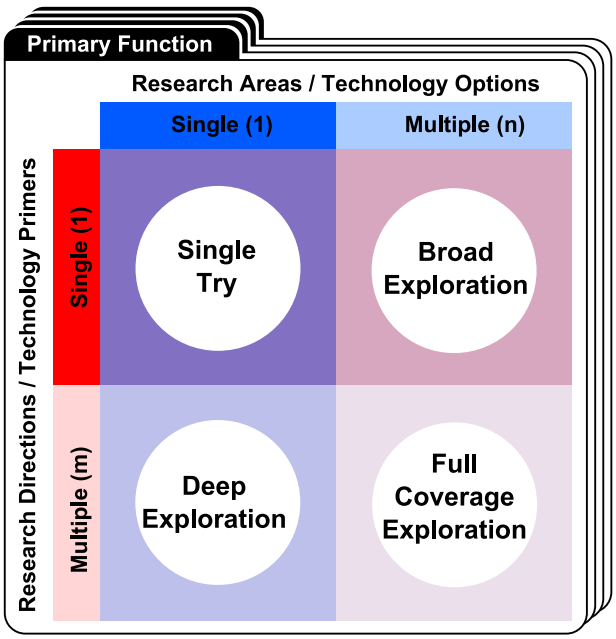

Figure 2.8: Extensiveness strategy. For each primary function, one can decide how much effort to put in. For a primary function one or more research areas can be investigated (in case of research) or one or more technology options can be tried (in case of systems engineering) and for each of those areas/options, one or more research directions/technology primers can be explored/tried. Four types of extensiveness can be distinguished per primary function: *limited exploration*, *broad exploration*, *deep exploration* and *full coverage exploration*.

- *Project objectives:* What does the project want to achieve (*output*)?
    1. Technology development. Target is to develop technology primers and knowledge thereof:
        (a) Fundamental knowledge: delivers novel technology primer and knowledge about implications of variation of technology variables.
        (b) Application specific knowledge: takes technology primer and delivers knowledge about implications of variation of architecture variables.
    2. System development. Target is to work towards a system by integrating technology primers:
        (a) System architecture: delivers optimal architecture (sub-systems and requirements) for desired system, by utilizing technology primers and application specific knowledge thereof. Note: technology primers must exist, when this activity starts.
        (b) Implemented system: delivers a realization of the envisioned desired system by implementing the system architecture.
- *Project strategy:* How will the project do this? Which *activities* with which level of extensiveness and in which order?
    1. Activities:
        (a) Set up research activities:
            i. Fundamental research;
            ii. Applied research;

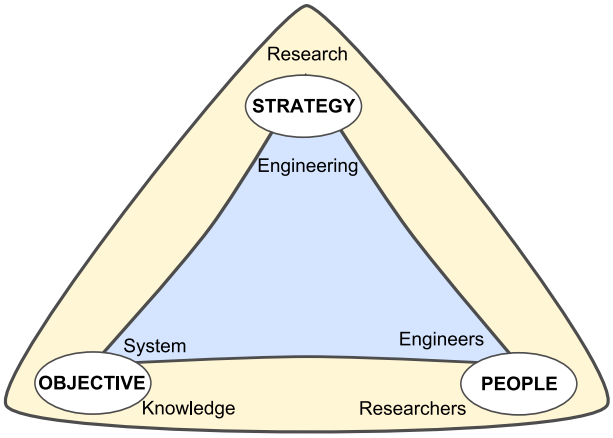

Figure 2.9: Objective-Strategy-People-Balance. The project plan must contain matching objectives, strategies and people involved.

   (b) Set up engineering activities:
      i. Systems engineering;
      ii. Engineering;

2. Timing:
   (a) Serial: (groups of) activities are executed after each other in sequence;
   (b) Parallel: (groups of) activities are executed at the same time;
3. Extensiveness: As shown in Figure 2.8, four types of extensiveness can be distinguished per primary function: *limited exploration*, *broad exploration*, *deep exploration* and *full coverage exploration*. Of course, the strategy can incorporate either *homogeneous* extensiveness (i.e. one equal level for all activities), or *differentiated* extensiveness (i.e. different levels for different activities).

- *People:* Who will do this? People have different roles:

1. Leaders: decide what to do;
2. Managers: make sure that what is decided to do, is done;
3. Researchers; perform research;
4. System Architects: make architectures;
5. Engineers: implement architectures.

How a role is fulfilled depends on internal (personal character, interest, goal, ...) and external factors (affiliation type (e.g. commercial principal, government, academics, contractors), targets from superior, ...).

The project plan choices can **not** be made independently for each of the elements. The objective-strategy-people-balance must be respected, see Figure 2.9. This triangle balances the three corner stones of the project plan. Notice that the Technology-Activities-People-Output diagram (Figure 2.7) summarizes all options, while the Objective-Strategy-People-Balance (Figure 2.9) actually illustrates how these options must be combined together in a project plan.

For example, if the aim is to produce knowledge (objective), then the strategy should be to set up research activities (either parallel or serial) by involving people that must (and want to) fulfill a researcher's role.

Example: Roles in Objective-Strategy-People blance
From a leader (project role), the expected output is a decision on what to do (project objective and project strategy). A leader, who is affiliated to the investor, would decide to realize the desired behavior as a system as cheap as possible while reducing failure risks (commercial driver). Instead, a leader affiliated to a research institute would decide to spend as much money as available on searching for new technologies for the desired behavior.

The first plan requires engineers (roles), the second plan requires researchers (roles), see Figure 2.7. People from a contractor company (target: aims for commercial earnings by implementing customer demands, reward mechanism: reward working system, reward cost savings), will aim at using proven technology to save time, money and reduce failure risks. People from a research institute (target: aims for new knowledge, reward mechanism: reward publications (journal papers, books, Ph.D. thesis)), will aim at trying new technologies and methods to produce published knowledge.

Clearly, the employee affiliation rewards have stronger influences on people behavior (it gives the people their most important/primary rewards: degrees, salary) than the project rewards (e.g. recognition from happy client). Hence, letting people from research institutes fulfill the engineering roles for the first plan, will result in publications on novel ideas, without a full working system in time. The same reasoning applies for letting people from contractor company fulfill the researcher role for the second plan: the contractor does not earn money from knowledge generation, hence the people do not get rewarded for publications.

Example 2.10: Example to illustrate (un)balancing the Objective-Strategy-People triangle.

After having agreed on the organizational content, through the above described procedure and considerations, the administrative content of the project plan can be added. The administrative content should follow directly from the organizational content. This is not further detailed here.

2.6.4 Project plan - People

The project plan determines the roles of people involved.

People Roles Different roles aim at different outputs (see Step 2, Section 2.6.3). Nevertheless, the way somebody fulfills his role depends on internal (personal character and interest/goals) and external factors (goals of employer affiliation type (e.g. client, investor, government)). People will fulfill their roles to earn the highest reward. Rewards can vary from e.g. job satisfaction (internal) and salary (external) to career opportunities, degrees and social recognition.

Rewards can come from the project, personal interest and from the affiliation. Goals of the affiliations (acting as employer) impose desired behavior from their people. Thus, their people are rewarded (e.g. financially, career opportunities, etc) accordingly. Therefore, often, if not always, the goals of the affiliation and of the people affiliated are aligned. This makes employer affiliation rewards have direct and stronger influence on people, while a project can only have indirect influence.

Conclusively, different project roles aim at different outputs, while the affiliations of the people who fulfill these roles have great influence on the content and format of this output.

Therefore, balancing the Objective-Strategy-People triangle (see Figure 2.9) implies understanding and acknowledging behavioral drivers (rewards) of the people involved in the project

	affiliation	commercial principal	government	academia	commercial contractor
project role	target	make profit on needed system	stimulate knowledge diffusion to companies and appl. targeted research	publish new technology and knowledge	make profit on implementing client demand
leader	make plan	desired system description	integrated applied novel technologies	bottom-up plan / try novelties	top-down plan / use proven tech.
manager	execute plan	reduced risk, cost & time	team binding	individual excellence	perfect plan execution
researcher	search and investigate	patents		papers, books, Ph.D. thesis, ...	patents
system architect	make architecture	architecture			architecture
engineer	implement architecture	working system			working system

Table 2.2: Example of **preferred outputs, attitudes and focus points** for different roles fulfilled by different affiliations. Preferred outputs and focus points are given for each role execution option as result of combination of role targets, affiliations and affiliation targets; the combination leads to different results for roles fulfilled by people from different affiliations

in order to align the content and format of the desired project outputs with the affiliation goals and their rewards (and vice versa). In this way, the reward mechanism of the employer will be directed in line with the project goals, such that roles are fulfilled for the benefit of the project.

Text box 2.10 gives a descriptive example of the relation between project roles and affiliations. It concludes with showing some possible unbalances. Such unbalances should simply be avoided by, once again, recognizing the importance of the Objective-Strategy-People-Balance (see Figure 2.9) when formulating objectives, strategies and choosing people, i.e. setting up the project plan.

Table 2.2 gives an example on **preferred outputs, attitudes and focus points** for each of the roles as result of combination of role targets, affiliations and affiliation targets; the combination leads to different preferences in results and attitudes for roles fulfilled by people from different affiliations.

People skills Skills of involved people are of course of major importance. Without going into details, it may be clear that skills can be classified into role competence and content knowledgeability. The first refers to whether a person suits his roles with respect to his competences. The later connects to the know-how and past experiences needed to contribute on the necessary content. These skills can be either attributed to the involved affiliation as a whole and to individual persons. At least the involved affiliation as a whole should encompass the skills needed for their appointed role. It can then be considered to assume that individuals

from the affiliation will benefit from the affiliation skills. Otherwise, individual people have to be assessed on skills as well.

People Involved versus Involved People For optimal project results, naturally, the people involved should be (and stay) involved people during the project. The author believes that an important prerequisite is the construction of a project plan that acknowledges the Objective-Strategy-People-Balance (see Figure 2.9).

During planning, the project plan is created (Step 0 to 2, Section 2.6.1 - 2.6.3) by people who accept leader roles within the context of the project. Thus, the actual first step for setting up the project is to choose one or more people that will fulfill leader roles. As indicated in Table 2.2, depending on their affiliation, these people will have preferences for certain objectives and strategies.

The project plan is shaped by negotiating these preferences and finally settling for an agreement, which should always acknowledge the Objective-Strategy-People-Balance. Since this process is crucial for the future project and influenced by people and affiliations, one should carefully select people and affiliations involved. To select people that will fulfill leader roles, the following two choices should be considered:

1. *People or Plan first:*
   (a) First a plan: first a plan is formulated and people are selected to fit the plan by matching roles, people and goals of affiliations;
      - Project creativity and ambitions depend on initiator;
   (b) First the people: first people are selected for leader roles, together they make up the project plan.
      - Outcomes of the jointly performed technology scan (Step 1, Section 2.6.2) are influenced by the affiliation goals and the interests of the people involved.
      - Initiator must perform a technology pre-scan (Step 1, Section 2.6.2), otherwise it is not clear who (which affiliation types, which discipline) to select at all;
      - Involved affiliations that first send leaders, later want to send people that fulfill one or more manager, researcher, system architect or engineer roles;
      - Be prepared to negotiate and to make compromises, but also to take leave of affiliations that do not fit within the settled objectives and strategy.
2. *Single or Mixed affiliation leader groups:*
   (a) *Single affiliation leader group:* leader roles fulfilled by people from same affiliation.
      - Project will have narrow scope;
   (b) *Mixed affiliation leader group:* leader roles fulfilled by people from different affiliations.
      - Project will have broad scope;

2.6.5 Project plan - Case examples

Naturally, for the same desired behavior (see Figure 2.7) different project plans can be formulated. Some case examples are given in this section to illustrate the concepts and framework discussed previously. The examples do not give strict guidelines, but merely show how the Objective-Strategy-People-Balance (see Figure 2.9) induces a variety of project-plans as function of choices on people, objectives and strategy.

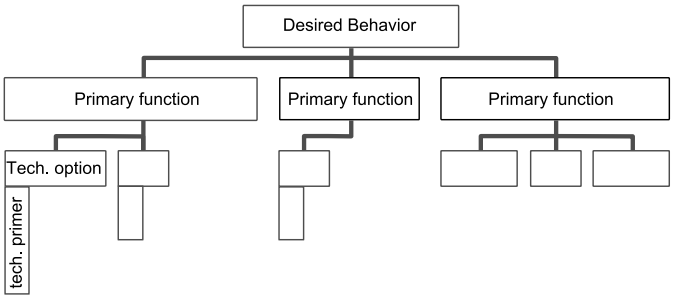

Figure 2.11: Case background: Output of technology pre-scan.

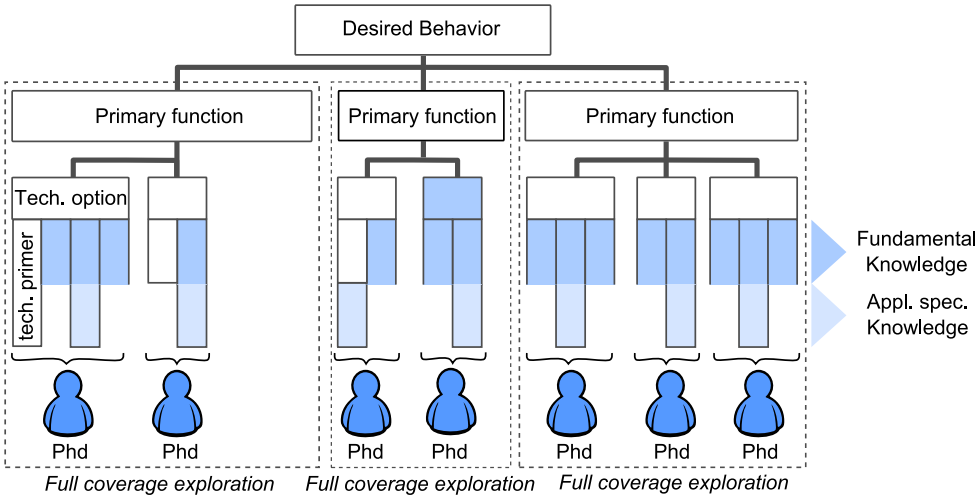

Figure 2.12: Case-1 Project-Plan: Fundamental and Applied research project. Colors indicate activities. Note that 'Phd' refers to Ph.D. student.

Case background
A commercial principal has stated some desired system behavior (Step 0, Section 2.6.1) for which a project is to be designed. The commercial principal can be seen as initiator. A technology pre-scan is executed, which revealed three primary functions for which a limited set of technology primers was found that leave some technology-gaps. This situation is sketched in Figure 2.11. Possibly some technology options and/or primers are missed, since the initiator may not be aware of some possibilities. During this pre-scan, the initiator may have consulted various people (internally and externally). It is clear that these people are not involved (i.e. have no project role) in the project (yet).

After his technology pre-scan, the initiator realizes that a system architecture can not be formed and some research activities are needed to work towards his desired system.

At this point the initiator has to make a choice on people-involvement (first a plan or first people, single or mixed affiliation leader group). For two of the four combinations, cases will describe different circumstances and decisions which lead to two examples of possible project plans[10].

Case-1: Pre-involvement of single affiliation leader group
The initiator has realized that the technology gap obstructs early implementations of his desired

[10]Note that the choice on people-involvement does not necessarily lead to four different project plans. The cases are meant to show how different choices lead to different plans, due to the necessity to comply with the Objective-Strategy-People-Balance. The balance implies that not all choices can be made independently.

system. Hence, he decides to form a group of leaders affiliated with research institutes. He selects people that work in research areas that match his identified technology options.

This group of leaders performed another technology-scan. Some of these people appear to have a wide interest area, which made them generate extra technology options. Altogether, the scan led to generate at least one technology primer for each of the technology options.

The leaders decided that the *project objective* is to develop novel technology for each of the primary functions (including the ones that have already some primers) up to the level of application specific knowledge. To do so, a matching *strategy* was formulated: set up fundamental research activities (*activity*) that perform a serial (*timing*) full coverage exploration (*extensiveness*). So, for each of the technology options, as many technology primers as possible should be investigated. The identified technology primers are used as initial research directions. Other directions may pop up. Per technology option, these investigations will be done in series. And per technology option (research area), the most promising novel technology primer will be selected for applied research, in order to deliver application specific knowledge for multiple technology options of each of the primary functions.

Now *people* have to be selected. Since research activities are planned, research people are needed. For each of the series exploration of each technology option, one researcher is appointed. Each of the researchers is made responsible to deliver fundamental knowledge for all identified technology primers in his research area and applied knowledge for (at least) one promising technology primer. To fulfill the *researchers roles*, the leaders have decided to select Ph.D. students, who want to study fundamental issues and produce knowledge by publishing papers and a Ph.D. thesis.

The complete project plan is illustrated in Figure 2.12. The choice on timing (serial per tech. option) implies the need for seven persons. Each researchers will contribute by creating new knowledge in his appointed research area and deliver for one proposing technology primer application specific knowledge. Each of these researchers may be managed/supervised by a senior researcher in the same research area. This manager will mainly focus on individual excellence of the Ph.D. student and help him to produce knowledge, which is also the goal of his affiliation. Furthermore, the supervisor and the Ph.D. student should both agree to study and publish fundamental and applied matters.

The personal goals, the goals of the affiliation and the agreed upon project goals are aligned by choosing the right strategy and the right people. The commercial principal realizes that at the end of the project, there will be now system implementation. However, he may expect a novel set of technology primers accompanied with application specific knowledge. Hence, after this project, architecting activities can start.

Case-2: After-involvement of mixed affiliation leader group

The initiator has realized that the technology gap obstructs early implementations of his desired system. However, he sees some available technology primers, some of them accompanied with application specific knowledge, other only with fundamental knowledge. The initiator believes that the identified technology options have enough potential. Hence the result of the technology pre-scan is accepted as output of Step 2 (Section 2.6.3).

Now, the initiator starts to set up a project plan by balancing objectives, goals and people. His plan is shown in Figure 2.13. He has decided that the *project objective* is to develop a system that implements his desired behavior. Since, he realizes that some technology-gaps need to be filled, his *project strategy* becomes threefold:

1. Set up parallel fundamental research activities for one technology option for the primary function that has no technology primers yet. Within one technology option, multiple

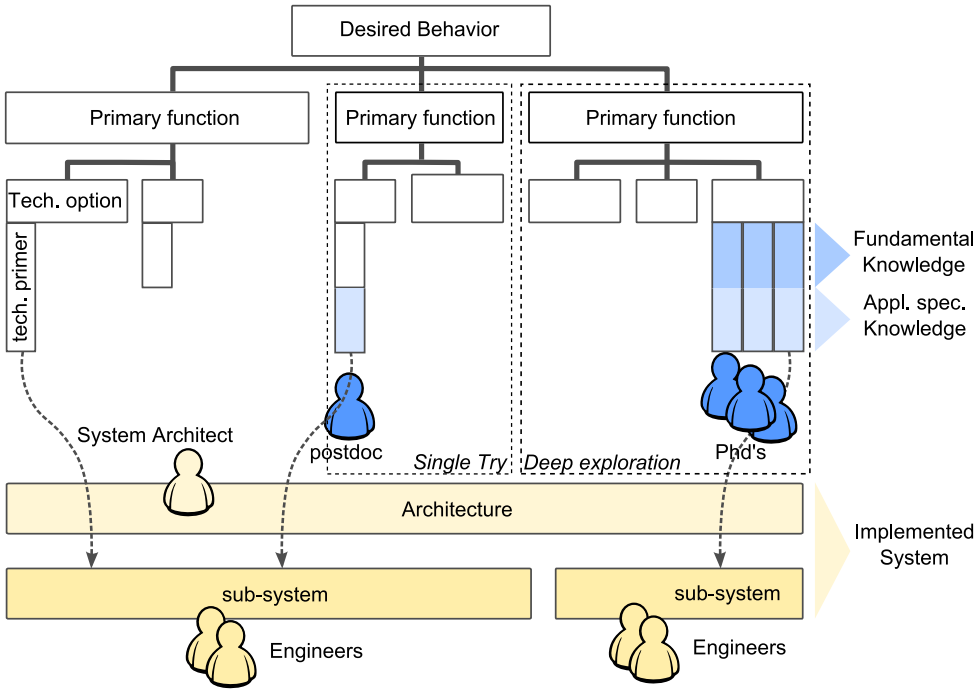

Figure 2.13: Case-2 Project-Plan: System development project with multiple research activities. Research is done by people from research affiliations, system integration is done by engineers at contractor companies. Note that 'Phd' refers to Ph.D. student.

research directions are explored (i.e. deep exploration) in parallel to try to increase chances of successful technology primer discovery. These activities are performed in parallel to do a deep exploration. The objective of these parallel deep explorations is to generate at least one technology primer;

2. Set up parallel applied research activities for the newly discovered technology primer and for the technology primer that only has some fundamental knowledge. The objective of these activities is to create application specific knowledge for one technology primer per primary function.

3. Set up engineering activities and systems engineering activities. The objective is to utilize the application specific knowledge of the technology primers to design a system architecture based on these primers and to implement this system.

The objectives and strategies are balanced. Now *people* have to be selected. Different roles are needed: fundamental researchers, applied researchers, system architects and engineers.

For the researcher roles, the initiator decides to ask people from universities (research affiliation). He understands the reward mechanism and decides to use Ph.D. students that want to create and publish fundamental knowledge for the parallel fundamental research activities. For the applied researcher roles, he opens postdoc[11]positions. He hopes to find postdoc researchers that want to bring their fundamental knowledge to application specific knowledge. Besides, these postdoc researchers are already more experienced, which will help to quickly get results.

For the systems engineering activities, i.e. integrating technology primers, the initiator opens a bid for contractor companies that employ system architects and engineers. However, these contractors can only start after the application specific knowledge has come available. Also,

these contractors should be willing to use the methods and technology that will be produced in the project.

Now, the initiator can start to search for actual people and affiliations that want to work in his project and follow his objectives and strategy. Likely, he will find these people, since he created a balanced project-plan. However, he did include some dependencies. If, research results are delayed, then he has to delay the start of the systems engineering activities. These dependencies will not obstruct his research activities. Also, the contractor company can understand this, since they can not start anyway without sufficient technology.

2.7 Falcon Project Approach Reflections

This section reflects on parts of the Falcon project plan and execution thereof. Section 2.7.1 summarizes the project plan using Section 2.5 and 2.6. Section 2.7.2 compares this plan and execution thereof with the presented application driven research project framework and insights in order to understand project dynamics and project outcomes.

2.7.1 Partial Falcon project plan summary

This Falcon project plan summary is distilled from public information on the ESI website (http://www.esi.nl) and put in the framework format (objectives, strategy, people).

Objectives *'The Falcon project will address the development of techniques and tools for the design of and implementation of professional systems. In particular it will focus on the optimization and decomposition of global requirements concerning system performance, reliability, and cost using a model-driven approach. Starting with high-level system models, system models will be created for different design abstraction levels to analyze and guide the (de-)composition and propagation of design requirements over system components.*

The project shall provide industrial critical evidence. Concepts shall be proven by demonstrators of components (related to item picking), and of optimal system design (integrated control and handling). At the end of the project the final demonstrator is expected to be a partial prototype of the "Distribution Centre of the future" proving the integral concept on an industrial relevant scale.'

[11] postdoc:a researcher who is involved in academic study beyond the level of a doctoral degree (http://wordnet.princeton.edu/).

Strategy - activities *'The research activities will be guided by three lines of attention.*

1. *Systems engineering, covering*
   - *architectural concepts for a Distribution Centre,*
   - *model based analyses and optimization of this type of systems (using the Effective Process Time principle, target cascading and optimal control theory),*
   - *model based engineering to generate proper control software.*
2. *System Operational Performance, covering*
   - *the actual control implementation to obtain the as designed system performance,*
   - *methods and algorithms to handle errors and exceptions and maintain system performance as best as possible,*
   - *the ability of the system in operation to handle new incoming items,*
   - *the use of vision and pattern recognition for the stacking of items,*
   - *the building and testing of demonstrators to prove industrial scale feasibility.*
3. *Critical component design (related to item handling and picking), covering*
   - *analysis of goods handling,*
   - *the design of a manipulator arm and grippers and real-time vision aspects involved,*
   - *the design of gropers (simple and robust grasping mechanisms).'*

Strategy - timing *'Given the specific application domain of the project the research will have strong multi-disciplinary aspects, requiring expertise in different technical and scientific domains, including algorithmics, embedded software, electronic hardware, mechatronics, etc. To be successful it will need to establish meaningful combinations of the analytic, modeling, and implementation techniques of the various disciplines.'*

In other words, it was planned to combine all developed knowledge and insights of the activities into demonstrators through a series of iterations. Also, these combined activities were to lead to exchanging knowledge to relate all activities to each other in a coherent way and to let different activities depend on each other, which must lead to one integral concept.

Hence a clear notion of teamwork and shared objectives was aimed to be created within the project.

Strategy - extensiveness On extensiveness, no explicit strategy was formulated.

People Several roles are defined in the Falcon project plan. Table 2.3 gives an overview of the planned personnel occupation (in fte) per affiliation type and per role.

2.7.2 Falcon project reflections

As discussed in Section 1.3.1, two major observations were done during the Falcon project execution: *coherence and teamwork* through knowledge exchange for integrated demonstrations between different project partners can be improved and executed activities have *smaller ties with the central application* and project objectives than might have been aimed for according to the project plan. Possible causes for these observations are found by comparing the Falcon project plan with the presented application driven research project framework.

Role	Affiliation Type	% fte	% fte total
Researchers			68 %
	University	80 %	
	ESI	20 %	
Project member			8 %
	University	6 %	
	Commercial Principal	94 %	
Coach / Professor			11 %
	University	91 %	
	Commercial Principal	9 %	
Manager			4 %
	ESI	75 %	
	Commercial Principal	25 %	
Engineer			9 %
	University	57 %	
	Commercial Contractor	43 %	

Table 2.3: Falcon project plan: people roles and affiliation types (total: 20.25 fte). Commercial principal is Vanderlande Industries B.V., Commercial Contractor is a mechatronic engineering company.

Top-down-bottom-up aspects The wide variety of planned research activities shows that several different technology options were identified as interesting research areas. The Falcon project plan leaves the choice of research directions to be filled in by the researchers during project execution. These research areas are not presented as part of a system architecture nor as part of primary functions. Instead, they are presented as part of a systems engineering process in which all results are proposed to be linked through iterations of top-down system decomposition analysis and system architecting activities. As such, project partners are expected to choose research directions, within their given areas, based on results of the system engineering analysis and sub-system definitions.

Looking back at the start of the Falcon project, researchers were asked to participate in system engineering activities and warehouse system architecting to find an optimal architecture. The joint analysis stranded due to absence of suitable technology, as explained in Section 2.2. What followed was an implicit process of individually selecting research directions for the given research areas. Implicit refers to the fact that researchers at some point, if an architecture is not formulated, make interest driven choices without central guidance or team interaction. Such individual selection process can be expected from individual goals and the affiliation type (academic) of the researchers involved, as discussed in Table 2.2.

Lessons learned:

> The strategy to jointly define a system architecture as central point from which research directions must be derived, while at the same time already having appointed researchers with research areas, leads to uncoordinated definition of research directions when architecting activities remain without results. System architecting results are obstructed in case of absence of technology, as is the case.
>
> Therefore, as suggested by the top-down-bottom-up framework, it is proposed to apply a different strategy to coordinate multidisciplinary teamwork. The activity of defining an architecture should not be put central. Instead, an explicitly communicated joint effort to identify primary functions should be chosen. From these primary functions, together, project partners can discuss on technology gaps and jointly define research directions to close technology gaps. In this way, mutual understanding arises and teamwork is needed to reach the shared goal of closing technology gaps together for the envisioned desired end-system behavior.

Section 2.4 presented some analysis. It shows how the analysis method is used to relate different research activities to the project. It may also serve as examples on how this analysis could have been jointly executed to create mutual goals and the selection of interdependent research areas (rather than individual areas).

Objective-Strategy-People balancing aspects The Objective-Strategy-People triangle of the Falcon project plan shows an unbalance. The objectives primarily point at formulating an optimal system architecture to derive sub-systems to be integrated and demonstrated by investigating off-the-shelf-techniques. A full integral concept of all developed tools and technology is aimed for. As discussed above, the strategy strives to follow the objectives by defining systems architecting activities as central starting point and integrating end-goal to start up research activities. A vast majority of researcher roles from academia were planed as apposed to negligible engineering roles, see Table 2.3.

Of course, the unbalance can be resolved by changing any of the three aspects. With respect to strategy; the central system engineering activities serve the objectives, but do not match the planned research activities (discussed above). With respect to people; The involved researchers match with the fact that research is required for the objectives, since technology gaps exist. However, the project objectives do not coincide with the academic reward mechanism. The external rewards for researchers come solely from their affiliation. For researchers, no reward mechanism exists in the Falcon project. The delivery of an integrated working system based on off-the shelve techniques (as proposed in project plan) would reward engineers from the commercial principal. However, such achievement does not contribute in new knowledge for publications. Hence, rewards for researchers remain void.

Lessons learned:

People involved in the project will naturally 'resolve' the Objective-Strategy-People unbalance by choosing for the strongest reward mechanism. This must and will happen such that personal objectives and strategies are matched to their roles and affiliation types. However, objectives and strategies of these personal balances will not coincide with the project objectives. Letting this happen implicitly leads to deterioration of multidisciplinary teamwork and mutually shared interdependent goals. Therefore, the strong benefits of the partial sum is lost.

For the Falcon project it implies: either altering objectives towards the objective of creating knowledge (see case-1, Section 2.6.5) or towards a systems engineering project with the people selected for it, see e.g. case-2 (Section 2.6.5). The project plan did not make an explicit statement on extensiveness strategy. Explicit discussions on this topic during project planning may help to focus strategy closer to objectives and people involved (as shown in Section 2.6.5).

2.8 Conclusions

Governments face the challenge of stimulating fast and interactive knowledge diffusion from academia to industry. Currently, many subsidies demand for application oriented projects with strong focus on early commercially applicable results. In technology disciplines, this led research projects to shift towards industrial standard systems engineering approaches. It gives a clear focus on the application, it gives a common language between project partners involved and seems to reduce project failure risks by decomposing the desired application into sub-systems with accompanied requirements. However, this approach is obstructed when technology options are lacking.

Section 2.8.1 summarizes the main ingredients of the framework introduced in this chapter to deal with challenges in application driven research projects. Section 2.8.2 uses the framework insights to give an alternative view on project interactions between industry and academia for these projects.

2.8.1 Framework conclusions

It was argued that if a top-down system decomposition can be done and requirements are set, then apparently all technology is available and engineers can finish the job in an engineering project with calculated risks and rewards for timely delivery of working systems. If the formulation of an architecture is obstructed by technology gaps, then research is needed, which raises the need for application driven research projects.

The importance of balancing objectives, strategy and people in an application driven research project was shown. Most importantly, due to opposing rewarding mechanisms, clear differences exist between researchers roles in academia an systems engineering roles in industry. Academic researcher roles target to produce new knowledge and novel technologies, driven by interest and not guaranteeing timely applicable results. Rewards are generated through publication of knowledge and e.g. a Ph.D. degree. As such, a academic researcher does not need a clear application focus. On the other hand, systems engineering roles will strive to derive the optimal architecture for the targeted application including sub-systems and requirements decomposition based on proven technology and given constraints.

Projects that strive to combine both may be obstructed by the intrinsic differences in approaches, roles and goals attached to different affiliation types. This chapter has proposed the top-down-bottom-up analysis framework that acknowledges these aspects to circumvent the obstructed formulation of a systems architecture. In this way, room is given to fill technology gaps through deploying researcher roles, while focus is generated for industry applications. The proposed framework and project model may serve as guidance to communicate and discuss project strategies and project roles for application driven research projects. In this way, it supports to establish multidisciplinary teamwork with shared project objectives.

Fundamental research will generate novel technologies and knowledge thereof by investigating the intrinsic technology variables (fundamental research). Next to fundamental research, the framework identifies applied research that aims to investigate and create knowledge for application specific architecture variables of certain technologies. Note that, to do so, no systems architecture nor requirements are needed, only the identification of architecture variables is needed. In this way, focus on applications can stimulate research areas in a healthy way. When knowledge and technology becomes available, then this technology can be utilized to finalize the application specific system architecture. Applying proven technology is a typical industrial commercial activity, executed as systems engineering role. It is not of interest (due to rewarding mechanism) for the researcher to put effort in this application phase.

2.8.2 Recommendations for application driven research projects

Setting up successful application driven research projects mainly depend on acknowledging different objectives of people connected to different affiliations. The reward mechanism for academic researchers is not suitable to let researchers change their research into engineering integration activities for generating application specific evidence. Whereas, current reward mechanism in industrial companies tend to oppose applying novel technologies, because such technology is not proven technology yet and hence has a higher risk of failure.

In application driven research projects, system engineers should be allowed to be open-minded in trying to operationalize this novel technology by accepting a certain failure risk. Within the project, the reward mechanism for this systems engineering role (independent of his affiliation type) should be changed, such that the project stimulates this quest for operationalization above e.g. management for reduction of failure risk.

For academic researchers, it is important to co-align their research areas of interest with the target application by selecting research areas that contribute to primary functions of the application.

This viewpoint better suits the purpose of government knowledge diffusion and application stimulation programs. In this way, novel knowledge really diffuses towards industry and the application driven research project stimulates early adoption and learning experiences for industry people. In this way, strengths of both roles are used: researchers search and develop relevant knowledge, system engineers strive to apply this knowledge (combined with important engineering experience), where clearly good interaction between both partners is needed to learn both ways.

Chapter 3

Dexterous Robot Hand Technology

Chapter 1 and Chapter 2 motivated the interest for human-like dexterous robotic hands. This chapter presents a brief overview of current standing of dexterous robotic hand technology and knowledge. This overview serves to motivate research directions to generate novel technologies within the research area of dexterous robotic hands.

First, Section 3.1 presents the desired behavior of a dexterous robotic hand and the identification of technologies involved. Section 3.2 continues with a brief literature survey on parts of these technology areas to identify promising research directions. Next, Section 3.3 takes the survey results into a set of conceptual design considerations for creating novel robotic hand technologies.

3.1 Desired Dexterous Robotic Hand Behavior

Dexterous robotic hands technology has shown major improvements in the last decade. However, it is still subject to research rather than ready for real world applications. Therefore, following the discussion in Chapter 2, available technology and knowledge thereof is not yet ready for application driven systems architecting and deploying commercial robotic systems. Hence, specific requirements and technical specifications for a particular application (e.g. domestic robotics or professional service robots) are not of any use yet.

Instead, this section gives a narrative description of the desired behavior and targeted operational environment of human-like dexterous robotic hands. Furthermore, the description is translated into a set of primary functions for a human-like dexterous robotic hand. These primary functions lead to identify involved research areas. Finally a (non-complete) set of possible requirement parameters is identified for a dexterous robotic hand system (see Chapter 2). While researching novel technologies, knowledge must be generated on how the design variables of the novel technology relate to achievable specifications for these parameters.

3.1.1 Functional wishes robotic hand

Many future robotic tasks require versatile end-effector interactions with a highly diverse set of objects and unstructured environments. The human hand has the greatest versatility of all living and lifeless end-effector instruments ever seen on earth. This makes its functional capabilities desirable to implement for robotics. Therefore,

the desired behavior of versatile robotic end-effectors
encompasses human-like hand functions.

Although highly complex, the term 'hand functions' needs some clarification in order to define more precisely **what** the desired robotic end-effector should do. Human hand functions are extensively discussed in [29] by applying an interesting multi-disciplinary (including robotics) viewpoint. Four hand functions are categorized in [29]:

- *Tactile sensing:* serves to effect contact between the person's stationary hand and a surface or object which may or may not be moving. In tactile sensing, the hand is always passive. Although not typically used for it, tactile sensing does provide some information about certain properties (e.g., surface texture, thermal conductivity).
- *Active haptic sensing:* serves to effect contact between the person's hand as it moves voluntarily over a surface or object. It involves the use of sensory inputs from receptors embedded in skin, muscles, tendons, and joints. This active mode is essential for identifying objects and extracting more precise information about their properties.
- *Prehension:* refers to those activities in which the hand reaches to grasp and hold an object. The configuration of the grasp is determined by the task objective and so will often change as the task progresses.
- *Non-prehensile skilled movements:* refer to a diverse class of activities ranging from the gestures made as part of communication, to the movements involved in e.g. wiping surfaces, pushing buttons and scratching ones back.

3.1.2 Primary functions for human-like dexterous robotic hand

The categorization of human hand functions gives already a set of primary functions. They will be re-formulated to focus on the future versatile robotic end-effector applications.

From a robotic technology perspective, the author prefers to look at tactile sensing as a prehensile supporting function, rather than seeing it as a stand alone primary function to be implemented to copy human functionality as is. Active haptic sensing is a highly complex task, because it does not only include numerous sensing units but also intelligent perception capabilities. As such, having in mind future robotic applications, this hand function is considered a separate technology area. Thus, for the aimed versatile robotic end-effectors, two primary functions are identified with several sub-functionalities as listed below:

- *Prehension*
  - *Dexterous grasping:* coordinated dexterous actions to restrain an object with respect to the hand palm, including reaching, grasping, holding and releasing the object;
  - *Dexterous manipulation:* changing the constrained object orientation and position by manipulating the fingers;
- *Non-prehensile skilled movements*
  Dexterous motions of one or multiple finger(s) without object constraining objectives.
  - *Free motion:* e.g. pre-shaping[1], gesturing, etc . . . ;
  - *Interactive motion:* e.g. scratching, pushing buttons, wiping surfaces, moving door-handles, (un)screwing bottles, etc. . . ;

[1] Pre-shaping: actions to prepare hand and finger configuration for grasping.

3.1.3 Requirement parameters for human-like dexterous robotic hand

As discussed in Section 2.2, a desired system is defined by a description of the desired behavior and a list of values for the requirement parameters. Fundamental research investigates which values can be achieved for certain requirement parameters as a function of technology variables. Hence, this section gives an overview of some relevant requirement parameters, without specifying particular desired values:

1. Form factor:
   (a) appearance, weight, dimensions;
2. Operating environment[2]:
   (a) workspace (static/dynamic constraints, geometry, object occlusions. . .);
   (b) items to be handled: dimensions, materials, shape, deformability, surface characteristics (e.g. roughness, friction coefficient (μ)), weight, inertia properties, mass distribution, max. contact pressure, max. acceleration[3], . . . ;
   (c) conditions: temperature, humidity, floor vibrations, EMC,. . . ;
   (d) human interaction;
3. Safety:
   (a) self-damage, environmental hazards, environmental damage;
4. Robustness:
   (a) reliability: operational robustness, i.e. ability to stay in operation without breaking down (measured by: mean time between failure (MTBF));
   (b) maintainability: how often is maintenance required, how long does maintenance take (mean time between maintenance (MTBM), mean time to maintain (MTTM));
   (c) yield: task robustness, i.e. ability to complete task successfully (quantified by 'yield', i.e. ratio of successful task trials over total task trials).
5. Energy: source (electric, hydraulic, . . .), consumption, efficiency;
6. Cost: investment, consumer price, maintenance cost, operating cost, . . . ;
7. Tolerances: position and/or force accuracy and precision[4];
8. Speed: grasping time, release time;

[2]Note: the environment for the projected future robotic applications is highly unstructured. Therefore, identifying a set of requirement parameters and attaching values to these parameters such that all situations are covered is considered impossible and not supportive for versatile end-effector development. Hence, the identification of requirement parameters is circumvented by choosing to investigate human-like dexterous hands. Nevertheless some parameters are listed to give the reader an idea on relevant aspects.

[3]Note: huge accelerations arise when releasing an item to place it, since it is decelerated by the landing surface. This constraint parameter indicates how gentile and how far above the surface an object can be released.

[4]Accuracy: the degree of closeness of measurements of a quantity to its actual (true) value. Precision: the degree to which repeated actions under unchanged conditions show the same result [http://en.wikipedia.org].

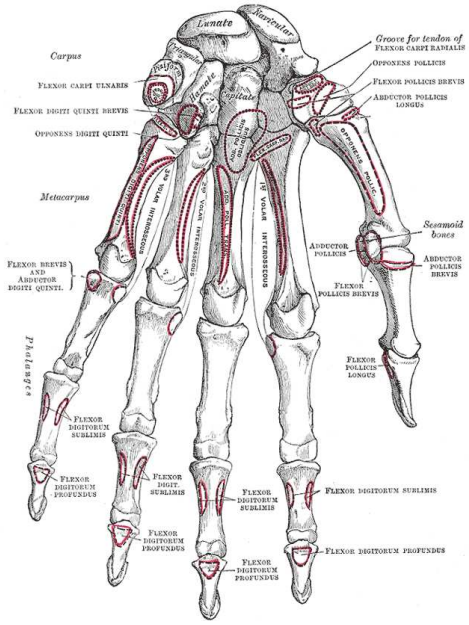

Figure 3.1: Bones of the left hand. Volar surface, source: [30].

3.1.4 Research areas

After having identified what the dexterous robotic hand should do, this section illustrates some robotic research directions involved that investigate **how** to achieve and implement this in robotics. From a robotic point of view, four elementary technology-options are involved for the dexterous end-effector:

1. *Mechanical & Kinematic structure:* refers to kinematics, mechanics and materials;
2. *Actuation System: refers to drive train and energy sources;*
3. *Measurement System:* refers to sensing feedback information for control system;
4. *Control System:* refers to decisions on actions to execute tasks;
   (a) High level controller: task coordinator determines what to do and how to do it (intention and planning) and how to handle new situations;
   (b) Low level controller: joint level control for motion and internal force regulation and dynamic interaction disturbance rejection.

The high level controller requires higher order intelligent autonomous and perceptive technologies in order to generate re-active and pro-active tasks and setpoints for (unstructured) situations. These perceptive technologies were identified as critical technologies on the robotics roadmap as well, Section 1.1.2. However, they are not the focus of this work. For human-like dexterous robotic hands, the human hand serves as example for inspiration on these technology-options, without aiming to literally copy the highly complex human hand structures. Brief comments are made on human hand equivalent 'technology'.

With regard to the mechanical & kinematic structure and the actuation system, 27 bones, 38 muscles and numerous tendons together form the complex structural elements of the human hand with four three digit fingers and one opposable two digit thumb, see Figure 3.1 and Figure 3.2. Not only these structural elements of the hand have contributed to its versatility. Also the soft tissues within the hand and the properties of the glabrous and hairy skin that

covers the palmar and dorsal surfaces, respectively [29]. Metabolic processes generate, store and use energy from digested food, i.e. human source of energy. Energy is transmitted as molecules through an extensive network of blood vessels.

The human measurement system contains several types of sensory receptors. The sensory mechanoreceptors within the skin provide the central nervous system with information about finger movements and the material and geometric properties of objects held within the hand [29]. Also visual information form the eyes is used to measure e.g. size, geometry of objects and relative distances. This group of sensors are called exteroceptive sensors [31]. The proprioceptive sensors sense movements and internal forces in the body. For example, muscle spindles sense length and shortening velocity of muscles and tendon organs sense tension in the tendons [31].

The human biomechanic control system is an extremely sophisticated system controlled by the Central Nervous System (CNS), both centrally controlled from the brain, high level control, (see also Figure 1.7) as well as having de-centralized low level control with reflexive control loops. Clever processing of a combination of various internal (e.g. intentions, feelings, etc) and external stimuli (from all sensory receptors) lead to decide on task planning, execution and according muscle control (high level control). Variations in muscle co-activation levels lead to changing intrinsic dynamics, i.e. stiffness and damping characteristics [32]. In the reflexive control loops, reflexes contribute to the dynamic interaction characteristics with the environment [31, 32].

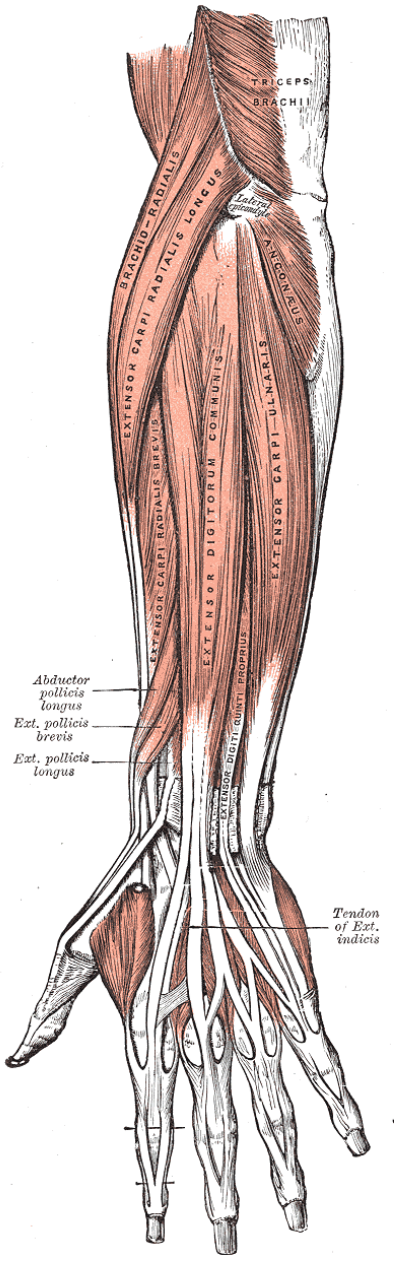

Figure 3.2: Hand muscles: Posterior surface of the left forearm. Superficial muscles, source: [30].

Both mechanisms together make up the dynamics of human body parts, as shown for human arms in [32]. These dynamics determine how postures (e.g. hand configurations) are maintained under the presence of external force disturbances. For slow (low bandwidth) disturbances, proprioceptive reflexes were shown to offer a flexible mechanism to adapt to chancing environments by quickly changing feedback gains as part of a learning (optimization) mechanism [32]. For fast disturbances (high bandwidth) these gains reduce to zero and only intrinsic dynamics remain. At the cost of metabolic energy, for posture maintaining tasks, humans use (near) maximum levels of muscle co-contraction to optimally adapt intrinsic dynamics for the given task (high stiffness) [32, 33]. Both mechanisms, adapting gains and changing levels of muscle co-activation, result in adapting stiffness of the human body part for optimal disturbance rejection. This human adaptation mechanism is described as impedance control in [34], which led to novel robotic interaction control strategies[5].

[5]It seems that [33] objects to the term 'impedance control' in this respect. According to [33], the goal of the CNS is to minimize a performance measure, rather than attaining a pre-specified reference impedance.

For grasping control, humans choose to use various grasp taxonomies to optimally utilize human hand dexterity to adapt the hand posture for the given task and object to be handled. The most common grasp types mostly referred to, were defined by Schlesinger as given in [35] and also extensively studied and further classified in [36, 37]: *cylindrical*, *tip*, *hook*, *palmar*, *spherical* and *lateral* grasp. For the analysis of robotic grasping, these are often categorized into *power grasps* and *finger-tip grasps*. To restrain objects, power grasps are formed by wrapping (enveloping) the fingers around an object. Finger-tip grasping is often used for manipulating the object [38].

3.2 Current Research Status

The previously given narrative description of the desired behavior for a human-like robotic hand led to identify several technology-options. Also some rough sketches were given on how human nature has implemented these technology-options.

For implementing these functions in robotics, the human hand should not be copied necessarily. It may be seen as source of inspiration and example. For each op the robotic technology-options, many different research directions exist. In the end, when integrating all technologies into one hand-design, the technology-options are interdependent and their applicability depend on the system architecture of the hand (see Chapter 2); e.g. designing a control strategy that heavily relies on tactile sensing, requires the existence and use of tactile sensor in the measurement system.

Within worldwide robotic research groups, starting in the early 1960's, researchers study the technology-options by trying different approaches and searching for alternative research directions. This section presents a brief (incomplete) overview of current status on various research directions for some of the technology-options. The purpose of this overview is to connect several approaches and contributions to identify promising design considerations and research directions for generating novel technology and knowledge for the desired human-like dexterous robot hand behavior.

3.2.1 Dexterity and grasp stability

The dexterity level determines the level of a device's ability of skilfully performing human like hand movements with and without restrained object. As such, dexterity refers to the physical capabilities of the human hand that make it highly versatile.

Salisbury found the minimum number of degrees of freedom (DOFs) to achieve dexterity to be nine for a robot hand with rigid, non rolling, non sliding contacts [7]. Hence he designed the Salisbury hand to have three fingers with three DOFs each [16]. Thereafter many other dexterous hands were designed, e.g. [17, 18, 19, 20, 21], see Figure 1.8.

To control these hands for prehension (dexterous manipulation and grasping), grasp stability became and still is an important research topic. Salisbury proposed a force closure rank condition for the rank of the grasp matrix to categorize stable and unstable grasps. However, this rank condition was found to be too restrictive. Bicchi and Kumar note that force closure does not guarantee stability and that any definition of stability must regard the grasp as a

However, in [32, 33], the author actually finds confirmation for impedance control theory. Discussions in [32, 33] describe maximum muscle co-activation levels as a human adaptation mechanism to optimize task performance. For posture maintaining tasks, altering to high stiffness values is exactly what is expected from an impedance controller.

dynamic system and describe the properties of the dynamic system when it is perturbed from an equilibrium configuration [39].

Indeed, Cutkosky and Kao showed that stability also depends on the fingertip compliance, the contact models and small changes in the grasp geometry [40]. For a full understanding of grasp stability Montana added a general condition for contact stability [41]. In [42], the idea of contact stability is extended to identify the class of equilibrium grasps, which showed that force closed grasps (concluded from positive definiteness of the grasped object stiffness, i.e.taking into account dynamics, e.g. controller, finger and contact stiffness) are stable, but not all stable grasps are force closed.

3.2.2 Grasp stiffness and interaction control

Cutkosky and Kao showed the importance of compliance in grasping by computing the overall stiffness matrix of a grasp, including structural, servo and geometric terms of the fingers [40]. This stiffness matrix (relating external forces to fingertip displacements) gives a direct measure for quasi-static stability, i.e. the matrix needs to be positive definite for stability.

From their analysis, Cutkosky and Kao clearly show that unmatched finger stiffness and applied contact forces may destabilize the grip. Besides analyzing the overall stiffness, they also present how to calculate required servo gains for a certain stiffness.

It is generally recognized that humans also regulate their stiffness according to the task they are dealing with. In [43] it is shown that some of the stiffness models in robotic grasping are indeed effective models for the human grasping behavior as well.

Besides using the stiffness matrix as a grasp stability measure, stiffness control has been (and still is) an interesting topic in view of interaction control of manipulators in general. Position and force control strategies (or hybrid combinations) tend to destabilize the controller in interaction tasks due to e.g. control loop delays, environment uncertainties, object location and object properties. In e.g. [44], intentionally using compliance and active stiffness control was already proposed as grasp control strategy.

Hogan [34, 45] generalized these approaches. He showed that controlling interaction tasks should not be seen as a matter of controlling the robot to some setpoint while minimizing the disturbances from the environment. These disturbances can not be minimized, because they have become dependent of the state of the interaction system. Hence, he proposed to approach it differently and control the impedance of the robot, i.e. the relation between the interacting forces and velocities [45, 46].

Based on Hogan's ideas, Stramigioli et al. pursued an impedance strategy for stable control of grasping tasks [47]. A virtual object connected to the fingertips through virtual spatial compliances prescribes the behavior of the grasping hand by measuring positions and calculating according fingertip forces that have to be applied by the controller as joint torque. Hence, no complex joint trajectories have to be generated. Instead the interaction behavior is defined by means of a desired system impedance such that the grasp is controlled passively, i.e. stable.

3.2.3 Programmable passive stiffness components

Actively generating impedance by means of control, can still render unstable behavior due to limited controller, sensor or actuator bandwidth or delays. Especially when non-backdriveable mechanics are used [48]. On the other hand, using direct drive (backdriveable) mechanics reveals other issues such as constant energy consumption for gravity compensation or external overload of the actuator due to fast impacts. Hence, for reasons of safety, passivity and stability,

Laurin-Kovitz et al. propose to control the impedance by incorporating programmable mechanical elements in the robot's drive system [48]. Inspired by human muscles, they developed a device with programmable stiffness and equilibrium position, using antagonistic non-linear springs. This antagonistic principle has been copied many times.

Nowadays, another reason for investigating variable stiffness components is found in safe human-robot interaction. In [49] the design trade-off considerations are presented with respect to safety and performance of robot arms. Variable stiffness components are believed to be helpful in this. For dexterous robot hands, safety in human-robot interaction is of course also an important issue.

Recently, researchers at DLR showed advances in dexterous grasping by combining impedance control with variable stiffness mechanisms [50, 51]. However, trajectory generation for finger grasp motion is not included in the specified desired finger behavior (i.e. impedance), whereas the impedance control scheme in [47] also naturally implements this as part of the desired physical behavior. For reasons of safety, miniaturization, intrinsic interaction control, stability and energy efficiency, they aim to develop their next DLR hand with tendon-driven joints. Variable stiffness components are used in the tendon drive lines [52]. They have chosen to implement variable stiffness by using non-linear springs on both antagonists for each joint [52], following [48].

3.2.4 Robot hand actuation

Despite all efforts, hardware complexity remains a bottleneck to get to a satisfying design. Back in the 80's, [17] already reported about the actuation challenges. In [7], Bicchi once again emphasized on the importance of finding suitable actuation methods and minimizing the amount of components.

Many different actuation methods (e.g. shape memory alloys [53], air muscles [54], fluidic actuators [20]) have been tried of which electromagnetic motors are still the most successful. However, due to volume restrictions, most of the grasping devices find their actuators positioned remotely outside the actual hand. To prevent backlash and other gearing difficulties, many common designs use tendon transmissions to drive the finger joints from outside the hand. One remarkable exception is found in the DLR II hand, where direct drive actuators are used in the joints. However, also at DLR the direct drive actuation method inside the fingers was found to be the limiting factor in reducing the dimensions. They decided to switch to tendon transmission as well [52].

Hirose and Umetani introduced another interesting finger actuation transmission [15]. Their 'softgripper' is an underactuated finger device that consists of a pulley routed tendon mechanism. The routing is such that some phalanges can be constrained, while others can still move. Hence, the n-DOF finger mechanism naturally conforms to any object shape, while it is simply controlled with only the traction of one pair of wires per finger. At the cost of manipulation dexterity, this underactuated mechanism allows to reduce the number of actuators (and sensors) significantly, while making it easier to grasp all kinds of irregular objects. Based on these principles the ARTS Lab has come up with some nice underactuated hands, e.g. RTR II [55]. Also in [56], this approach led to a novel compliant robust grasper, which utilizes structural compliance to enhance robustness. However, again at the cost of finger-tip grasping and dexterous manipulation.

3.2.5 Postural and force synergies

To reduce actuators and control complexity, recently robotic researchers (e.g [57, 58]) have adopted observations from neuro-scientists to investigate a different approach for dexterous grasping mechanisms and control. It was noticed and experimentally shown that even humans do not seem to control all of their 15 DOFs in their hand independently for all tasks. Depending on the task, several force synergies are observed, which describe coupled force (i.e. muscle activation) action patterns in grasping [59]. Also the majority of grasp postures (taxonomies) was shown to be based on two principal components [60]. In this way, the set of independent control variables (each synergy represents one control variable) is smaller than the number of independent actuators, which simplifies control. In [61], experiments show a different perspective on the origin of synergies in human hand control; a minimal intervention strategy. Nevertheless, if necessary, in human hands fine control is possible, since the actuators are present for the human hand.

In [57], an extensive analysis on motion and force controllability for robotic grasping hands with postural synergies is shown. These postural synergies can be virtually implemented, while maintaining full DOF actuation, to reduce control complexity. Also, synergies can be actually implemented in the mechanical design of the robotic hand, as in [58], where a sophisticated mechanism is used to switch between independent sets of so called 'eigenpostures', i.e. postural synergies for the robotic hand.

Postural synergies are described through the synergy matrix $S \in \mathbb{R}^{n_q \times n_z}$, whose columns describe the shapes of each synergy in the joint space $\mathcal{Q} \subset \mathbb{R}^{n_q}$, such that:

$$q_r = S \cdot z,$$

where $q_r \in \mathcal{Q}$ is the desired joint configuration belonging to the linear combination of synergies as selected by the synergy vector $z \in \mathbb{R}^{n_z}$ [57].

3.3 Design Considerations

The presented state of the art overview reveals interesting insights. This section will interconnect these insights to formulate design considerations from which novel concepts for robotic dexterous hands should be generated.

3.3.1 Design goals

For the presented dexterous hand functions, robotic system architectures need to be conceptualized and ultimately implemented. Tasks are executed under a wide variety of conditions and disturbances. The novel robotic architecture needs to address these circumstances. The state of the art discussion (Section 3.2) revealed some lessons learned, which lead to focus on the following requirement parameters as design goals:

- low weight;
- high energy efficiency;
- high robustness (task robustness and reliability);
- human dimensions;
- and low cost.

3.3.2 Robotic concept considerations

Some relevant design considerations are distilled from the previously discussed state of the art knowledge, to simulate generating concepts that address the given design goals.

Minimal component design Although the given design goals (Section 3.3.1) were tried to be respected, Section 1.3.2 showed that the required functions resulted in rather bulky implementations. The needed dexterity induced designs with many actuators to fully actuate all DOFs. This led to large dimensions, high weights, complex grasping control strategies and involvement of many (fragile) components (like sensors). All of these aspects endanger and degrade energy efficiency and robustness and result in costly designs. The author believes that this is not the right research direction to pursue.

Focus should be directed towards design for a minimal number of components. A minimal number of components, especially power actuators, allows to optimize dimensions, weight, costs and energy efficiency, while reliability and task robustness are improved due to a reduced amount of sensitive components and a lower control complexity.

Underactuation Combined control of position and mechanical compliance generally imposes a two DOFs control problem per joint. Hence, for a dexterous finger (i.e. three DOFs) with controlled compliance in each joint six power actuators per finger are needed, see e.g. [52]. Section 3.2.4 presented interesting example mechanisms to reduce the number of actuators, while at the same time control for power grasps is greatly simplified. A group of underactuated hands show interesting technologies that should be utilized for the benefit of minimizing the numbers of actuators. These underactuated hands are constructed in such a way that the degrees of freedom are coupled (see e.g. [15, 62]).

Variable mechanical compliance Furthermore, the importance of stiffness matching and interaction control strategies (such as impedance control) for grasp stability and grasping control have become clear. It was shown that the use of programmable impedance components, such as controllable mechanical compliance, can support this approach. Recently, within the robotic community, controllable mechanical compliance components have regained major interest for reasons of safety. However, besides for safety reasons, in grasping, it can be beneficial for other aspects as well.

The use of controllable mechanical compliance can be altered to its best for supporting the hand's interaction task and become part of the control strategy. In this way, the mechanics naturally solve part of the control difficulties, while also the amount of sensors could be reduced. The same task adaptation mechanism is found in human control of muscle co-activation (See Section 3.1.4). Reflexive loops are not fast enough for fast, high bandwidth, disturbances. Exactly the same holds for robotic control-loops with limited bandwidth and limited actuation accelerations.

Conclusively, variable mechanical compliance is believed to be advantageous for:

- Energy efficiency:
  - applying a constant force[6]: a non-backdriveable mechanism can keep an actuator configuration to maintain compliance and applied force without burning energy.

[6]Note: for this property, mechanical compliance does not necessarily need to be adjustable.

  - energy storage: variable amounts of energy can be stored to buffer energy from environment or actuator, which can be released to alter configurations when needed.

- Safety to environment: adjusting trade-off between desired task performance and safety to environment;

- Robustness:

  - disturbance rejection (task robustness): compliance determines how much configurations will change for force disturbances or how much force is build up in case of position disturbances. For both cases, variable compliance can be used to select a compliance for the benefit of desired disturbance rejection.
  - operational robustness (reliability): depending on the environment and task, compliance can help in preventing self-damage during task operation (safety for robot).

3.4 Conclusions

This chapter examined dexterous robot hand technology. Following the top-down-bottom-up analysis approach (see Chapter 2) and allowing anthropomorphic inspiration, four distinct primary functions for a human-like dexterous robotic hand were established; dexterous grasping, dexterous manipulation, free motion and interactive motion. Instead of defining specifications for such a robot hand, requirement parameters were identified, which can serve as test parameters during novel technology investigations, i.e. research.

Four elementary technology options were identified for the research area of dexterous robotic hands, by letting the human hand serve as source of inspiration: mechanical & kinematic structure, actuation system, measurement system, control system. A state of the art inspection on literature revealed an active research field on the topic of robotic hands. However, it also becomes clear that technology gaps need to be filled.

The literature review showed the need to focus first on some of the requirement parameters; weight reduction, energy efficiency improvement, increasing task and operational robustness, reducing dimensions and lowering costs. These goals are aimed to be reached by following a proposed set of design considerations: minimal component design, especially a minimal number of power actuators, through *underactuation* and *variable compliance* actuation. These considerations were formulated based on current knowledge on dexterous grasping, as presented in the state of the art review.

Chapter 4

Importance of Variable Compliance for Grasp Robustness

The previous chapter listed high task robustness as one of the major design goals (Section 3.3.1) for dexterous robotic hands. Task robustness refers to the ability to withstand perturbations and disturbances while continuing normal operations. The design considerations, as discussed in Section 3.3.2, advocate usage of variable compliance. One major reason for using variable compliance is to enhance disturbance rejection to improve task robustness.

The dexterous grasping tasks of a dexterous robotic hand will be the dominant tasks in many robotic applications. Therefore, this chapter focuses on robustness of (dexterous) grasping. To discover robustness, an effect analysis is presented for a set of identified disturbances. First, Section 4.1 gives a description of the robustness effect analysis. Then, in Section 4.2 the analysis is performed for a 1 DOF compliant gripper. Commonly known linear systems theory used in mechatronic engineering is applied for some intuitive 1 DOF gripper examples to show that various task-disturbance combinations lead to different preferred mechanical compliance settings. Thereafter, in Section 4.3, a multi-DOF robot hand example is used to apply known grasp robustness results from robotic literature, which again show the influence of various compliance settings for the dexterous grasper. Next, in Section 4.4, some other examples of dexterous skilled hand tasks are discussed to show that also for these tasks various compliance settings are desired.

4.1 Robustness Effect Analysis

Three of the four dexterous grasping tasks will be under investigation for the robustness effect analysis: **grasping**, **holding** and **releasing** (see Section 3.1.2). Before starting the actual effect analysis, first the possible disturbances are identified for which the effects are analyzed. Furthermore, a brief notion on two distinct holding strategies and three failure modes is given. Then, the actual analysis method is described and in the subsequent sections models are presented for the actual grippers under investigation.

4.1.1 Disturbance identification

Task robustness is endangered by all kinds of threats, as shown in Appendix A. Threats are use-case scenarios that (may) lead to failure of the executed dexterous hand task. Appendix A identifies three physical disturbances that make up a major part of all threats: **constant position** and **force** disturbances and **dynamic force** disturbances. Clearly, for grasping most

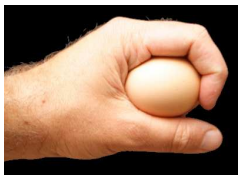

(a) Form closure: maintaining finger configuration (without exerting force) ensures holding egg.

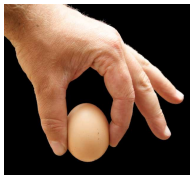

(b) Force closure: maintaining contact force ensures holding egg.

Figure 4.1: Form closure vs. force closure holding strategy.

disturbances will be more or less constant (i.e. quasi-static). However, dynamic disturbances may occur (see Appendix A) and hence are analyzed as well. i.e.

These disturbances can have either internal or external causes. Internal disturbances could be caused by e.g. measurement errors, external disturbances could come from e.g. environment interaction. In any case, this distinction does not change the disturbance type and is not relevant for a general disturbance and effect analysis for task robustness.

Combined with the three grasping tasks under investigation, a total of nine task-disturbance scenarios are analyzed for a 1 DOF gripper. Thereafter, a planar dexterous 3 DOF gripper example is used to present multi DOF grasp disturbance considerations.

4.1.2 Holding strategies

An object is held by maintaining contact forces on the object's surface, which completely or partially constrain the motions of the grasped object. Through the contacts, only unilateral forces can be applied on the object, i.e. pulling is not possible. Restraining an object with respect to the palm of the hand relies on establishing a static force equilibrium If the net external wrench[1] that acts on the object is zero, then the object is held.

Two basic holding (restraining, fixturing) strategies are distinguished to establish equilibrium, see Figure 4.1:

1. *Form closure:* If it can be assured that the object is geometrically constrained by the fingers, such that the object can not escape without changing geometry, then the object is held. Such force equilibrium does *not* rely on contact friction.

2. *Force closure:* If the object is not fully geometrically constrained by the fingers, friction forces are used to maintain force equilibrium.

In literature, these two strategies are extensively mentioned as robustness analysis metric (summarized in e.g. [7, 38, 39, 65]). Many different grasping control approaches arose based on the fact that a grasp has to be established through one of these two mechanisms.

For the presented analysis, it is assumed that force closure holding strategies are used for the grasping tasks. Form closure is not analyzed, since it 'simply' requires controlling infinite stiff configurations, in order to assure the 'form'. Note that this strategy endangers self-damage due to rigid structure. Also object damage is at risk, since infinite stiffness does not exist, which implies that small configurations changes will occur under certain disturbances, which will induce high contact forces. Furthermore, force closure is used more often, especially in case of dexterous manipulation.

[1] Wrench: generalized force co-vector, see e.g. [63, 64].

4.1.3 Failure modes

Any of the three disturbance types (constant position disturbance, constant force disturbance, dynamic force disturbance) can cause the grasp-task (grasping, holding, releasing) to fail. Failure is defined hereafter. For the analysis, three distinct failure modes are considered:

1. Damaging the object: contact force (at contact i) exceeds maximum allowable contact force before object damage occurs ($f_{ci} > f_{c,max}$);
2. Loosing the object: contact force does not meet minimum[2] needed contact force to maintain force closure ($f_{ci} < f_{c,min}$);
3. Positioning error: releasing object at wrong location ($x_o \neq x_{od}$);

If any of these failure modes occur, then the grasp-task is considered to have failed.

4.1.4 Effect analysis method

The goal of the subsequent effect analysis is to investigate, for each of the three grasping tasks, which grasper compliance settings are preferred in order to prevent failure modes from happening, while being exposed to one of the three disturbance types and pursuing a force closure holding strategy. Hence, these effect analysis investigate grasping robustness properties as a function of grasp compliance.

Section 4.2 presents effect analysis for a 1DOF compliant grasper, whereas Section 4.3 presents disturbance analysis for a planar dexterous 3DOF grasper. Both sections start with presenting the grasper model under consideration.

4.2 1DOF Disturbance Analysis for Variable Compliance

For this 1DOF analysis, a series elastic actuated 1DOF grasper is utilized as presented in Figure 4.2. The linear springs in each of the two 'fingers' represent mechanical compliance in the structure[3].

4.2.1 Simplified 1DOF grasper mechanism

The end-effector is rigidly attached to some manipulator (e.g. robot arm), which controls the end-effector position (x_h) at a desired end-effector position (x_{hd}). The end-effector position to control to (x_{hd}), is based upon known finger positions x_f and a measured object location ($\tilde{x}_o$) (for grasping task), which may be different from the actual object position x_o, or a desired release position (x_{od}) (for releasing task), see Figure 4.2.

After having arrived at x_h, the end-effector actuator changes x_a, see Figure 4.2. The grasper mechanism relies on a non-backdrivable feed-forward pre-setting of the actuator positions x_a. After presetting x_a, it is considered fixed (due to e.g. mechanical non-backdrivability) to that position[4]. Resulting contact forces (either to grasp or to release) depend on x_a, on the mechanical stiffness (k) and on the finger position x_f:

$$f_{ci} = (x_{ai} - x_{fi}) \cdot k, \tag{4.1}$$

[2]Note: the reader may notice a gap in English language; there exists no antonym of the verb 'to exceed'.

[3]Alternatively, one could see it as the controller stiffness (or as a combination of both structural and controller stiffness), for which it is then shown that different scenarios could use different feedback gains.

[4]Note: even if it is under continuous control, some reaction time is needed.

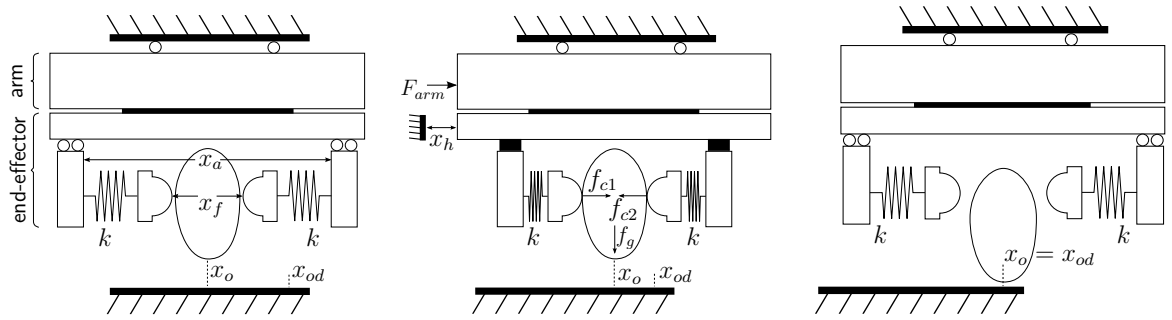

(a) Grasp: move actuator position x_a such that finger position x_f reaches contact points on object.

(b) Hold: move x_a such that mechanical springs (stiffness k) compresses to establish contact force f_{ci}. Actuator position is fixed (non-backdrivable). Arm is actuated (F_{arm}) to move end-effector with object from position x_h to some desired position x_{hd} such that object position x_o moves to desired position x_{od}.

(c) Release: move x_a to reduce contact force and release object at $x_o = x_{od}$.

Figure 4.2: 1DOF Grasper mechanism (nominal grasping sequence): utilizes force closure by ensuring $f_{c1}, f_{c2} \geq \frac{f_g}{2\mu}$, where f_g is gravity on object in vertical direction and μ is the contact friction coefficient. Due to non-backdrivability of actuator, x_a (and f_{ci}) can be maintained without using energy. Only moving x_a requires energy. Nominal (i.e. without disturbances) grasping behavior is sketched.

where $i \in \{1, 2\}$ denotes the contact (and finger) number[5]. The mechanical stiffness k determines to what extend disturbances will be rejected. As generally tried to be achieved in control, dynamic grasping control is tried to be minimized. This is done by steering x_a in feed-forward[6] and through a proper selection of stiffness k for disturbance rejection.

4.2.2 1DOF Grasper analysis parameters

Figure 4.2 shows the nominal behavior (i.e. no failure) for the grasper. From known gravitation force (object mass (m_o)), perpendicular to manipulation direction, and contact friction properties, the minimum needed contact forces can be calculated to establish force closure:

$$f_{c,min} = \frac{f_g}{2\mu}$$

The minimum contact forces make sure that no net force exist in gravitation direction. Notice that f_{c1} and f_{c2} have opposite positive direction, indicated by their vectors. The net force on the object (f_o) in manipulation direction (co-linear with f_{ci}) is:

$$f_o = f_{c1} - f_{c2}$$

Based upon object material properties, also a maximum allowable contact force ($f_{c,max}$) is determined.

Also some performance parameters will be used during analysis:

[5]Note: for this example, each contact force f_{ci} has one force component. This force is the force perpendicular to object surface, as indicated in Figure 4.2

[6]Note: feed-forward selection of x_a is based on assumed object geometry and known stiffness k and assuming a proper realization of x_h at x_{hd}.

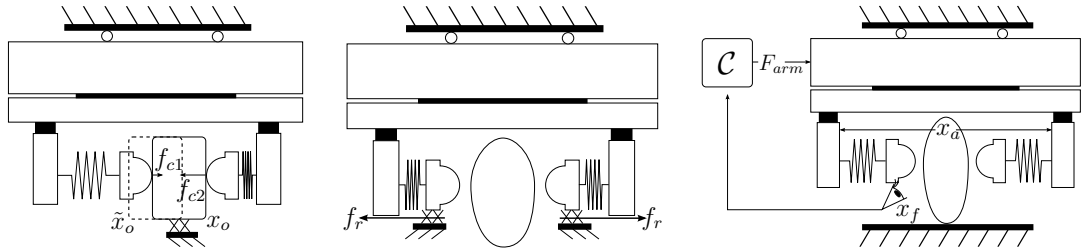

(a) Grasping with constant position disturbance.

(b) Grasping with constant force disturbance.

(c) Grasping with dynamic force disturbance.

Figure 4.3: Different disturbance scenarios for Grasp-task.

- $e_{h,max}$: End-effector position tolerance; maximum end-effector position error that grasper can handle before one of the failure modes occurs;
- e_o: Object positioning error ($e_o = x_o - x_{od}$); difference between true object location and desired location to place object (while holding, or after releasing).

The following paragraphs discuss the disturbance analysis for several combinations of end-effector tasks and disturbance types. Focus will be on qualitatively optimizing a stiffness value with respect to the three failure modes for the analyzed scenario, i.e. task robustness as function of k.

4.2.3 Grasp-task

- *Constant position disturbance:* See Figure 4.3(a); true position of object x_o to be grasped deviates from measured position $\tilde{x}_o$, while the object restrained to its position, as indicted in Figure 4.3(a). Based on $\tilde{x}_o$, x_{hd} is calculated and end-effector is controlled such that $x_h = x_{hd}$. Based on object properties, x_a is set to get desired contact forces. Due to $\tilde{x}_o \neq x_o$, x_f deviates from expected values for both fingers, resulting in undesired contact force changes (Δf_{ci}): increased f_{c2} and reduced f_{c1}. As shown by Equation 4.1, a **low value for** k will support to maintain $f_{c,min} \leq f_{ci} \leq f_{c,max}$, s.t. $e_{h,max}$ **is increased**.
- *Constant force disturbance:* See Figure 4.3(b); end-effector fingers are resisted with friction force (f_r) due to environment interaction. Based on object properties, x_a is set to get desired contact forces. However, f_r reduces f_{ci}, or even no contact will be established, hence a successful grasp is endangered. As soon as friction is resolved (due to e.g. lifting the hand a little bit), contact forces will be as desired.

  Note: if, during grasping, it is noticed that f_{ci} is too low, either x_a can be changed or k can be increased. However, this means that, once friction is resolved, $f_{ci} \geq f_{c,max}$. Furthermore, this action involves active grasp control, which was tried to be avoided by using the feed-forward strategy. The advantage is that x_a and k are controlled instead of f_{ci}, since directly controlling f_{ci} in case of interaction with unknown environments is physically meaningless, see [45, 46]. **Interaction control can utilize variable stiffness.**
- *Dynamic force disturbance:* See Figure 4.3(c); End-effector is moved to x_{hd} in order to put fingers on appropriate grasp positions. Controller $\mathcal{C}$ regulates x_f by applying robot arm force F_{arm}. The controlled motion of x_h induces oscillations on x_f, which disturb the finger positions. The lowest mechanical Eigen-frequency limits the achievable closed-loop position control bandwidth. The finger stiffness causes the lowest Eigen-frequency

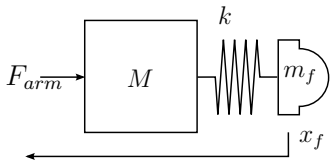

Figure 4.4: Equivalent model for grasping with dynamic force disturbance scenario.

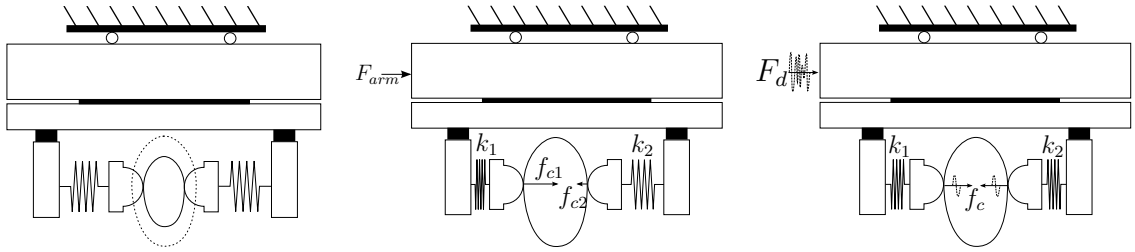

(a) Holding with constant position disturbance.

(b) Holding with constant force disturbance.

(c) Holding with dynamic force disturbance.

Figure 4.5: Different disturbance scenarios for Hold-task.

(ω_f) in the controlled system (see Figure 4.4), which can be increased by enlarging k, according to:

$$\omega_f \approx \sqrt{\frac{k}{m_f}},$$

where m_f is the mass of one finger and assuming $M >> m_f$, with M the total mass of the robot-arm and end-effector palm. Hence, **increasing** k, allows higher control bandwidths, which **reduces positioning errors (e_o)**, see e.g. Equation (1) in [66].

4.2.4 Hold-task

- *Constant position disturbance:* See Figure 4.5(a); based on object properties (such as dimensions), x_a is set to get desired contact forces. Since actual dimensions turn out to be smaller than expected, x_f deviates from expected values, resulting in undesired contact force reduction (Δf_{ci}). As shown by Equation 4.1, a **low value for** k supports to reduce Δf_{ci} and maintain $f_{c,min} \leq f_{ci} \leq f_{c,max}$.

- *Constant force disturbance:* See Figure 4.5(b); while holding object, the end-effector is accelerated ($\ddot{x}_h$) with constant force F_{arm} to move object. In steady state, the object accelerates ($\ddot{x}_o$) along with the end-effector, i.e. $\ddot{x}_o = \ddot{x}_h$. Hence, the contact forces change (Δf_{ci}) with respect to the preselected f_{ci}, such that the net force on the object has become $f_o = \Delta f_{c1} - \Delta f_{c2} = m_o \cdot \ddot{x}_o$. For the situation in Figure 4.5(b), the stiffness actually determines Δf_{ci} (assuming enough pre-tension s.t. f_{ci} remains positive). Considering k_i parallel springs, it can be seen that[7]:

$$\Delta f_{c1} = +\frac{k_1}{k_1 + k_2} m_o \cdot \ddot{x}_o, \quad \Delta f_{c2} = -\frac{k_2}{k_1 + k_2} m_o \cdot \ddot{x}_o, \tag{4.2}$$

where signs change if F_{arm} changes direction. Thus, e.g. if f_{ci} was set to be close to $f_{c,min}$, changing k to $k_1 > k_2$ supports to keep $f_{c2} > f_{c,min}$, while $f_{c1} < f_{c,max}$.

[7] See also Section 5.3.6.

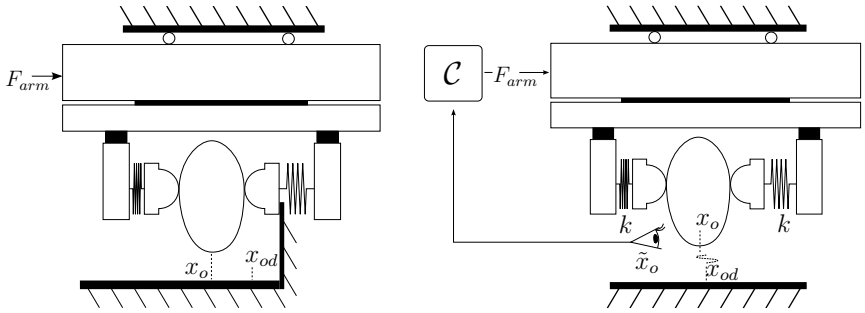

(a) Releasing with constant position disturbance.

(b) Releasing with dynamic force disturbance.

Figure 4.6: Different disturbance scenarios for Release-task.

In general, **distinguishing** k_i such that $k_1 \neq k_2$, supports to split the induced force disturbance over the contacts in order to prevent object damage or object slipping. Changing k equally (keeping $k_1 = k_2$) does not change anything to f_{ci}.

- *Dynamic force disturbance:* See Figure 4.5(c); desired behavior is set to hold end-effector and object stand still by applying a certain contact force $f_{c1} = f_{c2}$ (pre-load in springs). While holding object, the end-effector is accelerated ($\ddot{x}_h$) due to oscillating (i.e. no steady sate) disturbance force F_d. F_d is transferred to the object. The transfer function between the net force on the arm (F_d) and the net force on the object (f_o) is given by:

$$\frac{f_o(s)}{F_d(s)} = \frac{(k_1 + k_2)m}{mMs^2 + (k_1 + k_2)(m + M)}, \tag{4.3}$$

with $m := m_0 + 2m_f$ and assuming that contact remains. The object will vibrate, s.t. the contact forces will continuously change (Δf_{ci}), maximized by:

$$|\Delta f_{ci}| \leq \frac{k_i}{k_1 + k_2} f_o(s) = \frac{k_i m}{mMs^2 + (k_1 + k_2)(m + M)} F_d(s)$$

with cut-off frequency:

$$\omega_c = \sqrt{\frac{(k_1 + k_2)(m + M)}{mM}}$$

For dynamic $F_d(\omega)$ with frequencies ω, three ranges are differentiated:

1. $\omega < \omega_c$: $|\Delta f_{ci}| \approx \frac{k_i m}{(k_1+k_2)(m+M)} \cdot |F_d|$[8];
2. $\omega > \omega_c$: $|\Delta f_{ci}| \approx \frac{k_i}{Ms^2} \cdot |F_d|$;
3. $\omega = \omega_c$: $|\Delta f_{ci}|$ depends on the damping.

Assuming that damping is large enough, worst case contact force deviations are found for $\omega \leq \omega_c$, hence **reducing stiffness** $(k_1 + k_2)$, reduces ω_c, s.t. larger parts of dynamic disturbances become **harmless**. Also known as low-pass filtering.

4.2.5 Release-task

- *Constant position disturbance:* See Figure 4.6(a); robot-arm is moving to desired release position x_{od}. However, due to interaction between environment and finger (or object), the

[8]Note: $\omega = 0$ implies constant F_d, inducing constant acceleration $\ddot{x}_h = \ddot{x}_o = \frac{F_d}{m+M}$. Hence, substituting $F_d = (m + M) \cdot \ddot{x}_0$, gives Equation 4.2 again.

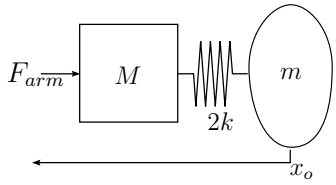

Figure 4.7: Equivalent model for releasing object with dynamic force disturbance scenario ($m = m_o + 2m_f$).

object is obstructed. As long as x_h moves on, one spring compresses and the according f_{ci} is increased, endangering $f_{ci} > f_{c,max}$. Through Equation 4.1 it is clear that for smaller values of k, greater x_h displacements are allowed until damage occurs. Hence, **smaller values of** k increase allowable reaction time, i.e. **increased safety margins**.

- *Constant force disturbance:* Consider again Figure 4.3(b); x_a is set to reduce contact forces and detach fingers from object to release. end-effector fingers are resisted with friction force (f_r) due to environment interaction. However, f_r opposes the release force on the fingers, hence releasing is endangered. Unlike in the grasping scenario, in this case increasing k or x_a is harmless and does support to release the object. Increasing x_a would induce larger x_f position displacements. Hence **increasing** k **is favorable**.

- *Dynamic force disturbance:* See Figure 4.6(b) End-effector is moved to x_{od} in order to bring object to appropriate release position. Controller $\mathcal{C}$ regulates x_f ($= x_o$, as long as object is held) by applying robot arm force F_{arm}. The motion tracking control of x_h induces oscillations on x_o, which induces $x_o \neq x_{od}$, s.t. $e_o \neq 0$. The lowest mechanical Eigen-frequency limits the achievable closed-loop position control bandwidth. For the grasped system, an equivalent model is given in Figure 4.7. The finger stiffness causes the lowest Eigen-frequency (ω_e) in the controlled system (see Figure 4.4), which can be increased by enlarging k, according to:

$$\omega_e \approx \sqrt{\frac{2k}{m}},$$

assuming $M >> m$. Hence, **increasing** k, allows higher control bandwidths, which **reduces positioning errors (**e_o**)**, see e.g. Equation (1) in [66].

4.3 3DOF Disturbance Analysis for Variable Compliance

Through a series of simple 1 DOF grasper examples, the previous section showed that different task-disturbance scenarios, require different compliance values for optimal disturbance rejection. As discussed in Section 3.2.1 and 3.2.2, the stiffness matrix of a grasp can be used to study robustness of a grasp. In this section, the stiffness matrix is worked out for an illustrative example of a simple planar 'dexterous' hold-task, based on results found in [40]. The examples serve to discuss and illustrate (in an accessible manner) the influence of robot finger stiffness on grasp robustness for dexterous grasping. The same failure modes apply (Section 4.1). For this more dexterous case, the position now also includes a desired orientation of the object.

4.3.1 Planar 2 finger dexterous grasper

The analysis utilizes a description of kinematics based on screw theory using twists and wrenches, i.e geometrical instantaneous velocities of a body and geometrical forces acting on a body respectively (See e.g. [63, 65, 64]). The following notations are used:

- $T_i^{k,j}$: Twist of body i w.r.t. body j expressed in coordinates of reference frame Ψ_k.
- W_i^k: Total wrench on body i expressed in coordinates of reference frame Ψ_k.
- $W_{i,ci}^k$: Wrench on body i, due to interaction at contact point ci, expressed in coordinates of reference frame Ψ_k.

The 'dexterous' planar hold situation to be analyzed is illustrated in Figure 4.8(a). For this planar example, only three coordinates are needed; two translation displacements (x, y) and one rotational orientation (θ_z). Hence the twist is considered a (simplified) vector in $\mathbb{R}^{3\times1}$:

$$T_i^{k,j} = \begin{pmatrix} \omega_{z,i} \\ v_{x,i} \\ v_{y,i} \end{pmatrix},$$

where $\omega_{z,i}$ denotes the angular velocity (i.e. $\dot{\theta}_z$) of body i relative to body j expressed in coordinate frame k, and $v_{x,i}, v_{z,i}$ denote the instantaneous velocity (relative to frame j) of a point (virtually) fixed in body i that passes through the origin of frame k. The wrench is considered a co-vector in $\mathbb{R}^{1\times3}$:

$$W_i^k = \begin{pmatrix} \tau_{z,i} & f_{x,i} & f_{y,i} \end{pmatrix},$$

where f_x, f_y denote the linear force and τ_z the momentum about ω_z, acting on the origin of frame k applied to body i.

Because stiffness is a linearized concept, valid around a local equilibrium, only small perturbations around the given configuration of Figure 4.8(a) are examined. Hence, infinitesimal displacements and infinitesimal forces around this equilibrium are considered, which will be denoted by δ; e.g. δT is an infinitesimal deformation twist, which is regarded a infinitesimal displacement.

Thus, it is aimed to derive the object stiffness matrix $\mathcal{K}_o$ for the given planar grasp, as illustrated in Figure 4.8(a), which relates infinitesimal object wrenches to infinitesimal object twists around the given configuration, given by: $\delta W_e^T = \mathcal{K}_o \cdot \delta T_o$.

Contact model When contact is established between the object and the finger-tip, the contact transmits forces and motions from and to the object. Many different contact models exist, which either model dynamics or kinematics or both, either local quasi-static or globally full dynamics (see a.o. [65, 67]). For the quasi-static robustness analysis at hand, it is considered sufficient to model the contact through kinematic constraints, assuming contact persists and the contact point location does not change significantly over the surface (coincides with small perturbations assumption).

$\mathcal{H}_i \in \mathbb{R}^{n_{ci}\times3}$ sets the contact model by defining the transmitted n_{ci} degrees of freedom of contact i. As depicted in Figure 4.8(b), contact forces and displacements for contact i are defined in the contact coordinate frame Ψ_{ci}, which is co-aligned with the object surface in the contact point, i.e. y_c-axis lies along tangential direction of object surface, x_c-axis lies in normal direction of object surface. The contact forces in Ψ_{ci} are given by $f_{ci} \in \mathbb{R}^{1\times n_{ci}}$. For this planar case, the contact forces f_{ci} always contain a normal component, f_{ix}, and, depending on the contact model $(\mathcal{H}_i)$, f_{ci} can also contain a tangential (f_{iy}) friction component. A rotational friction component would imply rolling friction, which is considered physically meaningless (slippage during rolling is contained in the tangential friction forces). So, in non of the contact models it is considered. The accompanying velocity components are represented by $\dot{\epsilon}_i \in \mathbb{R}^{n_{ci}\times1}$

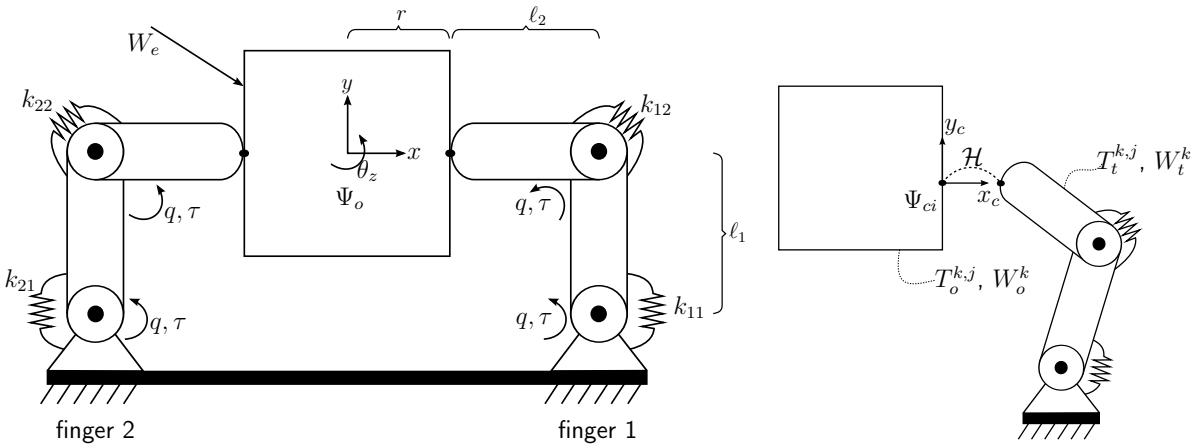

(a) Planar 3 DOF hold situation with two 2-DOF compliant robotic fingers. Reference frame Ψ_o is the reference frame attached to the object, which (for given configuration) coincides with a fixed world coordinate frame $\Psi_w = \Psi_o$. Joint configurations are denoted by q and joint torques are given by τ.

(b) Finger-object contact model. Contact reference frame Ψ_c is co-aligned with object surface in contact point. $\mathcal{H}$ sets the contact model by defining the transmitted DOFs of the contact.

Figure 4.8: 3DOF quasi-static dexterous hold scenario for stiffness analysis. Subscript o indicates *object*, t *finger-tip* and c *contact*. Dimensions r, ℓ_1, ℓ_2 define half object width and length of phalanx 1 and 2 of each finger respectively.

and the infinitesimal contact displacements by $\delta\epsilon_i \in \mathbb{R}^{n_{ci}\times 1}$. Altogether, the contact model is defined by the following constraint equations:

$$\mathcal{H}_i : \begin{cases} \dot{\epsilon}_i & = & \mathcal{H}_i \cdot T_t^{k,j} = \mathcal{H}_i \cdot T_o^{k,j} \\ \mathcal{H}_i^T \cdot f_{ci}^T & = & \left(W_t^k\right)^T = \left(W_o^k\right)^T \end{cases}, \tag{4.4}$$

where the twists and wrenches are defined in Figure 4.8(b). One can recognize that an infinitesimal contact displacement ($\delta\epsilon_i$) is found through a scalar multiplication with dt (being an infinitesimal time-step[9], $\delta\epsilon_i = \dot{\epsilon}_i \cdot dt$, such that also $\delta\epsilon_i = \mathcal{H}_i \cdot \delta T_t^{k,j} = \mathcal{H}_i \cdot \delta T_o^{k,j}$.

A point-contact-without-friction (PwoF) model is used when the contact patch is very small and the surfaces of the hand and object are slippery. A hard finger contact (HF) model is used when there is significant contact friction, but the contact patch is small, so that no appreciable friction moment exists[10] [65]. For each of the models, $\mathcal{H}$ is defined as follows:

$$\mathcal{H}_{PwoF} = \begin{pmatrix} 0 & 1 & 0 \end{pmatrix} \quad \Leftrightarrow \quad f_{ci} = \begin{pmatrix} f_{ix} \end{pmatrix}, \quad \dot{\epsilon}_i = \begin{pmatrix} x_{ci} \end{pmatrix} \tag{4.5}$$

$$\mathcal{H}_{HF} = \begin{pmatrix} 0 & 1 & 0 \\ 0 & 0 & 1 \end{pmatrix} \quad \Leftrightarrow \quad f_{ci} = \begin{pmatrix} f_{ix} & f_{iy} \end{pmatrix}, \quad \dot{\epsilon}_i = \begin{pmatrix} x_{ci} \\ y_{ci} \end{pmatrix} \tag{4.6}$$

For the analysis it is assumed that the contact forces remain inside the cone of friction of each contact i.

Initial equilibrium configuration Robustness properties of the planar dexterous grasper are discussed for the given configuration in Figure 4.8. The geometric finger Jacobians[11] (J_1, J_2)

[9] Note: dt must be infinitesimal since the space of twists is a non-linear non-flat space, such that this time scaling can only hold locally.

[10] A soft-finger soft finger contact (SF) model is used in situations in which the surface friction and the contact patch are large enough to generate significant friction forces and a friction moment about the contact normal. However, in this planar example, such SF model can not exist.

[11] See e.g. [64].

of both fingers map infinitesimal joint displacements to infinitesimal finger-tip twists: $\delta T_t^{ci,w} = J_i \cdot \delta q_i$ and, dually, wrenches on the finger-tip are mapped to joint torques; $\delta \tau_i^T = J_i^T \cdot (\delta W_t^{ci})^T$, with $\delta q_i \in \mathbb{R}^2$ the infinitesimal joint displacement vector and $\delta \tau_i \in \mathbb{R}^{1\times 2}$ the infinitesimal joint torques about a given configuration of finger i . Note that the twist is denoted w.r.t. the fixed world reference frame $\Psi_w = \Psi_o$ and both the twist and the wrench are expressed in each of the finger contact frame coordinates (Ψ_{ci}).

For this configuration, the geometric finger Jacobians expressed in Ψ_{ci} are found to be:

$$J_1 = \begin{pmatrix} 1 & 1 \\ -\ell_1 & 0 \\ -\ell_2 & -\ell_2 \end{pmatrix}, \qquad J_2 = \begin{pmatrix} 1 & 1 \\ -\ell_1 & 0 \\ \ell_2 & \ell_2 \end{pmatrix}, \tag{4.7}$$

The *sub*-grasp-matrix G_i for **contact** i defines the coordinate change that maps the wrench on the object *due to interaction at contact* i, expressed in the associate contact frame Ψ_{ci} ($W_{o,i}^{ci}$), to the wrench expressed in world coordinates Ψ_w ($W_{o,i}^{w}$). Dually, its transpose (G_i^T) maps the twist of the object expressed in Ψ_w to a twist expressed in Ψ_{ci}:

$$G_i : \begin{cases} \left(W_{o,i}^{w}\right)^T &= G_i \cdot \left(W_{o,i}^{ci}\right)^T \\ T_o^{ci,w} &= G_i^T \cdot T_o^{w,w} \end{cases} \tag{4.8}$$

The sub-grasp-matrices for this configuration are:

$$G_1 = \begin{pmatrix} 1 & 0 & r \\ 0 & 1 & 0 \\ 0 & 0 & 1 \end{pmatrix}, \qquad G_2 = \begin{pmatrix} 1 & 0 & -r \\ 0 & 1 & 0 \\ 0 & 0 & 1 \end{pmatrix} \tag{4.9}$$

These sub-grasp-matrices are used in the remainder of the analysis.

For the reader who is familiar with grasping literature; in order not to be confused, it is important to realize that this sub-grasp-matrix is a sub-block of what is called the *complete* Grasp Matrix of the grasping system in [65]. Hence, it is called the sub-grasp-matrix in order to clarify this distinction.

The total wrench on the object expressed in world coordinates, W_{co}^{w}, due to interactions at all n_c contacts in the grasp system is simply given by the sum of each of the interaction wrenches. Hence,

$$\left(W_{co}^{w}\right)^T = \sum_{i=1}^{n_c} \left(W_{co,i}^{w}\right)^T = \sum_{i=1}^{n_c} G_i \cdot \left(W_{co,i}^{ci}\right)^T \tag{4.10}$$

For the reader who is familiar with special Euclidean spaces; consider a homogeneous matrix H_k^l, which denotes the change of coordinates from a coordinate frame Ψ_k to another coordinate frame Ψ_l:

$$H_k^l = \begin{pmatrix} R_k^l & p_k^l \\ 0 & 1 \end{pmatrix}, \quad R_k^l \in SO(3), \quad p_k^l \in \mathbb{R}^3 \tag{4.11}$$

The homogeneous matrix can be used as matrix representation of the elements of the special Euclidean group $SE(3)$, i.e. a Lie group. The lie algebra $se(3)$ of the group is defined as the tangent space to the identity of the group. The twist is the element of the algebra $se(3)$ corresponding to the translation of the tangent element $\dot{H}$ at H to the identity. Coordinate changes for twists and wrenches are given by the adjoint mapping [63, 64]:

$$Ad_{H_k^l} : \begin{cases} T_i^{l,j} & = & Ad_{H_k^l} \cdot T_i^{k,j} \\ \left(W_i^k\right)^T & = & Ad_{H_k^l}^T \cdot \left(W_i^l\right)^T \end{cases}, \qquad Ad_{H_k^l} = \begin{pmatrix} R & \mathbb{I}_3 \\ \tilde{p}R & R \end{pmatrix} \tag{4.12}$$

Hence, $G_i^T = Ad_{H_w^{c_i}}$, which also shows that G_i holds for both dynamic and quasi static analysis (also noted in[65]) $\square$

4.3.2 Grasp stiffness matrix: $\mathcal{K}_o$

The following discussion aims to derive the stiffness matrix for the grasped object, following [40], without considering the contact geometry, since the object has flat contact surfaces. The grasp stiffness matrix $\mathcal{K}_o \in \mathbb{R}^{3\times3}$ defines the relation between the required external wrench δW_e to induce object displacement δT_o^w, expressed in Ψ_w coordinates:

$$\left(\delta W_e^w\right)^T = \mathcal{K}_o \cdot \delta T_o^{w,w}, \tag{4.13}$$

where

$$\mathcal{K}_o = \sum_i^{n_c} K_{oi}, \tag{4.14}$$

with K_{oi} the object stiffness matrix due to finger-tip contact i. For this example $n_c = 2$. The finger-tip stiffness of each finger are structurally in parallel, which is why the sum can be used to add all stiffnesses to find the total stiffness.

The analysis will derive K_{oi}, i.e. the object stiffness matrix due to one finger-tip contact i. For one finger-tip contact i, the joint compliance matrix $C_{qi} \in \mathbb{R}^{n_{qj}\times n_{qi}}$, with n_{qi} the number of joints of the finger with finger-tip contact i (in this example $n_{qi} = 2$), is given by:

$$\delta q_i = C_{qi} \cdot \delta \tau_i^T, \qquad \text{with} \quad C_{qi} = \begin{pmatrix} \frac{1}{k_{i1}} & 0 \\ 0 & \frac{1}{k_{i2}} \end{pmatrix}, \tag{4.15}$$

where joint stiffness k_{ij} models structural joint stiffness and/or controller stiffness. Substituting the geometric finger Jacobian, Equation 4.7, gives:

$$\delta T_t^{ci,w} = J_i \cdot C_{qi} \cdot J_i^T \cdot \left(\delta W_t^{ci}\right)^T, \tag{4.16}$$

from which the finger-tip compliance $C_{fi} \in \mathbb{R}^{3\times3}$ is defined by[12]: $C_{fi} = J_i C_{qi} J_i^T$. The finger-tip compliance seen through the contact, $C_{ci} \in \mathbb{R}^{n_{ci}\times n_{ci}}$, is found be applying the contact

[12] $C_{fi} = J_i C_{qi} J_i^T$ is called a pull-back of C_{qi} from joint space to $se(3)$, see Chapter 5, Definition 5.33.

constraints (and assuming stiff contacts[13]). Hence, substitution of Equation 4.4 gives:

$$\delta\epsilon_i = \mathcal{H}_i \cdot C_{fi} \cdot \mathcal{H}_i^T \cdot \delta f_{ci} = C_{ci} \cdot \delta f_{ci}, \tag{4.17}$$

which, if invertible[14], gives the finger-tip stiffness seen through the contacts: $K_{ci} = (C_{ci})^{-1}$. Thus, the transmitted contact forces are related to the transmitted contact displacements as follows:

$$\delta f_{ci} = K_{ci} \cdot \delta\epsilon_i, \qquad \text{with} \quad K_{ci} = \left(\mathcal{H}_i C_{fi} \mathcal{H}_i^T\right)^{-1}. \tag{4.18}$$

However, not all forces are transmitted to the object, hence the object contact stiffness (K_{pi}) is found by substituting Equation 4.4:

$$\left(\delta W_o^{ci}\right)^T = \mathcal{H}_i^T \cdot \left(\mathcal{H}_i C_{fi} \mathcal{H}_i^T\right)^{-1} \cdot \mathcal{H}_i \cdot \delta T_o^{ci,w}, \tag{4.19}$$

such that $K_{pi} = \mathcal{H}_i^T \cdot \left(\mathcal{H}_i C_{fi} \mathcal{H}_i^T\right)^{-1} \cdot \mathcal{H}_i$. Finally, applying the sub-grasp-matrix coordinate transformation (Equation 4.8), gives:

$$\delta\left(W_o^w\right)^T = G_i \cdot \mathcal{H}_i^T \cdot \left(\mathcal{H}_i C_{fi} \mathcal{H}_i^T\right)^{-1} \cdot \mathcal{H}_i \cdot G_i^T \cdot \delta T_o^{w,w}, \tag{4.20}$$

from which the object stiffness matrix K_{oi} due to finger-tip contact i is found to be:

$$K_{oi} = G_i \cdot \mathcal{H}_i^T \cdot \left(\mathcal{H}_i \cdot J_i \cdot C_{qi} \cdot J_i^T \cdot \mathcal{H}_i^T\right)^{-1} \cdot \mathcal{H}_i \cdot G_i^T. \tag{4.21}$$

Thus, combining Equation 4.21 with 4.14 leads to the total grasp stiffness matrix of the grasped object, $\mathcal{K}_o$. These results are generally applicable for a full 6-DOF analysis.

Grasp stiffness matrix inspection For hard finger contacts ($\mathcal{H}_i = \mathcal{H}_{HF} \quad \forall i$, see Equation 4.5), the grasp stiffness matrix for the given configuration is found to be:

$$\mathcal{K}_o = \begin{pmatrix} \frac{r^2(k_{12}+k_{22})}{{\ell_2}^2} & \frac{-r(k_{12}+k_{22})}{\ell_1\ell_2} & \frac{r(k_{12}-k_{22})}{{\ell_2}^2} \\ \frac{-r(k_{12}+k_{22})}{\ell_1\ell_2} & \frac{(k_{12}+k_{11}+k_{22}+k_{21})}{{\ell_1}^2} & \frac{k_{22}-k_{12}}{\ell_1\ell_2} \\ \frac{r(k_{12}-k_{22})}{{\ell_2}^2} & \frac{k_{22}-k_{12}}{\ell_1\ell_2} & \frac{k_{12}+k_{22}}{{\ell_2}^2} \end{pmatrix} \tag{4.22}$$

From this stiffness matrix, interesting robustness observations can be made [40]:

- Grasp equilibrium: If the stiffness matrix $\mathcal{K}_o$ is *full rank*, the grasp is a force closure grasp. Hence the grasp can establish a force equilibrium to hold the object.
  - Clearly, in this case, for hard finger contacts, the given stiffness matrix is full rank;
- Stability: If $\mathcal{K}_o$ is *positive definite*, then the grasp is stable. This stability refers to the natural preference of the grasping system to return to the equilibrium grasp after a (small) disturbance. As such, it respects the dynamic stability criterion as advocated in e.g. [39].
  - This analysis holds only for small perturbations, because no full dynamic system is investigated. Stiffness is considered dominant (w.r.t to inertia and damping) in quasi-static situations.

[13] Note: if applicable, contact compliance occurs in series with C_{fi}. Hence, if necessary, contact compliance can be simply included, by adding to C_{ci} a $n_{ci} \times n_{ci}$ contact compliance matrix expressed in the transmittable contact coordinates of contact i.

[14] Note: for e.g. underactuated fingers, this map is non-invertible. This is treated in Chapter 5 and Chapter 6.

  - The given stiffness matrix is full rank as long as $k_{ij} > 0$. For some combinations of non-positive k_{ij} (due to e.g. controller stiffness), $\mathcal{K}_o$ may become negative definite, i.e. an instable grasp;
  - Still, in literature, grasp performance metrics are discussed and have not settled yet. Some suggestions point towards usage of the grasp stiffness matrix as performance metric, as in e.g. [40]. The level of stability is measured by evaluating which hand/grasp creates a more stable grasp. More stable refers to a stronger tendency to return to an equilibrium after a disturbance, i.e. disturbance rejection. So, in fact, in that sense stability and disturbance rejection are equal. Some approaches measure the level of stability by comparing Eigen values of the stiffness matrix, which indicate how sensitive the grasp is for small perturbations in various directions. Be aware, to compare different grasps and hands based on Eigen values in different configurations, a coordinate free generalization is needed [68]. Nevertheless, the sign of Eigen values is not influenced by a choice of coordinates.

- Center of Compliance: The center of compliance is the position and orientation of a coordinate frame Ψ_{cc} in space. The frame is positioned such that defining the stiffness matrix in that frame renders a diagonal stiffness matrix. In that case, each of the non-zero elements of $\mathcal{K}_o$ defines the stiffness along the belonging principal direction of Ψ_{cc}. These elements are the principal stiffnesses. Also, an applied force along a line through the center of compliance does *not* produce moments on the object.

  - The position and orientation, together with the stiffness values give a direct interpretation of disturbance rejection in each of the directions.
  - Naturally, a negative stiffness value would imply pushing the grasp further away from its equilibrium after a disturbance. This is typically unstable behavior. Hence, if the stiffness values are positive, then $\mathcal{K}_o$ is positive definite, implying a stable grasp.

4.3.3 Disturbance analysis

The planar grasp example is finished by examining the center of compliance and the principal stiffnesses. Consider a coordinate transformation H^w_{cc}, which transforms the coordinates from Ψ_{cc} to Ψ_w, as given by Equation 4.11, and parameterized as follows:

$$H^w_{cc} = \begin{pmatrix} \cos(\theta_{cc}) & -\sin(\theta_{cc}) & x_{cc} \\ \sin(\theta_{cc}) & \cos(\theta_{cc}) & y_{cc} \\ 0 & 0 & 1 \end{pmatrix},$$

with x_{cc}, y_{cc} and θ_{cc} the positions and orientations of Ψ_{cc} w.r.t. Ψ_w. Then $\mathcal{K}_o$ changes coordinates by substituting the coordinate transformation (see Equation 4.12) into Equation 4.13, such that

$$(\delta W^{cc}_e)^T = \left(Ad_{H^w_{cc}}\right)^T \cdot \mathcal{K}_o \cdot Ad_{H^w_{cc}} \cdot \delta T^{cc,w}_o, \tag{4.23}$$

with

$$Ad_{H^w_{cc}} = \begin{pmatrix} 1 & 0 & 0 \\ y_{cc} & \cos(\theta_{cc}) & -\sin(\theta_{cc}) \\ -x_{cc} & \sin(\theta_{cc}) & \cos(\theta_{cc}) \end{pmatrix}.$$

The diagonalized stiffness matrix $\tilde{\mathcal{K}}_o$ becomes

$$\tilde{\mathcal{K}}_o = \left(Ad_{H^w_{cc}}\right)^T \mathcal{K}_o Ad_{H^w_{cc}}, \tag{4.24}$$

which is symmetric and must have zero elements in the off-diagonal elements. Hence, equating the left off-diagonal elements of $\tilde{\mathcal{K}}_o$ to zero, gives three equations for three unknowns: x_{cc}, y_{cc} and θ_{cc}, which, after solving for these variables, gives the center of compliance Ψ_{cc} as function of the grasp parameters ℓ_i, r and k_{ij}. The position of Ψ_{cc} is[15]:

$$\begin{aligned} x_{cc} &= \frac{r\cdot(k_{21}k_{12}+k_{11}k_{12}-k_{21}k_{22}-k_{11}k_{22})}{k_{11}k_{12}+4k_{12}k_{22}+k_{21}k_{12}+k_{11}k_{22}+k_{21}k_{22}} \\ y_{cc} &= \frac{4r\ell_1\cdot k_{22}k_{12}}{\ell_2\cdot(k_{11}k_{12}+4k_{12}k_{22}+k_{21}k_{12}+k_{11}k_{22}+k_{21}k_{22})} \end{aligned} \tag{4.25}$$

The principal stiffnesses are found on the diagonal of $\tilde{\mathcal{K}}_o$ by substituting these Ψ_{cc} positions and orientation in Equation 4.24. The orientation of Ψ_{cc} contains the directions that belong to each of the principal stiffnesses.

Through a series of examples, it will be shown how different stiffness values (k_{ij}) change the center of compliance and hence alter the displacement response (δT_o) effected by an applied external wrench $\delta W_e^w = (0 \quad 0 \quad f_y)$, see Figure 4.9. For the sake of simplicity of the example, some arbitrary values are chosen: $r = 0.5$, $\ell_1 = \ell_2 = 1$ and $k_{11} = k_{21} = k$.

- $k_{12} = k_{22} = k$: see Figure 4.9(a), Ψ_{cc} lies on the force application line. Hence, as shown, the object only displaces in y direction. This can be verified by calculating $\delta T_o^{w,w}$:

$$\delta T_o^{w,w} = \mathcal{K}_o^{-1} \cdot \delta W_e^w = \begin{pmatrix} 0 \\ 0 \\ \frac{1}{2k} \end{pmatrix} \cdot f_y$$

- $k_{12} > k_{22}$: see Figure 4.9(b), $k_{12} = 2k, k_{22} = k$. Ψ_{cc} does *not* lie on the force application line. Hence, as shown, the object displaces in y direction and rotates clockwise:

$$\delta T_o^{w,w} = \mathcal{K}_o^{-1} \cdot \delta W_e^w = \begin{pmatrix} -\frac{1}{4k} \\ 0 \\ \frac{3}{8k} \end{pmatrix} \cdot f_y$$

- $k_{12} < k_{22}$: see Figure 4.9(c), $k_{12} = k, k_{22} = 2k$. Ψ_{cc} does *not* lie on the force application line. Hence, as shown, the object displaces in y direction and rotates counter clockwise:

$$\delta T_o^{w,w} = \mathcal{K}_o^{-1} \cdot \delta W_e^w = \begin{pmatrix} \frac{1}{4k} \\ 0 \\ \frac{3}{8k} \end{pmatrix} \cdot f_y$$

- $k_{12} > k_{22}$: see Figure 4.10, some $k_{12} = 2k, k_{22} = k$ with $k = 5\ N/rad$ arbitrarily chosen. The applied wrench is now defined in Ψ_{cc} coordinates: $\delta W_e^{cc} = (0 \quad 10 \quad 10)$. Naturally, Ψ_{cc} does lie on the force application line. The resulting object displacement expressed in Ψ_{cc} is:

$$\delta T_o^{cc,w} = \tilde{\mathcal{K}}_o^{-1} \cdot \delta \left(W_e^{cc}\right)^T = \begin{pmatrix} 0.7 & 0 & 0 \\ 0 & 0.08 & 0 \\ 0 & 0 & 0.04 \end{pmatrix} \cdot \begin{pmatrix} 0 \\ 10 \\ 10 \end{pmatrix} = \begin{pmatrix} 0 \\ 0.8 \\ 0.4 \end{pmatrix}$$

  Clearly, as implied by the (inverse of the) principal stiffnesses in $\tilde{\mathcal{K}}_o^{-1}$, the x_{cc} direction is more compliant than the y_{cc} direction. Hence, although the applied force is equal in both

[15] The orientation θ_{cc} is not printed, because the general expression for the orientation θ_{cc} requires too much space on paper, while not necessary for the remaining discussion.

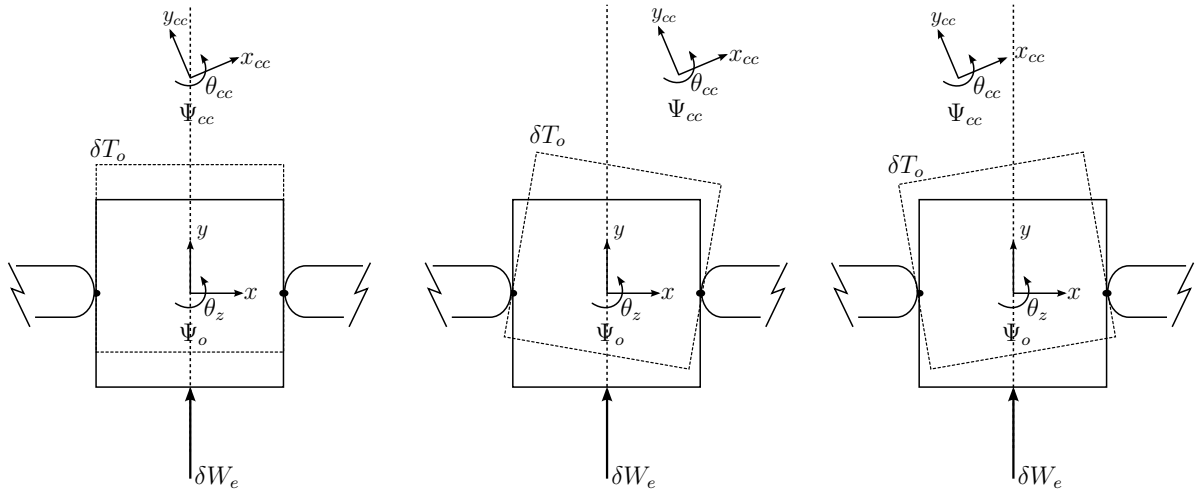

(a) $k_{12} = k_{22} = k$ (b) $k_{12} > k_{22}$ (c) $k_{12} < k_{22}$

Figure 4.9: 3DOF disturbance analysis for different robot finger stiffness values. The position of the center of compliance changes for each combination of robot finger stiffness values. Infinitesimal displacement δT_o is induced by external wrench: $\delta W_e = (0 \quad 0 \quad f_y)$.

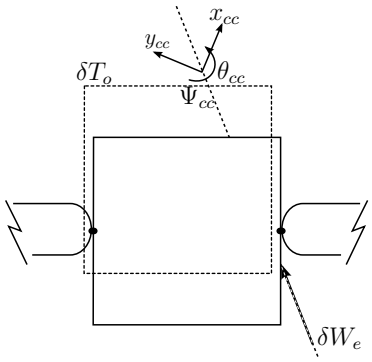

Figure 4.10: 3DOF disturbance situation for differentiated robot finger stiffness values ($k_{12} > k_{22}$). For the given position of Ψ_{cc} (as a result of stiffness settings), the applied force does not induce rotations. The principal stiffnesses, directly related to the actual stiffness of the springs, represent stiffness in each of the principal directions. In this situation, apparently, the principal stiffnesses are not equal, since the object displaces more in one direction than the other direction.

directions, $\delta T_o^{cc,w}$ shows a larger displacement along x_{cc}. In world coordinates (Ψ_w), this displacement is given by:

$$\delta T_o^{w,w} = Ad_{H_{cc}^w} \cdot \delta T_o^{cc,w} = \begin{pmatrix} 0 \\ -0.05 \\ 0.9 \end{pmatrix}$$

As depicted in Figure 4.10, the object translates along the force application line, without rotational displacement.

The examples have shown how different stiffness settings change the grasp configuration response for external disturbances, which can be utilized for the benefit of task-robustness. It was illustrated how to determine the grasp stiffness matrix, and its relation to robustness (grasp equilibrium, stability and disturbance rejection). It was shown how robot finger stiffness differentiations, alter the center of compliance and influence the configuration response to disturbances. The center of compliance and the notion of principal stiffnesses have shown to be helpful and intuitive in discussing the disturbance rejection properties.

Although not discussed, of course, also the other configuration parameters ℓ_i and r influence these characteristics. This clearly follows from the expressions for $\mathcal{K}_o$ and the position of Ψ_{cc}. Following the presented analysis, the reader can easily verify that the choice of contact model takes a major part in all of the discussed results above. For example, substituting the PwoF model for one of the two contacts will reduce the rank of $\mathcal{K}_o$, i.e. no force closure.

4.4 Variable Compliance for Skilled Movements

The analysis so far treated robustness properties for dexterous grasping. Also for the other hand tasks, dexterous manipulation and non-prehensile skilled movements, different stiffness preferences arise for different tasks.

For dexterous manipulation, one can imagine that some level of stiffness is needed to enforce the desired trajectory. At the same time, as presented in Section 4.3, some level of compliance for certain non task related directions supports to react compliantly (small contact force changes) against position disturbances.

In case of interactive motion tasks, also different preferences may arise; While applying a force on a surface (e.g. dust wiping, scratching somebodies bag, etc), the surface geometry may be difficult to measure. Hence, position disturbances are likely to happen. For these situations, being compliant in the force application direction supports to reduce force deviations. At the same time, stiffness in perpendicular directions can be useful to maintain a motion trajectory along which the force is applied to the surface. For some other interactive motion tasks, the hand must maintain its finger and hand configuration, while the arm is exerting a certain force to e.g. open a drawer, to manipulate a door handle or to turn a light switch. To apply this force at the right point, the finger configuration should not change. Hence, stiffness is required.

4.5 Conclusions

A series of examples for different grasping tasks and disturbance scenarios have been presented to show the differing stiffness preferences for different scenarios.

1DOF disturbance analysis conclusions With a 1DOF series elastic actuated gripper mechanism it is shown that grasping, holding and releasing while experiencing position, force or dynamic force disturbances require different stiffness values to optimally avert disturbances and avoid failure. Hence, already simple examples show that variable stiffness helps for disturbance rejection which improves task-robustness.

While aiming to maintain a certain applied force (force closure grasp strategy), different stiffness values will not change the total net force transferred to the object. However, the relative difference between several finger stiffness values does change the internal contact forces. Furthermore, the stiffness determines how much position deviation occurs under force disturbance. For position disturbances, a high stiffness value supports to reduce positioning errors, while low values help to increase end-effector positioning error tolerances (without exceeding contact force limits).

In industry, often one of the fingers is rigidly connected to the end-effectors, i.e. $k = \infty$. The presented analysis also holds for such anti-symmetric grasper mechanism, with different stiffness values for each of the fingers. Therefore, it is concluded that the examples have shown the relevance for variable stiffness.

3DOF disturbance analysis conclusions The 3DOF planar 'dexterous' grasper examples have shown how different stiffness settings change the grasp configuration response for external disturbances. The grasp stiffness matrix showed that in a multi-DOF situation, in which disturbances have different directions, depending on desired and allowable responses, different disturbance responses can be selected for different directions by differentiating robot finger stiffness values. Hence, altering robot finger stiffness values improves task-robustness.

The presented 3DOF treatment represents a simple multi DOF example. Already such a simple example clarifies the importance of understanding and changing robot finger stiffness for the huge set of possible situations in the unstructured environment. The treatment generalizes to a full 6DOF situation. As such, the examples served the objective to motivate the benefits of variable compliance for dexterous robot hands.

The structural robot finger compliance is preferably implemented mechanically (as opposed to implementing it by active control), as discussed in Section 3.3.2.

General conclusions The interest for variable compliance in dexterous grasping was elaborated on. An overview on illustrative 1DOF and 3DOF planar dexterous simple grasp examples showed that different scenarios require different stiffness settings for optimal (with respect to successful task completion) disturbance rejection and hence to improve task robustness. Furthermore, implementing variable compliance mechanically adds operational robustness by ensuring mechanical safety, without relying on bandwidth limited controllers. Hence, mechanical variable compliance is found to be of interest for novel dexterous robotic hand concepts and will therefore be utilized and investigated in this thesis.

In addition: through the application of a simple dexterous planar grasping example, known results from grasping literature have been synthetically combined and comprehensively presented as a digestible entrance point for people starting in the field of robotic grasping.

Chapter 5

Natural Space Decompositions

Besides variable compliance, Chapter 3 presented the aim to utilize underactuation for novel robotic finger concepts. To evaluate such robotic concepts through analysis and simulation, kinematic and dynamic models of the physical robotic system are used.

The involved kinematic relations are commonly modeled by mathematical maps. Specific examples of interest for this work are kinematic chains (e.g. robot fingers), modeled with a geometric Jacobian $J(q)$, the drive-train of an underactuated robotic finger, modeled through the transmission matrix T or actuation Jacobian J_a (see Section 3.2.5), and the grasp system of a grasped object, modeled by the grasp matrix G (see Section 4.3).

For kinematic analysis and control purposes, inverse kinematics may be needed. However, kinematic maps may be non-bijective, i.e. non-invertible. For example, the actuator Jacobian of underactuated robot fingers is non-bijective. As the kinematic map represents physical behavior, the physically equivalent solution refers to the unique solution of the inverse problem found in nature. These solutions are of particular interest for modeling and analyzing kinematics, since they describe the expected physical behavior. The weighted pseudo-inverse is of course a well-known solution for the inverse problem.

Nevertheless, physically equivalent results are less trivial.This chapter presents a study on non-bijective maps, aiming to derive and understand the unique *physically equivalent solution* for the inversion problem of these maps in kinematic modeling of physical systems. The presentation in this chapter aims to arrive at that particular solution (as a special case of the weighted pseudo-inverse) from a geometrical and physical perspective, closely related to the modeling problem. As such, the presented analysis tools are aimed to contribute in understanding the physical properties of robotic systems, and especially in robotic grasping and robotic finger analysis and design.

Furthermore, it will become clear that metrics attached to the spaces play a crucial role. The chapter contributes in discussing candidate metrics for physically equivalent inverse kinematic maps and introduces a mixed dissipation-mass metric for damped free motions. These results will be directly applied for the analysis and control of the robotic finger concept in the following chapter.

5.1 Inverses of non-Bijective Physical Maps

This section describes the inverse problem of non-bijective physical maps[1]. Based on this problem definition, the section ends by presenting an outline of the remaining chapter.

[1]Note: the notion of phyiscal maps is defined later, see Definition 5.5.

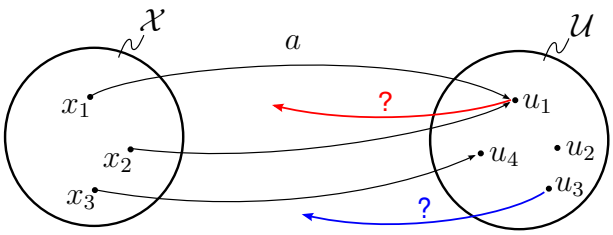

Figure 5.1: Non-bijective map a. Inversion problem.

5.1.1 General non-bijective map

Consider two vector spaces $\mathcal{X} \subseteq \mathbb{R}^n$ and $\mathcal{U} \subseteq \mathbb{R}^m$ with properly defined inner-products. Hence, these vector spaces are Hilbert spaces. In general any abstract space could be considered. For the presented discussion in this chapter, considering Hilbert spaces suffices. Furthermore, consider a linear map a that takes elements from $\mathcal{X}$ to $\mathcal{U}$:

$$a : \mathcal{X} \mapsto \mathcal{U} \quad ; \quad u = a(x), \qquad u \in \mathcal{U}, x \in \mathcal{X} \tag{5.1}$$

In general, for such a map, different classes can be distinguished by the following definitions:

Definition 5.1 (surjective)**.** *A map a, as defined in Equation 5.1, is called surjective if every element of $\mathcal{U}$ is mapped to by at least one element of $\mathcal{X}$ (also called* **onto***).*

Definition 5.2 (injective)**.** *A map a, as defined in Equation 5.1, is called injective if elements of $\mathcal{U}$ are mapped to by at most one element of $\mathcal{X}$ (also called* **one-to-one***).*

Definition 5.3 (bijective)**.** *A map a, as defined in Equation 5.1, is called bijective if it is injective* **and** *surjective.*

Thus, a non-bijective map is either non-surjective or non-injective or both.

The inverse map[2] of a, *if it exists*, is indicated by $a^{-1} : \mathcal{U} \mapsto \mathcal{X}$, such that

$$a \circ a^{-1} = id_{\mathcal{U}}, \quad a^{-1} \circ a = id_{\mathcal{X}},$$

where $id_{\mathcal{X}}$, $id_{\mathcal{U}}$ represent the identity elements on $\mathcal{X}$ and $\mathcal{U}$, respectively. Thus, for a given $u_p \in \mathcal{U}$, the inverse map a^{-1} selects a solution $x_s \in \mathcal{X}$ for which $a(x_s) = u_p$. In order for this inverse map to exist, be uniquely defined and be defined for all $u \in \mathcal{U}$, a must be bijective.

However, in general, the map a can be non-bijective. For example, having a non-injective and non-surjective map, implies that different elements in $\mathcal{X}$ map to the same element in $\mathcal{U}$ as well as that some elements in $\mathcal{U}$ can never be reached. This is illustrated in Figure 5.1. Clearly, for a being non-injective, for some $u_p \in \mathcal{U}$ **multiple** inverse elements $x_s \in \mathcal{X}$ give $a(x_s) = u_p$ (the inverse solution is not unique), while a being non-surjective, implies that for some $u_p \in \mathcal{U}$ there exists **no** inverse element $x_s \in \mathcal{X}$ that gives exactly $a(x_s) = u_p$. Exact inverse solutions are defined in the following definition.

Definition 5.4 (exact inverse solution)**.** *Consider the map a as defined in Equation 5.1. For a given $u_p \in \mathcal{U}$, any $x_s \in \mathcal{X}$ for which $a(x_s) = u_p$, is called an exact inverse solution of $u_p \in \mathcal{U}$.*

Conclusively, for non-surjective maps, no exact inverse solution exists, while for non-injective maps, multiple exact non-unique inverse solutions exist. Hence, for a non-bijective map, the inverse map of a is non-trivial and requires a pseudo-inverse map, denoted by $a^{\#}$.

[2] See any textbook on calculus.

5.1.2 Physical map

In this chapter, the map a, as given in Equation 5.1, is considered to represent a map in a physical system. To clarify this discussion, the following two definitions are introduced and used throughout the chapter.

Definition 5.5 (physical (vector)[3] map)**.** *Consider a physical system Σ. A map $a : \mathcal{X} \mapsto \mathcal{U}$, where $\mathcal{X}$ and $\mathcal{U}$ have a mathematical structure of a Hilbert space, is called a physical vector map if $\mathcal{X}$ and $\mathcal{U}$ are representing physical quantities in Σ, i.e. velocities and forces.*

Examples of physical maps of interest for this work are the geometric Jacobian $J(q)$, which models a kinematic chain (found in e.g. robot fingers), the transmission matrix T or actuation Jacobian J_a (see Section 3.2.5), which models the drive-train of an underactuated robotic finger and the grasp matrix G, which models the grasp system of a grasped object (see Section 4.3).

5.1.3 Problem definition

Clearly, as holds for the general maps discussed in Section 5.1.1, also physical maps can be non-bijective. Well-known pseudo-inverses are available to produce pseudo-inverse solutions for non-bijective maps [69]. However, especially in the case of physical maps, these pseudo-inverses are often misused, due to their pure numerical interpretation without considering the actual physical representation of the problems that are solved. This is clearly discussed in e.g. [70, 71], where the authors advocate coordinate invariant pseudo-inverses (i.e. the results should not depend on the choice of coordinates).

In physical systems, nature selects a unique inverse solution, see e.g. Section 5.3. Hence, for a pseudo-inverse problem, mathematically there exist multiple inverse solutions, while nature 'selects' one particular unique solution, if it concerns inverting a physical map. This is captured in the notion of a physically *equivalent* inverse map, as is introduced in this work.

Definition 5.6 (physically equivalent inverse map)**.** *Consider a physical map a, as defined in Definition 5.5. A pseudo-inverse map $a^{\#} : \mathcal{U} \mapsto \mathcal{X}$ that maps any $u_p \in \mathcal{U}$ to the inverse solution $x_s \in \mathcal{X}$, which coincides with the actual unique solution found in the real physical system, is called the physically equivalent inverse map.*

Remark 5.1. *For a bijective physical map, the physically equivalent inverse map coincides with its unique inverse map.*

The physically equivalent inverse map is needed for the analysis of physical systems which encompass physical maps. In this work, this is used in the subsequent chapters, where the insights on the physically equivalent inverse map are used for analyzing the novel robotic finger finger concept and for controller synthesis. Therefore, the goal of this chapter is:

1. to describe the weighted generalized (pseudo-) inverse map;
2. to describe the physically equivalent inverse map as particular instantiation of the weighted generalized (pseudo-) inverse;

[3] Abuse of notation: throughout the chapter, the physical vector map will be called physical map.

The weighted generalized (pseudo-) inverse is well described in literature (e.g. [69, 72, 73, 71]). Hence, the explanation and description of the the weighted generalized (pseudo-) inverse map in this chapter (goal 1) does not yield new results. It presents the weighted generalized inverse from a geometrical point of view for completeness of the description and understanding of physically equivalent inverse maps.

Remark 5.2. *Clearly, a physically equivalent inverse map must be coordinate invariant. Vice-versa, being a coordinate invariant inverse map is not sufficient for being a physically equivalent inverse map.*

As explained in [70, 71], nature does not care about coordinates. Hence, any (pseudo-) inverse of a physical map must at least be coordinate invariant. Nevertheless, it is important to realize that for any physical map, many coordinate invariant pseudo-inverse maps may exists [71], while only one of these many coordinate invariant solutions is the physically equivalent inverse map. Thus, the goal is not just to find a coordinate invariant pseudo-inverse, but to understand and describe the particular physically equivalent inverse map.

5.1.4 Chapter outline

The chapter is organized as follows. First, Section 5.2 extends a bit more on the notion of physical maps as introduced in Definition 5.5. Then, Section 5.3 gives an example of a physically equivalent solution for the inverse relation of a map in a physical system, i.e. the grasp system. Throughout the chapter, the grasp system is used as a case example to naturally explain the presented material. Next, a general geometrical description of non-bijective mappings is given in Section 5.4, from which the general mathematical inverse follows in Section 5.5.

Then in Section 5.6, the results are applied to the example grasp system, which shows how the general inverse maps relates to the physically equivalent solution. It is shown that the choice of metrics plays a central role. Next, Section 5.7 introduces a particular class of dual Hilbert spaces, physical dual spaces, and defines physical dual elements to show the physical interpretation of physical inverse problems. This understanding supports the analysis and clarifies physically ill-posed inverse problems. Also, physical dual elements rely on properly chosen metrics.

Finally, Section 5.8 introduces some physical dual spaces together with their associated metric, ready to be applied for specific modeling situations of mechanical systems. For a particular modeling situation, damped free motions, the physical dual space and associated metric need further analysis, which is presented in Section 5.9 leading to a novel metric and specific insights. Insights and results of this chapter will be used for the analysis and controller design of the underactuated robot finger concept.

5.2 Properties of Physical Maps

This section presents some physical interpretations that follow from the mapping properties of a physical map a, as defined in Definition 5.5. These interpretations will be used and referred to throughout the chapter.

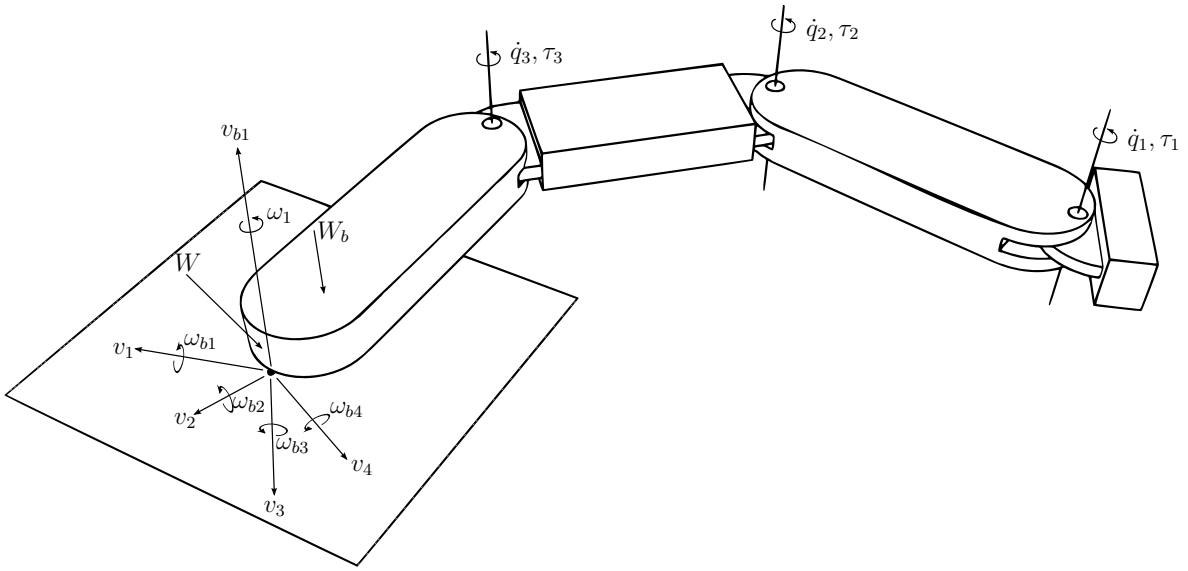

Figure 5.2: Example of robotic finger with three joints. The geometric Jacobian represents a physical map, defined by: $J(q) : T_q\mathcal{Q} \mapsto se(3) \quad ; \quad T = J(q) \cdot \dot{q} \qquad T \in se(3), \dot{q} \in T_q\mathcal{Q}, q \in \mathcal{Q}$, where $T \in se(3)$ are the twists of the finger-tip containing translational velocities and rotational velocities $T = (\omega^T, v^T)^T$ (see e.g. [67]) and $\dot{q}, \tau$ are the joint velocities and joint torques respectively. Note that $\operatorname{im} J(q) \subset se(3)$. Hence, there are blocked motions: For the presented configuration q, the translational velocity v_{b1} is blocked and the rotational velocities $\omega_{b1}, \omega_{b2}, \omega_{b3}, \omega_{b4}$ are blocked and hence modeled to be non-existent. Whereas the translational velocities v_1, v_2, v_3, v_4 and the rotational velocity ω_1 can exist. $W_b \in se^*(3)$ represents an externally applied wrench at the finger-tip, which contains only force components along the axis v_{b1}, whereas $W \in se^*(3)$ represents any wrench applied at the finger.

5.2.1 Non-surjective physical map

The elements in $\mathcal{U}$ that are reachable through a, are contained in the image of a, denoted by $\operatorname{im} a$ and defined by:

$$\operatorname{im} a = \{u \in \mathcal{U} \mid u = a(x), x \in \mathcal{X}\}$$

Consider the physical map a to be non-surjective. Hence, not all elements in $\mathcal{U}$ are mapped to, which implies that the image of a non-surjective map a is a subset of $\mathcal{U}$: $\operatorname{im} a \subset \mathcal{U}$. Hence, searching for the inverse of any $u_p \notin \operatorname{im} a$, implies that one is searching for an $x_s \in \mathcal{X}$ that would have to ignore the modeled physical map properties to produce (through map a) the requested u_p. Clearly, the modeled physical properties can not be ignored and hence no (exact) $x_s \in \mathcal{X}$ exists.

As stated in Definition 5.5, $\mathcal{U}$ and $\mathcal{X}$ represent either forces or velocities in the physical system Σ. As shown above, a non-surjective physical map a induces a particular subspace on $\mathcal{U}$, i.e. the image of a. Physical interpretations for this subspace are given below for both physical quantities. Clarifying examples are given afterwards.

Definition 5.7 (blocked motions)**.** *Consider physical map a, as defined in Definition 5.5, and consider the according Hilbert spaces $\mathcal{X}$ and $\mathcal{U}$, as defined in Definition 5.5, to represent* **velocities***. The velocities $u \notin \operatorname{im} a \subset \mathcal{U}$ are called blocked motions. These are the motions in $\mathcal{U}$ which can not be achieved by any motion in $\mathcal{X}$.*

Example: consider the robot finger as shown in Figure 5.2. The robot finger is a physical system. The geometric Jacobian $J(q)$, which is a physical map in the robot finger, maps the joint velocities $\dot{q}$ to the finger-tip twist T:

$$J(q) : T_q\mathcal{Q} \mapsto se(3) \quad ; \quad T = J(q) \cdot \dot{q} \qquad T \in se(3), \dot{q} \in T_q\mathcal{Q}, q \in \mathcal{Q},$$

with $\mathcal{Q}$ the joint configuration space. As shown in Figure 5.2, due to the design of the finger $\operatorname{im} J(q) \subset se(3)$. Hence, some finger-tip motions can not exist. These are called blocked motions, indicated by subscript $_b$ in Figure 5.2. Note: $J(q)$ depends on the configuration q. Hence, the indicated blocked motions hold for the given configuration.

Definition 5.8 (non-producible forces)**.** *Consider physical map a, as defined in Definition 5.5, and consider the according Hilbert spaces $\mathcal{X}$ and $\mathcal{U}$, as defined in Definition 5.5, to represent* **forces***. The forces $u \notin \operatorname{im} a \subset \mathcal{U}$ are called non-producible forces. These are the forces in $\mathcal{U}$ which can not be produced or generated (and hence can not be resisted) by any force in $\mathcal{X}$.*

Example: consider the grasp matrix $G : \mathcal{F}_c \to \mathcal{W}_{co}$ as given in Equation 5.4, which is a physical map for the general grasp system. The grasp system is a physical system, illustrated in Figure 5.3. Assume, $\mathcal{W}_{co} \subset se^*(3)$, such that $\operatorname{im} G \subset se^*(3)$. Then, any applied disturbance wrench $W_d \notin \operatorname{im} G$ can not be resisted by producing any set of contact forces $f_c \in \mathcal{F}_c$. These $W_d \notin \operatorname{im} G$ are called non-producible wrenches.

Example: consider again the robot finger as shown in Figure 5.2. The transposed geometric Jacobian, $J^T(q)$ maps a wrench $W \in se^*(3)$ on the finger-tip to the joint torques τ:

$$J^T(q) : se^*(3) \mapsto T_q^*\mathcal{Q} \quad ; \quad \tau = J^T(q) \cdot W \qquad W \in se^*(3), \tau \in T_q^*\mathcal{Q}, q \in \mathcal{Q}.$$

Notice that $\operatorname{im} J^T(q) = T_q^*\mathcal{Q}$, which implies that there exists no $\tau \notin \operatorname{im} J^T(q)$. Hence, any $\tau \in T_q^*\mathcal{Q}$ can be produced through some $W \in se^*(3)$, i.e. there exist no wrench $W \in se^*(3)$ that can induce non-producible joint torques.

Related to the physical system Σ, in this work, the inverse problem of searching the inverse element $x_s \in \mathcal{X}$ for a given element $u_p \in \mathcal{U}$ is categorized by the following definition.

Definition 5.9 (physically ill-posed inverse problem)**.** *Consider physical map a, as defined in Definition 5.5, and the according Hilbert spaces $\mathcal{X}$ and $\mathcal{U}$, as defined in Definition 5.5, which represent physical quantities in a mechanical system. Then, trying to find the inverse element $x_s \in \mathcal{X}$ for a given $u_p \in \mathcal{U}$ for the given physical map a, is said to be a physically ill-posed inverse problem if the given $u_p \in \mathcal{U}$ physically violates physical laws of the physical system Σ with physical map a.*

Remark 5.3. *Consider a physical system Σ with physical map a (Definition 5.5), which is assumed to map* **velocities***. Furthermore, it is assumed that velocities can be applied on $\mathcal{U}$. Then, proposing to apply any blocked motion $u_p \notin \operatorname{im} a$ and trying to find the according inverse element $x_s \in \mathcal{X}$, is considered a physically ill-posed inverse problem.*

Example: consider again the robot finger shown in Figure 5.2 with Geometric Jacobian $J(q)$. As discussed previously, there are blocked motions in the physical system. Hence, proposing to apply a twist $T \notin \operatorname{im} J(q)$ and searching for the joint velocities $\dot{q}$ that belong to this twist generates a *physically ill-posed inverse problem*. This is physically ill-posed, because such a twist can not be applied without violating physical laws of the modeled system (with physical map $J(q)$), since there are no motions $\dot{q} \in T_q\mathcal{Q}$ which allow for the proposed twist.

In order to make it a physically well-posed problem, extra DOFs should be modeled by introducing extra joints, in such a way that the proposed twist is not a blocked motion anymore.

Remark 5.4. *Consider a physical system Σ with physical map a (Definition 5.5), which is assumed to map* **forces**. *Furthermore, it is assumed that forces can be applied on $\mathcal{U}$. Then, proposing to apply any force $u_p \in \mathcal{U}$, including non-producible forces $u_p \notin \operatorname{im} a$, and trying to find the according inverse element $x_s \in \mathcal{X}$, does not generate a physically ill-posed inverse problem.*

Example: consider again the grasp matrix $G : \mathcal{F}_c \to \mathcal{W}_{co}$ as given in Equation 5.4, which is a physical map for the general grasp system. The grasp system is a physical system, illustrated in Figure 5.3. Assume, $\mathcal{W}_{co} \subset se^*(3)$, such that $\operatorname{im} G \subset se^*(3)$. As previously noticed, any applied disturbance wrench $W_d \notin \operatorname{im} G$ can not be resisted any set of contact forces $f_c \in \mathcal{F}_c$. Nevertheless, applying such a wrench does not violate any physical law in the system. The effect would be that the object leaves equilibrium.

If a physically ill-posed inverse problem occurs, clearly, the model is incompetent for the posed problem. Throughout this chapter, several more examples will arise that may help to clarify the definitions and show the importance of their implications.

5.2.2 Non-injective physical map

Consider the physical map a to be non-injective, such that multiple elements in $\mathcal{X}$ map to the same element in $\mathcal{U}$. Hence, the elements $u_p \in \mathcal{U}$ have multiple inverse elements $x_s \in \mathcal{X}$, which all produce exactly the requested $u_p \in \mathcal{U}$. This raises the question which element to choose as solution for the inverse problem.

Mathematically (numerically), one can choose any $x_s \in \mathcal{X}$ as inverse solution. However, as stated in Section 5.1.3, nature has one particular solution for the inversion of physical map a, i.e. the physically equivalent inverse solution (see Definition 5.6). In this work, these solutions are of interest, since the mappings that are studied originate from physical systems.

The elements in $\mathcal{X}$ that are mapped to zero in $\mathcal{U}$ through a, are contained in the kernel of a, denoted by $\ker a$ and defined by:

$$\ker a = \{x \in \mathcal{X} \mid a(x) = 0\}$$

The physical map a is considered to be a non-injective map. Hence, multiple elements in $\mathcal{X}$ map to the same element in $\mathcal{U}$. This implies that the kernel of the non-injective physical map a is a non-empty subset of $\mathcal{X}$: $\ker a \subset \mathcal{X}$.

This implication is intuitively verified by considering two elements $x_1, x_2 \in \mathcal{X}$ which both map to the same $u_1 \in \mathcal{U}$, where $x_1 \notin \ker a$, such that $a(x_1) = u_1$. Take any $x_k \in \ker a$

($a(x_k) = 0$) and notice that x_2 must be any linear combination of x_1 and any x_k, i.e. $x_2 = x_1 + x_k$ such that indeed:

$$a(x_2) = a(x_1 + x_k) = a(x_1) + a(x_k) = a(x_1) = u_1.$$

Clearly, if the kernel of a is empty, a is injective.

As stated in Definition 5.5, $\mathcal{U}$ and $\mathcal{X}$ represent either forces or velocities in the physical system Σ. As shown above, a non-injective physical map a induces a particular subspace on $\mathcal{X}$, i.e. the kernel of a. Physical interpretations for this subspace are given below for both physical quantities. Clarifying examples are given afterwards.

Definition 5.10 (null-space motions)**.** *Consider physical map a, as defined in Definition 5.5, and consider the according Hilbert spaces $\mathcal{X}$ and $\mathcal{U}$, as defined in Definition 5.5, to represent* **velocities***. The velocities $x \in \ker a \subset \mathcal{X}$ are called null-space motions. These are the motions in $\mathcal{X}$ which do not affect any motion in $\mathcal{U}$.*

Definition 5.11 (self-balanced forces)**.** *Consider physical map a, as defined in Definition 5.5, and consider the according Hilbert spaces $\mathcal{X}$ and $\mathcal{U}$, as defined in Definition 5.5, to represent* **forces***. The forces $x \in \ker a \subset \mathcal{X}$ are called self-balanced forces. These are the forces in $\mathcal{X}$ which do not affect any force in $\mathcal{U}$.*

Example: consider again the robot finger as shown in Figure 5.2. Notice that an externally applied force $W_b \in se^*(3)$, which contains only force components along the translational axis v_{b1}, does **not** induce any non-zero torque around the joint axes. Furthermore, it was already shown that motions along this direction are blocked. Hence, an externally applied force along the translational axis v_{b1} does not produce any torque around the joint axes, while it also does not induce any motion. Therefore, it must hold that the force is equilibrated, without any torque action around the joint axes. Hence, the externally applied force is said to be self-balanced by the modeled mechanism. Thus, it may be expected that $W_b \in \ker J^T(q)$.

The given physical interpretations and definitions (in particular Definition 5.7, 5.8 and 5.9) will be of importance for the discussion on physically equivalent inverses and the understanding of physical implications of posed inverse problems, rather then merely considering the inverse problems as mathematical problems. Throughout the chapter, examples are used to further clarify the concepts.

5.3 Physical Example: The Grasp System

As introduced, the topic of this chapter is the study of non-bijective mappings in model representations of physical systems. To give a motivating example of such a mapping, this section discusses the grasp system. A simple example is used to illustrate most mathematical concepts as discussed along this chapter. Hence, the example serves to clarify ideas and concepts.

5.3.1 The general grasp system

The inversion problem of the grasping system is presented as motivation for the discussion on non-bijective kinematic maps. Section 4.3.1 presented the sub-grasp-matrix G_i for contact i

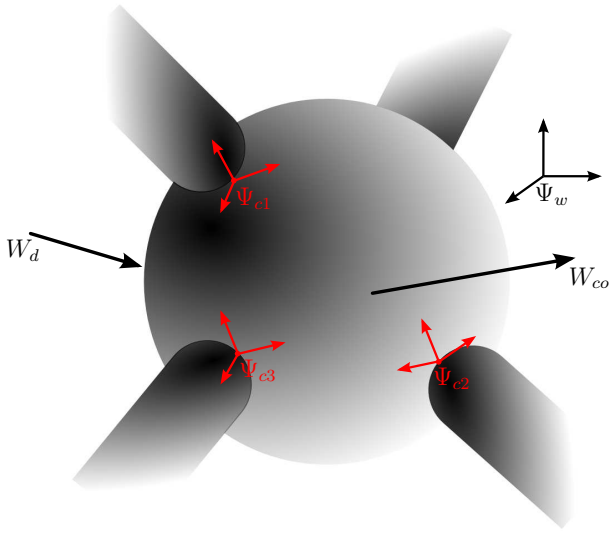

Figure 5.3: General grasp system with $n_c = 4$ contact points, i.e. three contact frames are shown; Ψ_{c1}, Ψ_{c2} and Ψ_{c3}. All contact forces f_c together generate a total wrench on the object: $W_{co}^T = G \cdot f_c^T \quad \in se^*(3)$. A possible external disturbance wrench is denoted by $W_d \in se^*(3)$.

as coordinate change from contact coordinates Ψ_{ci} to some chosen world coordinate frame Ψ_w (see Equation 4.8). Instead of a planar grasp, now a general 6 DOF grasp with n_c contact points is considered as shown in Figure 5.3.

The same notations apply. However, the twist $T_i^{k,j}$ and wrench W_i^k are now 6 DOF vectors and co-vectors, defined as in e.g. [63, 64]:

$$T_i^{k,j} \in se(3)$$

$$W_i^k \in se^*(3)$$

This also coincides with other known usages in grasping, such as in [65].

The *complete*[4] grasp matrix $\tilde{G}$ is constructed by following [65] and recalling Equation 4.10 and the sub-grasp matrix as given in Equation 4.8:

$$\tilde{G} = \begin{pmatrix} G_1 & \dots & G_{n_c} \end{pmatrix}$$

such that with all wrenches stacked together into one co-vector, Equation 4.10 becomes:

$$\left(W_{co}^w\right)^T = \begin{pmatrix} G_1 & \dots & G_{n_c} \end{pmatrix} \cdot \begin{pmatrix} \left(W_{co,1}^1\right)^T \\ \vdots \\ \left(W_{co,ci}^{ci}\right)^T \end{pmatrix} \tag{5.2}$$

$$= \tilde{G} \cdot \left(W^{ci}\right)^T, \tag{5.3}$$

with W^{ci} a $6n_c$ co-vector containing all transmitted wrenches due to all n_c contact interactions and $W_{co}^w \in se^*(3)$ is the total wrench on the object due to contact interactions (expressed in *any* arbitrary frame Ψ_w).

Furthermore, the n_c contact models $\mathcal{H}_i$ (see Equation 4.4) can be taken together into one contact constraint matrix $\mathcal{H}$:

$$\mathcal{H} = \text{blockdiag}(\mathcal{H}_1, \dots, \mathcal{H}_{n_c})$$

[4]Note: 'Complete' refers to including all $6n_c$ twist components [65].

Notice that in this general 6 DOF case, also soft finger contact (SF) models can exist (see Section 4.3.1) and $\mathcal{H}_i$ has become a $n_{ci} \times 6$ matrix, see e.g. [65][5]. Taking together the contact models and the complete grasp matrix, results in the well-known *grasp matrix* G of the grasp system:

$$G : \mathcal{F}_c \rightarrow \mathcal{W}_{co}, \tag{5.4}$$

with

$$G = \tilde{G}\mathcal{H}^T \qquad \in \mathbb{R}^{6\times n_t},$$

where $\mathcal{F}_c \subset \mathbb{R}^{1\times n_t}$ is the space of transmittable contact forces with n_t the total number of transmittable contact force components:

$$n_t = \sum_{i=1}^{n_c} n_{ci}$$

Hence,

$$(W_{co}^w)^T = G \cdot f_c^T, \qquad f_c \in \mathcal{F}_c \tag{5.5}$$

with co-vector

$$f_c = (f_{c1} \quad \dots f_{cn_{ci}}).$$

Dually, as shown in Equations 4.4 and 4.8, the transpose (G^T) maps the twist of the object to the transmittable contact velocities:

$$\dot{\epsilon} = G^T \cdot T_o^{w,w} \qquad T_o^{w,w} \in se(3), \dot{\epsilon} \in T_{\epsilon_c}\mathcal{E}_c, \tag{5.6}$$

with $\dot{\epsilon}^T = (\dot{\epsilon}_1 \quad \dots \quad \dot{\epsilon}_{n_{ci}})$, where $T_\epsilon\mathcal{E}_c \subset \mathbb{R}^{n_t\times 1}$ is the space of all transmittable contact velocities, which is tangent to the contact configuration manifold $\mathcal{E}_c$ at contact configuration $\epsilon \in \mathcal{E}_c$[6]. Notice that $\mathcal{F}_c = T_\epsilon^*\mathcal{E}_c$, which is the co-tangent space of $\mathcal{E}_c$ at contact configuration $\epsilon \in \mathcal{E}_c$[7]. Hence the elements $f_c \in \mathcal{F}_c$ are co-vectors.

In general, the object can be subject to an external disturbance wrench $W_d \in se^*(3)$. The total wrench on the object is denoted by $W_o \in se^*(3)$, such that[8]:

$$W_o^T = W_{co}^T + W_d^T = G \cdot f_c^T + W_d^T. \tag{5.7}$$

Notice that the grasp is in equilibrium if $W_o = 0$.

5.3.2 General grasp inversion problem

Consider either the case that the grasp task is to maintain equilibrium for a certain disturbance W_d, or to induce motion on the object due to contact interaction, i.e. $W_o \neq 0$. Equation 5.7 shows that it is necessary to generate either $W_{co} = -W_d$ or a certain desired $W_{co} = W_o \neq 0$.

In any case, for a given desired $W_{co} \in se^*(3)$, suitable contact forces f_c have to be found that generate the desired W_{co}. From Equation 5.4 it is clear that this involves (pseudo-) inversion of the map G (grasp matrix), such that the (pseudo-) inverse map:

$$G^\# : se^*(3) \mapsto \mathcal{F}_c, \tag{5.8}$$

produces contact forces $f_c \in \mathcal{F}_c$ that must generate the desired wrench $W_{co}^T = G \cdot f_c^T$.

[5]Note: without any difference, in [65] transposed notations are used.
[6]Note: notation $T_y\mathcal{Y}$ denotes a tangent space of the manifold $\mathcal{Y}$ at element $y \in \mathcal{Y}$, see e.g. [74]
[7]Note: notation $T_y^*\mathcal{Y}$ denotes a co-tangent space of the manifold $\mathcal{Y}$ at element $y \in \mathcal{Y}$, see e.g. [74]
[8]Note: if coordinates are considered, to sum these wrenches, they must be expressed in the same coordinates.

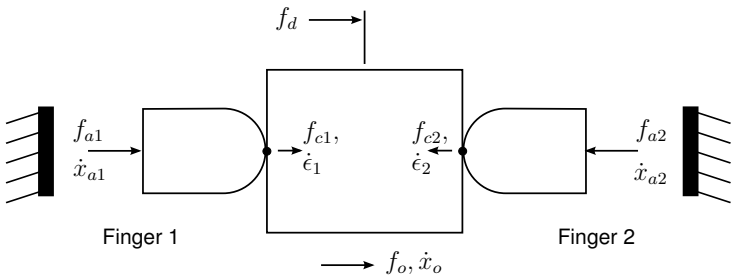

Figure 5.4: 1 DOF Grasping system; finger 1 and finger 2 exert contact forces f_{c1} and f_{c2} on the object. According finger-tip contact displacement is modeled by ϵ_{ci} and contact velocity $\dot{\epsilon}_{ci}$. Contact forces are generated by ideal force actuators f_{ai}. The actuator displacements are represented by $\dot{a}_i$. The object is subject to a disturbance force f_d. The total force on the object is $f_o = f_d + G \cdot f_c^T$. The object displacement is given by $\dot{x}_o$. In this illustrated situation, the fingers, the object and the contacts are considered rigid. Note that the arrow heads point in the positive directions of the variables.

However, the grasp matrix in general can be a non-bijective map. As discussed in Section 5.1, for such maps, the inverse relation must be a pseudo-inverse. Thus, the model representation of the kinematics of the physical grasp system is one of the examples for which non-bijective maps may arise.

Throughout this chapter, this general grasp system together with a simple grasp example are used to clarify several important notions on inverse relations in physical modeling. The simple grasp example is introduced in the next section.

5.3.3 Example: A simple grasp system

Consider the simple single DOF grasp system as presented in Figure 5.4. Only forces and displacements in the horizontal direction are considered. This grasp system is a simple instantiation of the general grasp system as discussed above.

The complete treatment of this simple grasp system example considers steady-state situations. For the example at hand, steady state is reached when velocities and accelerations are zero. Any disturbance force or a change of actuation forces induces accelerations. Naturally, in order to reach a steady state situation after applying such forces, damping is needed in the system. Hence, although not illustrated in Figure 5.4 and not mentioned anymore hereafter, damping is assumed to be present in the system to reach steady state. Note that damping does not influence the forces in the grasp system in steady state situation. Hence, the presented results are not affected by this assumption.

5.3.4 Example: Simple grasp system model

Since a simple 1DOF model is treated, the contact model must be a point-contact-without-friction (PwoF) contact model (see also e.g. Equation 4.4). Hence, for each of the two contacts, one transmitted force/velocity component is found, i.e. $n_t = 2$. In accordance with the presented general grasp system, the following variables and vector spaces are used for the model of the simple grasp system, as shown in Figure 5.4:

$$\begin{array}{lcl@{\qquad\qquad}lcl} f_c & \in & \mathcal{F}_c = T^*\mathcal{E}_c \subseteq \mathbb{R}^2 & f_d, f_o, f_{co} & \in & \mathcal{F}_E = T^*\mathcal{X}_x \subseteq \mathbb{R} \\ \epsilon_c & \in & \mathcal{E}_c \subseteq \mathbb{R}^2 & x_o & \in & \mathcal{X} \subseteq \mathbb{R} \\ \dot{\epsilon}_c & \in & T_\epsilon\mathcal{E}_c \subseteq \mathbb{R}^2 & \dot{x}_o & \in & T_x\mathcal{X} \subseteq \mathbb{R} \end{array} , \tag{5.9}$$

with

$$f_c = \begin{pmatrix} f_{c1} & f_{c2} \end{pmatrix}, \quad \dot{\epsilon} = \begin{pmatrix} \dot{\epsilon}_1 \\ \dot{\epsilon}_2 \end{pmatrix}.$$

and f_d an object disturbance force, f_{co} the force on the object due to contact interactions at all contacts and f_o the total force on the object. Furthermore, x_o and $\dot{x}_o$ are the object position on the object configuration space $\mathcal{X}$ and object velocity on the tangent space $T_x\mathcal{X}$, respectively. Whereas ϵ_c and $\dot{\epsilon}_c$ are the contact positions on the contact position space $\mathcal{E}_c$ and the contact velocities on the tangent space $T_\epsilon\mathcal{E}_c$, respectively.

Intuitively, one can see that the contact forces f_{ci} add up (taking into account the choice of references, see Figure 5.4) to create a force on the object, hence the grasp matrix is found at once:

$$G = \begin{pmatrix} 1 & -1 \end{pmatrix} \tag{5.10}$$

and the kinematics of the grasp system are described by (see Equation 5.7):

$$f_o = f_d + f_{co} = f_d + G \cdot f_c^T. \tag{5.11}$$

Dually, for the contact velocities the kinematics are given by:

$$\dot{\epsilon} = G^T \cdot \dot{x}_o, \tag{5.12}$$

which shows, as expected, that the contact velocities are **constrained** to the object velocities (assuming contact is maintained): $\dot{\epsilon}_1 = \dot{x}_o, \quad \dot{\epsilon}_2 = -\dot{x}_o$.

Infinitesimal variations

Remark 5.5. *In general, $\mathcal{X}$ and $\mathcal{E}_c$ van be curved manifolds. Instead of considering (contact and object) velocities on the tangent spaces $T_\epsilon\mathcal{E}_c$ and $T_x\mathcal{X}$, one could consider* **infinitesimal** *displacements $\delta\epsilon$ and δx_o around an equilibrium configuration ϵ and x_o.*

An infinitesimal displacement, as proposed in the above given remark, is found through a scalar multiplication of the velocities ($\dot{\epsilon}$ or $\dot{x}$) with an infinitesimal time-step dt: $\delta x_o = \dot{x}_o \cdot dt$, $\delta\epsilon = \dot{\epsilon} \cdot dt$. Note that dt must be infinitesimal, since a general non-linear space is a curved space, such that time scaling only holds locally without effecting the configuration. The scalar multiplication involves only scaling of the elements, hence these infinitesimal displacements are still elements of the tangent spaces: $\delta x_o \in T_\epsilon\mathcal{E}_c$, $\delta x_o \in T_x\mathcal{X}$.

Naturally, also the tangent map G^T applies locally for infinitesimal displacements around an equilibrium configuration ϵ, x_o:

$$\delta\epsilon = G^T \cdot \delta x_o$$

and for the co-tangent elements, infinitesimal changes of the forces are given by:

$$\delta f_o = \delta f_d + G \cdot \delta f_c^T$$

Linear variations Note that, in this case, since $\mathcal{X}$ and $\mathcal{E}_c$ are linear spaces and since the (co-)tangent mappings G,G^T are linear constant maps, the previously introduced infinitesimal variations may be any variation (instead of only infinitesimal variations) around a given equilibrium configuration ϵ, x_o and equilibrating forces f_c, $f_o = 0$ (in equilibrium, the net forces on the object are zero). These linear variations are denoted with Δ. Hence, the following linear grasp system equations are found:

$$\Delta\epsilon_c = G^T \cdot \Delta x_o, \tag{5.13}$$

around a certain equilibrium configuration ϵ, x_o, and the changes in forces are given by:

$$\Delta f_{co} = G \cdot \Delta f_c^T, \tag{5.14}$$

around a force equilibrium, i.e. $f_c \in \ker G$, $f_o = 0$, $f_d = 0$, such that the change in the net force on the object is given by:

$$\Delta f_o = f_d + G \cdot \Delta f_c^T \tag{5.15}$$

5.3.5 Example: Simple grasp inversion problem

Consider the grasp system in equilibrium for initial contact forces f_c, and no disturbance, $f_d = 0$, such that $f_o = 0$. Next, consider the case that some disturbance force $f_d \neq 0$ is applied to the object. In order to maintain force equilibrium, $f_o = 0$, the contact forces f_c must change such that $\Delta f_o = 0$. Equation 5.15 shows that it must hold that:

$$G \cdot (\Delta f_c^T) = -f_d. \tag{5.16}$$

Hence, to find the required change in contact forces, $\Delta f_c \in \mathcal{F}_c$, the pseudo-inverse map $G^{\#}$ is needed as discussed in Equation 5.8. The goal is to investigate the physically equivalent inverse solution, i.e. selecting the change in contact forces that nature would 'select' to counterbalance the disturbance.

Physically well-posed inverse problem The given G (see Equation 5.10) is a surjective and non-injective map. As discussed in Section 5.2.2, multiple Δf_c can be found that all map to the same desired $-f_d$. Furthermore, notice that $\operatorname{im} G = \mathcal{F}_E$, such that any $f_d \in \mathcal{F}_E$ can be reached through G, i.e. G is surjective. Thus, there are no non-producible $f_d \in \mathcal{F}_E$ in the grasp system and hence all $f_d \in \mathcal{F}_E$ can be produced (and hence also resisted) through some choice of contact forces $\Delta f_c \in \mathcal{F}_c$ (if it is supposed that there are no limits to the contact forces that can be actuated). Therefore, this inverse problem is not physically ill-posed (See Definition 5.9) and hence said to be a physically well-posed inverse problem.

Moore-Penrose pseudo-inverse Mathematically, well-known pseudo-inverses are used to solve this inverse problem. For this particular case, the famous and often used *Moore-Penrose pseudo-inverse* gives [69]:

$$\Delta f_c^T = G^{\#}(-f_d) = -G^T(GG^T)^{-1} \cdot f_d = \begin{pmatrix} -\frac{1}{2} \\ \frac{1}{2} \end{pmatrix} \cdot f_d. \tag{5.17}$$

Numerically, this results indeed generates equality for Equation 5.16. Clearly, this numerical result is not (necessarily) the physically equivalent inverse solution.

Remark 5.6. *In fact, as it is written in Equation 5.17, it can not be the physically equivalent inverse map. Numerical equivalence would only be a coincidence. Notice that the map GG^T is a physically meaningless composition of maps, since G^T maps velocities to velocities, while G maps forces to forces. Obviously, some map is missing in between, which should map from velocities to forces. Also, the total composition $G^T(GG^T)^{-1}$ is physically incorrect, since the resulting physical quantities are velocities, due to the composition of G^T with $(GG^T)^{-1}$, while forces are expected.*

Throughout the chapter it will become clear that the missing map, as remarked above, is a metric on $T_\epsilon^*\mathcal{E}_c$. If this pseudo-inverse must model physical behavior, it will become clear that there is one specific metric on $T_\epsilon^*\mathcal{E}_c$ for physical equivalence. Furthermore, as shown later, the physically equivalent inverse map is then given by applying this specific metric for the *weighted generalized inverse* (see e.g. [69, 71]).

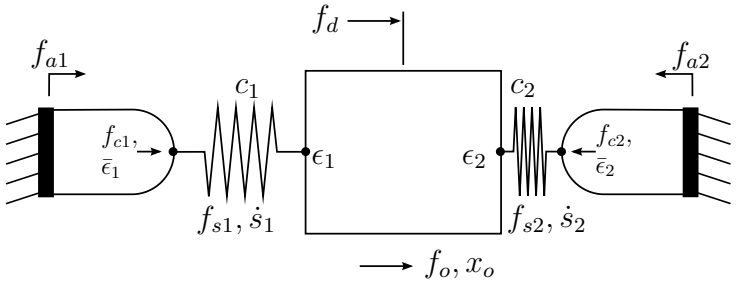

Figure 5.5: 1 DOF Grasping system; physical equivalence situation. Nature passively rejects a force disturbance by letting the compliance establish a new force equilibrium. The fixed world reaction force needed for the resulting equilibrium configuration ($f_{ai} = f_{ci}$) represent the physically equivalent contact forces. Notice that contact force f_{ci} is equal to force on spring f_{si} and that the contact is split into two spring attachment points, ϵ_i and $\bar{\epsilon}_i$, where $\Delta\epsilon_i = G^T \cdot \Delta x_0$ (Equation 5.13). The change of the spring lengths s_i of the linear springs is denoted by Δs_i.

5.3.6 Example: Physically equivalent solution

The goal is to investigate the physically equivalent inverse solution for the inverse problem as given in the previous section, Section 5.3.5.

Consider a steady-state situation for the simple grasp system in which, before applying the disturbance f_d, all velocities and accelerations are zero. In order to maintain this situation, the actuators are held at some position x_{ai}, see Figure 5.4.

In nature, such a situation is maintained by considering the situation as illustrated in Figure 5.5. As illustrated, linear springs are introduced to model limited (finite) stiffness of the robotic finger, the contacts and the stiffness of the controller in the original grasp system. So far, the grasp system has been modeled as a rigid kinematic system. However, in reality, rigid (infinite stiff) elements do not exist. Hence, the various sources of finite stiffness are consolidated into the model by adding (zero-length) linear springs with compliance c_1 and c_2 and spring lengths s_i. Hence, Figure 5.5 presents the physical equivalent situation under investigation.

Notice that the compliant decoupling splits the contact positions into two spring attachment points, ϵ_i and $\bar{\epsilon}_i$, for which still holds $\Delta\epsilon_i = G^T \cdot \Delta x_o$ and, *if* $\dot{s}_i = 0$, also $\Delta\bar{\epsilon}_i = G^T \cdot \Delta x_o$.

The forces on the springs f_{si} are given by:

$$f_{si} = \frac{1}{c_i} \cdot s_i = \frac{1}{c_i} \cdot (\epsilon_i - \bar{\epsilon}_i), \tag{5.18}$$

with s_i the lengths of the springs. Clearly, for any disturbance f_d, the object will displace, change the spring lengths (and hence the spring forces f_{si}) and find a new steady-state equilibrium position in which Equation 5.16 is satisfied again. In this steady-state the contact forces and the spring forces are equal, i.e. $f_{si} = f_{ci}$. Hence, the new set of physically equivalent contact forces result from object movement and according deformations of the springs[9].

Hereafter, the physical equivalent solution is derived through two approaches to gain insights from multiple perspectives.

Energy minimization It is well known that nature follows optimal behavior with respect to energy functions. Hence, it is expected to find the physically equivalent solution through the calculation of energy minimization for the given system.

[9]The required physically equivalent contact forces to be delivered by the actuators will be equivalent to the reaction forces of the fixed world in Figure 5.5, i.e. $f_{si} = f_{ai} = f_{ci}$. In fact, this resembles the disturbance scenario 'holding with constant force disturbance' as presented in Section 4.2, Figure 4.5(b).

In the simple grasp system under investigation, as shown in Figure 5.5, storage of elastic energy ($\mathbb{E}_s$) is found (in steady-state situations) as the only energy function present. For this linear system, the elastic storage energy is equal to the elastic co-energy ($\mathbb{E}_s^*$)[10]. The elastic (co-)energy stored in the linear springs is given by:

$$\mathbb{E}_{si} = \mathbb{E}_{si}^* = \frac{1}{2} c_i \cdot f_{si}^2. \tag{5.19}$$

The total (elastic) energy in the system is: $\mathbb{E} = \mathbb{E}_{s1} + \mathbb{E}_{s2}$. Assuming zero initial contact forces (i.e. unloaded springs), then the change in elastic energy due to a change in contact force ($\Delta f_c = \Delta f_{si}$) is given by:

$$\Delta\mathbb{E} \;=\; \frac{1}{2}\left(\Delta f_{c1}\right)^2 \cdot c_1 + \frac{1}{2}\left(\Delta f_{c2}\right)^2 \cdot c_2 \tag{5.20}$$

Furthermore, Equation 5.16 shows that the following equality is aimed for:

$$\Delta f_{c1} - \Delta f_{c2} = -f_d$$

Rewriting and substituting this force balance into Equation 5.20 gives:

$$\Delta\mathbb{E} = \frac{1}{2}\left(f_d^2 c_1 + \Delta f_{c2}^2 \cdot (c_1 + c_2) - 2 f_d \Delta f_{c2}\right)$$

Clearly, the change in stored energy is minimized for $\Delta f_{c2} \rightarrow \frac{\partial \Delta\mathbb{E}}{\partial \Delta f_{c2}}(\Delta f_{c2}) = 0$. Solving $\frac{\partial \Delta\mathbb{E}}{\partial \Delta f_{c2}}(\Delta f_{c2}) = 0$ for Δf_{c2} leads to the following physically equivalent solution:

$$\begin{array}{ll} \Delta f_{c2} & = \frac{c_1}{c_1+c_2} \cdot f_d \\ \Delta f_{c1} & = \frac{-c_2}{c_1+c_2} \cdot f_d \end{array}, \tag{5.21}$$

Elementary physics The physically equivalent contact forces can also be derived by applying laws from standard physics. Hence, the following presentation shows the derivation of the physically equivalent solution without explicitly using knowledge on nature's preference to optimize behavior with respect to energy functions.

Consider again Figure 5.5 and recall Equation 5.16, then force equilibrium is found for:

$$f_d = -G \cdot \Delta f_c^T,$$

where the required forces Δf_c^T are changes in contact forces added to any set of initial set of equilibrating ($f_o = 0$) contact forces.

Next, the two finger compliances are put together into a compliance matrix C:

$$C = \begin{pmatrix} c_1 & 0 \\ 0 & c_2 \end{pmatrix}, \tag{5.22}$$

such that

$$\Delta f_c^T = C^{-1} \cdot \Delta s = C^{-1} \cdot \Delta\epsilon,$$

[10] Note: writing energy as a function of the port variable (force), instead of the state variable (spring elongation), gives a co-energy storage function [63, 64].

where it is used that the contact displacement $\Delta\epsilon$ equals the spring deformation Δs, since the finger is fixed to the fixed world, i.e. $\dot{\bar{\epsilon}} = 0 \rightarrow \Delta\bar{\epsilon} = 0$. Substituting Equation 5.13 gives the change in contact forces related to the change in object position (Δx_o):

$$\Delta f_c^T = C^{-1} \cdot \Delta\epsilon = C^{-1} \cdot G^T \cdot \Delta x_o. \tag{5.23}$$

This is pre-multiplied with G and Equation 5.16 is substituted, such that it must hold that

$$f_d = GC^{-1}G^T \cdot \Delta x_o,$$

which, after inversion, gives:

$$\Delta x_o = \left(GC^{-1}G^T\right)^{-1} \cdot f_d.$$

Finally, the physically equivalent solution is found by substituting this into Equation 5.23:

$$\begin{aligned} \Delta f_c^T &= C^{-1} \cdot G^T \cdot \Delta x_o & (5.24)\\ &= C^{-1} \cdot G^T \cdot \left(GC^{-1}G^T\right)^{-1} \cdot f_d & (5.25)\\ &= \begin{pmatrix} -\frac{c_2}{c_1+c_2} \\ \frac{c_1}{c_1+c_2} \end{pmatrix} \cdot f_d & (5.26) \end{aligned}$$

Naturally, this result coincides with Equation 5.21.

Conclusions: physically equivalent solution For the simple grasp system, the inverse problem was formulated as finding the equilibrating contact forces for a given disturbance f_d. The kinematics of the grasp system are modeled by the map G, which is a non-injective and surjective map. Hence, multiple combinations of contact forces give a numerically (mathematical) correct solution. The physically equivalent solution was found by acknowledging the existence of finite stiffness in the kinematics. The solutions were obtained by using these insights from physics and adapting the model accordingly. Such observations have been presented before [75, 76].

The author wishes to use the results to present that modeling of kinematics through non-bijective maps must not be a pure mathematical exercise, but rather a modeling task that acknowledges the physics behind. And to clarify through examples the properties and implications of the inverse problem.

Notice that the mathematical solution in Equation 5.17, the Moore-Penrose pseudo-inverse, is a particular case, which holds for $c_1 = c_2$. As discussed before, the Moore-Penrose pseudo-inverse solution does not account for the actual physics attached to the pseudo-inverse problem.

5.4 Geometrical Description of General non-Bijective Map

The previous section presented an example of a non-bijective kinematic map in a model representation of a physical system. Also, the physically equivalent solution was discussed. This section presents a geometrical description of the inverse problem of a general non-surjective and non-injective (i.e. non-invertible) map, as a continuation of the discussion in Section 5.1.

For the reason of completeness and importance for physically meaningful analysis, combined insights are presented from a geometric viewpoint, aimed to contribute and enhance the understanding of the geometrical relations of non-bijective maps. In the next section, these insights will also be used to derive a mathematical description of the generalized pseudo-inverse as well as to study the kinematics of underactuated robot fingers (see Chapter 6 and Chapter 7) and kinematics in general. Other helpful references to study a geometric description of pseudo-inverses are found in [72, 73].

5.4.1 Map decomposition

The section gives a geometrical presentation of the pseudo-inverse problem of a general **non-surjective** and **non-injective** linear map a, as defined in Equation 5.1. Along the discussion for this general map, the pseudo-inversion of a specific physical map (Definition 5.5) and its physically equivalent pseudo inverse map (Definition 5.6) is presented as particular solution.

To describe the inversion problem, it is split into two parts: (1) selecting an $x_s \in \mathcal{X}$ for a given u_p being element of the blocked motions (or non-producible forces), i.e. $u_p \notin \operatorname{im} a$, and (2), selecting one $x_s \in \mathcal{X}$, while multiple $x_s \in \mathcal{X}$ all map to the given $u_p \in \mathcal{U}$. To separate the two distinct inversion problems, a full-rank decomposition is used to decompose the map a into two maps.

Theorem 5.1 (Full-rank decomposition)**.** *Consider a linear map a, as defined in Equation 5.1, and a $k \in \mathbb{R}$; $k = \dim(\operatorname{im} a) > 0$ with $k < \dim \mathcal{U} = m$ (i.e. a is non-surjective) and $k < \dim \mathcal{X} = n$ (i.e. a is non-injective[11]), then there is always an intermediate vector space $\mathcal{V} = \mathbb{R}^k$, with $\dim \mathcal{V} = k$, such that the map a can be written as the composition of two linear maps:*

$$a =: f \circ c,$$

where $c : \mathcal{X} \to \mathcal{V}$, with $\dim(\operatorname{im} c) = \dim \mathcal{V}$ and $\ker c = \ker a \neq \emptyset$ (i.e. c is surjective and non-injective) and where $f : \mathcal{V} \to \mathcal{U}$, with $k = \dim(\operatorname{im} f) < \dim \mathcal{U}$ and $\dim(\ker f) = \dim \mathcal{V} - \dim(\operatorname{im} f) = 0$ such that $\ker f = \emptyset$ (i.e. f is non-surjective and injective).

Proof. Vector spaces $\mathcal{X}$,$\mathcal{V}$,$\mathcal{U}$ are finite dimensional. Recall[12] that (after choosing bases, which is shown later in Section 5.5.1) in spaces $\mathcal{X}$,$\mathcal{V}$,$\mathcal{U}$, every linear map $a : \mathcal{X} \mapsto \mathcal{U}$, $c : \mathcal{X} \mapsto \mathcal{V}$ and $f : \mathcal{V} \mapsto \mathcal{U}$ can be represented as a $m \times n$ matrix A, a $k \times n$ matrix C and a $m \times k$ matrix F, respectively. Hence, the full-rank decomposition of map a is represented by a full-rank factorization[13] of matrix A, given by: $A =: FC$.

Then it is used that for the given matrix A, there always exists a singular value decomposition, such that A can be written as:

$$A = U_1 \cdot \begin{pmatrix} \Sigma_k & 0 \\ 0 & 0 \end{pmatrix}_{m \times n} \cdot U_2^T, \qquad \Sigma_k = \begin{pmatrix} \sigma_1 & & 0 \\ & \ddots & \\ 0 & & \sigma_k \end{pmatrix}_{k \times k},$$

where the diagonal $k \times k$ matrix Σ_k holds the k positive singular values σ_i on the diagonal and where U_1 is a $m \times m$ matrix and U_2 is a $n \times n$ matrix of which the columns/rows are linearly independent. Since all σ_i are positive, by taking the square roots of the singular values, the middle matrix can be split into a $m \times k$ matrix and a $k \times n$ matrix, such that:

$$\begin{aligned} A &= \underbrace{U_1 \cdot \begin{pmatrix} \sqrt{\Sigma_k} \\ 0 \\ \vdots \\ 0 \end{pmatrix}_{m \times k}}_{F} \cdot \underbrace{\begin{pmatrix} \sqrt{\Sigma_k} & 0 & \dots & 0 \end{pmatrix}_{k \times n} \cdot U_2^T}_{C} \\ &= F \cdot C. \end{aligned}$$

[11] Recall that $\dim(\ker a) = \dim \mathcal{X} - \dim(\operatorname{im} a)$, hence $\dim(\ker a) > 0$ and $\ker a \neq \emptyset$, i.e. a is non-injective.
[12] Standard definition of a linear map in linear algebra.
[13] A prove of full-rank factorization is also given in e.g.[69].

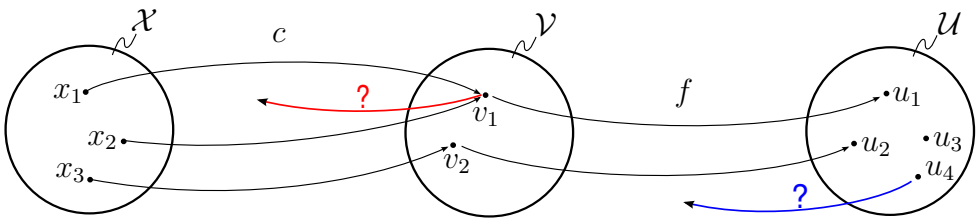

Figure 5.6: Decomposition of a non-injective and non-surjective map a: $a =: f \circ c$. c is a surjective and non-injective map, while f is an injective and non-surjective map.

Since U_1 and U_2 have linearly independent columns/rows, it follows that F is a $m \times k$ matrix with rank k, such that the matrix F indeed represents the injective and non-surjective map f and it follows that C is a $k \times n$ matrix with rank k, such that the matrix C indeed represents the non-injective and surjective map c. □

With respect to the surjective and injective properties of the map a, it is useful to note the following remarks.

Remark 5.7. *For the map a being non-injective and surjective, a trivial and obvious full-rank decomposition, as given in Theorem 5.1, is given by $a = c$, with f the identity map.*

Remark 5.8. *For the map a being non-surjective and injective, a trivial and obvious full-rank decomposition, as given in Theorem 5.1, is given by $a = f$, with c the identity map.*

Thus, following Theorem 5.1, the full-rank decomposition of the linear map a into two maps is illustrated in Figure 5.6 and given by:

$$a =: f \circ c \quad : \quad \mathcal{X} \to \mathcal{U}, \tag{5.27}$$

with

$$c : \mathcal{X} \to \mathcal{V}$$
$$f : \mathcal{V} \to \mathcal{U},$$

where $\mathcal{V} = \mathbb{R}^k$ is another vector space with $k := \dim(\operatorname{im} a)$, and such that c is a surjective and non-injective map (i.e. $\ker c = \ker a \neq \emptyset$ and $\dim(\operatorname{im} c) = k$) and such that f is an injective and non-surjective map (i.e. $\dim(\operatorname{im} f) = \dim(\operatorname{im} a) < m$ and $\ker f = \emptyset$). Hence, inversion of map c corresponds to the second part (2) of the inversion problem and inversion of map f corresponds to the first part (1) of the inversion problem.

Note that inversion of both c and f requires pseudo-inversion. However, both of them deal with only one subproblem of the full non-bijective inversion problem, as indicated in Figure 5.6.

From here, the inversion problems of both sub-maps are treated in separate sections. Thereafter, these two are connected again to complete the geometrical description of the total inversion problem.

5.4.2 $c^{\#}$: Surjective and non-injective map

The inversion of the non-injective and surjective map c is examined:

$$c^{\#} : \mathcal{V} \to \mathcal{X}$$

As discussed in Section 5.2.2, the fact that c is not-injective suggests the existence of a subspace $\mathcal{X}_n \subset \mathcal{X}$ from which c maps the elements $x \in \mathcal{X}_n$ to the zero element in $\mathcal{V}$. These elements

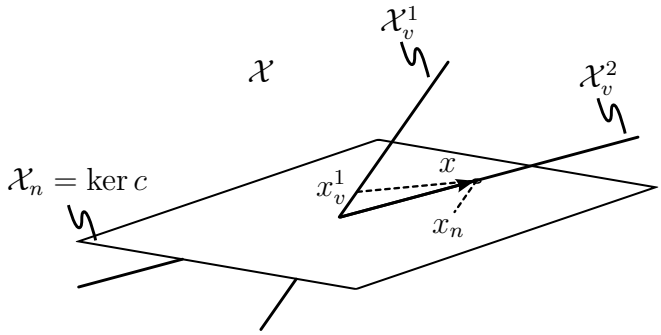

Figure 5.7: Non-uniqueness of complementary space $\mathcal{X}_v$. $\mathcal{X}_n = \ker c$ is intrinsically defined. However, any $\mathcal{X}_v$ for which $\mathcal{X}_n \oplus \mathcal{X}_v = \mathcal{X}$ can be the complementary space. Hence, also the projection of any $x \in \mathcal{X}$ (unless $x \in \mathcal{X}_n$) is not unique and depends on the choice of complementary space. As illustrated, for $\mathcal{X}_n \oplus \mathcal{X}_v^2 = \mathcal{X}$, the projection of $x \in \mathcal{X}$ results in some $(x_n, x_v^2) = (\emptyset, \bullet)$, i.e. the projection on $\mathcal{X}_n$ is zero, since x fully coincides with $\mathcal{X}_v^2$. For $\mathcal{X}_n \oplus \mathcal{X}_v^1 = \mathcal{X}$, the projection of $x \in \mathcal{X}$ results in some $(x_n, x_v^1) = (\bullet, \bullet)$, i.e. the projections on both spaces are non-zero.

$x \in \mathcal{X}_n$ do not contribute to any effect on $\mathcal{V}$ and therefore can be added to any solution of $c^{\#}$. Hence, the existence of elements $x \in \mathcal{X}_n$ gives rise to have multiple $x \in \mathcal{X}$ that map to the same $v \in \mathcal{V}$, i.e. c is a non-injective map. Not surprisingly, as shown in Section 5.2.2, $\mathcal{X}_n$ is the kernel of c:

$$\mathcal{X}_n := \ker c \subset \mathcal{X} \tag{5.28}$$

Nevertheless, c is a surjective map, implying that all $v \in \mathcal{V}$ are mapped to, i.e. $\operatorname{im} c = \mathcal{V}$. Since $\mathcal{X}_n$ has taken out all redundant elements, the elements $x \notin \mathcal{X}_n$ must have a invertible (bijective) relation with elements $v \in \mathcal{V}$. However, while $\mathcal{X}_n$ is intrinsically defined, the subspace which contains these elements $x \notin \mathcal{X}_n$ is not unique at all.

Non-unique complementary spaces Since $\mathcal{X}_n$ is a subspace of $\mathcal{X}$, a complementary space $\mathcal{X}_v$ is needed to complete splitting $\mathcal{X}$ into subspaces, such that:

$$\mathcal{X} = \mathcal{X}_n \oplus \mathcal{X}_v.$$

Hence, it must hold that $\dim \mathcal{X}_v = \dim \mathcal{V} = k$ and therefore $\dim \mathcal{X}_n = n - k$.

However, as illustrated in Figure 5.7, it is of major importance to realize that this complementary space $\mathcal{X}_v$ is by no means unique and it is not intrinsically defined, i.e. there are infinite arbitrary complementary spaces. By choosing any complement, a vector $x \in \mathcal{X}$ can be expressed in a unique way as the sum of an element in the kernel and an element in the complement.

As shown in Figure 5.7, an element $x \in \mathcal{X}$ is projected onto $\mathcal{X}_n$ along the complementary space $\mathcal{X}_v$, and, $x \in \mathcal{X}$ is projected onto $\mathcal{X}_v$ along $\mathcal{X}_n$. Hence, different complementary spaces also result in different projections of $x \in \mathcal{X}$ onto the subspaces.

On $\mathcal{X}$, only the kernel of c defines an intrinsic subspace. Hence, also the projection of any $x \in \mathcal{X}$ onto $\mathcal{X}_n$ and $\mathcal{X}_v$ is not intrinsically defined (unless $x \in \mathcal{X}_n$, i.e. the element belongs solely and completely to $\mathcal{X}_n$), see Figure 5.7.

Orthogonal complementary space One *option* to construct the complementary space $\mathcal{X}_v$ is to use the inner-product on $\mathcal{X}$, which is induced by the metric M_x on $\mathcal{X}$ and called the M_x-weighted inner-product (note that $\mathcal{X}$ is a Hilbert space, see Section 5.1.1; hence it has an inner-product).

Definition 5.12 (M-weighted inner-product)**.** *Consider some Hilbert space $\mathcal{P} \subset R^n$. Then the inner-product defined by the metric M on $\mathcal{P}$ is called the M-weighted inner-product and in coordinates given by:*

$$\langle p_1, p_2 \rangle := \bar{p}_1^T \cdot M \cdot \bar{p}_2, \qquad p_1, p_2 \in \mathbb{R}^n,$$

where $p_1, p_2 \in \mathbb{R}^n$ are coordinate vectors, which represent the elements $p_1, p_2 \in \mathcal{P}$ for chosen bases (See Section 5.5.1). Furthermore, the $n \times n$ matrix M, called metric M, is a positive-definite symmetric matrix, which represents[14] *the M-weighted inner-product in coordinates of the chosen bases.*

Definition 5.13 (M-norm)**.** *Consider the M-weighted inner-product as defined in Definition 5.12 for Hilbert space $\mathcal{P}$. The M-norm of $p \in \mathcal{P}$ is defined by [71]:*

$$||p||^2 := \langle p, p \rangle \qquad p \in \mathcal{P}$$

Through application of the M_x-weighted inner-product, a unique (i.e. unique for the given metric M_x) so-called orthogonal complementary space can be constructed.

Definition 5.14 (orthogonal spaces)**.** *Let $\mathcal{X}$ be a Hilbert space. Two subspaces $\mathcal{X}_n \subset \mathcal{X}$ and $\mathcal{X}_v \subset \mathcal{X}$ are called orthogonal if:*

$$\langle x_v, x_n \rangle = 0, \qquad \forall x_n \in \mathcal{X}_n, \quad \forall x_v \in \mathcal{X}_v, \tag{5.29}$$

which is denoted by the perp-symbol $^\perp$: $\mathcal{X}_n = \mathcal{X}_v^\perp$.

Hence, from all possible complementary spaces, $\mathcal{X}_v$ can be constructed by taking that particular subspace orthogonal to $\mathcal{X}_n$ which preserves[15] $\mathcal{X} = \mathcal{X}_n \oplus \mathcal{X}_v$, such that this constructed $\mathcal{X}_v$ is called the *orthogonal complement* of $\mathcal{X}_n$, denoted by:

$$\mathcal{X}_v = \mathcal{X}_n^\perp = (\ker c)^\perp, \tag{5.30}$$

and uniquely defined by the metric M_x on $\mathcal{X}$. Clearly, different metrics give different orthogonal complementary spaces. Hence, different metrics on $\mathcal{X}$ not only define different complementary spaces, but also result in different projections of $x \in \mathcal{X}$ onto the subspaces.

(Pseudo-) inverse solution (set) The abstract separation of spaces is illustrated in Figure 5.8. It clearly illustrates the mapping properties and the related separation of spaces. These insights show the various solutions of the pseudo-inversion of c for any given $v_p \in \mathcal{V}$.

Multiple exact solutions (see Definition 5.4) exist: for any $v_p \in \mathcal{V}$ the solution can be composed by one unique (for the chosen complement $\mathcal{X}_v$) element from $\mathcal{X}_v$ plus any redundant element from $\mathcal{X}_n$. Thus, for any given $v_p \in \mathcal{V}$ there exists a set of exact inverse solutions (see Definition 5.4), $\mathcal{X}_s$:

$$\mathcal{X}_s := x_v + \mathcal{X}_n \qquad v_p \in \mathcal{V}, x_v \in \mathcal{X}_v \tag{5.31}$$

such that $v_p = c(x_s) \quad \forall x_s \in \mathcal{X}_s$ and where $x_v \in \mathcal{X}_v$ is the representative element of the redundant elements $x_s \in \mathcal{X}_s$ that all map to the same given $v_p \in \mathcal{V}$. Note that the representative $x_v \in \mathcal{X}_v$ is the projection of any $x_s \in \mathcal{X}_s$ onto $\mathcal{X}_v$ along $\mathcal{X}_n$, see Figure 5.9(b).

The set $\mathcal{X}_s$ is a linear variety contained in $\mathcal{X}$ [73]. Clearly, the set does **not** depend on the choice of the complementary space. However, the representative $x_v \in \mathcal{X}_v$ will change for different complementary spaces, see Figure 5.9(b). Hence, in the case of an orthogonal complementary space, it depends on the choice of the metric M_x.

[14] Note: the inner-product itself is a abstract bilinear map: $\mathcal{P} \times \mathcal{P} \mapsto \mathbb{R} \quad ; \quad \langle p_1, p_2 \rangle \mapsto \mathbb{R}$, $p_1, p_2 \in \mathcal{P}$, which, for given coordinates, is represented by matrix M, see e.g. [77]

[15] Note: two subspaces can be orthogonal without giving a direct sum of the total space.

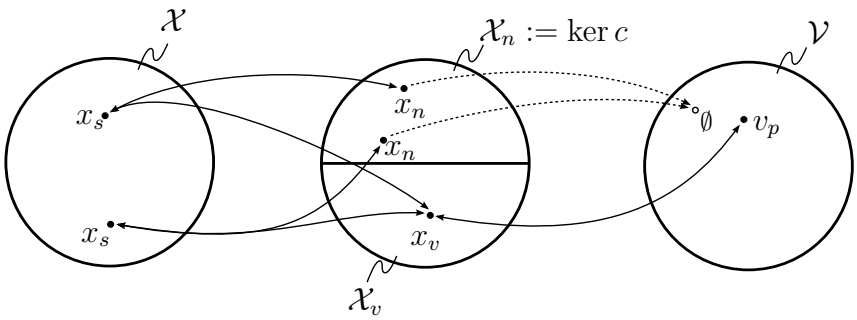

Figure 5.8: Splitting $\mathcal{X}$ into $\mathcal{X}_n$ and $\mathcal{X}_v$ through the kernel of c. Elements $x \in \mathcal{X}$ are split into $x_n \in \mathcal{X}_n$ and $x_v \in \mathcal{X}_v$, such that $x_n \oplus x_v = x$. Clearly, all $x_n \in \mathcal{X}_n$ map to $\emptyset \in \mathcal{V}$, whereas all $x_v \in \mathcal{X}$ map to some $v \in \mathcal{V}$ and all $v \backslash \emptyset \in \mathcal{V}$ are mapped to by $x_v \in \mathcal{X}_v$, i.e. bijective relation. Multiple exact solutions exist for the pseudo-inversion of any $v_p \in \mathcal{V}$; these are composed out of one element from $\mathcal{X}_v$ for each $v_p \in \mathcal{V}$ plus any redundant element from $\mathcal{X}_n$.

Definition 5.15 (pseudo-inverse map $c^\#$)**.** *Consider the map c and spaces $\mathcal{X}$ and $\mathcal{V}$ as given in Equation 5.27. The map that, for any given $v_p \in \mathcal{V}$, selects the representative $x_v = x \in \mathcal{X}_v \cap \mathcal{X}_s$, which is mapped to the given $v_p \in \mathcal{V}$ by c, is called the pseudo-inverse map $c^\#$.*

Clearly, the pseudo-inverse map depends on the choice of the complementary space. Hence, in the case of an orthogonal complementary space, it depends on the choice of the metric M_x.

Independent of the choice of complementary space, the only properly defined space for which a bijective map with $\mathcal{V}$ can be found is the quotient space $\mathcal{Q}_x = \mathcal{X}/\ker c$. This vector space $\mathcal{Q}_x$ is the space whose elements $q_x \in \mathcal{Q}_x$ represent sets of elements $x \in \mathcal{X}$ that are equivalent under $\ker c$, i.e. the elements $q_x \in \mathcal{Q}_x$ are equivalent classes of vectors $x \in \mathcal{X}$, see Figure 5.9(a). It holds that $\dim \mathcal{Q}_x = \dim \mathcal{V}$ and the map between $\mathcal{Q}_x$ and $\mathcal{V}$ is the only intrinsic bijection.

Clearly, every $q_x \in \mathcal{Q}_x$ represents a linear variety $\mathcal{X}_s$, see Figure 5.9(b) and by choosing a particular complementary space $\mathcal{X}_v$, a representative element $x \in \mathcal{X}_v \cap \mathcal{X}_s$ for all $x \in \mathcal{X}_s$ is chosen, being the the projection of all $x \in \mathcal{X}_s$ along $\ker c$ onto $\mathcal{X}_v$ (see Figure 5.9(b)). The map from any given $v_p \in \mathcal{V}$ to this representative $x_v \in \mathcal{X}_v$ is called the pseudo-inverse map: $x_v = c^\#(v_p)$ and depends on the choice of $\mathcal{X}_v$.

Physically equivalent pseudo-inverse map As said, different metrics on $\mathcal{X}$ give different orthogonal complementary spaces and therefore also different projections of $x \in \mathcal{X}$ onto the subspaces and hence also different pseudo-inverse solution sets, see Equation 5.31.

Section 5.1.3 discussed that nature has one particular (pseudo-)inverse solution for a physical non-injective and non-surjective map a. Hence, for the physically equivalent pseudo-inverse map of a physical non-injective and surjective map c, the natural orthogonal complementary space of $\mathcal{X}_n$, called $\mathcal{X}_v$, needs to be found, which involves finding the metric which is used to describe the complementary space that is found in nature, i.e. in the physical system.

Remark 5.9. *Even in the particular case, in which $\mathcal{X}$ can be considered a Euclidean space (a Hilbert space generalizes the notion of Euclidean space), where all vectors are represented with components of equal physical units, then the intrinsic metric (and hence intrinsic inner-product) of the Euclidean space may not be the metric that describes the complementary space found in nature, i.e. in the physical system.*

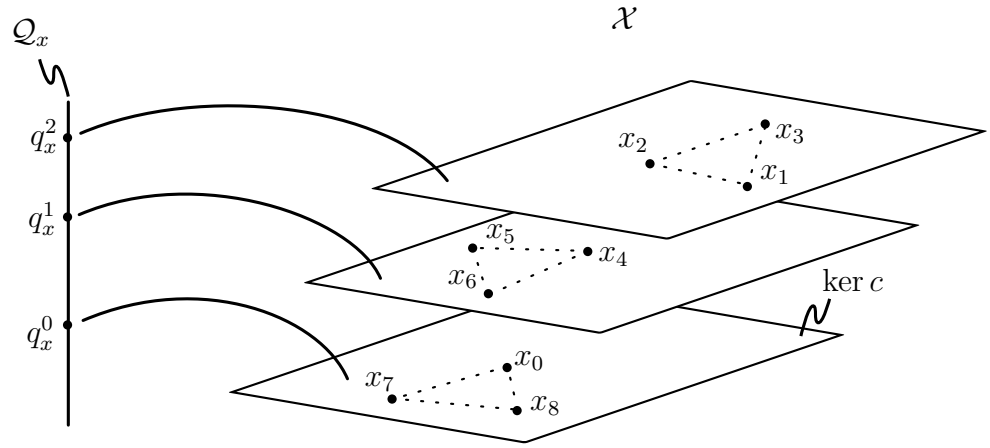

(a) Quotient space $\mathcal{Q}_x$. Elements $q_x \in \mathcal{Q}_x$ represent equivalence classes under the equivalence of $\ker c$.

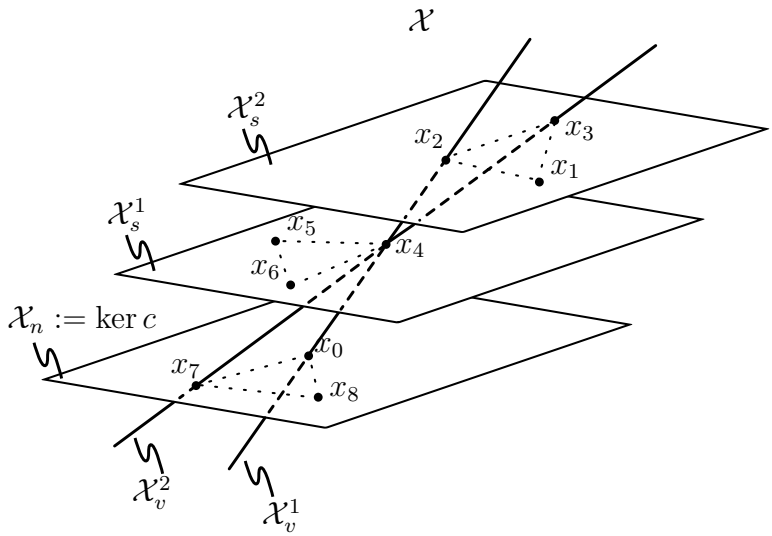

(b) Linear varieties $\mathcal{X}_s$ with different representative elements depending on the choice of $\mathcal{X}_v$: e.g. for complementary space $\mathcal{X}_v^1$, elements $x_0, x_2, x_4 \in \mathcal{X}_v^1$ are representatives of $\mathcal{X}_n$, $\mathcal{X}_s^1$ and $\mathcal{X}_s^2$ respectively, while for complementary space $\mathcal{X}_v^2$, elements $x_3, x_4, x_7 \in \mathcal{X}_v^2$ are the representatives. The linear varieties itself do not change, i.e. the subsets $\mathcal{X}_s^1$ and $\mathcal{X}_s^2$ always contain the same elements.

Figure 5.9: The solution set illustrated as quotient space $\mathcal{Q}_x$ and linear variety $\mathcal{X}_s$. The linear varieties $\mathcal{X}_s$ coincide with the equivalence classes under $\ker c$ that are represented by the elements q_x of the quotient space $\mathcal{Q}_x$. Every $x_v = x \in \mathcal{X}_v \cap \mathcal{X}_s$ is a unique (For the chosen $\mathcal{X}_v$) representative for $\mathcal{X}_s$ and all $x_s \in \mathcal{X}_s$ project along $\mathcal{X}_n = \ker c$ to the same x_v, e.g. $x_1, x_3 \in \mathcal{X}_s^2$ project to $x_2 \in \mathcal{X}_v^1$. Basically, by choosing a particular complement $\mathcal{X}_v$, a representative $x_v \in \mathcal{X}_s$ for all $x \in \mathcal{X}_s$ is chosen, being the the projection of all $x \in \mathcal{X}_s$ along $\ker c$ onto $\mathcal{X}_v$.

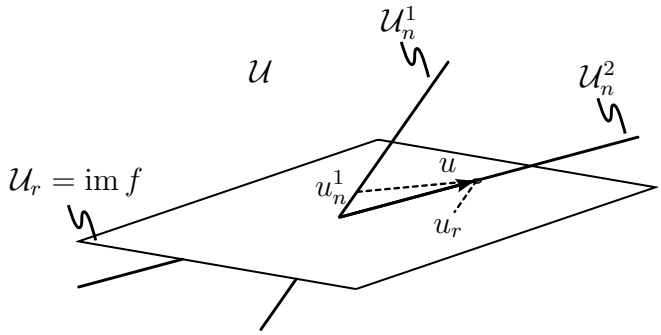

Figure 5.10: Non-uniqueness of complementary space $\mathcal{U}_n$. $\mathcal{U}_r = \operatorname{im} f$ is intrinsically defined. However, any $\mathcal{U}_n$ for which $\mathcal{U}_r \oplus \mathcal{U}_n = \mathcal{U}$ can be the complementary space. Hence, also the projection of any $u \in \mathcal{U}$ (unless $u \in \mathcal{U}_r$) is not unique and depends on the choice of complementary space. As illustrated, for $\mathcal{U}_r \oplus \mathcal{U}_n^2 = \mathcal{U}$, the projection of $u \in \mathcal{U}$ results in some $(u_r, u_n^2) = (\emptyset, \bullet)$, i.e. the projection on $\mathcal{U}_r$ is zero, since u fully coincides with $\mathcal{U}_n^2$. For $\mathcal{U}_r \oplus \mathcal{U}_n^1 = \mathcal{U}$, the projection of $u \in \mathcal{U}$ results in some $(u_r, u_n^1) = (\bullet, \bullet)$, i.e. the projections on both spaces are non-zero.

5.4.3 $f^\#$: Injective and non-surjective map

The inversion of the injective and non-surjective map f is examined:

$$f^\# : \mathcal{U} \to \mathcal{V}$$

The fact that f is injective suggests the existence of a subspace $\mathcal{U}_r \subset \mathcal{U}$ to which f maps elements $v \in \mathcal{V}$ in a one-to-one manner. This implies that every $v \in \mathcal{V}$ is mapped to a unique $u \in \mathcal{U}_r$. $\mathcal{U}_r$ is intrinsically defined and given by the image of f:

$$\mathcal{U}_r := \operatorname{im} f \tag{5.32}$$

Note that, because of f being injective, $\ker f = \emptyset$. Hence, the choice of $\mathcal{U}_r$ constructs a bijective (invertible) map between $\mathcal{V}$ and $\mathcal{U}_r$ and hence $\dim \mathcal{U}_r = \dim \mathcal{V} = k$.

Non-unique complementary spaces Because f is non-surjective and $\mathcal{U}_r$ is a subset of $\mathcal{U}$, a complementary subspace $\mathcal{U}_n$ is needed to complete splitting $\mathcal{U}$ into subspaces, such that:

$$\mathcal{U} = \mathcal{U}_r \oplus \mathcal{U}_n,$$

with $\dim \mathcal{U}_n = m - k$. The complementary space $\mathcal{U}_n$ holds elements $u \in \mathcal{U}$ to which *non* of the elements $v \in \mathcal{V}$ are mapped to.

Again, similar to the illustration in Figure 5.7, Figure 5.10 stresses that this complementary space $\mathcal{U}_n$ is by no means unique and it is not intrinsically defined. Only the the image of f defines a unique subspace of $\mathcal{U}$, being $\mathcal{U}_r$. By choosing any complement, any vector $u \in \mathcal{U}$ can be expressed in a unique way as the sum of an element in the image and an element in the complement. Only elements in the image are mapped to by f.

As shown in Figure 5.7, an element $u \in \mathcal{U}$ is projected onto $\mathcal{U}_r$ along the complementary space $\mathcal{U}_n$, and, $u \in \mathcal{U}$ is projected onto $\mathcal{U}_n$ along $\mathcal{U}_r$. Hence, different complementary spaces also result in different projections of $x \in \mathcal{X}$ onto the subspaces.

Orthogonal complementary space Again, the complementary space $\mathcal{U}_n$ can be constructed by using the inner-product on $\mathcal{U}$, which is induced by the metric M_u on $\mathcal{U}$ and called the M_u-weighted inner-product, see Definition 5.12 (note that $\mathcal{U}$ is a Hilbert space, see Section 5.1.1; hence it has an inner-product).

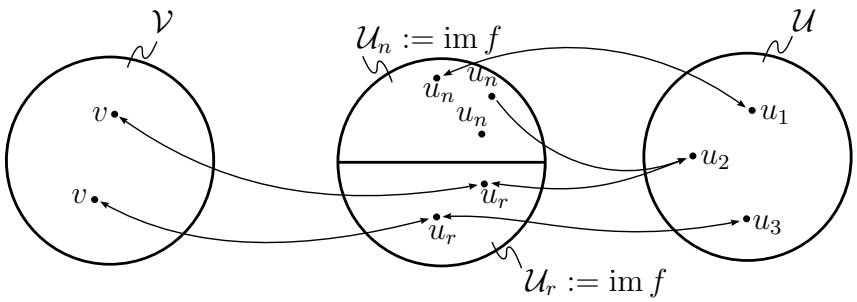

Figure 5.11: Splitting $\mathcal{U}$ into $\mathcal{U}_n$ and $\mathcal{U}_r$ through the image of f. Elements $u \in \mathcal{U}$ are split into $u_n \in \mathcal{U}_n$ and $u_r \in \mathcal{U}_r$, such that $u_n \oplus u_r = u$. Clearly, all $u_r \in \mathcal{U}_r$ are mapped to by $v \in \mathcal{V}$ in i.e. bijective relation. Notice that: $u_1 \in \mathcal{U}$ can not be reached (no existence of exact inverse), for $u_2 \in \mathcal{U}$ only its part in $\mathcal{U}_r$ can be reached (no existence of exact inverse) and $u_3 \in \mathcal{U}$ is fully reached (exact inverse does exist!).

Through application of the M_u-weighted inner-product, $\mathcal{U}_n$ is constructed as a unique (i.e. unique for the given metric M_u) so-called orthogonal complementary space, see Definition 5.14, and which is denoted by:

$$\mathcal{U}_n = \mathcal{U}_r^{\perp} = (\operatorname{im} f)^{\perp}, \tag{5.33}$$

and uniquely defined by the metric M_u on $\mathcal{U}$. Notice that $\mathcal{U}_n$ holds the **blocked motions** or the **non-producible forces** (Section 5.2.1). Clearly, different metrics M_u give different orthogonal complementary spaces and also result in different projections of $u \in \mathcal{U}$ onto the subspaces.

Pseudo-inverse solution The abstract separation of spaces is illustrated in Figure 5.11. It clearly illustrates the mapping properties and the related separation of spaces. These insights show that the inverse map of f can never select an exact solution for elements in $\mathcal{U}$ that partially or fully coincide with $\mathcal{U}_n$. This is illustrated in Figure 5.11.

Clearly, for any given $u_p \in \mathcal{U}_r$, there exists an exact inverse element $v_s \in \mathcal{V}$ such that $u_p = f(v_s)$. Whereas, for any given $u_p \notin \mathcal{U}_r$ only the part that is coincides with $\mathcal{U}_r$ can be reached from some $v_s \in \mathcal{V}$, i.e. only the projection of u_p onto $\mathcal{U}_r$ along the complementary space $\mathcal{U}_n$ can be reached from some $v_s \in \mathcal{V}$.

Therefore, for a given $u_p \in \mathcal{U}$, the corresponding $v_s \in \mathcal{V}$ which is mapped to the projection of u_p onto $\mathcal{U}_r$ by f, is called the pseudo-inverse solution of u_p and does not always yield an exact solution[16] (see Definition 5.4). Hence, the following definition is given.

Definition 5.16 (pseudo-inverse map $f^{\#}$)**.** *Consider the map f and spaces $\mathcal{U}$ and $\mathcal{V}$ as given in Equation 5.27. The map that selects the element $v_s \in \mathcal{V}$ which f maps to the projection of u_p onto $\mathcal{U}_r$ for any given u_p, is called the pseudo-inverse map $f^{\#}$.*

Remark 5.10. *Since projection along $\mathcal{U}_n$ is used, the pseudo-inverse map $f^{\#}$ is by no means unique and depends on the choice of $\mathcal{U}_n$. Here, Hilbert spaces are considered for which $\mathcal{U}_n$ can be chosen to be the orthogonal complementary space of $\mathcal{U}_r$, which is uniquely defined by the metric M_u on $\mathcal{U}$. Clearly, different choices of M_u, give different complementary spaces and hence different projections and different pseudo-inverse maps.*

[16] Exact solutions are found for $u_p \in \mathcal{U}_r$ for which it holds that the projection of onto $\mathcal{U}_r$ along $\mathcal{U}_n$ always equals the element u_p itself and is independent of the chosen complementary space $\mathcal{U}_n$.

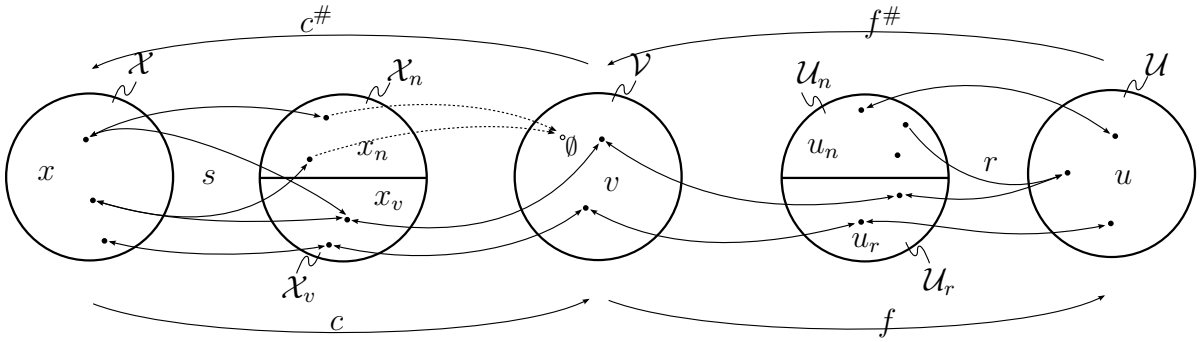

Figure 5.12: Complete composition of forward and backward mapping of map a. The decomposition of a was defined by: $a =: f \circ c$, and the inverse relation follows from the illustration, $a^\# := c^\# \circ f^\#$, which is a known result from calculus. Mappings s and r denote coordinate changes, see Section 5.5.

For the non-injective and surjective map c, it was discussed that there exists an intrinsic bijection for the quotient space under equivalence of the kernel of c. There is **no** intrinsic bijection for the injective and non-surjective map f, since the only intrinsically defined subspace on $\mathcal{U}$ is $\operatorname{im} f$. All elements $u \in \mathcal{U}$ which project to the same $u_r \in \mathcal{U}_r$ could be called equivalent and hence belong to the same equivalence class. The elements $q_u \in \mathcal{Q}_u$ of the quotient space $\mathcal{Q}_u$ for the described equivalence relation, represent these equivalence classes. To each of these elements, there is one unique $v_s \in \mathcal{V}$ associated, i.e. a bijective map exists between $\mathcal{Q}_u$ and $\mathcal{V}$. However, since the equivalence relation relies on the projection along $\mathcal{U}_n$, it depends on the arbitrary choice of $\mathcal{U}_n$, such that is **not** intrinsically defined and hence, also the bijective map is **not** intrinsically defined.

Physically equivalent pseudo-inverse map Section 5.1.3 discussed that nature has one particular (pseudo-)inverse solution for a physical non-injective and non-surjective map a. Hence, for the physically equivalent pseudo-inverse map of a physical injective and non-surjective map f, the natural orthogonal complementary space of $\mathcal{U}_r$, called $\mathcal{U}_n$, needs to be found, which involves finding the metric which is used to describe the complementary space that is found in nature, i.e. in the physical system.

Remark 5.11 (repeated)**.** *Even in the particular case, in which $\mathcal{U}$ can be considered a Euclidean space (a Hilbert space generalizes the notion of Euclidean space), where all vectors are represented with components of equal physical units, then the intrinsic metric (and hence intrinsic inner-product) of the Euclidean space may not be the metric that describes the complementary space found in nature, i.e. in the physical system.*

5.4.4 $a^\#$: Complete description

Inversion of both submaps c and f has been investigated and presented geometrically. As presented in Figure 5.12 and defined in Equation 5.27, the total description is found through composition of both submaps c and f. As known from common calculus, but also clearly illustrated in Figure 5.12 by following the mapping arrows backwards, the composition of the inverse relation is given by:

$$a^\# := c^\# \circ f^\# \tag{5.34}$$

All previously discussed properties of the pseudo-inversion of the submaps can now be combined together to describe the pseudo-inverse relations of the total non-injective and non-surjective map a, hence:

For any $u_p \in \mathcal{U}$ and the given map a, the set $\mathcal{X}_s \subset \mathcal{X}$ of (pseudo-)inverse solutions is given by:

$$\mathcal{X}_s := a^{\#}(u_p) + \mathcal{X}_n \qquad u_p \in \mathcal{U},$$

where

- the set $\mathcal{X}_s$ is a linear variety contained in $\mathcal{X}$ (see e.g. [73]);
- the pseudo-inverse map $a^{\#}$ selects the representative element of all redundant elements in $\mathcal{X}_s$, i.e. the projection of all $x \in \mathcal{X}_s$ along $\mathcal{X}_n$ onto $\mathcal{X}_v$, which a maps to the projection of u_p onto $\mathcal{U}_r$ along $\mathcal{U}_n$;
- any $x \in \mathcal{X}_n$ can not reach $\mathcal{U}$, i.e. these elements impose redundancy to the mapped spaces, since they can be added to **any** (pseudo-)inverse solution $x_s \in \mathcal{X}$ without effecting $\mathcal{U}$;
- for any $u_p \in \mathcal{U}_n$ and $u_p \notin \mathcal{U}_r$ ($u_p \cap \mathcal{U}_r = \emptyset$), the projection of this u_p onto $\mathcal{U}_r$ is zero (hence also $a^{\#}(u_p) = 0$), i.e. these u_p can **not** be reached through a and, if a is a physical map, these are called **blocked motions** or **non-producible forces**;
- for any $u_p \in \mathcal{U}_r$ and $u_p \notin \mathcal{U}_n$ ($u_p \cap \mathcal{U}_n = \emptyset$), all $x_s \in \mathcal{X}_s$ are **exact** inverse solutions of the given u_p (see Definition 5.4), such that for this u_p, indeed $a(x_s) = u_p \quad \forall x_s \in \mathcal{X}_s$;
- any $u_p \in \mathcal{U}$ with $u_p \cap \mathcal{U}_r \neq \emptyset$ and with $u_p \cap \mathcal{U}_n \neq \emptyset$ can only be reached **partially**; $a(x_s) \neq 0 \neq u_p \quad \forall x_s \in \mathcal{X}_s$. Note, the part $u_r \in \mathcal{U}_r$ (i.e. the projection of the given u_p onto $\mathcal{U}_r$) can be reached and is always equal for all **multiple** $x \in \mathcal{X}$ (redundancy in $\mathcal{X}_n$);

Instead of being non-injective and non-surjective, the mapping properties (injectivity and surjectivity) of a may coincide with either of the properties of map f or c (instead of both). In that case, it is clear that a does not need to be decomposed and the pseudo-inversion of a directly follows the presented discussion of either map c or f, see Remark 5.7 and Remark 5.8.

Remark 5.12. *As shown for both maps, c and f, the pseudo-inverse map is constructed based on a separation of spaces which defines the projection directions in $\mathcal{X}$ and $\mathcal{U}$. As discussed, the complementary spaces $\mathcal{X}_v$ and $\mathcal{X}_n$ of the intrinsic subspaces $\mathcal{X}_n$ and $\mathcal{U}_r$ are not unique. Since $\mathcal{X}$ and $\mathcal{U}$ are Hilbert spaces, the orthogonal complement is a well defined choice for $\mathcal{X}_v$ and $\mathcal{X}_n$, and is uniquely defined by the M_x- and M_u-weighted inner-product. Hence the orthogonal complements are determined by the choice of metrics M_x and M_u.*

Physically equivalent pseudo-inverse map As discussed, the (pseudo-)inverse solution for a non-injective and non-surjective map a and hence also for a non-injective and non-surjective physical map a, requires the selection of complementary spaces $\mathcal{X}_v$ and $\mathcal{U}_n$. Geometrically speaking, these complements are by no means unique. For the physically equivalent pseudo-inverse map, the structure of the Hilbert spaces is used by utilizing the inner-product to construct orthogonal complementary spaces. Hence, searching for the Physically equivalent pseudo-inverse map becomes equivalent to determining the metrics which can be used to describe the complementary space that is found in nature, i.e. in the physical system.

5.5 Mathematical Description of non-Bijective Map

The geometrical description presented in the previous section (Section 5.4) is now followed to derive a mathematical (numerical) description of the pseudo-inverse map $a^{\#}$. The solution itself is not new, since the core of the mathematical description of the pseudo-inverse will be the weighted generalized inverse, see e.g. [69, 71, 72, 73].

Nevertheless, the discussion completes the geometric description and serves to enhance insights for studying and interpreting linear maps that represent physical maps in physical systems, such as the actuation Jacobian of underactuated robot fingers.

5.5.1 Attaching coordinates

The geometrical description used abstract elements and spaces. Bases and coordinates need to be considered for each of the vector spaces to do calculations and work out numerical solutions. First a brief summary on coordinates is given, then particular coordinates are chosen to describe the problem at hand.

Bases and coordinate vectors The concepts of bases and coordinate vectors are shortly summarized here. The concepts are discussed by taking vector space $\mathcal{X}$ as example as defined in Section 5.1.1.

Consider again the abstract vector space $\mathcal{X}$ of dimension n over the field of reals $\mathbb{R}$ with abstract elements $x \in \mathcal{X}$, which may represent anything. An ordered[17] base for $\mathcal{X}$ is constructed by picking n different elements $e_i \in \mathcal{X}$ and letting them be the base B:

$$B = \{e_1, \ldots, e_n\} \qquad e_i \in \mathcal{X}$$

Then, the function ψ_B maps every element $x \in \mathcal{X}$ to its coordinate representation for the base B, i.e.:

$$\psi_B : \mathcal{X} \mapsto \mathbb{R}^n \quad ; \quad x \mapsto \bar{x} = (x_1, \ldots, x_n)^T \qquad x \in \mathcal{X}, \bar{x} \in \mathbb{R}^n, x_i \in \mathbb{R},$$

where $\bar{x}$ represents the coordinate vector with coordinates x_i being real numbers. The inverse map, ψ_B^{-1}, maps the coordinate vector to its abstract element in the following way:

$$\psi_B^{-1} : \mathbb{R}^n \mapsto \mathcal{X} \quad ; \quad x = \sum_{i=1}^{n} e_i \cdot x_i \qquad x, e_i \in \mathcal{X}, x_i \in \mathbb{R},$$

which shows that any abstract element $x \in \mathcal{X}$ can be found by a linear combination of the basis elements. Hence, $\bar{x}$ represents the **coordinate vector** which holds an ordered sequence of numbers, called **coordinates**, which form a column vector, of which their values indicate 'how much of each basis element is needed' (hence B must be ordered such that the indexes of the coordinates x_i correspond to the indexes of the basis elements e_i) to form the element $x \in \mathcal{X}$, for which $\bar{x}$ is the numerical representative.

Clearly, choosing another base, i.e. picking other elements in $\mathcal{X}$ as basis elements, generally requires another linear combination of those new basis elements to form the same element $x \in \mathcal{X}$. Hence, the coordinates x_i and hence the coordinate vector $\bar{x}$ change for different bases, while the corresponding abstract element $x \in \mathcal{X}$ remains the same, see also Figure 5.13.

[17] Using an ordered base allows to index the basis elements and hence index the corresponding coordinates.

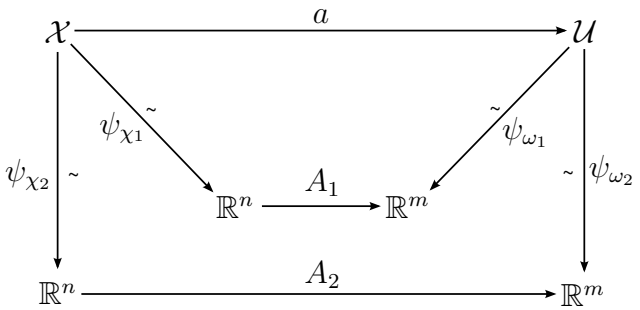

Figure 5.13: Commutative diagram showing different coordinate representations for the same abstract objects; spaces $\mathcal{X}$ and $\mathcal{U}$ and linear map a. The (invertible) map ψ_{χ_1} maps elements $x \in \mathcal{X}$ to coordinate vectors in $\mathbb{R}^n$ for the chosen base χ_1. The (invertible) map ψ_{ω_1} maps elements $u \in \mathcal{U}$ to coordinate vectors in $\mathbb{R}^m$ for the chosen base ω_1. The matrix A_1 represents the map a for the bases χ_1 and ω_2, while the matrix A_2 represents the map a for the bases χ_2 and ω_2. The commutative diagram shows that any abstract element $u \in \mathcal{U}$ as a result of mapping $x \in \mathcal{X}$ to $u \in \mathcal{U}$ through map a, can be found through $u = \psi_{\omega_1}^{-1} \circ A_1 \psi_{\chi_1}(x)$ or $u = \psi_{\omega_2}^{-1} \circ A_2 \psi_{\chi_2}(x)$ and must be the same.

Remark 5.13 (coordinate invariant solutions)**.** *Consider any problem for which the solution is given by the abstract element $x_s \in \mathcal{X}$. Consider the problem to be solved numerically in coordinates of base B_1 and the found solution to be some set of numbers, i.e. coordinate vector $\bar{x}_1$. Then it should be realized that $\bar{x}_1$ represents the element $x_s \in \mathcal{X}$ for the chosen base B_1. Hence, the actual solution is $x_s \in \mathcal{X}$ of which $\bar{x}_1$ is a numerical representative. Choosing another base B_2 and solving the same problem leads to another set of numbers, i.e. coordinate vector $\bar{x}_2$ is found. However, it should represent the same element $x_s \in \mathcal{X}$. If both solutions indeed represent the same element $x_s \in \mathcal{X}_s$, then the numerical solutions are called coordinate invariant.*

Remark 5.14. *Clearly, solutions that describe physical quantities in physical systems should be coordinate invariant, since nature (physical laws) does not care about coordinates. Coordinates are merely a human choice to represent the problem numerically. Hence, as said in Section 5.1.3, a physical equivalent solution must be coordinate invariant. However, a coordinate invariant solution is not necessarily a physically equivalent solution.*

Coordinate representation of map a Consider again the Hilbert spaces $\mathcal{X}$ and $\mathcal{U}$ and the linear map a, as given in Equation 5.1. For a particular choice of bases on $\mathcal{X}$ and $\mathcal{U}$, the linear map a can be represented as a $m \times n$ matrix, which will be denoted by its capital symbol, i.e. A. Any linear map a may be represented by many matrices, since the elements of A depend on the choice of bases. This is illustrated in the commutative diagram as shown in Figure 5.13.

Thus, for the current discussion for some chosen set of bases, the map a is represented by a $m \times n$ matrix A, such that the abstract mapping $a : \mathcal{X} \mapsto \mathcal{U} \quad ; \quad u = a(x) \quad x \in \mathcal{X}, u \in \mathcal{U}$ is represented by:

$$\bar{u} = A \cdot \bar{x} \qquad \bar{u} \in \mathbb{R}^m, \bar{x} \in \mathbb{R}^n, \tag{5.35}$$

with $\operatorname{rank} A = k$ and the (pseudo-)inverse map is denoted by $A^{\#}$.

Furthermore, for a chosen set of coordinates, the full-rank decomposition of a into c and f (see Theorem 5.1) is represented in matrix notation by $A = FC$, which is known as the full-rank factorization of a matrix [69]. F is a $m \times k$ full column-rank matrix[18] and C a $k \times n$

[18] Full column-rank: the number of columns is equal to $\operatorname{rank} F = \dim(\operatorname{im} f) = \dim(\operatorname{im} a) = k$.

full row-rank matrix[19] which represent the maps f and c respectively. Hence,

$$\begin{aligned} \bar{v} &= C \cdot \bar{x} \qquad \bar{v} \in \mathbb{R}^k, \bar{x} \in \mathbb{R}^n \\ \bar{u} &= F \cdot \bar{v} \qquad \bar{u} \in \mathbb{R}^m, \bar{v} \in \mathbb{R}^k, \end{aligned}$$

and

$$A^{\#} = C^{\#} F^{\#}. \tag{5.36}$$

In the remainder of this section, $C^{\#}$ and $F^{\#}$ will be investigated separately, parallel to subsections 5.4.2 and 5.4.3.

Original coordinates As discussed, the choice of bases and coordinates is arbitrary. Nevertheless, among all possible choices of bases, there are some choices which are suited to the schematics which are used for describing a problem or model. Even if they are not unique, from now on, these bases are called the **original bases**. The corresponding coordinates are called the **original coordinates**.

In practical situations, often the original bases are implicitly chosen. Fore example, when physical systems are considered, for which the map a is a physical map, the (implicitly) used bases often coincide with the physical quantities and attached variables of the physical model.

> To give a practical example of original bases and coordinates, see the example in Section 5.3.3 and Figure 5.4. The arrows indicating the lines of application for the contact forces represent the bases of the space $\mathcal{F}_c$ for which the matrix G is given. This intuitive choice of bases is called the original bases. The coordinates are given by the components f_{c1} and f_{c2} of the coordinate vector $\bar{f}_c \in \mathbb{R}^2$, which represents the element $f_c \in \mathcal{F}_c$. Notice that in Section 5.3.3, an abuse of notation is used, since the notation in Section 5.3.3 does not show a distinction between the element $f_c \in \mathcal{F}_c$ and its coordinate vector representation.

Before starting the calculations for the mathematical description of the pseudo-inverse map $a^{\#}$, the maps a, c and f are given a numerical representation by the matrices A,C and F respectively. Hence, bases are chosen for $\mathcal{X}$ and $\mathcal{U}$ and coordinates for $\mathcal{V}$ follow automatically. These chosen coordinates, either implicitly or explicitly defined, are considered the original coordinates.

Remark 5.15 (abuse of notations)**.** *From now on, the bar in the notation of coordinate vectors, which indicates coordinate vectors, is left out. Hence, abstract elements $x \in \mathcal{X}$ and their coordinate vector representations $\bar{x} \in \mathbb{R}^n$ are both denoted by x. From the context it follows whether the abstract element is meant or the representative coordinate vector.*

Let $\chi = \{\chi_1, \ldots, \chi_n\}$ be the original basis for $\mathcal{X}$ and $\omega = \{\omega_1, \ldots, \omega_m\}$ the original basis for $\mathcal{U}$. The according elements $x = (x_1, \ldots, x_n) \in \mathbb{R}^n$ are the coordinate vectors of which their components x_i are the original coordinates with respect to the original base χ. Also, $u = (u_1, \ldots, u_m) \in \mathbb{R}^m$ are the original coordinates of $\mathcal{U}$. Furthermore, the useful concept of a basis matrix is used, as defined in [73]:

Definition 5.17 (basis matrix)**.** *Any subspace $\mathcal{N}$ can be represented by a matrix N whose columns are a basis of $\mathcal{N}$, so that $\mathcal{N} = \operatorname{im} N$. Such a matrix is called a basis matrix of $\mathcal{N}$ and it follows that $\mathcal{N} = \operatorname{span}(\operatorname{col} N)$.*

[19] Full row-rank: the number of rows is equal to $\operatorname{rank} C = n - \dim(\ker c) = n - \dim(\ker a) = k$.

5.5.2 $C^{\#}$: Inversion of surjective and non-injective map

Consider the following basis matrices and coordinates for the subspaces $\mathcal{X}_n$ and $\mathcal{X}_v$ of $\mathcal{X}$ as introduced in Section 5.4.2:

- X_n is a $n \times (n-k)$ basis matrix of $\mathcal{X}_n$ (defined in Equation 5.28) expressed in the original coordinates, i.e. the columns of X_n are vectors in $\mathbb{R}^{n-k}$ expressed as components on the original basis χ. The elements $x_n = (x_{n1}, \ldots, x_{ni}, \ldots, x_{n(n-k)}) \in \mathbb{R}^{n-k}$ are $n-k$-dimensional vectors of which their components x_{ni} form the coordinates with respect to the base of $\mathcal{X}_n$.
- X_v is a $n \times k$ basis matrix of $\mathcal{X}_v$ expressed in the original coordinates. The elements $x_v = (x_{v1}, \ldots, x_{vi}, \ldots, x_{vk}) \in \mathbb{R}^k$ are k-dimensional vectors of which their components x_{vi} form the coordinates with respect to the base of the non-unique complementary space $\mathcal{X}_v$.

The pseudo-inversion of C is worked out as follows. Coordinate transformation s is defined to relate the subspace coordinates, x_{ni} and x_{vi}, to the original coordinates, see also Figure 5.12.

Definition 5.18. *Consider basis matrices X_n and X_v as given above and let s be the coordinate transformation, represented by the $n \times n$ matrix S:*

$$S = \begin{pmatrix} X_n & X_v \end{pmatrix}, \tag{5.37}$$

such that, as a consequence of the definition of the basis matrices X_n and X_v, the coordinates x_{ni} and x_{vi} are transformed to the original coordinates x through map s as follows:

$$x = S \cdot \begin{pmatrix} x_n \\ x_v \end{pmatrix} = X_n \cdot x_n + X_v \cdot x_v \tag{5.38}$$

With Definition 5.18 and using that $\operatorname{span}(\operatorname{col} X_n) = \ker C$ implies $CX_n = 0$, it is found that:

$$\begin{aligned} v &= CS \cdot \begin{pmatrix} x_n \\ x_v \end{pmatrix} && (5.39)\\ &= CX_n \cdot x_n + CX_v \cdot x_v && (5.40)\\ &= CX_v \cdot x_v, && (5.41) \end{aligned}$$

Property 5.1. *The term CX_v, as given in Equation 5.41, is a $k \times k$ invertible matrix.*

Proof. C is a $k \times n$ matrix with $\operatorname{rank} C = k$ (full row-rank) and X_v is a $n \times k$ matrix with $\operatorname{rank} X_v = k$ (full column-rank). Notice, by construction $\operatorname{span}(\operatorname{col} X_v) \notin \ker c$, therefore $\operatorname{im} C = \operatorname{im}(CX_v)$. Hence, C maps all linearly independent columns of X_v to different independent $v \in \mathcal{V}$ (no elements mapped to zero). Naturally, $\operatorname{im} C = \operatorname{im}(CX_v) \Rightarrow \dim(\operatorname{im}(CX_v)) = \dim(\operatorname{im} C) = \dim \mathcal{V} = k \Rightarrow \operatorname{rank}(CX_v) = \operatorname{rank} C = k$. CX_v is a $k \times k$ matrix, hence CX_v is full rank and therefore invertible. □

Taking Equation 5.41 and applying Property 5.1, gives:

$$x_v = (CX_v)^{-1} \cdot v \tag{5.42}$$

Finally, Equation 5.42 is pre-multiplied with X_v and substituted into Equation 5.38 to derive:

$$x = X_v \cdot (CX_v)^{-1} \cdot v + X_n \cdot x_n, \tag{5.43}$$

from which the set $\mathbb{X}_s \subset \mathbb{R}^n$ is found and given by:

$$\mathbb{X}_s := X_v \cdot (CX_v)^{-1} \cdot v_p + X_n \cdot x_n \qquad v_p \in \mathbb{R}^k, \forall x_n \in \mathbb{R}^{n-k}, \tag{5.44}$$

which represents the set $\mathcal{X}_s \subset \mathcal{X}$ (see Equation 5.31) of multiple exact inverse solutions (see Definition 5.4) for any $v_p \in \mathcal{V}$ for the chosen bases χ. Hence, for the chosen bases χ, $\mathbb{X}_s$ holds the coordinate vectors that represent all multiple exact inverse solutions of a given coordinate representation of $v_p \in \mathcal{V}$, such that $v_p = C \cdot x_s \quad \forall x_s \in \mathbb{X}_s$.

Orthogonal complementary spaces To complete the mathematical description, the complementary space $\mathcal{X}_v$ is **chosen** to be the orthogonal complementary space of $\mathcal{X}_n$ (see Definition 5.14), such that:

$$\mathcal{X}_v := \mathcal{X}_n^{\perp} = \ker c^{\perp} \tag{5.45}$$

Since $\mathcal{X}$ is a Hilbert space, the orthogonal complement $\mathcal{X}_v$ is a well defined choice and uniquely defined by the M_x-weighted inner-product, which is represented by the choice of metric M_x.

Then, for the chosen complementary space $\mathcal{X}_v$, as defined in Equation 5.45, a basis matrix X_v is worked out in the following theorem.

Theorem 5.2. *Consider $\mathcal{X}_v$ chosen to be the orthogonal complementary space of $\mathcal{X}_n = \ker c$ as defined in Equation 5.45. Then, a suitable basis matrix X_v for the orthogonal complementary space $\mathcal{X}_v$ is given by:*

$$X_v = M_x^{-1} \cdot C^T$$

Proof. By construction, X_v is a $n \times k$ full column-rank matrix and C is a $k \times n$ full row-rank matrix. $\operatorname{rank} X_v = \operatorname{rank} C = k$. Let X_n be the basis matrix of $\mathcal{X}_n$; by construction $X_v^T M_x X_n = 0$ ($\mathcal{X}_v = \mathcal{X}_n^{\perp}$, see Definition 5.14) and $CX_n = 0$ ($\mathcal{X}_n = \ker C$). Therefore, $X_v^T M_x = C$, which gives after rewriting and using symmetry of M_x (i.e. $M_x^{-1} = M_x^{-T}$): $X_v = M_x^{-1} \cdot C^T$. □

Substituting Theorem 5.2 into Equation 5.44, gives a complete description of the solution set $\mathbb{X}_s$ for the specific choice of $\mathcal{X}_v$, i.e. using the orthogonal complement as given in Equation 5.45:

$$\mathbb{X}_s := M_x^{-1} C^T \cdot \left(C M_x^{-1} C^T\right)^{-1} \cdot v_p + X_n \cdot x_n, \qquad v_p \in \mathbb{R}^k, \forall x_n \in \mathbb{R}^{n-k}, \tag{5.46}$$

The following theorem presents a well-known and useful property of the found solution set.

Theorem 5.3. *Let Equation 5.46 define the solution space $\mathbb{X}_s$, which contains the representative coordinate vectors of all exact inverse elements $x \in \mathbb{X}_s$ for a given $v_p \in \mathcal{V}$ for the chosen base χ and letting $\mathcal{X}_v$ be the orthogonal complement of $\mathcal{X}_n$, as given in Equation 5.45. Then, of all possible solutions $x_s \in \mathcal{X}_s$, for a given $v_p \in \mathcal{V}$, the minimum M_x-norm solution x_{ms} for the chosen coordinates is represented by:*

$$x_{ms} = M_x^{-1} C^T \cdot \left(C M_x^{-1} C^T\right)^{-1} \cdot v_p,$$

such that:

$$||M_x^{-1} C^T \left(C M_x^{-1} C^T\right)^{-1} \cdot v_p||^2 \leq ||M_x^{-1} C^T \left(C M_x^{-1} C^T\right)^{-1} \cdot v_p + X_n \cdot x_n||^2 \qquad v_p \in \mathbb{R}^k, \forall x_n \in \mathbb{R}^n$$

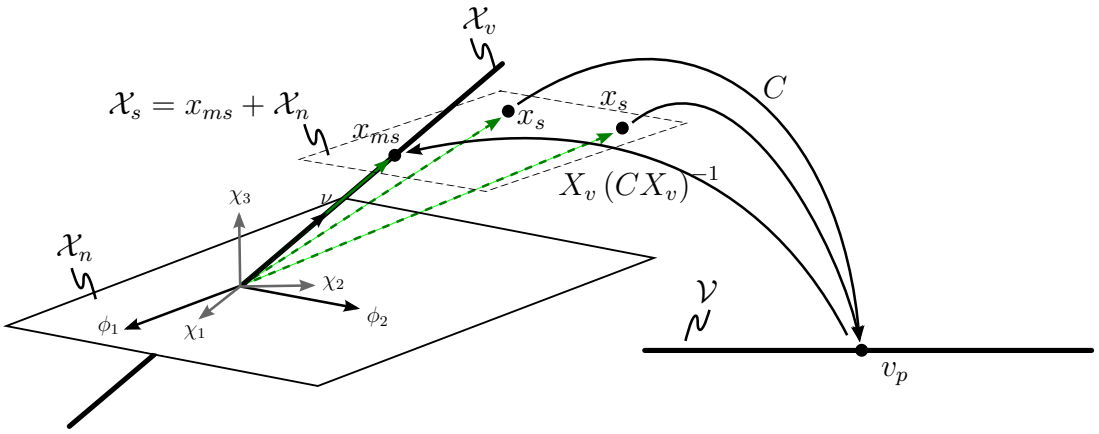

Figure 5.14: Geometric representation of projections on $\mathcal{X}$. This example assumes $n = 3, k = 1$ and $\dim \mathcal{X}_v = 1$, $\dim \mathcal{X}_n = 2$ and $\dim \mathcal{V} = 1$. The original base on $\mathcal{X}$ is given by the vectors $\{\chi_1, \chi_2, \chi_3\}$, the bases of the subspaces $\mathcal{X}_n$ and $\mathcal{X}_v$ are given by the vectors $\{\phi_1, \phi_2\}$ and $\{\nu\}$ respectively. Note that $\operatorname{col} X_n = \{\phi_1, \phi_2\}$ and $\operatorname{col} X_v = \{\nu\}$. All solutions of the inverse problem for the given $v_p \in \mathcal{V}$ are in the set $\mathcal{X}_s$. The minimal M_x-norm solution is the projection of any $x_s \in \mathcal{X}_s$ on $\mathcal{X}_v$ along $\mathcal{X}_n$, illustrated with x_{ms}. Going from x_s to v_p and back to x_{ms} is given by the map: $X_v\ (CX_v)^{-1} C$, i.e. the projection matrix.

Proof. Working out the norms (see Definition 5.13) and using the orthogonal construction of $\mathcal{X}_v$, i.e. $X_n^T \cdot M_x \cdot X_v = 0$, shows that:

$$||X_v\,(CX_v)^{-1} \cdot v_p||^2 = v_p^T \cdot (CX_v)^{-T}\, X_v^T \cdot M_x \cdot X_v\,(CX_v)^{-1} \cdot v_p = L$$

and

$$||M_x^{-1}C^T\left(CM_x^{-1}C^T\right)^{-1} \cdot v_p + X_n \cdot x_n||^2 = L + x_n^T X_n^T M_x X_n x_n.$$

M_x is positive definite, therefore $x_n^T X_n^T M_x X_n x_n > 0 \quad \forall x_n \backslash 0 \in \mathcal{X}_n$ and $x_n^T X_n^T M_x X_n x_n = 0$ with $x_n = 0$, which proofs the theorem. □

Hence, the minimum solution x_{ms} has no component in $\mathcal{X}_n$, i.e. $x_v = 0$.

Notice that x_{ms} being the minimum M_x-norm solution can also be understood by considering x_{ms} the orthogonal projection of all solutions $x_s \in \mathcal{X}_s \subset \mathcal{X}$ onto $\mathcal{X}_v$ along $\mathcal{X}_n$. Consider $v_p = C \cdot x_s \quad \forall x_s \in \mathcal{X}_s$ and find that $x_{ms} = M_x^{-1}C^T\left(CM_x^{-1}C^T\right)^{-1} C \cdot x_s$, where $M_x^{-1}C^T\left(CM_x^{-1}C^T\right)^{-1} C$ is the orthogonal projection matrix on $\mathcal{X}_v$ as illustrated in Figure 5.14. Orthogonal projections are extensively discussed in [73].

Conclusion Since C is a non-injective and surjective map, a set of multiple exact solutions is found for the inversion from any $v_p \in \mathcal{V}$. Letting $\mathcal{X}_v$ be the orthogonal complementary space of $\mathcal{X}_n$, defined through the M_x-weighted inner-product, resulted in the following solution set $\mathbb{X}_s$ for the chosen original bases χ:

$$\mathbb{X}_s := M_x^{-1}C^T \cdot \left(CM_x^{-1}C^T\right)^{-1} \cdot v_p + X_n \cdot x_n, \qquad v_p \in \mathbb{R}^k, \forall x_n \in \mathbb{R}^n. \tag{5.47}$$

Hence, following Definition 5.15, the pseudo-inverse map $c^{\#}$ is represented, for a chosen bases and coordinates, by the matrix $C^{\#} = M_x^{-1}C^T \cdot \left(CM_x^{-1}C^T\right)^{-1}$, which gives the minimum M_x-norm solution, such that $x_{ms} = C^{\#} \cdot v_p = M_x^{-1}C^T \cdot \left(CM_x^{-1}C^T\right)^{-1} \cdot v_p$ is the smallest solution with respect to the M_x-norm.

5.5.3 $F^{\#}$: Inversion of injective and non-surjective map

The inversion of the injective and non-surjective map f is examined:

$$f^{\#} : \mathcal{U} \to \mathcal{V}$$

Consider the following basis matrices and coordinates for the subspaces $\mathcal{U}_r = \operatorname{im} F$ (see Equation 5.32) and the non-unique complementary space $\mathcal{U}_n$ of $\mathcal{U}$ as introduced in Section 5.4.3:

- U_n is a $m \times (m-k)$ basis matrix of $\mathcal{U}_n$ expressed in the original coordinates, i.e. the columns of U_n are coordinate vectors in $\mathcal{U}$ expressed as components on the original basis ω. The vectors
$$u_n = (u_{n1}, \ldots, u_{ni}, \ldots, u_{n(m-k)}) \in \mathbb{R}^{m-k} \tag{5.48}$$
are $m-k$-dimensional coordinate vectors of which their components u_{ni} form the coordinates with respect to the base of $\mathcal{U}_n$.

- U_r is a $m \times k$ basis matrix of $\mathcal{U}_r$ expressed in the original coordinates. The vectors
$$u_r = (u_{r1}, \ldots, u_{ri}, \ldots, u_{rk}) \in \mathbb{R}^{k} \tag{5.49}$$
are k-dimensional coordinate vectors of which their components u_{ri} form the coordinates with respect to the base of $\mathcal{U}_r$.

The pseudo-inversion of F is worked out as follows. Coordinate transformation r is defined to relate the subspace coordinates, u_{ri} and u_{ri}, to the original coordinates, see also Figure 5.12.

Definition 5.19. *Consider basis matrices U_n and U_r as given above and and let r be the coordinate transformation, defined by the $m \times m$ matrix R:*

$$R = \begin{pmatrix} U_n & U_r \end{pmatrix}, \tag{5.50}$$

such that, as a consequence of the definition of the basis matrices U_n and U_r, the coordinates u_{ni} and u_{ri} are transformed to the original coordinates u through map r as follows:

$$u = R \cdot \begin{pmatrix} u_n \\ u_r \end{pmatrix} = U_n \cdot u_n + U_r \cdot u_r \tag{5.51}$$

As previously discussed, F maps v only to subspace $\mathcal{U}_r$. Thus, in general, for a given $u \in \mathcal{U}$, an exact solution $v_s \in \mathcal{V}$, for which F maps v_s to the given u does not exist.

Orthogonal complementary spaces To complete the mathematical description, the complementary space $\mathcal{U}_n$ is **chosen** to be the orthogonal complementary space of $\mathcal{U}_r$ (see Definition 5.14), such that:

$$\mathcal{U}_n := \mathcal{U}_r^{\perp} = \operatorname{im} f^{\perp} \tag{5.52}$$

Since $\mathcal{U}$ is a Hilbert space, the orthogonal complement $\mathcal{U}_n$ is a well defined choice and uniquely defined by the M_u-weighted inner-product, which is represented by the choice of metric M_u.

Then, in order to eliminate the unreachable coordinates u_n from the element u (see Equation 5.51), it is pre-multiplied with $U_r^T M_u$:

$$\begin{aligned} U_r^T M_u \cdot u &= U_r^T M_u U_n \cdot u_n + U_r^T M_u U_r \cdot u_r & (5.53)\\ &= U_r^T M_u U_r \cdot u_r, & (5.54) \end{aligned}$$

where it was used that $\operatorname{span}(\operatorname{col} U_n) = \mathcal{U}_r^{\perp} = \operatorname{im}(F)^{\perp}$ implies $U_r^T M_u U_n = 0$.

Theorem 5.4. *The term $U_r^T M_u U_r$, as given in Equation 5.54, is a $k \times k$ invertible matrix.*

Proof. U_r is a $m \times k$ matrix with $\operatorname{rank} U_r = k$, i.e. full column-rank. Metric M_u is a full rank $m \times m$ matrix, such that $M_u U_r$ is a $m \times k$ full column-rank matrix. $M_u U_r$ is then multiplied with U_r^T, a $k \times m$ full row-rank matrix, such that $U_r^T M_u U_r = U_r^T M_u U_r$ is a $k \times k$ matrix with rank k, i.e. full rank, which implies $U_r^T M_u U_r$ is invertible. □

Taking Equation 5.54 and applying Theorem 5.4, gives:

$$u_r = \left(U_r^T M_u U_r\right)^{-1} \cdot U_r^T M_u \cdot u \tag{5.55}$$

Since $\operatorname{im} F = \mathcal{U}_r$ and F is a $m \times k$ full column-rank matrix ($\operatorname{rank} F = k$), then an obvious and suitable choice for basis matrix U_r is given by:

$$U_r := F \tag{5.56}$$

Now, $u = F \cdot v$ is substituted into Equation 5.55 and Equation 5.56 is applied:

$$u_r = \left(F^T M_u F\right)^{-1} \cdot F^T M_u F \cdot v = v,$$

which shows $v = u_r$ (and also $\mathcal{V} = \mathcal{U}_r$). Hence, the **reachable part** of u, u_r, is found by substituting $v = u_r$ into Equation 5.55:

$$v = \left(F^T M_u F\right)^{-1} \cdot F^T M_u \cdot u \tag{5.57}$$

To complete the mathematical description, also the **unreachable part** of u, u_n is described. The reachable coordinates u_r are eliminated from the element u, by pre-multiplying u (Equation 5.51) with $U_n^T M_u$:

$$U_n^T M_u \cdot u \;=\; U_n^T M_u U_n \cdot u_n, \tag{5.58}$$

where it was used that $\operatorname{span}(\operatorname{col} U_n) = \mathcal{U}_r^\perp = \operatorname{im}(F)^\perp$ implies $U_n^T M_u U_r = 0$. For similar reasons as given in Theorem 5.4, $U_n^T M_u U_n$ is a $(m-k) \times (m-k)$ invertible matrix. Hence for a given $u \in \mathcal{U}$, u_n is found to be:

$$u_n = \left(U_n^T M_u U_n\right)^{-1} U_n^T M_u \cdot u \tag{5.59}$$

Theorem 5.5. *Consider $\mathcal{U}_n$ chosen to be the orthogonal complementary space of $\mathcal{U}_r = \ker c$ as defined in Equation 5.52. Then, a suitable basis matrix U_n for the orthogonal complementary space $\mathcal{U}_n$ is given by:*

$$U_n = M_u^{-1} \cdot \ker F^T$$

Proof. By construction $U_r^T M_u U_n = 0$ and also (consider Equation 5.56) $F^T M_u U_n = 0$. Furthermore, $F^T \cdot \ker F^T = 0$. Therefore, $M_u U_n = \ker F^T$, which gives: $U_n = M_u^{-1} \cdot \ker F^T$. □

With these results the geometric descriptions of Section 5.4.4, can be mathematically described by the following statements:

Definition 5.20. *Consider any $u_p \in \mathcal{U}$, represented by the coordinate vector[20] $u_p \in \mathbb{R}^m$, let $v_p \in \mathcal{V}$, represented by the coordinate vector $v_p \in \mathbb{R}^k$, be given by Equation 5.57:*

$$v_p = \left(F^T M_u F\right)^{-1} \cdot F^T M_u \cdot u_p \qquad u_p \in \mathbb{R}^m, \tag{5.60}$$

[20] Recall the abuse of notation, as noted in Remark 5.15.

and let the unreachable part $u_n \in \mathcal{U}_n$, represented by the coordinate vector $u_n \in \mathbb{R}^{m-k}$ (Equation 5.48), be given by Equation 5.59:

$$u_n = \left(U_n^T M_u U_n\right)^{-1} U_n^T M_u \cdot u_p \qquad u_p \in \mathbb{R}^m,$$

then:

1. *v_p is called the* **exact** *inverse element (see Definition 5.4) of u_p, such that $u_p = F \cdot v_p$, if $u_p \in \mathcal{U}_r$, i.e. $u_n = 0$.*
2. *v_p is called the* **partial inverse** *element of u_p, such that $u_p \neq F \cdot v_p \neq 0$, if $u_p \in \mathcal{U}_r \oplus \mathcal{U}_n$, i.e. $v_p \neq 0, u_n \neq 0$.*
3. *v_p is called non existent, i.e. $v_p = 0$, such that $F \cdot v_p = 0 \neq u_p$, if $u_p \in \mathcal{U}_n$.*

The following theorem presents a well-known and useful property of the above given solution.

Theorem 5.6. *Consider Definition 5.20, where Equation 5.60 defines (pseudo-) inverse solution v_p for a given $u_p \in \mathcal{U}$. Note that $F \cdot v_p \in \mathcal{U}_r \quad \forall v_p \in \mathcal{V}$ and recall that $\mathcal{U}_n$ is chosen to be the orthogonal complement of $\mathcal{U}_r$, as given in Equation 5.52. For any (partial) inverse solution v_p, as given in Equation 5.60, $F \cdot v_p$ produces the M_u-least squares error with respect to the given u_p:*

$$||u_p - F \cdot v_p||^2 \leq ||u_p - y||^2, \qquad \forall u_p \in \mathcal{U}, \forall y \in \mathcal{U}_r$$

Thus, out of all candidates $y \in \mathcal{U}_r$, $F \cdot v_p \in \mathcal{U}_r$ has the 'smallest distance' on $\mathcal{U}$ to the desired u_p, measured with the M_u-norm.

Proof. For any set of orthogonal vectors $a, b \in \mathcal{U}$, it is well known that $||a+b||^2 = ||a||^2 + ||b||^2$ (see e.g. [73]).Since $(u_p - Fv_p) \in \mathcal{U}_n$ and $(Fv_p - y) \in \mathcal{U}_r$, $(u_p - Fv_p)$ and $(Fv_p - y)$ are two orthogonal vectors. Hence,

$$\begin{aligned} ||u_p - y||^2 &= ||u_p - Fv_p + Fv_p - y||^2 \\ &= ||u_p - Fv_p||^2 + ||Fv_p - y||^2 \geq ||u_p - F \cdot v_p||^2 \end{aligned}$$

□

Notice that Fv_p being the M_u-least squares error can also be understood by considering Fv_p the orthogonal projection (along $\mathcal{U}_n = \mathcal{U}_r^\perp$) of $u_p \in \mathcal{U}$ onto the reachable set $\mathcal{U}_r$ expressed in the original coordinates u on the original base $\{\omega\}$. Thus, $Fv_p = F\left(F^T M_u F\right)^{-1} \cdot F^T M_u \cdot u_p$, where $F\left(F^T M_u F\right)^{-1} \cdot F^T M_u$ is the orthogonal projection matrix for $u_p \in \mathcal{U}$ on $\mathcal{U}_r$ as illustrated in Figure 5.15. Orthogonal projections are extensively discussed in [73].

Conclusion Since F is a non-surjective and injective map, generally no exact solutions are found for the inversion from any $u_p \in \mathcal{U}$. For $\mathcal{U}_n$ being the orthogonal complementary space of $\mathcal{U}_r$, defined through the M_u-weighted inner-product, the (partial) inverse element $v_p \in \mathcal{V}$, for the chosen original bases ω, is given by:

$$v_p = F^{\#} \cdot u_p = \left(F^T M_u F\right)^{-1} \cdot F^T M_u \cdot u_p \qquad u_p \in \mathcal{U}, \tag{5.61}$$

which gives $F \cdot v_p \in \mathcal{U}_r$ closest (M_u-least squares error) to u_p. Hence, following Definition 5.16, the pseudo-inverse map $f^{\#}$ is represented, for a chosen bases and coordinates, by the matrix $F^{\#} = \left(F^T M_u F\right)^{-1} \cdot F^T M_u$.

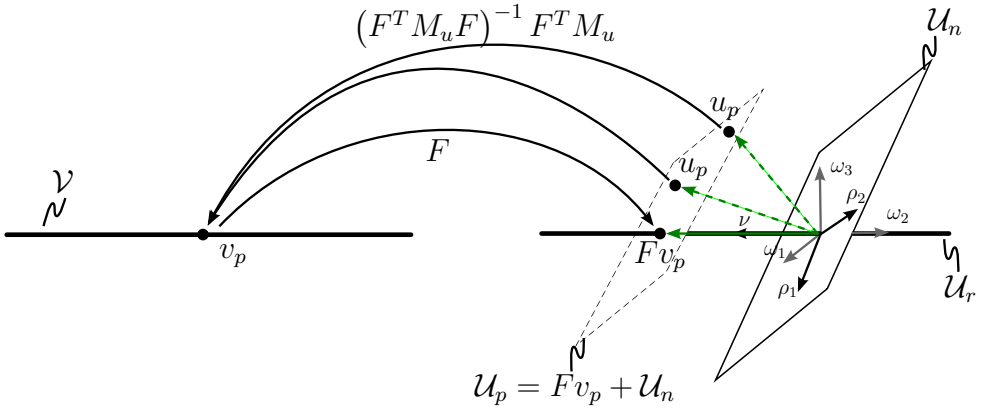

Figure 5.15: Geometric representation of projections on $\mathcal{U}$. This example assumes $m = 3, k = 1$ and $\dim \mathcal{U}_r = 1$, $\dim \mathcal{U}_n = 2$ and $\dim \mathcal{V} = 1$. The original base on $\mathcal{U}$ is given by the vectors $\{\omega_1, \omega_2, \omega_3\}$, the bases of the subspaces $\mathcal{U}_n$ and $\mathcal{U}_r$ are given by the vectors $\{\rho_1, \rho_2\}$ and $\{\nu\}$ respectively. Note that $\operatorname{col} U_r = \{\rho_1, \rho_2\}$ and $\operatorname{col} X_n = \{\nu\}$. For all $u_p \in \mathcal{U}_p$, the same non-exact inverse element $v_p \in \mathcal{V}$ is found, which F maps to the element $Fv_p \in \mathcal{U}_r$, expressed in the original base. Fv_p is the M_u-least squares error element with respect to u_p, i.e. it is the projection of any $u_p \in \mathcal{U}_p$ on $\mathcal{U}_r$ along $\mathcal{U}_n$. Going from u_p to v_p and back to Fv_p is given by the map: $F\left(F^T M_u F\right)^{-1} \cdot F^T M_u$, i.e. the projection matrix.

Multiple $u_p \in \mathcal{U}$ have the same (partial) inverse element, i.e. v_p is the partial inverse element for all $u_p \in \mathcal{U}_p \subset \mathcal{U}$:

$$\mathcal{U}_p := F \cdot v_p + \mathcal{U}_n, \qquad v_p \in \mathcal{V}$$

The non reachable part of $u_p \in \mathcal{U}$ is given by:

$$u_n = \left(U_n^T M_u U_n\right)^{-1} U_n^T M_u \cdot u \tag{5.62}$$

i.e. the projection of u_p on $\mathcal{U}_n$, expressed in subspace coordinates u_{ni}.

5.5.4 $A^{\#}$: Complete mathematical description

A mathematical description for the inversion of any element $u_p \in \mathcal{U}$ to some element $x_s \in \mathcal{X}$ for the given map $a : \mathcal{X} \mapsto \mathcal{U}$ has been investigated by considering coordinates such that matrix C and F represent the maps c and f. The complete inversion of the original map a, represented by the matrix A is found by the composition of C and F. This composition is illustrated in Figure 5.16 and given by the composition of both submaps, see Equation 5.36.

In accordance with the geometrical description given in Section 5.4.4, the following mathematical description is found for the inversion of the non-bijective map a, given by matrix A (taking together Equation 5.46, 5.61 and 5.62) for the chosen original bases χ and ω on $\mathcal{X}$ and $\mathcal{U}$ respectively:

Definition 5.21. *Consider (sub)spaces, elements and maps as defined throughout this chapter and let them be represented by their according coordinate vectors and matrices, as defined throughout this chapter. For any element $u_p \in \mathcal{U}$, represented by the coordinate vector $u_p \in \mathbb{R}^k$, and the given map a, represented by the matrix A, the set $\mathbb{X}_s \subset \mathbb{R}^n$ of (pseudo-) inverse solutions is given by:*

$$\mathbb{X}_s = M_x^{-1} C^T \left(C M_x^{-1} C^T\right)^{-1} \cdot \left(F^T M_u F\right)^{-1} F^T M_u \cdot u_p + X_n \cdot x_n, \qquad \forall x_n \in \mathbb{R}^{n-k}, u_p \in \mathbb{R}^k,$$

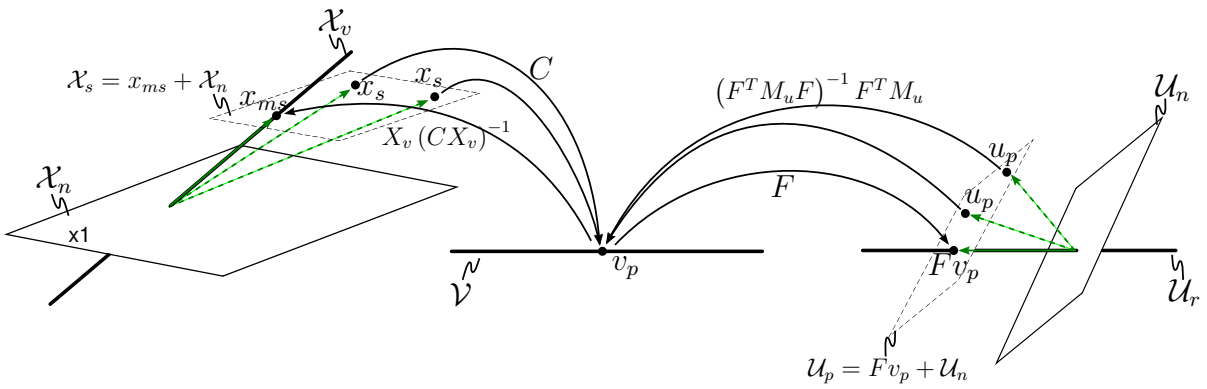

Figure 5.16: Complete composition of forward and backward mapping of map a, represented by matrix A. The decomposition of A is defined by: $A =: FC$, and the inverse relations follows from the illustration, composed by $A^{\#} := C^{\#} \circ F^{\#}$.

and the unreachable part $u_n \in \mathcal{U}_n$, represented in coordinates $u_n \in \mathbb{R}^{m-k}$, is given by[21]*:*

$$u_n = \left(U_n^T M_u U_n\right)^{-1} U_n^T M_u \cdot u_p \qquad u_p \in \mathcal{U},$$

where:

1. *the pseudo-inverse map $a^{\#}$ is represented by the matrix: $A^{\#} = M_x^{-1} C^T \left(C M_x^{-1} C^T\right)^{-1} \cdot \left(F^T M_u F\right)^{-1} F^T M_u$, which selects, for a given $u_p \in \mathcal{U}$, within the set $\mathbb{X}_s$, the minimum M_x-norm element, represented in coordinates by $x_{ms} \in \mathbb{X}_s$:*

$$\begin{aligned} x_{ms} &:= A^{\#} \cdot u_p = C^{\#} F^{\#} \cdot u_p \\ &= M_x^{-1} C^T \left(C M_x^{-1} C^T\right)^{-1} \cdot \left(F^T M_u F\right)^{-1} F^T M_u \cdot u_p \qquad u_p \in \mathbb{R}^k, \end{aligned} \tag{5.63}$$

   and which gives the coordinate vector $A \cdot x_{ms} \in \mathbb{R}^k$, which represents the element in $\mathcal{U}_r$ closest (M_u-least squares error) to $u_p \in \mathcal{U}$.

2. *for $u_p \in \mathcal{U}_r$, with $u_n = 0$, $\mathbb{X}_s$ holds all* **exact** *inverse elements of u_p, such that $u_p = A \cdot x_s \quad \forall x_s \in \mathbb{X}_s$;*

3. *for $u_p \in \mathcal{U}_n$ with $u_p \cap \mathcal{U}_r \neq \emptyset$, $\mathbb{X}_s$ holds all* **partial inverse** *elements of u_p, such that $A \cdot x_s \neq 0 \neq u_p \quad \forall x_s \in \mathbb{X}_s$ is the M_u-least square error with respect to u_p.*

4. *for $u_p \in \mathcal{U}_n$, with $A \cdot u_p = 0$ and $u_n \neq 0$, $\mathbb{X}_s$ does not hold inverse elements, i.e. $\operatorname{span} \mathbb{X}_s = \mathcal{X}_n$, such that $A \cdot x_s = 0 \neq u_p$*

Remark 5.16. *The set $\mathbb{X}_s$ (see Definition 5.21) is equal for multiple $u_p \in \mathcal{U}$. $\mathbb{X}_s$ is equal for all $u_p \in \mathcal{U}_p \subset \mathcal{U}$:*

$$\mathcal{U}_p := A \cdot x_s + \mathcal{U}_n, \qquad x_s \in \mathbb{X}_s$$

5.5.5 Conclusions

The inverse relation for the map a, mathematically represented by A, was shown and calculated analogues to the intuitive coordinate free geometrical analyses presented in Section 5.4.

[21] Note: the reader may recognize a projection: $\tilde{u} = U_n \cdot \left(U_n^T M_u U_n\right)^{-1} U_n^T M_u \cdot u_p$, is the coordinate vector ($\tilde{u} \in \mathbb{R}^k$) of the projection of $u_p \in \mathbb{R}^k$ onto $\mathcal{U}_n$ given in the original coordinates ω of $\mathcal{U}$, where it is used that $\tilde{u} = U_n \cdot u_n$ (Definition 5.19).

The resulting matrix representation of the pseudo-inverse map $a^{\#}$, presented in Equation 5.63 by $A^{\#}$, is well-known as the **weighted generalized inverse** of matrix A [69, 71]. Nevertheless, in this section a different approach was taken to explain and investigate the properties of non-bijective maps. A separation of spaces $\mathcal{X}$ and $\mathcal{U}$ into complementary subspaces was used as starting point for an intuitive geometrical description. Mathematically this was worked out by defining suitable subspace bases and coordinates through a coordinate transformation.

The intuitive description led to the mathematical summary of all mapping properties, stated in Definition 5.21. From the discussion it is important to realize that the pseudo-inverse map depends on the choice of complementary spaces $\mathcal{X}_n$ and $\mathcal{U}_v$. These spaces are by no means unique and hence the pseudo-inverse solution is not unique.

The inner-products on the Hilbert spaces $\mathcal{X}$ and $\mathcal{U}$ can be used to construct orthogonal complementary spaces. For such a choice, the complementary spaces depend on the choice of metrics M_x and M_u. This is also reflected in the mathematical description given in Definition 5.21, which encompass metrics M_x and M_u.

Of particular interest is the property that the inverse solution in Equation 5.63, gives a minimum M_x-norm solution in $\mathcal{X}$ and produces the M_u-least squares error in $\mathcal{U}$ [71], while the non-reachable parts are found in $\mathcal{U}_n$.

Physically equivalent pseudo-inverse map For the physically equivalent pseudo-inverse map, the structure of the Hilbert spaces is used by utilizing the inner-product to construct orthogonal complementary spaces. Hence, searching for the Physically equivalent pseudo-inverse map boils down to determining the metrics which can be used to describe the complementary space that is found in nature, i.e. in the physical system.

The insights will be of major importance for usage of the remainder of this chapter (continuing on physically equivalence) as well as for the analysis and control of an underactuated robot finger, see Chapter 6 and Chapter 7.

5.6 Example Continued: Applying Mathematical Inverse

The insights and results obtained from the geometrical and mathematical description of non-bijective maps and in particular the inversion problem of these maps is applied to the physical example introduced in Section 5.3. Also the relation between the inverse solution and the physically equivalent solutions is discussed for this particular case. This will then be extended to more general cases in the next section, Section 5.7.

5.6.1 Example: Simple grasp force decomposition

Geometric inverse description Consider again the simple grasp system as presented in Section 5.3.4 and Figure 5.4. Elements and spaces are used as given in Equation 5.9, where the space of contact forces $\mathcal{F}_c$ is a Hilbert space with metric M_f, which needs to be determined, such that (following Definition 5.12):

$$\langle f_1, f_2 \rangle := f_1 \cdot M_f \cdot f_2^T, \qquad f_1, f_2 \in \mathcal{F}_c, \tag{5.64}$$

Recall that $\mathcal{F}_c$ contains co-vectors (represented by row vectors).

Section 5.3.5 discusses the inversion problem. The inversion of G deals with a surjective and non-injective map. Since G is surjective, G does not need to be decomposed, see Remark 5.7.

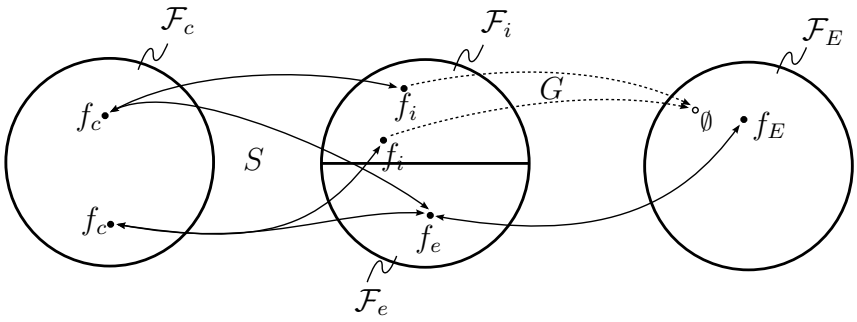

Figure 5.17: Splitting $\mathcal{F}_c$ into $\mathcal{F}_i$ and $\mathcal{F}_e$ through the kernel of G. Elements $f_c \in \mathcal{F}_c$ are split into $f_i \in \mathcal{F}_i$ and $f_e \in \mathcal{F}_e$, such that $f_i \oplus f_e = f_c$. Clearly, all $f_i \in \mathcal{F}_i$ map to $\emptyset \in \mathcal{F}_e$, whereas all $f_e \in \mathcal{F}_e$ map to some $f \in \mathcal{F}_E$ and all $f_E \backslash \emptyset \in \mathcal{F}_E$ are mapped to by $f_e \in \mathcal{F}_e$, i.e. bijective relation.

Hence, Section 5.4.2 shows that the required contact forces to resist f_d are given by the set $\mathcal{F}_s$ (see Equation 5.31 and Equation 5.46):

$$\mathcal{F}_s := G^{\#} \cdot (-f_d) + \mathcal{F}_i \qquad f_d \in \mathcal{F}_E, \tag{5.65}$$

where $\mathcal{F}_i$ is intrinsically defined by the map G (following Equation 5.28):

$$\mathcal{F}_i = \ker G$$

and the elements $G^{\#} \cdot (-f_d)$ are contained in the non-unique complementary space $\mathcal{F}_e$:

$$G^{\#} \cdot (-f_d) \in \mathcal{F}_e$$

For this complementary space, $\mathcal{F}_e$, the orthogonal complement is chosen, such that (following Equation 5.30):

$$\mathcal{F}_e = \ker G^{\perp}.$$

Thus, $\mathcal{F}_e$ is induced by the inner-product and hence uniquely defined by the metric M_f. Clearly, $\mathcal{F}_c$ is decomposed into $\mathcal{F}_i$ and $\mathcal{F}_e$. This is illustrated in Figure 5.17. Notice that the dimension of both subspaces is 1.

Geometric interpretation Both spaces have a clear interpretation: $\mathcal{F}_i$ represents internal forces and $\mathcal{F}_e$ holds the external forces.

The internal forces represent the self-balanced forces *as a result of applied contact forces* that have no effect on the global motion of the object [76], because they are in $\ker G$ and hence produce $f_{co} = 0$, i.e. no object motion induced trough contact forces. For the given example, the internal force has a clear physical interpretation: the internal force is the amount of compression (i.e. squeezing) of the object (assuming that the object has finite stiffness) along the horizontal direction of the applied forces (i.e. the basis for the internal force coincides with this application line). For higher order grasp systems, with $n_c > 2$, the physical interpretation of the bases of the internal forces is non-trivial, see e.g. [78].

Furthermore, $\mathcal{F}_e$ contains the unique external force inducing elements, that generate $f_{co} \neq 0$ *as a result of applied contact forces*. Thus, to resist f_d, Equation 5.65 shows that the contact forces f_c must equal at least $G^{\#} \cdot (-f_d)$ plus optionally any $f_i \in \mathcal{F}_i$.

Mathematical inverse description Following Section 5.5.2, it is noticed that G is given for the original bases of $\mathcal{F}_c$, which lies along the arrows indicating the lines of application for the contact forces. The coordinates along these bases are given by the components f_{c1} and

f_{c2} of the coordinate vector $f_c \in \mathbb{R}^2$, which represents the elements $f_c \in \mathcal{F}_c$, where the abuse of notation is used, see Remark 5.15.

Then the coordinate transformation S is given by:

$$S = \begin{pmatrix} F_e & F_i \end{pmatrix}, \tag{5.66}$$

with F_e the 2×1 basis matrix of $\mathcal{F}_e$ expressed in the original bases of $\mathcal{F}_c$ and F_i the 2×1 basis matrix of $\mathcal{F}_i$ expressed in the original bases of $\mathcal{F}_c$. Therefore, the coordinate change defines:

$$f_c^T = S \cdot \begin{pmatrix} f_i \\ f_e \end{pmatrix},$$

with f_i the single coordinate of $\mathcal{F}_i$ and f_e the single coordinate of $\mathcal{F}_e$ for their new bases as represented by the according basis matrices F_i and F_e.

Finally, after proceeding the analysis parallel to Section 5.5.2, from Equation 5.46, the mathematical description of the set of all possible solutions of the investigated inverse problem are found:

$$\mathcal{F}_s := M_f^{-1} G^T \cdot \left(G M_f^{-1} G^T\right)^{-1} \cdot (-f_d) + F_i \cdot f_i, \qquad f_d \in \mathcal{F}_E, \forall f_i \in \mathcal{F}_i, \tag{5.67}$$

Naturally, it follows that for any desired $f_{co} \in \mathcal{F}_E$ (recall $f_o = f_{co} + f_d$, with $f_{co} = G \cdot f_c^T$), the required set of generating contact forces expressed in the original base is found to be:

$$\mathcal{F}_g := M_f^{-1} G^T \cdot \left(G M_f^{-1} G^T\right)^{-1} \cdot f_{co} + F_i \cdot f_i, \qquad f_{co} \in \mathcal{F}_E, \forall f_i \in \mathcal{F}_i, \tag{5.68}$$

such that $\forall f_c \in \mathcal{F}_g$, $f_{co} = G f_c^T = G G^{\#} f_{co} + G F_i \cdot f_i = G G^{\#} f_{co} = f_{co}$, with f_i the internal force coordinate with respect to the base of $\mathcal{F}_i$.

It is noticed that the minimum M_f-norm solution $f_{mc} \in \mathcal{F}_g$, that produces the desired f_{co}, is given by:

$$f_{mc}^T = G^{\#} \cdot f_{co} = M_f^{-1} G^T \cdot \left(G M_f^{-1} G^T\right)^{-1} \cdot f_{co} \tag{5.69}$$

Internal forces Recall that the examined situation assumes maintaining finger-object contact. Therefore the contact forces must be at least positive and, for force closure[22], have a minimum $f_{c,min} \geq 0$. Hence:

$$f_c \geq f_{c,min} \quad \Rightarrow \quad M_f^{-1} G^T \cdot \left(G M_f^{-1} G^T\right)^{-1} \cdot f_{co} + F_i \cdot f_i \geq f_{c,min} \qquad f_{co} \in \mathcal{F}_E, \forall f_i \in \mathcal{F}_i. \tag{5.70}$$

Therefore, the internal forces can not be chosen arbitrarily. As intuitively understandable, some object squeezing is needed to maintain the grasp, where the amount of squeezing is determined by choosing f_i:

$$F_i \cdot f_i \geq f_{c,min} - M_f^{-1} G^T \cdot \left(G M_f^{-1} G^T\right)^{-1} \cdot f_{co} \qquad f_{co} \in \mathcal{F}_E, \forall f_i \in \mathcal{F}_i. \tag{5.71}$$

5.6.2 Physically equivalent solution

The simple grasp inversion problem as given in Equation 5.8 and discussed in Section 5.3.5 was solved by applying three different approaches. It was already concluded that Equation 5.25

[22] Note: in e.g. [65] it is shown that for force closure grasps, the lower limits of f_c are determined by the friction cones.

represents the physically equivalent inverse solution. The weighted pseudo-inverse, as geometrically presented in Section 5.6.1, also led to find an pseudo-inverse map $G^{\#}$, being the minimum M_f-norm solution (Equation 5.69). Yet, a metric M_f still needs to be found in order to let the $G^{\#}$ coincide the physically equivalent inverse solution, Equation 5.25. Hence, M_f must be the metric which induces a decomposition of spaces which is equivalent to the decomposition of spaces found in nature, i.e. in the real physical system.

Physically consistent metrics In order to find the appropriate metric M_f, it must be recognized that any candidate metric M_f must at least induce a coordinate invariant inner-product, as clearly presented in [70, 71]. Arbitrary metrics may lead to misleading coordinate invariant (hence physical inconsistent) results [71]. Such a case arises when the Euclidean inner-product is used on the vector space $\mathcal{F}_c$, while $\mathcal{F}_c$ would be represented with components of different physical units [71]. Applying a scaling metric (e.g. choosing the identity matrix, while attaching different units to the unitary elements) to make the physical units work out, still may not lead to coordinate invariant results. Clearly, nature has one unique solution for this inversion problem, which certainly does not depend on the coordinates used to describe the problem.

For this particular case, $\mathcal{F}_c$ does contain components with equal units, namely $[N]$ (Newton). Hence, applying the Euclidean norm gives coordinate invariant results. Notice that, by applying the Euclidean norm on $\mathcal{F}_c$ (i.e. M_f the identity metric, $M_f = \mathbb{I}_2$), Equation 5.69 reduces to the Moore-Penrose pseudo-inverse (Equation 5.17). This makes the Moore-Penrose a particular case of the weighted generalized inverse.

However, considering Remark 5.6, it is not clear whether this identity metric, maps the velocities (or infinitesimal displacements) to forces, as must be the case (see Remark 5.6).

Physically equivalent solution Nevertheless, coordinate invariance does not necessarily imply physical equivalence. Hence, in order to let Equation 5.69 be the physically equivalent solution, metric M_f must make Equation 5.69 coincide with the known physically equivalent solution, Equation 5.25.

Easy inspection reveals that $M_f = C$ (given in Equation 5.22) lets both solutions coincide. This implies that the natural metric on $\mathcal{F}_c$ must be the compliance matrix C, as given in Equation 5.22.

Again, considering Remark 5.6, indeed C^{-1} maps infinitesimal displacements to forces, as shown in Equation 5.23; $\Delta f_c^T = C^{-1} \cdot \Delta\epsilon$. Hence, the map $GM_f^{-1}G^T = GC^{-1}G^T$ is a physical meaningful composition of maps:

$$GC^{-1}G^T : T_x\mathcal{X} \overset{G^T}{\to} T_\epsilon\mathcal{E}_c \overset{C^{-1}}{\to} \mathcal{F}_c \overset{G}{\to} \mathcal{F}_E$$

Hence, also from this perspective, the found metric is physically meaningful.

Furthermore, for $M_f = C$, Equation 5.69 produces the minimum C-norm solution, given by:

$$f_{mc}^T = C^{-1}G^T \cdot \left(GC^{-1}G^T\right) \cdot f_{co},$$

which minimizes the C-norm quantity:

$$||f_{mc}||^2 = f_{mc} \cdot C \cdot f_{mc}^T,$$

which is recognized as an elastic energy function, i.e. it is twice the total elastic co-Energy, $\mathbb{E}^*$, in the grasp system[23], see Equation 5.20. Hence, the physically equivalent solution for

[23]Notice that the contact forces that minimize $\mathbb{E}^*$ also minimize $2\mathbb{E}^*$ i.e. $\{f_{mc} \in \mathcal{F}_c | \min(\mathbb{E}^*)\} = \{f_{mc} \in \mathcal{F}_c | \min(2\mathbb{E}^*)\}$.

the simple grasp inversion problem can be described by applying the weighted generalized pseudo-inverse and using the metric $M_f = C$.

Conclusion For the inverse problem in the simple grasp example, the physically equivalent pseudo-inverse map is found by letting the metric M_f on $\mathcal{F}_c$ be the compliance matrix, C, of the grasp system. Note that M_f and hence C are numerically denoted in the original coordinates of $\mathcal{F}_c$, i.e. the contact forces along the lines of application. Hence, also, for these original coordinates, C is simply given by a diagonal matrix with on the diagonal the compliance of each of the contacts corresponding to the contact force coordinates, see Equation 5.22.

The found physically equivalent pseudo-inverse map, $G^{\#}$, gives a minimum M_f-norm solution, which, for $M_f = C$, gives a physical quantity that corresponds to elastic co-energy. Hence, also the minimized quantity of the pseudo-inverse map corresponds with the physical quantity that was minimized, which led to derive the physically equivalent solution in Equation 5.21.

From the geometrical discussion, it is clear that the minimum M_f-norm solution is the projection of all exact inverse solutions in $\mathcal{F}_s$ (see Equation 5.65) along $\mathcal{F}_i = \ker G$ onto $\mathcal{F}_e$. Out of all possible choices for the complementary space $\mathcal{F}_e$, the orthogonal complement was used, induced by the inner-product. Hence, the metric M_f on the space of contact forces $\mathcal{F}_c$ determines the complementary space and hence the projection direction and also the minimized norm, which is induced by the inner-product.

5.6.3 General grasp system: Force decomposition

Section 5.3.2 presented the inverse problem for the $6 \times n_t$ grasp matrix G of the general grasp system, as summarized in Equation 5.8. Following the geometric treaty and mathematical discussion on general non-bijective maps (Section 5.4 and Section 5.5), the set $\mathcal{F}_s \subset \mathcal{F}_c$ is the set of inverse solutions for any desired $W_{co} \in se^*(3)$, given by (see Definition 5.21):

$$\mathcal{F}_s := M_f^{-1} G_c^T \left(G_c M_f^{-1} G_c^T \right)^{-1} \cdot \left(G_f^T M_w G_f \right)^{-1} G_f^T M_w \cdot W_{co} + F_i \cdot f_i \quad \forall f_i \in \mathcal{F}_i, W_{co} \in \mathcal{W}_o, \tag{5.72}$$

with full-rank decomposition $G = G_f \cdot G_c$ and with $\operatorname{rank} G = \text{row-rank}\, G_c = \text{column-rank}\, G_f = k$. G_c is a $k \times n_t$ matrix which represents a surjective and non-injective map, while G_f is a $6 \times k$ matrix representing a non-surjective and injective map.

Furthermore, the $n_t \times n_t$ matrix M_f and the 6×6 matrix M_w are the metrics that represent the inner-products on $\mathcal{F}_c$ and $se^*(3)$ of the grasp system, respectively. As discussed, the choice of metric is not unique and is used to define the decomposition of orthogonal complementary spaces. As opposed to the Euclidean space, there exists no intrinsic metric for M_w on $se^*(3)$ and $se(3)$ (see e.g. discussion in [79], which is based on the PhD dissertation of J. Loncaric (1985)). Candidate coordinate invariant metrics for M_w could follow from the dynamics involved for a specific inverse problem, e.g. the twists of a rigid body could be decomposed based on the kinetic energy metric [71].

Force decomposition The physically intuitive decomposition of forces follows from the decomposition of spaces through the constructed coordinate changes (Section 5.5). The following subspaces are distinguished:

- **Internal forces:** as seen in the simple grasp example:

$$\mathcal{F}_i = \ker G, \quad \dim(\mathcal{F}_i) = n_t - k,$$

represents the internal forces, with F_i the $n_t \times (n_t - k)$ basis matrix expressed in the original contact force coordinates and $f_i \in \mathbb{R}^{1\times(n_t-k)}$ the internal force coordinates. As opposed to the simple grasp example, for higher order grasp systems, with $n_c > 2$, the physical interpretation of the bases (directions) of the internal forces is non-trivial, see e.g. [78]. However, still, the intuition of squeezing the object holds.

- **Minimum M_f-norm elements:** the orthogonal complement of $\mathcal{F}_i$, $\mathcal{F}_e$, represents the set of minimum M_f-norm elements that impose (and resist) external forces on the object, i.e. $W_{co} \neq 0$:

$$\mathcal{F}_e = \mathcal{F}_i^{\perp} = \ker G^{\perp}, \quad \dim(\mathcal{F}_e) = k,$$

  which completes the decomposition of the space of contact forces for a specific choice of metric M_f: $\mathcal{F}_c = \mathcal{F}_i \oplus \mathcal{F}_e$.

- **Producible wrenches:** the producible wrenches are contained in:

$$\mathcal{W}_r = \operatorname{im} G, \quad \dim(\mathcal{W}_r) = k,$$

- **Non-producible wrenches:** the orthogonal complement of $\mathcal{W}_r$, which follows from a chosen (non-intrinsic) metric M_w, holds the *non-producible* wrenches:

$$\mathcal{W}_n = \mathcal{W}_n^{\perp} = \operatorname{im} G^{\perp}, \quad \dim(\mathcal{W}_n) = 6 - k.$$

  The non-producible wrenches are the wrenches that can not be resisted or generated. Hence, for the object wrench W_{co} the following situation are recognized:

  - $W_{co} \in \mathcal{W}_n$; the required W_{co} contains non-producible wrenches. Hence, a disturbance can not be fully rejected, i.e. the object may slip and the grasp fails and/or a desired object motion can not be fully induced. Thus, such a grasp is not force closed.
  - $W_{co} \notin \mathcal{W}_n$; the required W_{co} does not contain non-producible forces and can be fully resisted/generated.

  Note that the grasp matrix G generally is a function of the contact points and depends on the assumed contact model $\mathcal{H}_i$ (Equation 5.4). Hence G changes for each grasp configuration, which implies that also $\mathcal{W}_n$ changes, i.e. the set of non-producible (irresistible) wrenches depends on the chosen grasp configuration. Intuitively; humans choose their grasp according to expected disturbances, i.e. they make sure that their chosen grasp corresponds to maintaining these disturbance wrenches in $\mathcal{W}_r$.

This force decomposition gives a physical example of the inverse problem of physical maps as generically discussed in the previous sections. It allows to separate different force-acting components of the grasp, which has been used and shown to be useful for grasp analysis and grasping control, e.g. [80, 81, 82, 76, 83]. Clearly, for a physically equivalent decomposition, specific choices of metrics need to be used which correspond to the given phsycial system.

Physical equivalence Within the solution set $\mathcal{F}_s$, $f_{ms} \in \mathcal{F}_s$ is the minimum M_f-norm element:

$$f_{ms} := M_f^{-1} G_c^T \left(G_c M_f^{-1} G_c^T\right)^{-1} \cdot \left(G_f^T M_w G_f\right)^{-1} G_f^T M_w \cdot W_{co} \qquad W_{co} \in se^*(3), \qquad (5.73)$$

which generates $G \cdot f_{ms}^T \in \mathcal{W}_r$ closest (M_w-least squares error) to $W_{co} \in se^*(3)$. As discussed, in order to maintain static equilibrium for all $W_{co} \in se^*(3)$, force closure is needed. Hence it is needed that G is a surjective map such that $\mathcal{W}_n = \emptyset$ and f_{ms} solely follows from the metric on $\mathcal{F}_c$ ($f_{ms} = M_f^{-1} G^T \left(G M_f^{-1} G^T\right)^{-1} \cdot W_{co}$).

Consider this situation and consider the grasp system a static passive system. Then, for a given disturbance $W_d \in se^*(3)$, the resulting $f_c \in \mathcal{F}_s$ may re-establish equilibrium again: $W_o = W_d + G \cdot f_c^T$. This physical passive system of forces chooses f_{ms} by minimizing elastic energy in the system (e.g. contacts, structural compliance), as intuitively expected from the simple grasp example and also discussed in [75, 76].

Therefore, for such a (quasi-)static kinematic system, the compliance weighting matrix is of special interest, since it minimizes potential energy of the system and yields the action of a body in a potential field [75]. In this case, the force equilibrating action (i.e. the passive system response) is the action to be found.

Hence, for physical equivalence, M_f should be the concatenated $n_t \times n_t$ contact compliance matrix $\mathcal{C}_c$ expressed in the transmitted coordinates along bases of f_c. Hence, for the total grasp system with n_c contacts:

$$\mathcal{C}_c = \text{blockdiag}\left(C_{c1}, \cdots, C_{cn_c}\right),$$

with C_{ci} representing the total compliance through which contact forces f_{ci} are transmitted for contact i. Thus, C_{ci} holds the compliance components for contact i seen through the contact (in absence of other contacts), expressed in the transmitted coordinates of contact i (along the base of f_{ci}).

Considering a robot finger, the compliance C_{ci} is a series chain of joint (controller) compliance C_{qi}, mechanical/structural compliance C_{si} and (soft) contact compliance $\bar{C}_{ci}$ (see e.g. Equation 4.16):

$$C_{ci} = \bar{C}_{ci} + \mathcal{H}_i \left(J_i C_{qi} J_i^T + C_{si}\right) \mathcal{H}_i^T, \tag{5.74}$$

with $\bar{C}_{ci}$ the $n_{ci} \times n_{ci}$ matrix representing the contact compliance in the transmitted contact coordinates, and C_{si} the 6×6 structural compliance matrix expressed in twist ($se(3)$) coordinates. See also [40], Equation 11-14, which (however) does not include $\bar{C}_{ci}$.

5.6.4 Conclusions

The example of the grasp system has been used to show the application of the geometrical description of the inversion problem. The separation of spaces resulted in physically interpretable spaces, i.e. internal and external forces.

Furthermore, for force closure, the physically equivalent solution was discussed and shown to be the minimum M_f-norm solution if G is a surjective and non-injective map, while using compliance metrics for M_f. This compliance metric represents the compliance through which the contact forces f_c and the object wrenches W_o are transmitted. Hence, with such a metric, a minimum elastic energy solution is found, which is physically equivalent behavior of passive (natural) systems.

5.7 Duality for Physically Equivalent Solutions

As shown through the given example, for the inversion of non-bijective maps, the choice of metrics is of major influence when physical systems (e.g. kinematics) are modeled in order to get physically equivalent results.

Necessarily, physical consistent metrics should be used to make sure that the physical units work out properly and the results are coordinate invariant [70, 71]. And, as noticed in the given grasp system example, out of all possible coordinate invariant metrics, one metric gives physically equivalence.

Remark 5.17 (physically equivalent metric)**.** *Consider the inversion problem of a non-bijective physical map a for the physical system Σ, as presented in Section 5.1.3 and solved in Definition 5.21. The physically equivalent solution is given by the minimum M_x-norm M_u-least squares solution $x_{ms} \in \mathcal{X}_s$, with M_x and M_u the physically equivalent metrics of the spaces $\mathcal{X}$ and $\mathcal{U}$ in the model representation of the system Σ.*

Acknowledging nature's preference to optimize behavior with respect to physical scalar functions, the following definition is given:

Definition 5.22 (physically sensible norm)**.** *Consider Hilbert space $\mathcal{X}$, which represents physical quantities in a physical system Σ, as used in Definition 5.5. A norm on $\mathcal{X}$, $||x||^2$, induced by the M_x-weighted inner-product, as defined in Definition 5.12, is called a physically sensible norm on $\mathcal{X}$ if it represents a physically meaningful scalar function of Σ, like energy or power.*

Physically meaningful scalar function of real physical systems, like energy or power, are clearly coordinate invariant, since there are no coordinates in nature. Hence, any metric M_x, which is a coordinate representation of the above given physically sensible norm for a arbitrarily chosen base, is coordinate invariant. Clearly, independent of the choice of base, such metric M_x represents the same physical quantity for a given abstract element $x \in \mathcal{X}$.

Definition 5.23 (candidate physically equivalent metric)**.** *Consider $\mathcal{X}$ and Σ as used in Definition 5.22. A metric M_x on space $\mathcal{X}$, which induces a physically sensible norm on $\mathcal{X}$, as defined in Definition 5.22, is called a candidate physically equivalent metric.*

This section introduces the concept of physical dual spaces as a useful concept to check validity of a proposed physically equivalent inverse solution. The next section will then use these results to investigates several candidate physically equivalent metrics.

5.7.1 Dual spaces

A dual space is a well-known mathematical concept, defined by the following definition.

Definition 5.24 (dual space)**.** *The dual vector space to a real vector space $\mathcal{X}$ is the vector space, denoted $\mathcal{X}^*$, of linear operators $F : \mathcal{X} \to \mathbb{R} \quad ; \quad x^*(x) \mapsto \mathbb{R}$, with elements $x^* \in \mathcal{X}^*$.*

The notation $x^*(x)$ denotes the elements of the dual spaces as functions that operate on $x \in \mathcal{X}$. In coordinates, $\mathcal{X}$ contains vectors (denoted by column arrays), therefore the dual space elements $x^* \in \mathcal{X}^*$ contain co-vectors, denoted as row arrays, such that $\mathcal{X}^* \times \mathcal{X} \mapsto \mathbb{R}$ can be written as $x^* x \quad x^* \in \mathcal{X}^*, x \in \mathcal{X}$.

Associated isomorphisms The associated isomorphisms[24] for the inner-product on $\mathcal{X}$ allow to attach to each $x \in \mathcal{X}$ a unique dual element $x^* \in \mathcal{X}^*$ and to define an inner-product on $\mathcal{X}^*$. This is mathematically explained in e.g. [77] and summarized hereafter. Dual elements associated in this manner will be used for the analysis of pseudo-inverse maps. Note that in general there is no intrinsic isomorphism between two dual spaces, hence the associated isomorphism

[24] Note: an isomorphism is a bijective map between two vector spaces.

for the inner-product, as used here, is a particular choice motivated by the orthogonal space decomposition as presented before.

Recall the M_x-weighted inner-product for a Hilbert space $\mathcal{X}$, Definition 5.12, and notice that an inner-product is a bilinear map. The bilinear map for the M_x-weighted inner-product on $\mathcal{X}$ is abstractly represented by $\mathbb{G}_x$:

$$\mathbb{G}_x : \mathcal{X} \times \mathcal{X} \mapsto \mathbb{R} \quad ; \quad \langle x_1, x_2 \rangle \mapsto \mathbb{R} \qquad x_1, x_2 \in \mathcal{X} \tag{5.75}$$

> **Note:** in the notations in the metric M_x and the M_x-weighted inner-product $\mathbb{G}_x$, the subscript $_x$ refers to a Hilbert space $\mathcal{X}$.

For chosen bases on $\mathcal{X}$, the inner-product $\mathbb{G}_x$ is represented by a matrix M_x, called metric, as shown in Definition 5.12. For the bilinear map $\mathbb{G}_x$, a linear map $\mathbb{G}_x^\flat : \mathcal{X} \mapsto \mathcal{X}^*$, called flat map of $\mathbb{G}_x$, is defined by:

$$x^* = \mathbb{G}_x^\flat(x_1) \quad s.t. \quad x^*(x_2) = \mathbb{G}_x(x_1, x_2) = \langle x_1, x_2 \rangle \qquad x_1, x_2 \in \mathcal{X}, \tag{5.76}$$

which is invertible, due to positive definiteness of the inner-product $\mathbb{G}_x$.

Definition 5.25 (M_x-associated isomorphisms)**.** *For a given inner-product $\mathbb{G}_x$, as defined in Equation 5.75 and represented by metric M_x, the linear maps $\mathbb{G}_x^\flat$ and its inverse map (called sharp map, denoted $\mathbb{G}_x^\sharp$), as defined in Equation 5.76, are called the M_x-associated isomorphisms for the inner-product $\mathbb{G}_x$.*

Note that in coordinates, the M_x-weighted inner-product is represented by the metric M_x, and for the same coordinates, the flat map $\mathbb{G}_x^\flat$ is represented by the same matrix M_x. Hence, in coordinates, for given $x_1, x_2 \in \mathcal{X}$, the M_x-weighted inner-product is given by $\langle x_1, x_2 \rangle = x_1^T M_x x_2$, whereas for a given $x_1 \in \mathcal{X}$ the M_x-associated isomorphism (flat map $\mathbb{G}_x^\flat$) allows to associate a dual element $M_x \cdot x_1 = (x^*)^T \in \mathcal{X}^*$, such that indeed the image of x_2 under this $x^* = x_1^T M_x$ is represented by: $x^* x_2 = x_1^T M_x x_2 = \langle x_1, x_2 \rangle$, as required by Equation 5.76. These associated dual elements, for the particular choice of isomorphisms, being the M_x-associated isomorphisms, are named M_x-associated dual elements.

Definition 5.26 (M_x-associated dual elements)**.** *Let $\mathbb{G}_x$ be the M_x-weighted inner-product on $\mathcal{X}$, as defined in Equation 5.75. Then the M_x-associated isomorphisms, as defined in Definition 5.25, associate to each $x \in \mathcal{X}$ a unique dual element $x^* \in \mathcal{X}^*$. These associated dual elements are called M_x-associated dual elements.*

The M_x-associated isomorphisms also allow to define an inner-product $\mathbb{G}_x^*$ on the dual space, given by:

$$\mathbb{G}_x^*(x_1^*, x_2^*) = \mathbb{G}_x^{-1}(x_1^*, x_2^*) = \mathbb{G}_x((\mathbb{G}_x^\flat)^{-1}(x_1^*), (\mathbb{G}_x^\flat)^{-1}(x_2^*)) \qquad x_1^*, x_2^* \in \mathcal{X}^*, \tag{5.77}$$

which shows that this inner-product $\mathbb{G}_x^*$ on $\mathcal{X}^*$ for elements $x_1^*, x_2^* \in \mathcal{X}^*$ is equal to the inner-product $\mathbb{G}$ on $\mathcal{X}$ for the M_x-associated dual elements $x_1, x_2 \in \mathcal{X}$, given by the associated isomorphisms: $x_1 = (\mathbb{G}^\flat)^{-1}(x_1^*)$, etc.

Definition 5.27 (M_x-induced inner-product)**.** *For a given inner-product $\mathbb{G}_x$ on $\mathcal{X}$, as defined in Equation 5.75 and represented by metric M_x, the particular inner-product $\mathbb{G}_x^*$ on $\mathcal{X}^*$, which is induced by the associated isomorphisms for $\mathbb{G}_x$, as defined in Equation 5.77, is called the M_x-induced inner-product.*

Property 5.2 (inverse metrics for M_x-induced inner-product)**.** *Let $\mathcal{X}$ be a Hilbert space with M_x-weighted inner-product $\mathbb{G}_x$, which is represented by metric M_x for chosen coordinates. Let $\mathcal{X}^*$ be the dual space of $\mathcal{X}$ and consider M_x-associated dual elements (as defined in Definition 5.26) for the elements in $\mathcal{X}$ and $\mathcal{X}^*$. Furthermore, let the inner-product on $\mathcal{X}^*$, $\mathbb{G}_x^*$, be given by the M_x-induced inner-product (as defined in Definition 5.27). Then $\mathbb{G}_x^*$ is represented by M_x^{-1} for the chosen coordinates, such that the inner-product on $\mathcal{X}^*$ is calculated by:*

$$\langle x_1^*, x_2^* \rangle := x_1^* \cdot M_x^{-1} \cdot (x_2^*)^T \qquad x_1^*, x_2^* \in \mathcal{X}^*,$$

Proof. Let $x_1, x_2 \in \mathcal{X}$ be represented by coordinate vectors x_1, x_2 and use the associated isomorphism $\mathbb{G}_x^\flat$, represented by M_x, to define the (M_x-associated) dual elements in $\mathcal{X}^*$:

$$x_1^* = x_1^T M_x, \qquad x_2^* = x_2^T M_x \qquad x_1^*, x_2^* \in \mathcal{X}^*.$$

Using that $\mathbb{G}^\flat$ is invertible gives $x_1^* M_x^{-1} = x_1^T$ and $x_2^* M_x^{-1} = x_2^T$.

The inner-product $\mathbb{G}_x^*$ on $\mathcal{X}^*$ is chosen to be the M_x-induced inner-product of $\mathbb{G}$, as defined in Definition 5.27. Thus, let matrix M_x^* represent the metric on $\mathcal{X}^*$. Then, for the constructed M_x-associated dual elements and for $\mathbb{G}_x^*$ being the M_x-induced inner-product, it must hold that (according to Equation 5.77):

$$\begin{aligned} \mathbb{G}_x^*(x_1^*, x_2^*) &= \mathbb{G}_x(M_x^{-1}(x_1^*)^T, M_x^{-1}(x_2^*)^T) \\ &\Leftrightarrow \quad x_1^* M_x^* (x_2^*)^T = x_1^* M_x^{-1} M_x M_x^{-1} (x_2^*)^T = x_1^* M_x^{-1} (x_2^*)^T, \end{aligned}$$

from which it follows that indeed: $M_x^* = M_x^{-1}$. □

Remark 5.18. *Notice that for the particular choice of associating dual elements through the inner-product $\mathbb{G}_x$ of $\mathcal{X}$ (i.e. M_x-associated dual elements) and letting the M_x-induced inner-product be the inner-product on $\mathcal{X}^*$, it holds that M_x-associated dual elements have equal norms:*

$$||x||^2 = \langle x, x \rangle = \langle x^*, x^* \rangle = ||x^*||^2 \qquad \forall x \in \mathcal{X}, \forall M_x x = (x^*)^T \in \mathcal{X}^*. \tag{5.78}$$

5.7.2 Dual maps

Next to duality for vector spaces, the concept of duality also exists for linear maps.

Definition 5.28 (dual maps)**.** *Let $\mathcal{X}$,$\mathcal{U}$ be vector spaces and $\mathcal{X}^*$,$\mathcal{U}^*$ their dual spaces. Consider the linear map $a : \mathcal{X} \mapsto \mathcal{U}$. The dual map of a, $a^* : \mathcal{U}^* \mapsto \mathcal{X}^*$ is defined by:*

$$x^*(x) = u^*(u) \qquad \forall x \in \mathcal{X}, \forall u \in \mathcal{U}, \forall x^* \in \mathcal{X}^*, \forall u^* \in \mathcal{U}^*$$

Corollary 5.1. *Consider Definition 5.28 and notice that the operation of the given map a in coordinates is represented by $u = A \cdot x \quad x \in \mathcal{X}, u \in \mathcal{U}$, with A a matrix representing the map a. In coordinates, the dual map a^* is given by the matrix A^T such that in coordinates $(x^*)^T = A^T \cdot (u^*)^T \quad x^* \in \mathcal{X}^*, u^* \in \mathcal{U}^*$.*

Proof. In coordinates $x^*(x) = u^*(u)$ is represented by $x^* x = u^* u$, which is verified to be equal for the dual matrix maps A and A^T: $x^* x = x^T (x^*)^T = x^T A^T (u^*)^T = u^* A x = u^* u$. □

5.7.3 Dual subspaces

First duality for subspaces is discussed, then these duality properties are used to discuss some particular dual subspaces, i.e. dual subspaces of the kernel and the image of a map.

Intrinsic subspace in dual space Consider a vector space $\mathcal{X}$ and its dual space $\mathcal{X}^*$ with dimension n, as defined in Definition 5.24, where $\mathcal{X}$ and $\mathcal{X}^*$ -for the moment- do **not** have any other structure like an inner-product.

Now, consider a subspace on $\mathcal{X}$ of dimension $k < n$: $\mathcal{X}_s \subset \mathcal{X}$. Without any extra structure, a subspace $\mathcal{X}_s^0 \subset \mathcal{X}^*$ of dimension $n-k$, can be intrinsically defined on $\mathcal{X}^*$ based on $\mathcal{X}_s$:

$$\mathcal{X}_s^0 := \{x^* \in \mathcal{X}^* | x^*(x) = 0, x \in \mathcal{X}\} \tag{5.79}$$

Subset $\mathcal{X}_s^0$ is called the annihilator of $\mathcal{X}_s$.

Dual sub-spaces for Hilbert spaces Extra structure is added to $\mathcal{X}$ in the form of an inner-product, represented by metric M_x, which makes $\mathcal{X}$ a Hilbert space. Furthermore, make dual space $\mathcal{X}^*$ a Hilbert space by adding the M_x-induced inner-product (see Definition 5.27).

For the given M_x-induced inner-product on $\mathcal{X}^*$, represented by M_x^{-1}, the orthogonal complementary space of $\mathcal{X}_s^0$ can be constructed. It is denoted by $(\mathcal{X}_s^0)^\perp$ and has dimension $n-(n-k)=k$, such that:

$$\mathcal{X}^* = \mathcal{X}_s^0 \oplus \left(\mathcal{X}_s^0\right)^\perp.$$

Notice that subspaces $(\mathcal{X}_s^0)^\perp$ and $\mathcal{X}_s$ have equal dimensions.

Definition 5.29 (M_x-associated dual subspace)**.** *Consider dual Hilbert spaces $\mathcal{X}$, with its inner-product represented by M_x, and $\mathcal{X}^*$ with M_x-induced inner-product, as defined in Definition 5.27 and represented by M_x^{-1}. Let $\dim \mathcal{X} = \dim \mathcal{X}^* = n$ and let $\mathcal{X}_s \subset \mathcal{X}$ be a subspace of $\mathcal{X}$ of dimension k. Then the subspace in the dual space $\mathcal{X}^*$ of dimension k, which contains all M_x-associated dual elements of $\mathcal{X}_s$, as defined in Definition 5.26, is called the M_x-associated dual subspace of $\mathcal{X}_s \subset \mathcal{X}$ and defined by:*

$$\mathcal{X}_s^* := \{x^* \in \mathcal{X}^* | x^* = \mathbb{G}_x^\flat(x_s), \forall x_s \in \mathcal{X}_s \subset \mathcal{X}\},$$

such that $\mathcal{X}_s^* \subset \mathcal{X}^*$ and where $\dim \mathcal{X}_s^* = k$ and $\mathbb{G}_x^\flat$ is the M_x-associated isomorphism as defined in Definition 5.25.

From this definition and the definition of the intrinsically defined annihilator in Equation 5.79, the following corollary follows naturally.

Corollary 5.2. *Consider $\mathcal{X}$, $\mathcal{X}^*$ and $\mathcal{X}_s^* \subset \mathcal{X}^*$ as defined in Definition 5.29. Let $\mathcal{X}_s^0 \subset \mathcal{X}^*$ be the annihilator of $\mathcal{X}_s$, as given in Equation 5.79. Then, $\mathcal{X}_s^0$ is the orthogonal complementary space of $\mathcal{X}_s^*$ for the M_x-induced inner-product (as defined in Definition 5.27 and represented by metric M_x^{-1}) on $\mathcal{X}^*$, such that:*

$$\mathcal{X}_s^* = \left(\mathcal{X}_s^0\right)^\perp$$

Proof. It is proven that $\mathcal{X}_s^* = (\mathcal{X}_s^0)^\perp$.

Consider $\mathcal{X}$, $\mathcal{X}^*$ and $\mathcal{X}_s^* \subset \mathcal{X}^*$ as defined in Definition 5.29 and define arbitrary dual coordinate bases for $\mathcal{X}$ and $\mathcal{X}^*$ such that their elements can be represented by coordinate vectors and their inner-products are represented by the metrics M_x and M_x^{-1} respectively. Then, through the construction of $\mathcal{X}_s^0$, it holds that:

$$x_s^0 \cdot x_s = 0 \qquad \forall x_s \in \mathcal{X}_s, \forall x_s^0 \in \mathcal{X}_s^0 \subset \mathcal{X}^*.$$

Also by construction of $\mathcal{X}_s^*$, as defined in Definition 5.29, it holds that:

$$x_s = M_x^{-1}(x_s^*)^T \qquad \forall x_s \in \mathcal{X}_s, \forall x_s^* \in \mathcal{X}_s^*$$

Substituting the latter relation in the first relation, gives:

$$x_s^0 M_x^{-1} (x_s^*)^T = 0 \qquad \forall x_s^0 \in \mathcal{X}_s^0, \forall x_s^* \in \mathcal{X}_s^*,$$

which shows that the inner-product on $\mathcal{X}^*$, represented by M_x^{-1}, for any element $x_s^0 \in \mathcal{X}_s^0$ and any element $x_s^* \in \mathcal{X}_s^*$ is zero. This proves that subspaces $\mathcal{X}_s^*$ and $\mathcal{X}_s^0$ are orthogonal for inner-product M_x^{-1}. Furthermore, since their dimensions add to n, these subspaces are indeed orthogonal complementary subspaces, such that $\mathcal{X}_s^* = (\mathcal{X}_s^0)^\perp$ and $\mathcal{X}^* = \mathcal{X}_s^* \oplus \mathcal{X}_s^0$. □

Some M-associated dual subspaces Consider dual Hilbert spaces $\mathcal{X}$ and $\mathcal{X}^*$ with metric M_x on $\mathcal{X}$ and M_x-induced inner-product on $\mathcal{X}^*$, represented by metric M_x^{-1}. And let $\mathcal{U}$ and $\mathcal{U}^*$ also be dual Hilbert spaces with metric M_u on $\mathcal{U}$ and M_u-induced inner-product on $\mathcal{U}^*$, represented by metric M_u^{-1}. Furthermore, consider dual maps a and a^* as defined in Definition 5.31 and let the elements in $\mathcal{X}, \mathcal{X}^*$ and in $\mathcal{U}, \mathcal{U}^*$ be M_x- and M_u-associated dual elements respectively (see Definition 5.26).

Consider again the orthogonal complementary subspaces $\mathcal{X}_n = \ker a \subset \mathcal{X}$ and $\mathcal{X}_v = \mathcal{X}_n^\perp \subset \mathcal{X}$ with, for arbitrarily chosen coordinates, basis matrices X_n and $X_v = M_x^{-1} \cdot \operatorname{im} A^T$ respectively, as given in Section 5.5.2 and Theorem 5.2.

Remark 5.19. *For the given dual spaces and considering M_x-associated dual elements, it is found that the basis matrix of $\mathcal{X}_v^*$, i.e. the M_x-associated dual subspace of $\mathcal{X}_v = \mathcal{X}_n^\perp = \ker a^\perp$ (see Definition 5.29), is given by: $X_v^* = M_x \cdot M_x^{-1} \cdot \operatorname{im} A^T = \operatorname{im} A^T$. Since matrix A^T is the coordinate representation of dual map a^* (see Corollary 5.1), clearly $\mathcal{X}_v^* = \operatorname{im} a^* \subset \mathcal{X}^*$. Hence, $\ker a^\perp \subset \mathcal{X}$ and $\operatorname{im} a^* \subset \mathcal{X}^*$ are M_x-associated dual subspaces.*

From Corollary 5.2 it follows that $\mathcal{X}_v^* = \mathcal{X}_n^0$, such that $x_v^*(x_n) = 0 \quad x_v^* \in \operatorname{im} a^*, x_n \in \ker a$.

Consider again the orthogonal complementary subspaces $\mathcal{U}_r = \operatorname{im} a \subset \mathcal{U}$ and $\mathcal{U}_n = \mathcal{U}_r^\perp \subset \mathcal{U}$ with, for arbitrarily chosen coordinates, basis matrices U_r and $U_n = M_u^{-1} \cdot \ker A^T$ respectively, as given in Section 5.5.3 and Theorem 5.5.

Remark 5.20. *For the given dual spaces and considering M_u-associated dual elements, it is found that the basis matrix of $\mathcal{U}_n^*$, i.e. the M_u-associated dual subspace of $\mathcal{U}_n = \mathcal{U}_r^\perp = \operatorname{im} a^\perp$, is given by: $U_n^* = M_u \cdot M_u^{-1} \cdot \ker A^T = \ker A^T$. Since matrix A^T is the coordinate representation of dual map a^* (see Corollary 5.1), clearly $\mathcal{U}_n^* = \ker a^* \subset \mathcal{U}^*$. Hence, $\operatorname{im} a^\perp \subset \mathcal{U}$ and $\ker a^* \subset \mathcal{U}^*$ are dual subspaces.*

From Corollary 5.2 it follows that $\mathcal{U}_n^* = \mathcal{U}_r^0$, such that $u_n^*(u_r) = 0 \quad u_n^* \in \ker a^*, u_r \in \operatorname{im} a$.

5.7.4 Physical dual spaces

So far, it has been discussed that the inversion problem, described through decomposition of spaces, gives a physically meaningful decomposition of spaces and a physically equivalent solution if a physically equivalent metric is used (Definition 5.23). Now, with the notion on dual spaces, specific naming is introduced to denote usage of duality in physical systems, which allows to describe the pseudo-inverse map through duality, see next Section (Section 5.7.5).

Definition 5.30 (physical dual spaces)**.** *Consider a physical system Σ. Let Hilbert spaces $\mathcal{X}$ and $\mathcal{X}^*$, with inner-products $\mathbb{G}_x$ and $\mathbb{G}_x^*$, be dual spaces, as defined in Definition 5.24. Furthermore, let $\mathbb{G}_x^*$ be the M_x-induced inner-product, as defined in Definition 5.27. These dual Hilbert spaces with given associated inner-products are called physical dual spaces if the elements of $\mathcal{X}$ and $\mathcal{X}^*$ represent physical quantities in Σ and the associated norms, represented by M_x and M_x^{-1}, are physically sensible norms for Σ, as defined in Definition 5.22*

Analogues to the general definition of a dual map, see Definition 5.28, also specific naming is used for dual maps in representations of physical systems, the *physical dual map*, as defined hereafter.

Definition 5.31 (physical dual maps)**.** *Consider two sets of dual spaces $\mathcal{X}, \mathcal{X}^*$ and $\mathcal{U}, \mathcal{U}^*$ and the dual maps $a : \mathcal{X} \mapsto \mathcal{U}$ and $a^* : \mathcal{U}^* \mapsto \mathcal{X}^*$. If $\mathcal{X}, \mathcal{X}^*$ and $\mathcal{U}, \mathcal{U}^*$ are physical dual spaces, as defined in Definition 5.30, then a and a^* are called physical dual maps.*

The elements in physical dual spaces can be associated to each other. A specific choice of associating dual elements is specified and named in the following definition.

Definition 5.32 (physical dual elements)**.** *Consider physical dual spaces $\mathcal{X}$ and $\mathcal{X}^*$ with inner-products represented by M_x and M_x^{-1}, as defined in Definition 5.30, for a physical system Σ. The M_x-associated dual elements in $\mathcal{X}$ and $\mathcal{X}^*$, as defined in Definition 5.26, are called physical dual elements.*

Note that usage of, and referring to the above given definitions of physical dual spaces and physical dual elements implies specific choices: it implies that the spaces are Hilbert spaces with a particular choice on the inner-products and it implies that the dual elements are associated to each other through the inner-product, as defined in both definitions.

From Remark 5.18 it follows that the physically sensible norms of physical dual elements are equal. Hence the specific choice of associating dual elements as physical dual elements, as defined above, associates dual elements that are physical quantities which represent the same physical state of a physical system Σ.

5.7.5 Inspection of physically equivalent solution through duality

As said before, a physically equivalent pseudo-inverse map (see Definition 5.6) must be co-ordinate invariant. The notion of duality allows to inspect a pseudo-inverse map $a^\#$ (Definition 5.21), as shown hereafter. The notion of the pull-back of maps will be used and defined first.

Definition 5.33 (Pull-back)**.** *Consider vector spaces $\mathcal{X}$ and $\mathcal{U}$ and some map $a : \mathcal{X} \mapsto \mathcal{U}$. If an inner-product $\mathbb{G}_u$ is defined on the target space $\mathcal{U}$ and a is an injective map, then it is possible to define an associated inner-product on the domain space $\mathcal{X}$, which is called the pull-back[25] of $\mathbb{G}_u$ along a and given by:*

$$\mathbb{G}_x(x_1, x_2) = \mathbb{G}_u(a(x_1), a(x_2)) \qquad x_1, x_2 \in \mathcal{X},$$

which in coordinates is represented[26] by

$$M_x = A^T M_u A,$$

where the matrix A represents the injective map a, metric M_u the inner-product $\mathbb{G}_u$ and metric M_x the associated inner-product $\mathbb{G}_x$.

[25] Note: a pull-back exists for many maps and functions, here the pull-back is given for a bilinear map, i.e. the inner-product.

[26] Note: on $\mathcal{U}$ the inner-product is calculated by $u^T M_u u$ and elements $u \in \mathcal{U}$ are given by: $u = Ax$, such that the inner-product is equal to $x^T A^T M_u A x$ and hence $A^T M_u A$ can be used as a metric on $\mathcal{X}$ if it is positive definite.

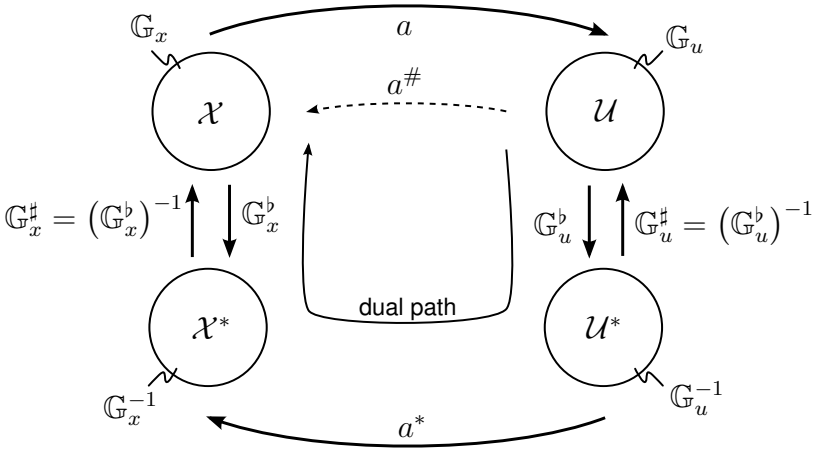

Figure 5.18: Coordinate invariant commutation diagram for pseudo-inverse map $a^\# = \left(\mathbb{G}_x^\flat\right)^{-1} \circ a^* \circ \mathbb{G}_u^\flat$, called dual path. $\mathbb{G}_x$ and $\mathbb{G}_u$ denote the inner-products on $\mathcal{X}$ and $\mathcal{U}$.

Coordinate invariant dual path Consider a physical system of which the physical quantities are represented by physical dual elements (Definition 5.32) on physical dual spaces (Definition 5.30) $\mathcal{X}$, $\mathcal{X}^*$ and $\mathcal{U}$, $\mathcal{U}^*$ with physically sensible norms (Definition 5.22) defined by their inner-products $\mathbb{G}_x$ and $\mathbb{G}_u$ respectively. Their associated isomorphisms are denoted by $\mathbb{G}_x^\flat$ and $\mathbb{G}_u^\flat$ respectively. The sets of dual spaces are connected through physical dual maps (Definition 5.31) a and a^*, given by:

$$\begin{aligned} a : \mathcal{X} \mapsto \mathcal{U} \quad &; \quad a(x) = u \quad x \in \mathcal{X}, u \in \mathcal{U} \\ a^* : \mathcal{U}^* \mapsto \mathcal{X}^* \quad &; \quad a^*(u^*) = x^* \quad x^* \in \mathcal{X}^*, u^* \in \mathcal{U}^*. \end{aligned}$$

For the above given representation of a physical system, given by physical dual spaces and physical dual maps, the pseudo-inverse map can be represented in a coordinate invariant commutation diagram, as shown in Figure 5.18.

From the commutation diagram it is clear that the pseudo-inverse map $a^\#$ could be given by the following composition, illustrated by the **dual path**:

$$a^\# = \mathbb{G}_x^\sharp \circ a^* \circ \mathbb{G}_u^\flat. \tag{5.80}$$

The dual path shows that no inversion is used and that commutation relies on the choice of inner-products $\mathbb{G}_x$ and $\mathbb{G}_u$. However, in order for the diagram to commute, the inner-products can not be chosen independently. Notice that there are two options for the associated isomorphisms[27]:

1. $\mathbb{G}_u^\flat$ is chosen and $\mathbb{G}_x^\flat$ follows, i.e.:

$$\mathbb{G}_x^\flat = a^* \circ \mathbb{G}_u^\flat \circ a, \tag{5.81}$$

which implies that the inner-product for $\mathbb{G}_x$ is given by:

$$\mathbb{G}_x(x_1, x_2) = \mathbb{G}_u(a(x_1), a(x_2)) \qquad x_1, x_2 \in \mathcal{X}, \tag{5.82}$$

which is called the pull-back of $\mathbb{G}_u$ along map a (Definition 5.33).

[27] It will be shown later that the appropriate option to use depends on the mapping properties of a.

2. $\left(\mathbb{G}_x^\flat\right)^{-1}$ is chosen and $\left(\mathbb{G}_u^\flat\right)^{-1}$ follows, i.e.:

$$\left(\mathbb{G}_u^\flat\right)^{-1} = a \circ \left(\mathbb{G}_x^\flat\right)^{-1} \circ a^* \tag{5.83}$$

which implies that the inner-product for $\left(\mathbb{G}_u\right)^{-1}$ on $\mathcal{U}^*$ is given by:

$$\left(\mathbb{G}_u\right)^{-1}(u_1^*, u_2^*) = \left(\mathbb{G}_x\right)^{-1}(a^*(u_1^*), a^*(u_2^*)) \qquad u_1^*, u_2^* \in \mathcal{U}^*, \tag{5.84}$$

which is called the pull-back of $\left(\mathbb{G}_x\right)^{-1}$ along dual map a^* (Definition 5.33).

Proof. The pull-back implications in the above options follows from the definition of the flat map, Equation 5.76, and the dual map, Definition 5.28, and the fact that M-induced inner-products are used on the dual spaces, Definition 5.27. Consider $x_1, x_2 \in \mathcal{X}$ and let $x_1^* = \mathbb{G}_x^\flat(x_1)$ such that $x_1^*(x_2) = \mathbb{G}_x(x_1, x_2)$ (Equation 5.76) and let $u_1 = a(x_1), u_2 = a(x_2) \in \mathcal{U}$ and let $u_1^* = \mathbb{G}_u^\flat(u_1)$ such that $u_1^*(u_2) = \mathbb{G}_u(u_1, u_2)$ (Equation 5.76). Because, $x_1^* = \mathbb{G}_x^\flat(x_1) = a^* \circ \mathbb{G}_u^\flat \circ a(x_1)$ it follows that $x_1^* = a^*(u_1^*)$. Then, a and a^* being dual maps, implies (Definition 5.28) $x_1^*(x_2) = u_1^*(u_2)$, which in this case for the given relations of the elements implies $\mathbb{G}_x(x_1, x_2) = \mathbb{G}_u(u_1, u_2) = \mathbb{G}_u(a(x_1), a(x_2))$. Equal arguments are used for the second implication. □

The above given options for the inner-products can **not** be arbitrarily used. A distinction is needed based upon the mapping properties of the dual maps a and a^*:

1. If a is a **non-injective and surjective map** then only option 2 is valid, i.e. Equation 5.83 is to be used. Map a being non-injective implies $\ker a \neq \emptyset$ and hence the given composition in Equation 5.81 is not positive definite and not an isomorphism. Whereas, map a being surjective implies that $\operatorname{im} a = \mathcal{U}$, such that $\ker a^* = \emptyset$ (see Remark 5.20 and notice that $\operatorname{im} a = \mathcal{U} \Rightarrow \operatorname{im} a^\perp = \emptyset \Rightarrow \ker a^* = \emptyset$) and Equation 5.83 is an isomorphism.

2. If a is an **injective and non-surjective map** then only option 1 is valid, i.e. Equation 5.81 is to be used. Map a being non-surjective implies $\operatorname{im} a \subset \mathcal{U}$, such that $\ker a^* \neq \emptyset$ (see Remark 5.20) and hence the given composition in Equation 5.83 is not positive definitive and not an isomorphism. Whereas, map a being injective implies that $\ker a = \emptyset$, such that Equation 5.81 is an isomorphism.

> Intuitively, the usage of the pull-back of the inner-products can be understood as having parts (represented as elements on different spaces) of the mechanical system that are directly connected and therefore posses physical quantities that correspond to the same value of equal physically sensible norms on both spaces.

Dual path in coordinates The dual path for the pseudo-inverse map $a^\#$, as shown in Figure 5.18, is now examined in coordinate representation (assuming arbitrarily chosen bases) for both mapping options as discussed for the commutation diagram, see Figure 5.18.

The map a is represented by the matrix A, the inner-products $\mathbb{G}_u$ and $\mathbb{G}_x$ are represented by the metrics M_u and M_x respectively and also the associated isomorphisms ($\mathbb{G}_u^\flat$,$\mathbb{G}_x^\flat$) are represented by the same matrices M_u and M_x.

In order to investigate both mapping options (as discussed above) separately, the map decomposition of Section 5.5 is followed. Matrix A is decomposed into C, which represents a non-injective and surjective map $c : \mathcal{X} \mapsto \mathcal{V}$, and F, which represents an injective and non-surjective map $f : \mathcal{V} \mapsto \mathcal{U}$, such that $A = FC$. Clearly, A, A^T and C, C^T and F, F^T represent physical dual maps. The physical dual space $\mathcal{V}^*$ is imposed through the associated

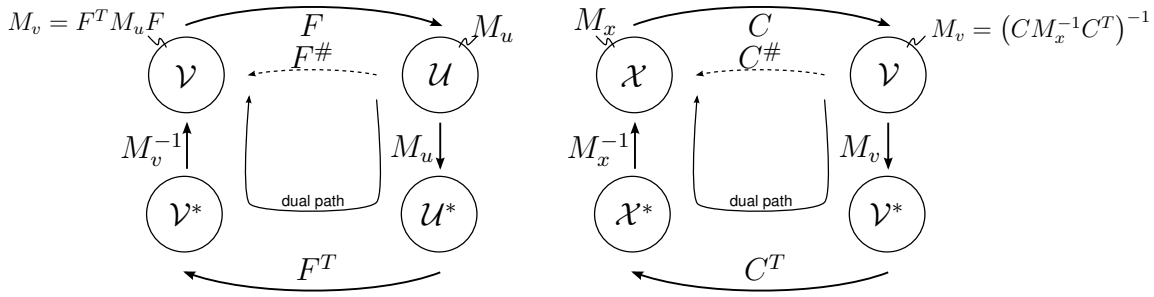

(a) Dual path for $F^\#$ (b) Dual path for $C^\#$

Figure 5.19: Dual paths in commutation diagrams for $C^\#$ and $F^\#$, represented in coordinates.

M_v-weighted inner-product on $\mathcal{V}$ with M_v the metric on $\mathcal{V}$, such that $F^T : \mathcal{U}^* \mapsto \mathcal{V}^*$ and $C^T : \mathcal{V}^* \mapsto \mathcal{X}^*$.

Both dual paths of the pseudo-inverse maps of maps C and F are discussed separately and shown in Figure 5.19:

1. Non-surjective and injective map F: As discussed above, in order for the commutation diagram (Figure 5.18) to commute, Equation 5.81 is used. Hence, for this case, the metric on $\mathcal{V}$ is given by the pull-back of M_u along F: $M_v = F^T M_u F$. Then the dual path in the commutation diagram in Figure 5.19(a) directly reveals the complete pseudo-inverse map:

$$F^\# = \left(F^T M_u F\right)^{-1} F^T M_u, \tag{5.85}$$

   which is recognized as the M_u-least squares solution and coincides with the pseudo-inverse map $F^\#$, as presented in Section 5.5.3.

   Hence, only metric M_u remains to be chosen. In order for M_u to be a candidate physically equivalent metric that generates a physically equivalent inverse map, M_u should induce a physically sensible norm.

2. Non-injective and surjective map C: As discussed above, in order for the commutation diagram (Figure 5.18) to commute, Equation 5.83 is used. Hence, for this case, the metric on $\mathcal{V}^*$ is given by the pull-back of M_x^{-1} along C^T: $M_v^{-1} = CM_x^{-1}C^T$, such that $M_v = \left(CM_x^{-1}C^T\right)^{-1}$. Then the dual path in the commutation diagram in Figure 5.19(b) directly reveals the complete pseudo-inverse map:

$$C^\# = M_x^{-1}C^T \left(CM_x^{-1}C^T\right)^{-1}, \tag{5.86}$$

   which is recognized as the minimum M_x-norm solution and coincides with the pseudo-inverse map $C^\#$, as presented in Section 5.5.2.

   Hence, only metric M_x remains to be chosen. In order for M_x to be a candidate physically equivalent metric that generates a physically equivalent inverse map, M_x should induce a physically sensible norm.

Conclusions The particular choice of dual Hilbert spaces, named physical dual spaces, with inverse inner-products and physical dual elements defined through the associated isomorphisms for the inner-products, gives a clear physical interpretation for the pseudo-inverse map. The interpretation is given in commutation diagrams, which directly show the relation of all maps and spaces involved in the pseudo-inverse map.

Coordinate invariance of the results is obtained if physically sensible norms are used, which is the case if physical dual spaces are considered. In that case, the related elements in all spaces can be interpreted as physical quantities, which are related through the various mappings in the commutation diagram.

The commutation depends on the chosen metrics. Metrics that induce physically sensible norms are considered candidate metrics that may render the physically equivalent pseudo-inverse map. Then the physical dual elements that are associated through a candidate metric can be used to check if the physical quantities of the corresponding dual elements are appropriate for the modeled situation.
Conclusively, using the properties of the physical dual system, as presented in Figure 5.18, reveals useful insights for the modeled physical inverse problem of map $a : \mathcal{X} \mapsto \mathcal{U}$ (Section 5.1) and for its pseudo-inverse solution.

5.7.6 Inverse properties from duality

Duality is a powerful concept to discover model properties of for example the inverse problem. This is illustrated by the following discussion. Consider Definition 5.21 again.

Parallel to the pseudo-inverse solution properties summarized in Definition 5.21, the three cases are re-examined to investigate the physical properties by utilizing physical duality and the commutation diagram (see Figure 5.18). Consider physical dual spaces (Definition 5.30) $\mathcal{X}^*$ and $\mathcal{U}^*$ for the Hilbert spaces $\mathcal{X}$ and $\mathcal{U}$ with metrics M_x and M_u. Furthermore, recall the definition of physical dual elements (Definition 5.32) and consider Remark 5.19 and Remark 5.20:

1. **Exact inverse ($u_p \in \mathcal{U}_r = \operatorname{im} a \subset \mathcal{U}$): Duality is used to verify that indeed $u_p \in \mathcal{U}_r = \operatorname{im} a$ has an exact inverse solution $x_s \in \mathcal{X}$.**

   Consider the dual path. The physical dual element of $u_p \in \mathcal{U}$ is given by $\left(u_p^*\right)^T = M_u \cdot u_p$. From Remark 5.20 it follows that the physical dual element u_p^* of any $u_p \in \mathcal{U}_r = \operatorname{im} a$ resides in $(\ker a^*)^\perp$. Thus, the dual map a^* takes $u_p^* \in (\ker a^*)^\perp$ to $x_s^* \in \mathcal{X}^*$, which is the physical dual element of the inverse solution $x_s \in \mathcal{X}$ ($x_s = M_x^{-1}(x_s^*)^T$). Hence, $u_p^* \in \operatorname{im} a$ is completely mapped to $\mathcal{X}^*$ and, through M_x^{-1}, to $x_s \in \mathcal{X}$.

2. **No inverse ($u_p \in (\operatorname{im} a)^\perp \subset \mathcal{U}$): Duality is used to verify that indeed $u_p \in \mathcal{U}_n = (\operatorname{im} a)^\perp$ has no inverse.**

   Consider the dual path. From Remark 5.20 it follows that the physical dual element u_p^* of any $u_p \in \mathcal{U}_n = (\operatorname{im} a)^\perp$ resides in $\ker a^*$. Clearly, the dual map a^* maps the physical dual element $u_p^* \in \ker a^*$ to 0. Thus, the dual path has shown that all dual elements u_p^* of $u_p \in (\operatorname{im} a)^\perp$ do not map to any element in $\mathcal{X}^*$, which confirms non-existence of the inverse element (other than zero).

3. **Partial inverse ($u_p \in \mathcal{U}$, $u_p \cap \mathcal{U}_n = \emptyset$, $u_p \cap \mathcal{U}_r = \emptyset$): Duality is used to verify that indeed a $u_p \in \mathcal{U}$ with components in both $\mathcal{U}_n = (\operatorname{im} a)^\perp$ and $\mathcal{U}_r = \operatorname{im} a$ has a partial inverse.**

   Consider $u_p = u_1 + u_2$ with $u_2 \in (\operatorname{im} a)^\perp$ and $u_1 \in \operatorname{im} a$ and reason along the dual path by using the previous two cases. It immediately follows that $x_s = M_1^{-1} A^T M_u \cdot u_p = M_1^{-1} A^T M_u \cdot u_1$. As expected, the dual path shows that only the component $u_1 \in \operatorname{im} a$ is mapped back and gives a partial inverse solution.

Physical properties One may recognize that forces and velocities may form physical dual spaces, if appropriate metrics are used (choices of metrics for physical dual spaces will be discussed in Section 5.8). As co-vectors, forces are functions that map velocity vectors to a instantaneous power.

To give the reader some intuition, for forces and motions previous general properties (listed above) can be interpreted and linked to the definitions of non-producible forces and blocked motions (see Section 5.2.1) as follows.

- Consider the elements on $\mathcal{X}$ and $\mathcal{U}$ to represent motions: those u_p that are non-reachable, i.e. $u_p \in (\operatorname{im} a)^{\perp}$ represent **blocked motions**. The fact that these motions are blocked is easily checked by noticing that the according physical dual elements u_p^* (through associated isomorphism), i.e. forces, reside in $\ker a^*$ and hence map to zero through the dual map a^*. Hence, forces on $\ker a^* \in \mathcal{U}^*$ that are physical dual elements with blocked motions $u_p \in (\operatorname{im} a)^{\perp} \subset \mathcal{U}$, can not (through a^*) impose forces on $\mathcal{X}^*$ and thus no motion on $\mathcal{X}$ and hence (through a) no motion on $\mathcal{U}$.
- Consider the elements on $\mathcal{X}$ and $\mathcal{U}$ to represent forces: those u_p that are non-reachable, i.e. $u_p \in (\operatorname{im} a)^{\perp}$ represent **non-producible forces**. The fact that these forces can not be produced through the kinematics is easily checked by noticing that the according dual motion elements u_p^* map to zero through the dual map a^*. Hence, motions on $\mathcal{U}^*$ that are co-aligned with (and induced by) non-producible forces $u_p \in (\operatorname{im} a)^{\perp} \subset \mathcal{U}$, do not (through a^*) impose motions on $\mathcal{X}^*$ (those motions u_p^* are known as null-space motions). Thus, no force on $\mathcal{X}$ exists that can resist or generate u_p to induce or resist null-space motions.

5.7.7 Physically ill posed inverse problem

Definition 5.9 poses a definition for a physically ill posed inverse problem. From the discussion on duality it is clear that a motion $u_p \notin \operatorname{im} a$ can not exist, since there is no corresponding motion $x_s \in \mathcal{X}$ that can produce this motion, nor a dual force u_p^* that can induce this motion (Remark 5.3).

If the inverse problem is raised for forces, then duality has shown that for a force $u_p \notin \operatorname{im} a$ there is no force $x_s \in \mathcal{X}$ that can generate (or resist) this force. Nevertheless, the force itself may exist (possibly applied from outside, externally). Hence duality shows that such a force induces (irresistible) null-space motions (Remark 5.4). It is not physically ill-posed.

Considering the dual spaces for the problem at hand by using proper physically equivalent metrics may hint for modeling errors that have caused physically ill-posed inverse problem. This is illustrated in the following example of inverse problem for the simple grasp system.

5.7.8 Example: dual simple grasp system inverse problem

Consider again the simple rigid grasp system as illustrated in Figure 5.4. Until now, the example was used to discuss the inverse problem for the grasp matrix G which maps forces. In this section, duality is applied to the example to illustrate previously discussed properties.

Equation 5.12 already presented a dual map G^T for the elements $\dot{\epsilon} \in T_{\epsilon}\mathcal{E}_c$ and $\dot{x}_o \in T_x\mathcal{X}$, which are the dual elements of the forces in the grasp system. Naively stating (forgetting previous results for the inverse problem of the forces in the grasp system) an inverse problem for this dual system, poses the problem to find $\left(G^T\right)^{\#}$, such that:

$$\left(G^T\right)^{\#} : T_{\epsilon}\mathcal{E}_c \mapsto T_x\mathcal{X}, \tag{5.87}$$

which describes the problem of finding the object motion as a result of contact motion.

> Notice that both $T_\epsilon\mathcal{E}_c, T^*_\epsilon\mathcal{E}_c$ and $T_x\mathcal{X}, T^*_x\mathcal{X}$ are dual spaces, since elements in $T^*_\epsilon\mathcal{E}_c$ and in $T^*_x\mathcal{X}$ map elements in respectively $T_\epsilon\mathcal{E}_c$ and $T_x\mathcal{X}$ to scalars. The scalar quantity mapped to is known as the physical quantity power. Indeed, the maps G and G^T are dual maps, such that e.g. $f_c\dot{\epsilon}_c = f_c \cdot A^T\dot{x}_o = \dot{x}_o^T \cdot Af_c^T = \dot{x}_o^T F_o^T$. However, a metric is needed in order to associate physical dual elements (as defined in Definition 5.32) along the dual path of the pseudo-inverse map to be found.

Physically ill-posed inverse problem Section 5.3.5 showed that the original problem describes the inversion of a surjective map for the object forces, such that any $f_{co} \in \mathcal{F}_E$ gives a physically well-posed inverse problem.

Notice that G^T is a non-surjective map, such that a physically ill-posed inverse problem could arise. This is indeed the case for inversion from elements $\dot{\epsilon} \in \left(\operatorname{im} G^T\right)^\perp \subset T_\epsilon\mathcal{E}_c$. Also intuitively, it can be easily understood that these elements give physically ill-posed inverse problems. Recall, that a rigid body model is used in Figure 5.4. Hence, elements $\dot{\epsilon} \in \left(\operatorname{im} G^T\right)^\perp \subset T_\epsilon\mathcal{E}_c$ have to violate the modeled rigid contact constraint in order to exist (i.e. $\dot{\epsilon} \in \left(\operatorname{im} G^T\right)^\perp$ are blocked motions). Thus, elements $\dot{\epsilon} \in \left(\operatorname{im} G^T\right)^\perp \subset T_\epsilon\mathcal{E}_c$ can not exist in this model, which for example could be squeezing (penetrating) finger motions.

Physically well-posed inverse problem Physically, the constraints need to be released to pursue the inverse problem for elements $\dot{\epsilon} \in \left(\operatorname{im} G^T\right)^\perp$. Hence, the model needs to be adapted. This is accomplished by modeling compliant contacts, as shown in Figure 5.5.

It was already established that on $T^*_\epsilon\mathcal{E}_c$, the physically equivalent metric M_f was found to be the compliance matrix C (Equation 5.22). Hence, the needed model adaptation is equivalent to letting the spaces be **physical dual spaces** for the associated isomorphisms for the M_f-weighted inner-product on $T^*_\epsilon\mathcal{E}_c$ (Definition 5.30). Therefore, the metric M_ϵ to be used on $T_\epsilon\mathcal{E}_c$ is given by; $M_\epsilon = M_f^{-1}$, such that the physical dual elements on $T_\epsilon\mathcal{E}_c$ are given by (see Definition 5.32) :

$$\delta\bar{\epsilon} = M_f \cdot f_c^T = C \cdot f_c^T \qquad \delta\bar{\epsilon} \in T_\epsilon\mathcal{E}_c, f_c \in T^*_\epsilon\mathcal{E}_c,$$

with $\delta\bar{\epsilon}$ the unblocked infinitesimal displacements[28] as illustrated in Figure 5.5.

Notice that the physical sensible quantity of the inner-products on both dual spaces represents elastic storage energy. To construct physical dual maps, also $T^*_x\mathcal{X}$ and $T_x\mathcal{X}$ need to be physical dual spaces with inverse metrics (M_x, M_F respectively and $M_x = M_F^{-1}$) that induce the same physical quantity, elastic energy storage. Since G^T is injective and non-surjective, Equation 5.81 is followed such that:

$$M_x = GM_\epsilon G^T = GM_f^{-1}G^T = \frac{1}{c_1} + \frac{1}{c_2} = \frac{c_1 + c_2}{c_1 c_2}, \tag{5.88}$$

which shows that metric M_x is the pull-back (see Definition 5.33) of M_ϵ along G^T. Not surprisingly, the metric M_x on the space of object motions ($T_\epsilon\mathcal{X}$) represents the total object

[28] Notice that the definition of the physical dual spaces with associated metrics M_f and M_f^{-1} imposes the physical dual elements of the contact forces to be contact displacements, instead of velocities. See Equation 5.13, where it is explained that both $\delta\epsilon$ and $\dot{\epsilon}$ are elements of the tangent space $T_\epsilon\mathcal{E}_c$.

stiffness[29]. And, as expected, the object displacement δx_o is dual to the force on the object f_o:

$$\delta x_o = M_F \cdot f_o \qquad \delta x_o \in T_\epsilon \mathcal{X}, f_o \in T^*_\epsilon \mathcal{X}.$$

Thus, G^T is the associated physical dual map, which gives:

$$\delta\bar{\epsilon} = \delta\epsilon = G^T \cdot \delta x_o,$$

It shows that for contact displacements induced by object displacements, it holds that $\delta\bar{\epsilon} = \delta\epsilon$, while the compliant separation of $\delta\bar{\epsilon}$ and $\delta\epsilon$ allows to reason about the effect of $\bar{\epsilon} \in \left(\operatorname{im} G^T\right)^\perp$ on the object displacement.

Physically equivalent inverse solutions The physically equivalent solution for the inverse problem given in Equation 5.87, using the adapted model as illustrated in Figure 5.5, is described with the three approaches discussed in this chapter. All resulting pseudo-inverse maps are equal for proper choices of metrics:

1. **Elementary physics - force equilibrium** (i.e. minimizing elastic energy): For any $\delta\bar{\epsilon}$ the object will displace δx_o such that elastic energy is minimized, which corresponds to zero net object force, i.e. $f_o = 0 \rightarrow f_{s1} = f_{s2}$. With spring forces $f_{si} = (\delta\bar{\epsilon}_i - \delta\epsilon_i) \cdot c_i^{-1}$ and contact displacement $\delta\epsilon = G^T \cdot \delta x_o$, the following equality is found:

   $$(\delta\bar{\epsilon}_1 - \delta x_o) \cdot c_1^{-1} = (\delta\bar{\epsilon}_2 + \delta x_o) \cdot c_2^{-1},$$

   which results in the inverse solution:

   $$\delta x_o = \frac{\delta\bar{\epsilon}_1 \cdot c_1^{-1}}{c_1^{-1} + c_2^{-1}} - \frac{\delta\bar{\epsilon}_2 \cdot c_2^{-1}}{c_1^{-1} + c_2^{-1}}$$

2. **Weighted inverse**: The inverse solution that produces the M_ϵ-least squares error for the injective and non-surjective map G^T is given by (see Equation 5.61 and notice that G^T follows pseudo-inverse of general injective and non-surjective map F and recall the metric M_ϵ on $T_\epsilon \mathcal{E}_c$ given by $M_\epsilon = M_f^{-1} = C^{-1}$):

   $$\begin{aligned} \delta x_o &= \left(G M_\epsilon G^T\right)^{-1} G M_\epsilon \cdot \delta\bar{\epsilon} = \left(G C^{-1} G^T\right)^{-1} G C^{-1} \cdot \delta\bar{\epsilon} \\ &= \frac{\delta\bar{\epsilon}_1 \cdot c_1^{-1}}{c_1^{-1} + c_2^{-1}} - \frac{\delta\bar{\epsilon}_2 \cdot c_2^{-1}}{c_1^{-1} + c_2^{-1}} \end{aligned}$$

3. **Dual path**: Applying the dual path for the physically equivalent inverse solution, as shown in Figure 5.19(a), requires a metric M_F on $T^*_x \mathcal{X}$ and a metric M_ϵ on $T_\epsilon \mathcal{E}_c$ and uses the physical dual spaces as constructed above. Hence, it is repeated that the metric $M_F = M_x^{-1}$ is given in Equation 5.88 as the pull-back of M_ϵ along G^T and that $M_\epsilon = M_f^{-1} = C^{-1}$. From Equation 5.80, the dual path solution is given by:

   $$\begin{aligned} \delta x_o &= M_F \cdot \overbrace{\left(G^T\right)^T \cdot \underbrace{M_\epsilon \cdot \delta\bar{\epsilon}}_{f_c^T}}^{f_o} = M_x^{-1} \cdot \overbrace{\left(G^T\right)^T \cdot \underbrace{M_\epsilon \cdot \delta\bar{\epsilon}}_{f_c^T}}^{f_o} \\ &= \left(\frac{c_1 + c_2}{c_1 c_2}\right)^{-1} G C^{-1} \cdot \delta\bar{\epsilon} \\ &= \frac{\delta\bar{\epsilon}_1 \cdot c_2}{c_1 + c_2} - \frac{\delta\bar{\epsilon}_2 \cdot c_1}{c_1 + c_2} = \frac{\delta\bar{\epsilon}_1 \cdot c_1^{-1}}{c_1^{-1} + c_2^{-1}} - \frac{\delta\bar{\epsilon}_2 \cdot c_2^{-1}}{c_1^{-1} + c_2^{-1}} \end{aligned} \tag{5.89}$$

[29] See also Section 5.6.3 and compare to metric M_f for G being surjective (force closure).

The example has illustrated that considering physical dual spaces for the problem at hand by using proper physically equivalent metrics may hint for modeling errors that cause a physically ill-posed inverse problem. Or, vice versa, if one does not want to adapt the model, it may hint and explain why the inverse problem is ill-posed and enhances understanding of the model.

5.7.9 Conclusions

Previous sections already indicated the importance of the choice of metrics for the decomposition of spaces and the accompanying physically equivalent inverse solution of kinematic maps in physical model representations. This section introduced the concept of the candidate physically equivalent metric, being the metric used to measure minimization of physical quantities that corresponds to natural behavior of the modeled physics.

Based on the well-known concept of mathematical dual spaces, physical dual spaces were introduced as a concept to distinguish particular dual spaces, constructed through the associated isomorphism for the metric-weighted inner-product. These dual spaces support to analyze the modeled physics and the according physical dual variables associated through the metric. It enabled to show the dual path as a physical explanation of the inverse problem, which supports to understand and resolve ill-posed modeling problems by considering the construction of dual spaces through proper physically equivalent metrics for the modeled situation.

Hence, the notion on physical dual spaces helps to verify and understand the implications of choices for metrics and hence supports model validation and hints for possible mistakes.

5.8 On the Choice of Metrics

Previous sections indicated the importance of properly chosen metrics to find physically equivalent inverse solutions in modeling problems and for the orthogonal decomposition of spaces. Therefore it is of interest to investigate candidate physical equivalent metrics. Understanding the attached physical dual spaces reveals modeling properties that support to understand the analysis of the model.

This section summarizes some dual spaces and their attached physical equivalent metrics for mechanical systems. Notice that these metrics are *candidate* physically equivalent metrics. Being a candidate physically equivalent metric does not imply that a specific metric, if used, will result in the correct physically equivalent solution. Also derived modeling properties are discussed, which are meant to be used for problem analysis in kinematic problems, as treated e.g. in the simple grasp examples throughout this chapter. These properties help to understand the choice of metrics for a specific problem.

5.8.1 Energy functions in mechanics

A mechanical system can be modeled with Hamiltonian mechanics. In Hamiltonian mechanics, the Hamiltonian $\mathbb{H}$ describes the total energy function of the system, see e.g. [64].

Conservative system The energy function for an isolated physical system is known to be described by the sum of the kinetic $\mathbb{H}_I(p,q)$ and potential energy $\mathbb{H}_C(q)$, being scalar functions, where $\mathbb{H}_I(p,q)$ depends on the generalized momenta, $p(t)$, and both depend on the generalized configuration variables, $q(t) \in \mathcal{Q}$ on the configuration manifold $\mathcal{Q}$. Thus:

$$\mathbb{H}(p,q) = \mathbb{H}_I(p,q) + \mathbb{H}_C(q), \tag{5.90}$$

where the kinetic energy can be written by:

$$\mathbb{H}_I(p,q) = \frac{1}{2} p(t) \cdot M(q)^{-1} \cdot p(t)^T \tag{5.91}$$

with $M(q)$ the mass matrix of the system with respect to the generalized coordinates. For such a system, the Hamiltonian equations describe the modeled behavior of the system:

$$\dot{p}(t)^T = -\frac{\partial \mathbb{H}}{\partial q(t)}(p,q) \tag{5.92}$$

$$\dot{q}(t) = \frac{\partial \mathbb{H}}{\partial p(t)}(p,q) = M(q)^{-1} \cdot p^T(t), \tag{5.93}$$

where $\dot{p} \in T_q^*\mathcal{Q}$ is the time derivative of the generalized momenta (co-vectors). And, $\dot{q} \in T_q\mathcal{Q}$ are velocities of the configuration changes.

Environment interaction Most physical systems interact with the environment and hence are not isolated. Interaction induces or extracts energy to or from the system due to externally applied forces (τ_{ext}) resulting from e.g. power-losses (dissipation) or external actuation. For interactions, the Hamiltonian Equation 5.92 changes to:

$$\dot{p}(t)^T = -\frac{\partial \mathbb{H}}{\partial q(t)} + \tau_{ext}^T, \tag{5.94}$$

with $\tau_{ext} \in T_q^*\mathcal{Q}$. Assuming linear damping B, the dissipation forces become:

$$\tau_{ext}^T = \tau_b(t)^T = B \cdot \dot{q}(t), \tag{5.95}$$

with B a linear damping matrix, which represents the dissipation function as function of the generalized coordinates.

Energy functions Conclusively, three energy functions are commonly known for a physical system; **potential energy** (gravitation and elastic storage), **kinetic energy** and dissipation, i.e. **power-loss**. Power-losses $P_b(t)$ are given by the change in energy in the system (also known as Rayleigh's dissipation function):

$$\begin{aligned} P_b(t) = \dot{\mathbb{H}}(t) &= \frac{d\mathbb{H}}{dt} = \left(\frac{\partial \mathbb{H}}{\partial q}\right)^T \dot{q} + \left(\frac{\partial \mathbb{H}}{\partial p}\right)^T \dot{p}^T \\ &= \left(\frac{\partial \mathbb{H}}{\partial q}\right)^T \frac{\partial \mathbb{H}}{\partial p} + \left(\frac{\partial \mathbb{H}}{\partial p}\right)^T \left(-\frac{\partial \mathbb{H}}{\partial q} + B\dot{q}\right) = \dot{q}(t)^T \cdot B \cdot \dot{q}(t) \end{aligned} \tag{5.96}$$

5.8.2 Physical dual spaces in mechanics

In [84], the given energy functions were briefly noted to obviously induce invariant metrics, i.e. physically consistent metrics. Hence physical equivalent candidate metrics may arise from these functions. Therefore these functions can be used to define inner-products for the physical dual spaces (Definition 5.30).

Nevertheless, different dual variables and modeling situations are involved for each of the candidate metrics. These are presented next and should be accounted for in specific modeling problems, when choosing a metric from the candidate metrics.

1. **(Quasi-) Statics:** Consider modeling a (quasi-) static situation for a given configuration $\tilde{q}$, with $\dot{q}(t) = 0 \quad \forall t$, $\dot{p}(t) = 0 \quad \forall t$ and applied external forces τ_{ext}^T. Quasi-static implies that only small configuration changes δq around $\tilde{q}$ are considered.

   For this situation, Power-losses (P_b, Equation 5.96) and Kinetic energy ($\mathbb{H}_I$, Equation 5.93, notice that $\dot{q} = 0 \Rightarrow p(t) = 0$) are zero. Hence, one energy function remains, i.e. $\mathbb{H}_C(q)$, which implies (see Equation 5.94): $\tau_{ext}^T = \frac{\partial \mathbb{H}}{\partial q(t)}$, such that infinitesimal displacements around $\tilde{q}$ give:

$$\delta\tau_{ext}^T = \frac{\partial^2 \mathbb{H}_\mathbb{C}}{\partial q^2}(\tilde{q}) \cdot \delta q,$$

   where $\delta\tau_{ext}^T$ represent infinitesimal forces and δq infinitesimal displacements.

   Hence, for this situation, a suitable candidate physically equivalent metric M_q on $T_q\mathcal{Q}$ for elements $\delta q \in T_q\mathcal{Q}$ is found to be:

$$M_q = \frac{\partial^2 \mathbb{H}_\mathbb{C}}{\partial q^2}(\tilde{q}),$$

   such that the physical dual elements (see Definition 5.32) on the dual space are given by $\delta\tau_{ext}^T = \frac{\partial^2 \mathbb{H}_\mathbb{C}}{\partial q^2}(\tilde{q}) \cdot \delta q \quad \in T_q^*\mathcal{Q}$, locally around $\tilde{q}$. And the physically sensible norm for the associated isomorphism is given by the (infinitesimal) change in potential energy:

$$\delta\mathbb{H}_\mathbb{C} = \delta q^T M_q \delta q = \delta q^T \frac{\partial^2 \mathbb{H}_\mathbb{C}}{\partial q^2}(\tilde{q})\delta q = \delta q^T \cdot \delta\tau_{ext}^T$$

   Notice, in absence of gravitation, this candidate metric represents a **stiffness matrix**, which has been used before.

2. **Undamped free motion:** Consider modeling an undamped free motion, i.e. $\dot{q}(t) \neq 0 \quad \forall t$. For this situation, Power-losses and Potential energy are zero. Hence, one energy function remains, i.e. Kinetic energy $\mathbb{H}_I(q)$, thus (recall Equation 5.93):

$$\dot{q}(t) = \frac{\partial \mathbb{H}_\mathbb{I}}{\partial p}(q) = M(q)^{-1} \cdot p(t)^T,$$

   which immediately suggests the associated isomorphism for the inner-product on $T_q^*\mathcal{Q}$ to be represented by the inverse mass matrix $M(q)^{-1}$, such that the $M(q)^{-1}$-weighted inner-product on $T_q^*\mathcal{Q}$ represents a kinetic energy function:

$$p(t) \cdot M(q)^{-1} \cdot p(t)^T = 2 \cdot \mathbb{H}_I,$$

   and the $M(q)^{-1}$-associated (see Definition 5.26) physical dual element is $\dot{q}(t) \in T_q\mathcal{Q}$:

$$\dot{q}(t) = M(q)^{-1} \cdot p(t)^T,$$

   such that $M_q = M(q)$ is the metric for the M_q-weighted inner-product on $T_q\mathcal{Q}$, being:

$$\dot{q}^T(t) \cdot M(q) \cdot \dot{q}(t),$$

   which shows that the physically sensible norm on $T_q\mathcal{Q}$ is given by a kinetic co-energy function equal to the kinetic energy function on $T_q^*\mathcal{Q}$:

$$2 \cdot \mathbb{H}_I = p(t) \cdot M(q)^{-1} \cdot p(t)^T = p(t) \cdot \dot{q}(t) = \dot{q}(t)^T M(q)\dot{q}(t).$$

   Thus, the **mass matrix** $M(q)$ induces physical dual elements $p(t)$ and $\dot{q}(t)$ and is a candidate physical equivalent metric for the given situation.

It may also be noticed that (recall Equation 5.93):

$$\frac{\partial \mathbb{H}_{\mathbb{I}}}{\partial p}(q) = \frac{\partial^2 \mathbb{H}_{\mathbb{I}}}{\partial p^2}(q) \cdot \delta p^T = M(q)^{-1} \cdot \delta p^T = \delta \dot{q}(t),$$

from which it follows that:

$$\delta p \cdot \frac{\partial^2 \mathbb{H}_{\mathbb{I}}}{\partial p^2}(q) \cdot \delta p^T = \delta p \cdot M(q)^{-1} \cdot \delta p^T = \delta \mathbb{E}_I, \tag{5.97}$$

is a $M(q)^{-1}$-weighted inner-product for the infinitesimal momenta changes $\delta p(t)$ on $T_q^*\mathcal{Q}$ around a given $q, \dot{q}$ and $p, \dot{p}$, which induces dual elements $\delta \dot{q}(t) \in T_q\mathcal{Q}$ that represent infinitesimal configuration velocity changes (infinitesimal accelerations) around given $q, \dot{q}$, based upon infinitesimal kinetic energy *changes*. Thus, the **mass matrix** $M(q)$ may also induce physical dual elements $\delta p(t)$ on $T_q^*\mathcal{Q}$ and $\delta \dot{q}(t) \in T_q\mathcal{Q}$.

3. **Damped free motion** Consider modeling a damped free motion, i.e. $\dot{q}(t) \neq 0 \quad \forall t$. For this situation, only Potential energy is zero. Hence, two energy function remains, i.e. Kinetic energy $\mathbb{H}_I(q)$ and Power-losses $P_b(t)$. The associated dual spaces and metric for kinetic energy is discussed above. The power-losses are investigated here.

   Recalling Equation 5.95 and Equation 5.96 and assuming the damping matrix to be positive definite immediately suggests an associated isomorphism for the M_q-weighted inner-product on $T_q\mathcal{Q}$, being the damping matrix B, such that the B-weighted inner-product on $T_q\mathcal{Q}$ represents the power-loss function $P_b(t)$ as given in Equation 5.96.

   The associated dual element is $\tau_b(t)^T = B \cdot \dot{q}(t) \in T_q^*\mathcal{Q}$. Hence, $M_\tau = M_q^{-1} = B^{-1}$ is the metric for the M_τ-weighted inner-product on $T_q^*\mathcal{Q}$, being:

$$\tau_b(t) \cdot B^{-1} \cdot \tau_b^T(t),$$

   such that the conserved energy for the associated isomorphism is given by a power-loss function:

$$P_b(t) = \tau_b(t) \cdot B^{-1} \cdot \tau_b(t)^T = \tau_b(t) \cdot \dot{q}(t) = \dot{q}(t)^T B \dot{q}(t). \tag{5.98}$$

   Thus, the **damping matrix** B induces physical dual spaces for elements $\tau_b(t) \in T_q^*\mathcal{Q}$ and $\dot{q}(t) \in T_q\mathcal{Q}$ and is a candidate physical equivalent metric for the given situation.

5.8.3 Conclusions

This section has presented various candidate physically equivalent metrics for different modeling problems and situations. For each of the three known energy functions, physical dual elements were discussed. It should be noticed that these different metrics all impose different dual elements and hence different variables on their dual spaces.

For the situation (3) of *damped free motions*, the damping matrix B was shown to be a candidate physically equivalent metric with associated dual elements $\dot{q}(t)$ and $\tau_b(t)$ $(= \dot{p}(t))$. However, It is noticed that for this situation also the mass metric is a candidate physically equivalent metric with associated dual elements $\dot{q}(t)$ and $p(t)$.

Both metrics seem equal candidates. Also intuitively, it may be recognized that for a damped free motion, damping and mass both influence energetics. However, their associated metrics have different norms attached.

Hence, the question arises how to combine both mass and damping effects into one metric. Or, which extra criteria can be distinguished for different situations within the setting of modeling damped free motions, for which one of the two metrics is suitable. These will be the topic of the next section, Section 5.9.

5.9 Physically Equivalent Metric for Damped free Motions

The previous section listed candidate physically equivalent metrics for several modeling problems. It concluded by raising the question how to combine both mass and damping effects into one metric for the case of damped free motions. This section contributes in understanding physically equivalent metrics by investigating damped free motions. For the linear case, the exact physically equivalent metric is derived. The implications for using this result are discussed and some expected implications for the non-linear case are given.

5.9.1 General problem definition

Briefly, the problem at hand is to find the metric that nature is minimizing for, for this specific case: damped free motion.

Motivation Finding the metric, does not just give a physically equivalent solution but may lead to better understand nature's optimization preferences for non-conservative dynamics and hence can be used to characterize physical properties of mechanisms (as will be done in Chapter 6 for the underactuated finger) and also for e.g. set-point (motion path) generation for motion control for which natural optimization solutions seem beneficial.

General model Consider damped free motions for a physical system with end-effector motions $T_e(t) \in se(3)$, modeled by the well known dynamic equations, given by[30]:

$$M(q) \cdot \ddot{q} + C(q, \dot{q}) \cdot \dot{q} + B \cdot \dot{q} = \tau_q^T = \tau_a^T + J(q)^T \cdot W_{ext}^T \quad (5.99)$$

$$T_e = J(q) \cdot \dot{q}, \quad (5.100)$$

with $q(t)$ the generalized configuration variables, i.e. $q(t) \in \mathcal{Q}$ on the configuration manifold $\mathcal{Q}$, $\tau_q^T(t) \in T_q^*\mathcal{Q}$ the net forces (co-vectors) and $\dot{q}(t) \in T_q\mathcal{Q}$ are generalized velocities of the configuration. Furthermore, $\tau_a(t) \in T_q^*\mathcal{Q}$ denote actuator forces and $W_{ext}(t)^T \in se^*(3)$ externally applied wrenches at the end-effector. The matrix $M(q)$ denotes the mass matrix, $C(q, \dot{q}) \cdot \dot{q}$ the Coriolis and centrifugal forces, B the constant linear damping and $J(q)$ the Jacobian of the end-effector, i.e. a kinematic map.

Problem definition Generally, the kinematic map $J(q)$ is non-bijective as discussed throughout this chapter. Applying some $W_{ext} \in \operatorname{im} J(q)$ will induce one unique set of motions $\dot{q}$ and T_e that follow from solving the given dynamics equation.

Nevertheless, if one observes or desires a certain $T_e(t)$, mathematically, for $J(q)$ being non-injective, multiple $\dot{q}$ can exist of which one $\dot{q}$ is the physically equivalent solution that belongs to $T_e(t)$ for the given system. Both the weighted pseudo-inverse and dual path solution give

[30] Note: all variables are functions of time, for shortness of notation, time variable t is left out

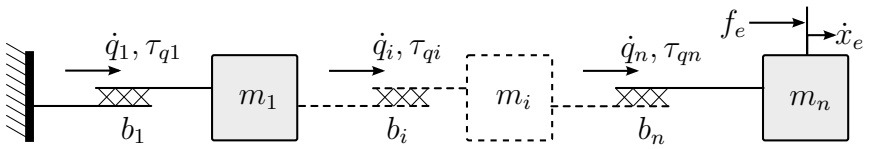

Figure 5.20: n-DOF Kinematic chain of n masses (m_i) connected through n prismatic joints q_i with linear damping b_i in the joints. The net torques on the joints are denoted by τ_{qi}.

solutions based on metrics for the spaces involved. The problem at hand is to find the metric M_q on $T_q\mathcal{Q}$ (or dually M_q^{-1} on $T_q^*\mathcal{Q}$) that induces the M_q-norm (see Definition 5.13) that nature is minimizing for in this specific case: damped free motion.

5.9.2 Method: Linear case

As announced, the results will be derived through examining the linear case as instantiation of the general case, as shown in Equation 5.99. Although, the results may not be directly copied to the general case, they will give useful insights for the general non-linear case.

Linear model The model of the linear instantiation of Equation 5.99 is illustrated in Figure 5.20. It presents a n-DOF kinematic chain of n masses (m_i) coupled through n linearly damped (b_i) prismatic joints, where q and $\dot{q}$ denote the joint-configuration and joint velocities, while $\dot{x}_e$ represents the end-effector velocity. Dually, τ_a represent the joint-actuation forces and f_e is the externally applied force at the end-effector.

From now on, merely for the sake of numerical examples, $n = 2$ is assumed. However, notice that the analytical results do apply for the general n-DOF linear case. Hence, the dynamic model is given by (see Equation 5.99):

$$M \cdot \ddot{q} + B \cdot \dot{q} = \tau_q^T = \tau_a^T + J \cdot f_e \tag{5.101}$$

$$\dot{x}_e = J \cdot \dot{q}, \tag{5.102}$$

where the mass matrix M and the damping matrix B are given by:

$$M = \begin{pmatrix} m_1 + m_2 & m_2 \\ m_2 & m_2 \end{pmatrix}, \qquad B = \begin{pmatrix} b_1 & 0 \\ 0 & b_2 \end{pmatrix}, \tag{5.103}$$

and the kinematic map J is given by:

$$J = \begin{pmatrix} 1 & 1 \end{pmatrix},$$

such that $J : T_q\mathcal{Q} \mapsto T\mathcal{X}_e \quad ; \quad \dot{x}_e = J \cdot \dot{q}$ with $\dot{q} \in T_q\mathcal{Q}$[31]$= \mathbb{R}^2$ and $\dot{x}_e \in T\mathcal{X}_e = \mathbb{R}$.

Method The physically equivalent inverse problem for this case is described by:

> *Consider a desired (or observed) $\dot{x}_{e,s} \in T\mathcal{X}_e$. Find $\dot{q}_s \in T_q\mathcal{Q}$ such that $\dot{q}_s$ is the minimum M_q-norm solution equal to $\dot{q}$ in the real physical system for the given situation and such that $\dot{x}_{e,s} = J \cdot \dot{q}_s$.*

The goal is:

> *Find the physically equivalent metric M_q for the above given inverse problem.*

[31] Note: for this linear case, $\mathcal{Q}$ is a flat manifold.

Clearly, $\operatorname{im} J = \mathbb{R}$ and $\ker J \neq \emptyset$. Hence, J is a surjective and non-injective map. Thus, as discussed throughout the chapter, a metric M_q is needed to find the pseudo-inverse of J (see Section 5.5.2):

$$J^{\#} = M_q^{-1} J^T \cdot \left(J M_q^{-1} J^T\right)^{-1}, \tag{5.104}$$

such that:

$$\dot{q}_s = J^{\#} \cdot \dot{x}_{e,s} \tag{5.105}$$

Note that the above given inverse problem is well posed, since every $\dot{x}_{e,s} \in T\mathcal{X}_e$ can be generated by at least one $\dot{q}$. Dually, inverting for $\tau_a \in \left(\operatorname{im} J^T\right)^{\perp}$ does not yield any solution, i.e. $\tau_a \in \left(\operatorname{im} J^T\right)^{\perp}$ represent non-producible forces that can not be (produced) resisted by any external force $f_e \in T_q^*\mathcal{Q} = \mathbb{R}$. Still, inverting from $\tau_a \in \left(\operatorname{im} J^T\right)^{\perp}$ is physically well posed, since these forces can be applied without violating any physical law. These forces will induce null-space motions, i.e. $\dot{q} \in \ker J$.

Thus, if the physically equivalent solution for the inverse problem of J is found, then also the physically equivalent metric M_q is found. Therefore, the approach will be to derive the physically equivalent solution by solving the dynamic equations and comparing this solution to the pseudo-inverse solution. It will be shown how the physically equivalent solution is found from this comparison.

5.9.3 Preview: Expectations

Before solving the dynamic equation, first, based on properties described in the previous section (Section 5.8), three cases are examined to establish some expectations for the physically equivalent metric to be found.

1. **Inducing motion:** consider $\dot{q}(t) = 0$, while $\ddot{q}(t) \neq 0$. Thus, no dissipation and the only obvious candidate metric left is given in Equation 5.97, i.e. the mass matrix M. Using $M_q = M$ induces the M-norm, which is expected to give a pseudo-inverse solution that minimizes the change of kinetic (co-)energy $\delta\mathbb{E}$. In that case,

$$J^{\#} = M^{-1} J^T \cdot \left(J M^{-1} J^T\right)^{-1} = \begin{pmatrix} 0 \\ 1 \end{pmatrix}, \tag{5.106}$$

   which corresponds to the fact that immediately after the moment that $\ddot{x}(t) \neq 0$, first q_2 starts to accelerate, before any motion (force) is transmitted to q_1.

2. **Steady state motion:** consider $\dot{q}(t) \neq 0$ and $\ddot{q}(t) = 0$. Thus, no accelerations, and the only candidate metric left is given in Equation 5.98, i.e. the damping matrix B. Using $M_q = B$ induces the B-norm, which is expected to give a pseudo-inverse solution that minimizes the dissipation losses $P_b(t)$. In that case,

$$J^{\#} = B^{-1} J^T \cdot \left(J B^{-1} J^T\right)^{-1} = \begin{pmatrix} \frac{b_2}{b_1+b_2} \\ \frac{b_1}{b_1+b_2} \end{pmatrix} \tag{5.107}$$

3. **Minimizing power-losses:** Assume that nature tries to minimize power losses $P_b(t)$ at a given time t, some known (or desired) $\dot{x}_e$ and no knowledge on metrics or a pseudo-inverse, etc. For this system, $P_b(t)$ at some time t, is given by (Equation 5.98):

$$P_b(t) = P_b = b_1 \cdot \dot{q}_1^2 + b_2 \cdot \dot{q}_2^2,$$

where time is neglected for $P_b, \dot{q}_1, \dot{q}_2$. From Equation 5.102 it is learned that: $\dot{q}_1 = \dot{x}_e - \dot{q}$. Substituting this into $P_b(t)$, gives

$$P_b = (b_1 + b_2)\dot{q}_2^2 - 2b_1\dot{x}_e\dot{q}_2 + b_1\dot{x}_e^2. \tag{5.108}$$

P_b is minimal for $\dot{q}_2$ at which the derivative is zero:

$$\frac{\partial P_b}{\partial \dot{q}_2}(\dot{q}_2) = 0 \quad \rightarrow \quad 2(b_1 + b_2)\dot{q}_2 - 2b_1\dot{x}_e = 0,$$

such that P_b is found to be minimal for:

$$\dot{q}_2 = \frac{b_1}{b_1 + b_2} \cdot \dot{x}_e \tag{5.109}$$

and

$$\dot{q}_1 = \dot{x}_e - \dot{q}_2 = \frac{b_2}{b_1 + b_2} \cdot \dot{x}_e \tag{5.110}$$

Comparing Equations 5.109 and 5.110 with Equation 5.107 leads to conclude that the starting assumption of case-3, 'nature minimizes power', can only (but may not necessarily) be true at all time t for which the system shows steady state motion, i.e. $\ddot{q}(t) = 0$.

5.9.4 Physically equivalent solution

As announced in the method, the physically equivalent solution is derived by solving the dynamic equations. Next, the solution is compared to the pseudo-inverse solution. It will be shown how the physically equivalent metric is found from this comparison.

Approach Consider the observed/desired $\dot{x}_e(t)$ to be the result of an externally applied step force $f_e(t)$ at time $t = 0$ (and hence consider $\tau_a(t) = 0 \quad \forall t$):

$$f_e(t) = \begin{cases} f_e & \forall t \geq 0 \\ f_0 & \forall t < 0 \end{cases},$$

and consider

$$\dot{q}(t) = \begin{cases} \dot{q}(t) & \forall t \geq 0 \\ \dot{q}_0 & \forall t < 0 \end{cases},$$

Also notice that, because of dissipation, the steady state situation for time $t < 0$, $\dot{q}(t) = \dot{q}_0 \quad \forall t < 0$, can only be maintained with some applied force, being $f_e(t) = f_0 \quad \forall t < 0$, such that it follows from the dynamic equations, Equation 5.101, that (notice: $\ddot{q}(t) = 0 \quad \forall t < 0$):

$$\dot{q}_0 = B^{-1}J^T \cdot f_0 \tag{5.111}$$

Solution The dynamic equation to be solved for $\dot{q}(t) \quad \forall t \geq 0$ is given in Equation 5.101. The differential equation is solved by considering the solution $\dot{q}(t)$ to consist of a homogeneous solution $\dot{q}_h(t)$ and a particular solution $\dot{q}_p(t)$, such that: $\dot{q}(t) = \dot{q}_h(t) + \dot{q}_p(t)$:

1. **Homogeneous solution:** For the homogeneous solution, the following autonomous system equation is solved for $\dot{q}_h(t)$:

$$M \cdot \ddot{q}_h(t) + B\dot{q}_h(t) = 0 \tag{5.112}$$

Using matrix exponentials and M and B being constant, gives the general solution:

$$\dot{q}_h(t) = e^{\tilde{A}t} C_1, \tag{5.113}$$

for some constant $n \times n$ matrix $\tilde{A}$ and n-dimensional vector C_1. $\tilde{A}$ is found by substituting Equation 5.113 into Equation 5.112

$$\left(M\tilde{A} + B\right) \dot{q}_h(t) = 0 \quad \rightarrow \quad \tilde{A} = -M^{-1}B \tag{5.114}$$

Thus, for M and B being constant, the homogeneous solution is found to be:

$$\dot{q}_h(t) = e^{-M^{-1}B \cdot t} C_1 \tag{5.115}$$

2. **Particular solution:** Since $f_e(t) \quad \forall t \geq 0$ is constant, the following particular solution is proposed:

$$\dot{q}_p(t) = C_3 \tag{5.116}$$

with C_3 some constant n-dimensional vector. C_3 is determined by substituting Equation 5.116 into the dynamic equation (Equation 5.101) and solving for C_3 (with B non-singular, i.e. some damping on each joint is needed to transmit forces/velocities):

$$BC_3 = J^T \cdot f_e \quad \rightarrow \quad C_3 = B^{-1}J^T \cdot f_e. \tag{5.117}$$

3. **Total solution:** The total function of interest, $\dot{q}(t) \quad \forall t \geq 0$, is found as:

$$\dot{q}(t) = e^{-M^{-1}B \cdot t} C_1 + B^{-1}J^T \cdot f_e, \quad \forall t \geq 0 \tag{5.118}$$

Then C_2 is solved by applying the initial condition $\dot{q}(0) = \dot{q}_0$, giving $C_1 = \dot{q}_0 - B^{-1}J^T \cdot f_e$. Hence, the joint velocities are given by:

$$\dot{q}(t) \;=\; e^{-M^{-1}B \cdot t} \left(\dot{q}_0 - B^{-1}J^T \cdot f_e\right) + B^{-1}J^T \cdot f_e, \quad \forall t \geq 0. \tag{5.119}$$

Substituting Equation 5.111 and considering changes with respect to the starting steady state situation, i.e. $\Delta f_e(t) = f_e - f_0$, $\Delta\dot{q}(t) = \dot{q}(t) - \dot{q}_0 \quad \forall t \geq 0$, finally results in:

$$\begin{aligned} \Delta\dot{q}(t) &= \dot{q}(t) - \dot{q}_0 \\ &= e^{-M^{-1}B \cdot t} \left(B^{-1}J^T \cdot f_0 - B^{-1}J^T \cdot f_e\right) + B^{-1}J^T \cdot f_e - B^{-1}J^T \cdot f_0 \\ &= \left(-e^{-M^{-1}B \cdot t} B^{-1}J^T + B^{-1}J^T\right) \cdot \Delta f_e, \qquad \forall t \geq 0, \end{aligned} \tag{5.120}$$

where it may be noticed that this result applies for a n-DOF linear kinematic system as illustrated in Figure 5.20.

Naturally, also the according observed (or desired) change in the end-effector velocity $\Delta\dot{x}_e(t)$ is found by applying the kinematic map J (Equation 5.102) to Equation 5.120, such that:

$$\Delta\dot{x}_e(t) = J \cdot \Delta\dot{q}(t) = \left(-Je^{-M^{-1}B \cdot t} B^{-1}J^T + JB^{-1}J^T\right) \cdot \Delta f_e, \qquad \forall t \geq 0 \tag{5.121}$$

with $\Delta\dot{x}_e(t) = \dot{x}_e(t) - \dot{x}_{e0} \quad \forall t \geq 0$ and $\dot{x}_e(t) = \dot{x}_{e0} \quad \forall t < 0$.

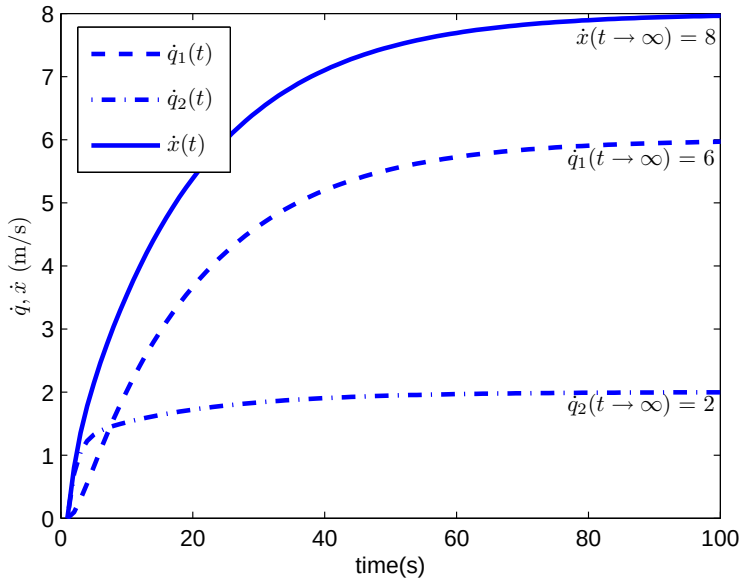

Figure 5.21: Arbitrary example of physically equivalent $\dot{q}(t)$ belonging to some $\dot{x}_e(t)$ (which is modeled as a response to constant force $f_e(t) = 1\ N$) $(m_1 = 2, m_2 = 1, b_1 = \frac{1}{6}, b_2 = \frac{1}{2}, f_e = 1)$. Notice: $\dot{q}_0 = 0, \dot{x}_{e0} = 0$.

Check steady state solution For the inspected situation, Equation 5.120 gives the physically equivalent velocity profile $\dot{q}(t)$ for a given $\dot{x}_e(t)$ as the result of an applied force, as given in Equation 5.121. Here it is shown that the solution for the inverse problem for *steady state motions* $(\ddot{q}(t) = 0)$ is easily found by considering $t \to \infty$.

In Section 5.9.3 the solution for *steady state motion* was expected to be given by (for shortness of notation, it is used that $\dot{q}_0 = 0, \dot{x}_{e0} = 0$):

$$\dot{q}(t) = J^{\#} \cdot x_e(t) = \begin{pmatrix} \frac{b_2}{b_1+b_2} \\ \frac{b_1}{b_1+b_2} \end{pmatrix} \cdot \dot{x}_e(t), \tag{5.122}$$

where $J^{\#}$ is taken from Equation 5.107 with metric B.

Inspection of Equation 5.120 and Equation 5.121 reveals that this expectation is generally true for damped free steady state motions. A numerical example, for $n = 2$, is used to give a brief illustration with arbitrary parameter values (listed in Figure 5.21).

The physically equivalent velocity profiles $\dot{q}(t)$ belonging to some $\dot{x}_e(t)$ are plot in Figure 5.21. The plot shows the steady state values, i.e. $\dot{q}(t \to \infty)^T = \begin{pmatrix} 6 & 2 \end{pmatrix} \quad [m/s], \quad \dot{x}_e(t \to \infty) = 8 \quad [m/s]$. Hence, it is verified that the steady state solution $\dot{q}(t \to \infty)$ is found with metric $M_q = B$, Equation 5.122, which resembles the physically equivalent solution found by solving the dynamic equation:

$$\dot{q}(t \to \infty) \quad = \quad \begin{pmatrix} \frac{b_2}{b_1+b_2} \\ \frac{b_1}{b_1+b_2} \end{pmatrix} \cdot \dot{x}_e(t \to \infty) = \begin{pmatrix} \frac{3}{4} \\ \frac{1}{4} \end{pmatrix} \cdot 8 = \begin{pmatrix} 6 \\ 2 \end{pmatrix} \quad \square$$

5.9.5 Result: Metric $M_q(t)$

For some observed end-effector velocity profile $\dot{x}_e(t)$, Equation 5.121, which happens to be the response to a constant force, the physically equivalent solution for $\dot{q}(t)$ was found, as given in Equation 5.120 (it describes the change with respect to a steady state situation, $\dot{x}_{e0}, \dot{q}_0$).

Now, the goal is to find $\dot{q}(t)$ for the given $\dot{x}_e(t)$ at each t by applying the weighted pseudo-inverse. Hence M_q needs to be determined for $J^{\#}$, as given in Equation 5.104.

Loosely speaking, $J^{\#}$ represents the ratio of $\dot{q}$ over $\dot{x}_e$ (see Equation 5.105), which varies in time as can be observed from the example in Figure 5.21. Therefore, a time dependent metric is expected.

Since $\dot{x}_e(t)$ is a scalar, it is noticed that $J^{\#}(t)$ may be written as:

$$J^{\#}(t) = \dot{q}(t) \cdot (\dot{x}_e(t))^{-1} \quad \forall \dot{q}(t) \neq 0, \forall \dot{x}_e(t) \neq 0$$

and $\dot{q}(t)$ being elements of the minimum M_q-norm solution, which is the case for the investigated physically equivalent solution.

Substituting the expressions for both velocity profiles, Equation 5.120 and Equation 5.121), gives the following interesting result:

$$\begin{aligned} J^{\#}(t) &= \left(-e^{-M^{-1}B\cdot t}B^{-1}J^T + B^{-1}J^T\right) \cdot f_e \cdot \left(-Je^{-M^{-1}B\cdot t}B^{-1}J^T + JB^{-1}J^T\right)^{-1} \cdot f_e^{-1} \\ &= \left(-e^{-M^{-1}B\cdot t}B^{-1}J^T + B^{-1}J^T\right) \cdot \left(-Je^{-M^{-1}B\cdot t}B^{-1}J^T + JB^{-1}J^T\right)^{-1} \\ &= DJ^T\left(JDJ^T\right)^{-1} \qquad \forall t, \end{aligned} \tag{5.123}$$

with

$$D = -e^{-M^{-1}B\cdot t}B^{-1} + B^{-1}$$

Comparing the derived equation for the pseudo-inverse, Equation 5.123, with the general description of $J^{\#}$, Equation 5.104, it is noticed that these two expressions equate for $D = M_q^{-1}$.

Therefore, it is concluded that the time dependent metric $M_q(t)$ is found to be:

$$M_q(t) = \left(-e^{-M^{-1}B\cdot t}B^{-1} + B^{-1}\right)^{-1} \qquad \forall t \backslash 0, \tag{5.124}$$

which is a smooth function of time, where $t = 0$ is excluded, since $M_q(0)$ is non-invertible.

5.9.6 Discussion: Properties of $M_q(t)$

For the derived physically equivalent metric $M_q(t)$, some properties are discussed hereafter.

Units and dual spaces The units of the physically equivalent metric $M_q(t)$, Equation 5.124, are found to be $\left(\frac{m}{Ns}\right)^{-1} = \frac{Ns}{m} \quad \forall t > 0$. Thus, the M_q-norm (see Definition 5.13) gives:

$$\dot{q}^T M_q \dot{q},$$

with units Nm/s, i.e. the physical sensible quantity mechanical *power*. From the units, it is clear that the induced physical dual elements are forces co-aligned with the joint velocities:

$$M_q(t) \cdot \dot{q}(t) = \tau_q(t) \quad \Leftrightarrow \quad \frac{Ns}{m} \cdot \frac{m}{s} = N,$$

Hence, in line with summarized properties in Section 5.8.2, the derived metric $M_q(t)$ induces an isomorphism for the physical dual elements $\dot{q}(t)$ on $T_q\mathcal{Q}$ and $\tau_q(t) \in T_q^*\mathcal{Q}$.

Steady state metric With Equation 5.124 it is easily verified that:

$$\lim_{t\to\infty} M_q(t) = B.$$

Notice that for the inspected case, $t \to \infty$ implies $\ddot{q}(\infty) = 0$, i.e. steady state motions. Hence, as expected, for steady state motions, i.e. $\ddot{q} = 0$, the metric $M_q(t)$ is constant and equal to dissipation metric B.

Time evolution of $M_q(t)$ The time dependency of $M_q(t)$ is investigated by its influence on $J^{\#}$, Equation 5.104, where $J^{\#}$ becomes a function of time as well: $J^{\#}(t)$.

In order to determine the time behavior of $M_q(t)$, its influence on $J^{\#}$ is investigated by comparing the time evolution of the $M_q(t)$ induced pseudo-inverse $J^{\#}_{pe}(t)$ with $J^{\#}_m$ (metric is M, mass) and $J^{\#}_b$ (metric is B, damping) for the $n = 2$-DOF kinematic chain for multiple arbitrary parameter sets. Notice that, because of linearity, the behavioral comparison results apply for any n-DOF chain and any (constant) parameter set (with B non-singular, i.e. some damping on each joint is needed to transmit forces/velocities).

The three pseudo-inverses $J^{\#}$ with different metrics are defined as follows:

$$J^{\#}_m = M^{-1}J^T \cdot \left(JM^{-1}J^T\right)^{-1} \tag{5.125}$$

$$J^{\#}_b = B^{-1}J^T \cdot \left(JB^{-1}J^T\right)^{-1} \tag{5.126}$$

$$J^{\#}_{pe}(t) = \left(M_q(t)\right)^{-1} J^T \cdot \left(J\left(M_q(t)\right)^{-1} J^T\right)^{-1} \qquad t \neq 0 \tag{5.127}$$

Hence, different metrics are used to produce a pseudo-inverse. Notice that all three $J^{\#}$ can be used for a mathematically correct inverse solution, with $J^{\#}_{pe}(t)$ the physically equivalent time dependent pseudo-inverse of J giving the physically equivalent solution. An arbitrary example is given in Figure 5.22 (used parameters are indicated in the figure caption), which illustrates the general observation.

From the behavioral time evolutions comparison it is concluded that:

1. $J^{\#}_{pe}(t) = J^{\#}_m \qquad \forall t \to 0$
2. $J^{\#}_{pe}(t) = J^{\#}_b \qquad \forall t \to \infty$

Conclusion: $M_q(t) = M$ for small t, $M_q = B$ for large t, which matches exactly the stated expectations in Section 5.9.3.

Energy usage The energy usage for each of the inverse solutions for the previously defined $J^{\#}(t)$ is compared. Total energy usage is kinetic (co-)energy plus power losses:

$$\mathbb{E}(t) = \int P_b(t) \cdot dt + \frac{1}{2}\left(\dot{q}(t)\right)^T M\dot{q}(t) = \int \left(\dot{q}(t)\right)^T B\dot{q}(t) \cdot dt + \frac{1}{2}\left(\dot{q}(t)\right)^T M\dot{q}(t),$$

where $q(t)$ is the according velocity profile, calculated for a belonging observed or desired end-effector velocity $\dot{x}_e(t)$, which can be described as the velocity profile resulting from applied $f_e(t)$. Different $q(t)$ are given for previously defined $J^{\#}(t)$:

$$\dot{q}_m(t) = J^{\#}_m \cdot \dot{x}_e(t) \tag{5.128}$$

$$\dot{q}_b(t) = J^{\#}_b \cdot \dot{x}_e(t) \tag{5.129}$$

$$\dot{q}_{pe}(t) = J^{\#}_{pe}(t) \cdot \dot{x}_e(t) \tag{5.130}$$

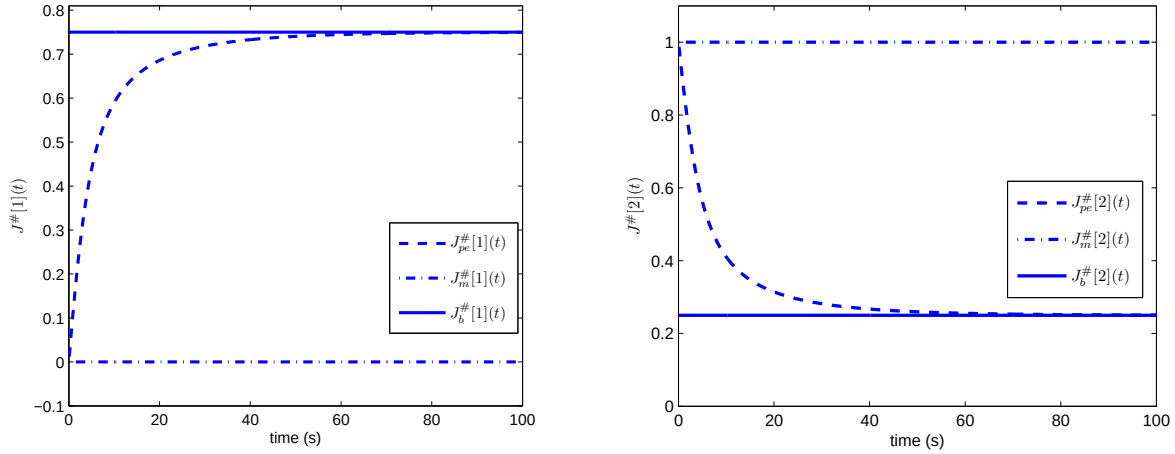

(a) $J^{\#}[1](t)$ (b) $J^{\#}[2](t)$

Figure 5.22: Arbitrary example of plots of $J^{\#}(t)$ for $n = 2$: $J^{\#}_{pe}(t)$, $J^{\#}_{m}(t)$, $J^{\#}_{b}(t)$ for $m_1 = 2, m_2 = 1, b_1 = \frac{1}{6}, b_2 = \frac{1}{2}$. Each plot shows one of the two components in $J^{\#}(t)$. The observed relative (compared) behavior of different $J^{\#}(t)$ for different metrics holds for any parameter set with B non-singular (damping is needed to transmit forces/velocities trough the chain).

Hence, different metrics[32] are used to produce a $\dot{q}(t)$.

The energy usage of above given solutions ($\dot{q}_m(t)$, $\dot{q}_b(t)$, $\dot{q}_{pe}(t)$) is denoted by $\mathbb{E}_m(t)$, $\mathbb{E}_b(t)$ and $\mathbb{E}_{ep}(t)$, respectively. These three are investigated by comparing their time evolutions for the $n = 2$-DOF kinematic chain for multiple arbitrary parameter sets. Notice that, because of linearity, the behavioral comparison results apply for any n-DOF chain and any (constant) parameter set (with B non-singular, i.e. some damping on each joint is needed to transmit forces/velocities).

An arbitrary example is given in Figure 5.23, which illustrates the general observations valid for all parameter sets:

- $0 < t < t_1$: $\mathbb{E}_{ep}(t) \leq \mathbb{E}_m(t) < \mathbb{E}_b(t)$
- $t_1 < t < t_2$: $\mathbb{E}_{ep}(t) \leq \mathbb{E}_b(t) << \mathbb{E}_m(t)$
- $t > t_2$: $\mathbb{E}_b(t) \leq \mathbb{E}_{ep}(t) << \mathbb{E}_m(t)$ and $\mathbb{E}_b(t) - \mathbb{E}_{ep}(t) = \kappa$, with $\kappa \in \mathbb{R}$.

where t_1 and t_2 depend on the parameters m_i and b_i. From the time dependent exponential in $M_q(t)$, with exponent $(M^{-1}B \cdot t)$, it can be understood that the parameters influence t_1 and t_2 as follows:

- $m_i \Uparrow \quad \Rightarrow \quad t_1, t_2 \Uparrow$
- $b_i \Uparrow \quad \Rightarrow \quad t_1, t_2 \Downarrow$

where $\Uparrow, \Downarrow$ indicate increments and decrements, respectively. Notice that for $t > t_2$ with $\dot{x}_e(t)$ going to steady state motion, $\dot{q}_b(t)$ results in lower energy consumption than $\dot{q}_{pe}(t)$.

These energetic observations together with the time evolution observations for $M_q(t)$, lead to the following useful proposition:

[32] Notice that all three $\dot{q}(t)$ give a mathematically correct inverse solution such that indeed $\dot{x}_e(t) = J \cdot \dot{q}(t)$, where $\dot{q}_{pe}(t)$ is the physically equivalent solution with $J^{\#}_{pe}(t)$ the physically equivalent time dependent pseudo-inverse of J.

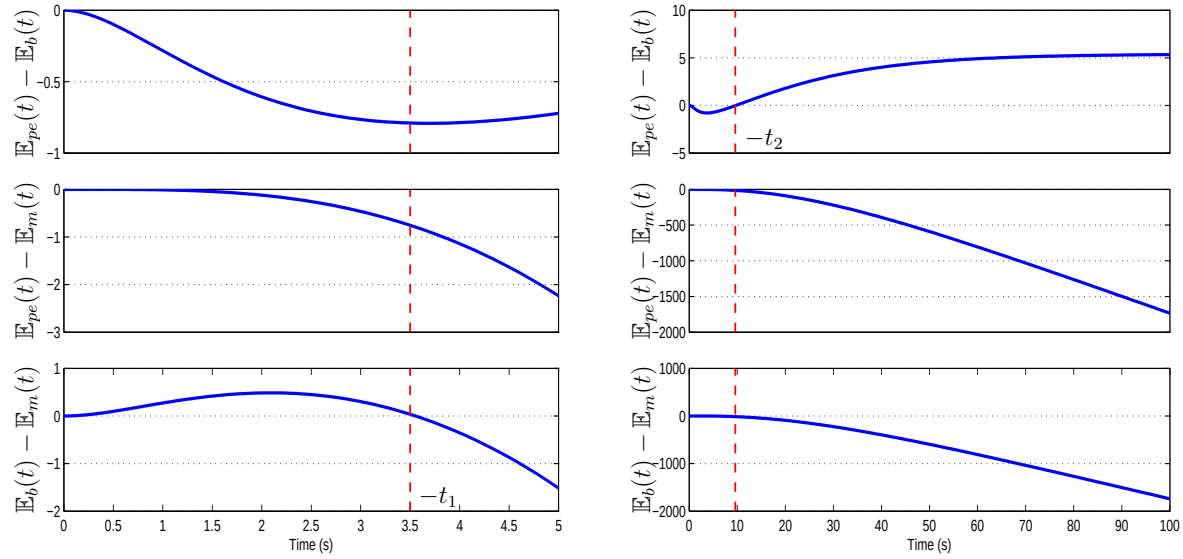

(a) Energy comparisons (Joules $[Nm]$) for $0 \leq t < 5\ s$, where t_1 indicates: $\mathbb{E}_b(t_1) = \mathbb{E}_m(t_1)$.

(b) Energy comparisons (Joules $[Nm]$) for $0 \leq t < 100\ s$, where t_2 indicates: $\mathbb{E}_b(t_2) = \mathbb{E}_{pe}(t_2)$.

Figure 5.23: Illustrative comparison plots of energy usage for different $\dot{q}(t)$ (calculated through $J_b^{\#}, J_m^{\#}$ and $J_{pe}^{\#}(t)$) that generate the same $\dot{x}_e(t)$: plots show differences $\mathbb{E}(t)_{pe} - \mathbb{E}(t)_b$, $\mathbb{E}(t)_{pe} - \mathbb{E}(t)_m$ and $\mathbb{E}(t)_b - \mathbb{E}(t)_m$ for different time scales and for arbitrary parameter set ($n = 2$): $m_1 = 2, m_2 = 1, b_1 = \frac{1}{6}, b_2 = \frac{1}{2}$. The observed relative (compared) behavior of different $J^{\#}(t)$ for different metrics holds for any parameter set with B non-singular (damping is needed to transmit forces/velocities trough the chain).

Remark 5.21. *Consider any observed or desired end-effector velocity profile $\dot{x}_e(t)$ of a linear kinematic chain (see Figure 5.20), which can be assumed to be the result of a sequence of n_f externally applied force steps Δf_{ei} at time instants t_i, such that (see Equation 5.121):*

$$\dot{x}_e(t) = \sum_{i=1}^{n_f} \Delta x_i(t - t_i)$$

with

$$\Delta x_i(t - t_i) = \begin{cases} 0 & t < t_i \\ \left(-Je^{-M^{-1}B\cdot(t-t_i)}B^{-1}J^T + JB^{-1}J^T\right) \cdot \Delta f_{ei}(t) & t \geq t_i \end{cases}$$

and

$$\Delta f_{ei}(t) = \begin{cases} 0 & t < t_i \\ \Delta f_{ei} & t \geq t_i \end{cases}$$

Then, two cases can be distinguished in order to estimate the $\dot{q}$ that are close to the physically equivalent $\dot{q}_{pe}(t)$ and which exactly generate $\dot{x}_e(t)$:

1. **relatively high frequent $\dot{x}_e(t)$:** *holds for $t_{i+1} - t_i \leq t_1$ (with t_{i+1} and t_i two consecutive time instants). Using $J_m^{\#}$, calculates the generating $\dot{q}_m(t) = J_m^{\#} \cdot \dot{x}_e(t)$ closest to $\dot{q}_{pe}(t)$ and lowest energy usage at any time t.*

2. **relatively low frequent $\dot{x}_e(t)$:** *holds for $t_{i+1} - t_i \geq t_2$. Using $J_b^{\#}$, calculates the generating $\dot{q}_b(t) = J_m^{\#} \cdot \dot{x}_e(t)$ closest to $\dot{q}_{pe}(t)$ and lowest energy usage at any time t.*

Notice that $M_q(t)$ is only the exact metric for the given velocity profile of $\dot{x}_e(t)$, being the result of externally applied force $f_e(t)$, where t is the running time-variable starting from the moment at which the force is applied. In practical situations, one observes or prescribes a desired $\dot{x}_e(t)$ for which the according $\dot{q}(t)$ are needed to be found trough the pseudo-inverse, without knowing t and, possibly, $\dot{x}_e(t)$ can not be assumed to be the result of one applied step force. Hence, the above given proposition gives interesting insights for these situations.

5.9.7 Conclusions and future work

Conclusions This section showed how to combine both inertia and dissipation effects into one metric for the attached dual spaces, $T_q\mathcal{Q}, T_q^*\mathcal{Q}$, of a kinematic map. For a linear map, the time dependent metric $M_q(t)$ was found. It induces a physically sensible norm, which measures power.

For steady state motions ($\ddot{q} = 0$), it has been shown that the natural metric is damping (B), while for instantaneous acceleration that induce or change motion, $M_q(t)$ gives minimization of the change of kinetic energy, which resembles the effect of the mass metric M.

The derived metric stems from the study on end-effector motions that can be described as being induced by an externally applied force. Such an assumption is needed, since the interplay between inertia and dissipation effects requires knowledge on previous states of the system in order to predict future states. This is reflected in the time dependency of the metric and in the different physical dual elements for metric M (momenta and velocities) and B (forces and velocities), as presented in the previous section, Section 5.8.2.

Nevertheless, the results have been interpreted for any motion as described in Remark 5.21. Hence, the results are detached from the motion assumption and have broader applicability.

Future work The metric $M_q(t)$ is derived for a general linear system. Hence, the mass matrix M is constant. In robotic systems, such as robotic fingers, oftentimes non-linear systems are found, implying a non-constant mass matrix $M(q)$ (Equation 5.99). If motions are studied for such mechanisms, the interplay between damping and inertia effects may change, since inertia varies. This induces accelerations $\ddot{q}(t) \neq 0$, while the end-effector may experience steady state motion $\ddot{x}_e(t) = 0$. Hence, for future work, it is interesting to see the effects of non-linearity on the metric.

Nevertheless, for cases in which the mass matrix does not (or negligibly) change (small or slow perturbations), the here presented linear results are applicable. This will be used and shown for the analysis of the robotic finger, presented in Chapter 6.

Remark 5.21 now uses qualitative descriptions of the interpretation of t_1 and t_2. In order to be able to be more specific, it would be interesting to find analytical parameter dependent functions for switching points t_1 and t_2. This involves solving the energetic equalities that define t_1 and t_2. If so, one has quantitative criteria to evaluate the choice of metrics for specific situations which require decomposition of spaces (such as for inverse problems or change of coordinates).

5.10 Conclusions

This chapter discussed the inverse relations of non-bijective maps in kinematic modeling of physical systems. For this specific class of non-bijective maps, the physically equivalent inverse solution has been introduced, being the unique inverse solution as found in the real physical behavior of the modeled system.

5.10 Conclusions

Various approaches were combined to arrive at the understanding of inversion of non-bijective maps, using geometrical coordinate free space-decompositions as natural way to understand and derive the mathematical description of the inverse relation in coordinates. As such, the minimum norm and least squares solution, being the well-known weighted pseudo-inverse, is contained in the complete description.

The physically equivalent solution of the inverse problem was shown to be related to the minimization of energy functions. It was shown to be mathematically described by the minimum norm and least squares inverse solution if the physically equivalent metric for the spaces involved is used.

Through a series of examples of the grasp system model, the intuitive interpretations of various concepts were explained, such as interpretations of the space decompositions, ill-posed inverse problems and physically equivalent metrics.

The concept of physical dual spaces and physical dual elements was introduced to show the dual path as physically equivalent solution for the inverse problem. The dual path allows to interpret the inverse problem in a physically meaningful way. Hence, physical dual spaces, with inverse metrics, were used to give insights to the physics behind the modeled inverse problem.

An overview of possible physical dual spaces is given for various energy functions and modeling variables in different cases. The chapter ends by presenting novel results and insights on the physically equivalent solution and physically equivalent metric for the case of damped free motions, which is shown to be time depended and induces minimization of the power, i.e. a physically sensible quantity, in the system.

These results will be directly applied for the analysis and control of the robotic finger concept in the following chapter.

Chapter 6

Novel Dexterous Robotic Finger Concept

Chapters 1, 2 and 3 discussed the interest for human-like dexterous robotic hands. Based on insights from these chapters, this chapter introduces a novel dexterous robotic finger concept to contribute in developing novel robotic hand technology and knowledge. In this work, the concept is studied in theory to verify and understand its properties before implementing it in practice in a possible later stage.

In Section 6.1, the design considerations from Chapter 3 are briefly summarized. Then Section 6.2 introduces the novel concept together with a port-Hamiltonian model in Section 6.3. The concept is analyzed and further clarified in a port-Hamiltonian framework in Section 6.5. As such, the analysis presents an interesting case-study for using port-Hamiltonian analysis. It also leads to some basic trade-offs for the design parameters, shown in Section 6.6.

The concept includes variable mechanical compliance and utilizes underactuation. Due to underactuation, the variable finger-tip compliance is non-trivial. Therefore, it is studied in Section 6.7, which results in an analytical description of the finger-tip compliance. The analysis heavily relies on insights and results of Chapter 5. The results are generally applicable for tendon-driven underactuated robotic fingers as well. The author has presented (parts of) this work in [85, 86].

6.1 Review of Design Considerations

Chapter 3 stated four primary functions for human-like dexterous robotic hands in future applications:

1. dexterous grasping: power grasping and tip grasping (see Section 3.1.4);
2. dexterous manipulation;
3. free finger motion;
4. interactive finger motion.

To focus research and technology development, for a subset of requirement parameters, general design goals were formulated:

- low weight;
- high energy efficiency;

- high robustness (task robustness and reliability);
- human dimensions;
- low cost.

Based on lessons learned from current state of the art, Chapter 3 translated these design goals into three design considerations for developing novel robotic hand technologies: utilizing **minimal component design**, **underactuation** and **variable mechanical compliance**.

A minimal number of components (especially actuators) allows to optimize dimensions, weight and energy efficiency, while operational robustness and reliability can be improved due to the reduction of sensitive components. The variable mechanical compliance and underactuation naturally support the hand functions and impedance control strategies, while complex control strategies may be avoided.

6.2 Novel Robotic Finger Concept

This work presents a novel dexterous robotic finger concept to be used for human-like robotic hands. The concept implements the discussed design considerations, as shown in Figure 6.1. It combines three key features:

1. an antagonistic underactuated actuation mechanism;
2. series-elastic tendon actuation with non-linear elastic elements (e.g. non-linear springs);
3. active joint locking mechanisms on the joints.

The presented concept is to be seen as a functional concept, without having worked out complete mechanical implementations that fulfill these functions. Before designing such mechanical concepts, it is chosen to first study the functional concept to verify its proposed properties and usability. Efforts on this functional analysis are presented in this thesis.

6.2.1 Review of design considerations

The conceptual properties of the presented robotic finger are briefly discussed with respect to the prescribed design considerations and desired hand/finger functions.

Variable mechanical compliance Antagonistic actuation with non-linear elastic elements in the driving tendons gives variable mechanical compliance [48]. This property is inspired by human stiffness control (see Section 3.1.4). However, combined control of position and mechanical compliance generally imposes a 2 DOF control problem per joint. Therefore, a dexterous finger (i.e. 3 DOF per finger for a hand with at least three fingers, see Section 3.2.1) and controlled compliance in each joint implies the need for six heavy power actuators per finger, see e.g. [52].

Minimal components and underactuation The underactuated 'softgripper' design ([15]) is adopted to reduce this amount of actuators and the number of sensors. Hence this choice supports a minimal components design.

Furthermore, the underactuated 'softgripper' finger naturally encloses and grasps (power grasps) a wide variety of object shapes. Hence, not only the amount of actuators is reduced, also no grasp trajectories have to be programmed. Thus, control complexity for grasping all kinds of irregular objects is decreased.

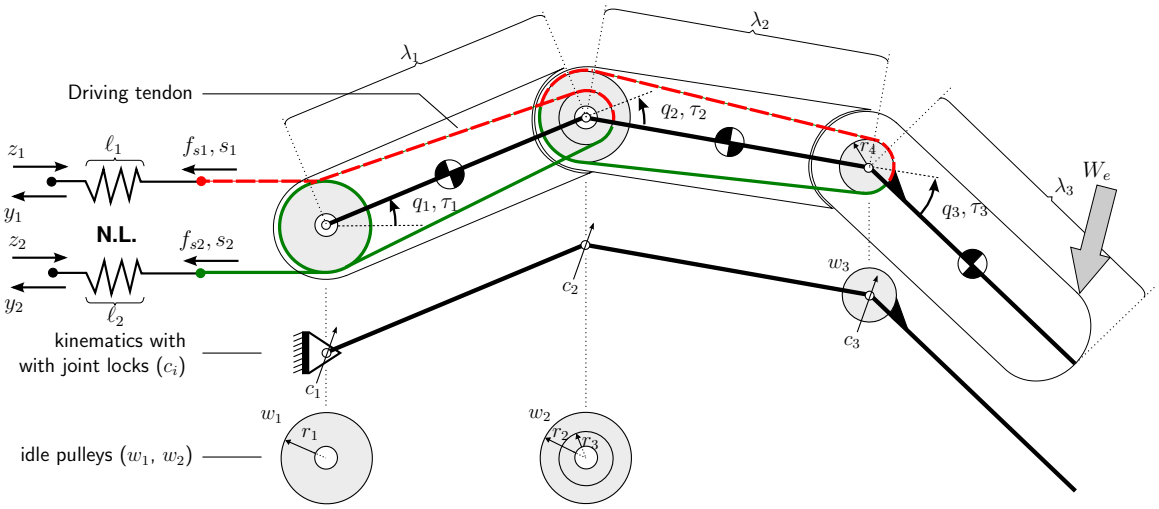

Figure 6.1: Conceptual drawing of novel robotic finger: The underactuated 'softgripper' principle is extended with joint locks and non-linear antagonistic elastic elements (denoted by $N.L.$ with length/state $\ell_j, j \in \{1, 2\}$) in series with the driving tendons. Pulleys 1 (w_1) and 2 (w_2) rotate freely on joint axes. Pulley 3 (w_3) is fixed to 3^{rd} phalanx. Variables $z = (z_1, z_2)^T$ denote the tendon actuation positions, lock switches are denoted with c_i, the relative motion of two attached phalanges is given by $\dot{q}_i$, where q_i is the relative joint angle of joint i and τ_i the torque on joint i. The externally applied wrench W_e represents environment interaction. The lengths of the phalanges are captured in $\lambda_i, i \in \{1, 2, 3\}$. Arrows indicate positive reference directions for attached variables.

Dexterity For underactuated fingers, the finger configuration is not fully reachable due to underactuation. Therefore the finger shape and configuration can not be steered to any desired location a priori, which is needed for e.g. pre-shaping in grasping, manipulation tasks, tip grasping, etc. Hence, underactuated fingers encompass reduced dexterity.

In the presented concept, this dexterity is restored by utilizing small sized mechanical locks on each joint: a lock can freeze and release the relative motion of two connected phalanges, without interfering with the free rotating (idle) pulleys on the joints. By means of switching control, the finger configuration space is fully reachable again.

Moreover, joint locking does not consume power (theoretically), since motions are constrained to zero velocity. Joint locking is also studied for control of parallel robot mechanisms [87].

Conclusion The underactuated principles are used to reduce control complexity and the number of large size power actuators, while keeping dexterity by using energy efficient small size joint locks. Furthermore, controlled mechanical compliance is introduced by a pair of non-linear elastic elements in series with the two antagonistic driving tendons.

6.2.2 Conceptual working principle

Some intuition on the proposed usage of the robotic finger is given. In the next sections, the port-Hamiltonian analysis helps to understand the working principle of the finger in more depth.

Finger functions From the listed robotic hand functions in Section 6.1 it is deduced that a single robotic finger needs to be able to dexterously alter its configuration, either in contact

(grasping objects, manipulating objects or interacting with environment) or freely moving (e.g. gesturing and pre-shaping). During interaction tasks, certain contact forces need to be applied.

Altering finger configuration The finger configuration is changed by controlling the tendon actuation positions ($z = (z_1, z_2)^T$) in differential mode (moving both tendons in opposite directions). Locks on each joint can freeze the relative motion of the attached phalanges (i.e. $\dot{q}_i = 0$). Notice that w_1 and w_2 always remain idle. Therefore, if a phalanx is constrained (either by external interaction or a lock), the other phalanges can still be moved through tendon actuation.

Thus, in case of object interaction, the phalanges naturally wrap around any shape if the tendon positions are moved differentially (power grasp). Whereas, the free moving finger configuration is steered by modulating the locks (switching on and off) and moving the tendon actuation positions (z) accordingly. A combination of both is used to execute non-enveloping grasps, such as tip-grasps, for which a particular pre-shape has to be maintained while grasping.

Altering finger compliance The mechanical compliance of the finger is controlled by driving z in common mode (moving both tendons in equal directions).

The compliance is used for disturbance rejection and to naturally establish contact forces during interaction in an energy efficient way. If the finger, due to external interaction, does not reach a finger configuration that belongs to the differential tendon actuation positions, then the elastic elements are (un)loaded (on top of a certain pre-load), which creates an external contact force on the interacting environment. The resulting contact force follows from the difference in preset configuration (differential tendon actuation positions) and the actual finger configuration together with the preset mechanical stiffness (common mode tendon actuation positions).

Control The finger can be controlled by simple position control for the tendon actuation positions (z) and by joint lock modulation. Notice that only (angular) position sensors are needed to measure the joint configuration and the tendon actuation positions, from which (for a known non-linear elastic function) the tendon stress (f_s) and the joint torques (τ) can be derived.

Since mechanical compliance is used, (relatively small) disturbances and other small interactions are rejected by the configured compliance. Furthermore, hand manipulations are generally relatively slow tasks. Hence, a low bandwidth position controller for the tendon actuation positions (z) suffices. It allows to use a non-backdriveable drive on the tendon actuation position. This is especially the case for holding tasks and other tasks that require maintaining finger configurations.

6.3 Model Variables

The presented robotic finger is analyzed in the next sections. Before setting up the complete model, first an overview is given of all relevant variables, spaces and involved mappings. These will be used throughout this chapter. The variables are generally time dependent functions. However, for shortness of notation, this is not explicitly reflected in the notation.

Remark 6.1. *Figure 6.1 addresses the mechanical locations and attachment points of the variables. The arrow-heads indicate positive reference directions for attached variables.*

- $q \in \mathcal{Q} \subset \mathbb{R}^3$**:** is the finger configuration (joint-angles) on the configuration manifold $\mathcal{Q}$.

- $\dot{q} \in T_q\mathcal{Q}$**:** is the time derivative of q, i.e. joint velocities, being elements (vectors) of the tangent space of $\mathcal{Q}$ at q.

- $\tau \in T_q^*\mathcal{Q}$**:** are torques on the joints, being elements (co-vectors) of the co-tangent space of $\mathcal{Q}$ at q.

- $s \in \mathcal{S} \subset \mathbb{R}^2$**:** are the positions of the tendons.

- $\dot{s} \in T_s\mathcal{S}$**:** are the time derivatives of s, being elements (vectors) of the tangent space of $\mathcal{S}$ at s.

- $f_s \in T_s^*\mathcal{S}$**:** are the tendon forces, being elements (co-vectors) of the co-tangent space $T_s^*\mathcal{S}$ at s.

- $\ell \in \mathcal{L} \subset \mathbb{R}^2$**:** are the states (elongations) of the non-linear elastic elements.

- $\dot{\ell} \in T_\ell\mathcal{L}$**:** are the time derivatives of ℓ, being elements (vectors) of the tangent space of $\mathcal{L}$ at ℓ.

- $f_\ell \in T_\ell^*\mathcal{L}$**:** are the elastic forces equal to f_s.

- $W_e \in se^*(3)_{H(q)}$**:** is the externally applied wrench (generalized 6 d.o.f. force) on the finger-tip (3^{rd} phalanx). The wrench space $se^*(3)_{H(q)} = T^*_{H(q)}SE(3)$ is the co-tangent space of the group of rigid transformations $H(q)$, called $SE(3)$, which denotes the special Euclidean group, at rigid transformation $H(q)$ [88].

- $T \in se(3)$**:** is the twist (generalized 6 d.o.f. rigid body motions) of the third phalanx, i.e. the finger-tip. The twist space $se(3)_{H(q)} = T_{H(q)}SE(3)$ is the tangent space of $SE(3)$ at $H(q)$ [88].

- $z \in \mathcal{Z} \subset \mathbb{R}^2$**:** are the actuator tendon positions that represent the positions of the actuators at the tendon ends.

- $u \in T_z\mathcal{Z}$**:** are the inputs that represent the velocities in the tangent space $T_z\mathcal{Z}$ of the tendon actuation position space $\mathcal{Z}$ at $z \in \mathcal{Z}$ (i.e. $u = \dot{z}$).

- $y \in T_z^*\mathcal{Z}$**:** are the outputs which represent the tendon forces in the co-tangent space of $\mathcal{Z}$ at z.

- λ_i**:** is the length of phalanx i captured in $\lambda_i, i \in \{1, 2, 3\}$.

Notice that the tangent and co-tangent spaces form dual spaces, see Section 5.7.1. All co-tangent spaces contain forces (co-vectors), which are functions on the tangent spaces that map the velocities (vectors) to the scalar quantity power.

Figure 6.2 shows the listed variables as elements of their different spaces. Also the inter-relating kinematic maps are depicted. The function $h_q : \mathcal{Q} \to SE(3)$ maps the joint configuration into a rigid body transformation for the finger-tip, while $f_s : \mathcal{Q} \to \mathcal{S}$ maps the joint

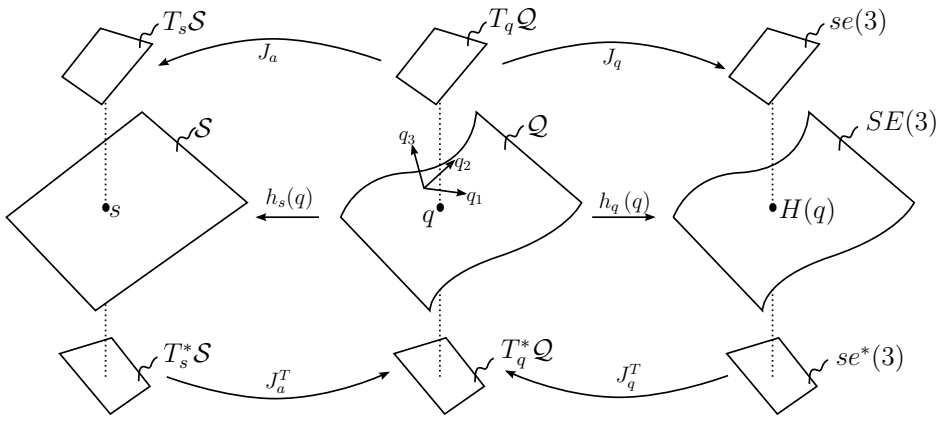

Figure 6.2: Model variables; The three joint-angles q_1, q_2, q_3 form a natural coordinate base to span the configuration space $\mathcal{Q}$.

configuration to the tendon positions.

In coordinates, where the three joint-angles q_1, q_2, q_3 (with unit radians), span the bases of the configuration space $\mathcal{Q}$ and the two tendon positions s_1, s_2, span the bases of $\mathcal{S}$, $h_s(q)$ follows from basic geometry:

$$h_s(q) : \begin{cases} s_1 &= r_1 \cdot q_1 + r_2 \cdot q_2 + \frac{r_2 r_4}{r_3} \cdot q_3 \\ s_2 &= -r_1 \cdot q_1 - r_2 \cdot q_2 - \frac{r_2 r_4}{r_3} \cdot q_3 \end{cases}, \tag{6.1}$$

which is re-written into matrix notation:

$$h_s(q) : \quad s = H_a \cdot q = \begin{pmatrix} r_1 & r_2 & \frac{r_2 r_4}{r_3} \\ -r_1 & -r_2 & -\frac{r_2 r_4}{r_3} \end{pmatrix} \cdot q, \tag{6.2}$$

with

$$H_a = \begin{pmatrix} r_1 & r_2 & \frac{r_2 r_4}{r_3} \\ -r_1 & -r_2 & -\frac{r_2 r_4}{r_3} \end{pmatrix} \tag{6.3}$$

The differential mappings (Jacobians) of h_q and h_s relate the tangent and co-tangent spaces in a dual manner. The geometric Jacobian $J_q(q)$, with short notation $J_q := J_q(q)$, defines the tangent map and dually the co-tangent map [88]:

$$\begin{array}{lcll} J_q & : & T_q\mathcal{Q} \to se(3) & (T = J_q \cdot \dot{q}) \\ J_q^T & : & se^*(3) \to T_q^*\mathcal{Q} & (\tau^T = J_q^T \cdot W_e^T) \end{array}. \tag{6.4}$$

which obviously depends on the finger configuration q. In coordinates, i.e. expressing T and W_e with respect to some reference frame, J_q is represented by a 6×3 matrix.

The actuation Jacobian J_a defines the (co-)tangent maps between the finger configuration and tendon position spaces:

$$\begin{array}{lcll} J_a & : & T_q\mathcal{Q} \to T_s\mathcal{S} & (\dot{s} = J_a \cdot \dot{q}) \\ J_a^T & : & T_s^*\mathcal{S} \to T_q^*\mathcal{Q} & (\tau^T = J_a^T \cdot f_s^T) \end{array}, \tag{6.5}$$

where, if coordinates are applied, J_a is represented by a 2×3 matrix. Hence, for the chosen coordinate bases:

$$J_a = \begin{pmatrix} r_1 & r_2 & \frac{r_2 r_4}{r_3} \\ -r_1 & -r_2 & -\frac{r_2 r_4}{r_3} \end{pmatrix} \tag{6.6}$$

Notice that J_a is constant and, numerically, it is equal to the configuration map H_a. However, they map different quantities and should therefore not be confused.

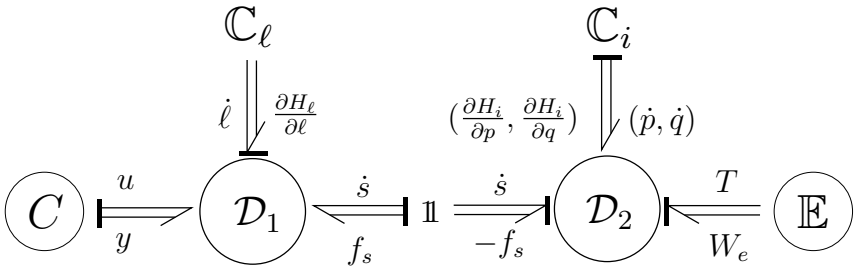

Figure 6.3: Generalized bond-graph model of the conceptual finger and its Dirac structures $\mathcal{D}_1, \mathcal{D}_2$, representing a port-Hamiltonian system with assigned effort causality in the direction of the bar on the bonds. The direction of the bond half-arrow indicates positive power flow.

6.4 Port-Hamiltonian Model

This section introduces a model of an idealized (rigid bodies, no friction, zero-length elastic elements, perfect locks and zero gravitaty) realization of the novel concept in a port-Hamiltonian framework and its underlying Dirac structure [64]. The Dirac structure represents the network topology of energy flows in the system. The power ports are interconnected such that power is conserved (as is the case in physical systems)[1].

This framework allows for an energy based, physically consistent, investigation of the conceptual properties for future implementation design and controller synthesis. The analysis of the conceptual properties is given in the next section, Section 6.5

6.4.1 Port-Hamiltonian model without locks

The generalized bond-graph model and its Dirac structure of the conceptual finger *without* locks is depicted in Figure 6.3. For completeness of the model, locks are added later (Section 6.4.2), but will not be part of the conceptual analysis. The locks are utilized by the controller for dexterous manipulation of the presented robotic finger, presented in Chapter 7.

Notice that all port variables are power conjugate variables, being the dual variables on the dual spaces, as presented in Figure 6.2. Figure 6.3 shows four different elements being interconnected through their ports on the Dirac structures $\mathcal{D}_1, \mathcal{D}_2$:

$\mathbb{C}_i$: Storage of generalized momenta $p = (p_1 \quad p_2 \quad p_3)$ of the three phalanges in kinetic energy, given by the Hamiltonian $H_i(p,q) = \frac{1}{2} p M^{-1}(q) p^T$. $M(q)$ is the mass matrix for the generalized coordinates q. The port is defined by the dual pair $\langle (\dot{p}, \dot{q}), (\frac{\partial H_i}{\partial p}, \frac{\partial H_i}{\partial q}) \rangle$.

$\mathbb{C}_\ell$: Storage of elastic states (elongations) $\ell = (\ell_1, \ell_2)^T$ of the two nonlinear elastic elements in potential energy, given by some Hamiltonian function $H_\ell(\ell)$. The port is defined by the dual pair $\langle \dot{\ell}, \frac{\partial H_\ell}{\partial \ell} \rangle$.

$\mathbb{E}$: The environment port is defined by the dual pair $\langle W_e, T \rangle$. It exerts a wrench W_e on the finger-tip (3^{rd} phalanx) and observes the twist T of the finger-tip.

[1] i.e. a generalization of Tellegen's theorem for electrical networks, see also [64] for a formal definition.

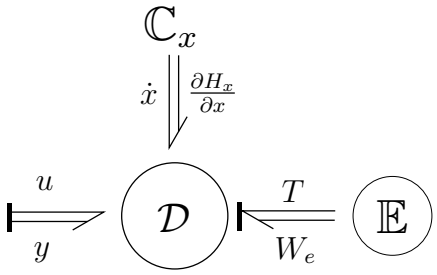

Figure 6.4: Reduced and combined total Dirac structure $\mathcal{D}$ with general storage element $\mathbb{C}_x$ and state vector $x = (p, q^T, \ell^T)^T$.

C : The control port is formed by the input-output dual pair $\langle u, y \rangle$, where the inputs $u = (u_1, u_2)^T$ represent the velocities of the tendon actuation positions z (i.e. $u = \dot{z}$) and their dual outputs $y = (y_1 \quad y_2)$ are the according actuation forces (equal to the tendon forces).

The $\mathbb{1}$-junction interconnects the two Dirac structures through their actuation transmission ports $\langle \dot{s}, f_s \rangle$, with $\dot{s}$ the time derivatives of the tendon positions s and f_s the forces in the tendons.

The Dirac structures $\mathcal{D}_1, \mathcal{D}_2$, in matrix form are given by:

$$\mathcal{D}_1 \quad : \quad \begin{pmatrix} \dot{\ell} \\ f_s^T \\ y^T \end{pmatrix} = \begin{pmatrix} 0 & -\mathbb{I}_2 & -\mathbb{I}_2 \\ \mathbb{I}_2 & 0 & 0 \\ \mathbb{I}_2 & 0 & 0 \end{pmatrix} \begin{pmatrix} \frac{\partial H_\ell}{\partial \ell} \\ \dot{s} \\ u \end{pmatrix} \tag{6.7}$$

$$\mathcal{D}_2 \quad : \quad \begin{pmatrix} \dot{p}^T \\ \dot{q} \\ \dot{s} \\ T \end{pmatrix} = \begin{pmatrix} 0 & -\mathbb{I}_3 & -J_a^T & -J_q^T \\ \mathbb{I}_3 & 0 & 0 & 0 \\ J_a & 0 & 0 & 0 \\ J_q & 0 & 0 & 0 \end{pmatrix} \begin{pmatrix} \frac{\partial H_i}{\partial p} \\ \frac{\partial H_i}{\partial q} \\ -f_s^T \\ W_e^T \end{pmatrix} \tag{6.8}$$

where, due to the $\mathbb{1}$-junction, the sign of f_s^T is opposite and $\mathbb{I}_n$ represents an $n \times n$ identity matrix.

Remark 6.2. *As a result of modeling positive power-flows going into the Dirac structure (standard modeling convention to preserve skew-symmetry of the Dirac structure), the tendon velocities $\dot{s}$ and input velocities $u = \dot{z}$ have opposite positive directions. This has no implications whatsoever, it is just a modeling choice.*

Notice that $\dot{p}$ represents the net torques on the joints: $\dot{p} = -\left(\frac{\partial H_i}{\partial q}\right)^T + \tau_s - \tau_e$, with $\tau_s^T = J_a^T \cdot f_s^T$ and $\tau_e = J_q^T \cdot W_e^T$.

The interconnection of Dirac structures is again a Dirac structure. Therefore, the network representation can be further reduced to one Dirac structure $\mathcal{D}$ (see Figure 6.4):

$$\mathcal{D} : \quad \begin{pmatrix} \dot{x} \\ \bar{y} \end{pmatrix} = \begin{pmatrix} J & g(x) \\ -g^T(x) & 0 \end{pmatrix} \cdot \begin{pmatrix} \frac{\partial H_x}{\partial x} \\ \bar{u} \end{pmatrix} \tag{6.9}$$

with 8×8 skew-symmetric matrix J, and 8×8 input-output matrix $g(x)$:

$$J = \begin{pmatrix} 0 & -\mathbb{I}_3 & J_a^T \\ \mathbb{I}_3 & 0 & 0 \\ -J_a & 0 & 0 \end{pmatrix}, \qquad g(x) = \begin{pmatrix} 0 & -J_q^T \\ 0 & 0 \\ -\mathbb{I}_2 & 0 \end{pmatrix},$$

where the consolidated state vector $x = (p, q^T, \ell^T)^T$, the total consolidated input vector $\bar{u} = (u^T, W_e)^T$ and the total consolidated output vector $\bar{y} = (y, T^T)^T$. Furthermore, the full system Hamiltonian is given by: $H_x(x) = H_i(p, q) + H_\ell(\ell)$. Hence, the port-Hamiltonian system is represented by the following dynamic (Hamiltonian) equations:

$$\begin{cases} \dot{x} & = J\frac{\partial H_x}{\partial x}(x) + g(x)\bar{u} \\ -\bar{y} & = g(x)^T\frac{\partial H_x}{\partial x}(x) \end{cases} \tag{6.10}$$

Each bond represents power flow between the ports to which it is connected. Power is defined by the dual product of the power conjugate port variables. Conservation of energy through the external ports $(\bar{u}, \bar{y})$ and the storage port $(\dot{x}, \frac{\partial H_x}{\partial x})$ is confirmed by recognizing the skew-symmetry of the Dirac structure:

$$\begin{pmatrix} \dot{x} \\ \bar{y} \end{pmatrix}^T \cdot \begin{pmatrix} \frac{\partial H_x}{\partial x} \\ \bar{u} \end{pmatrix} = 0 \tag{6.11}$$

Thus, the total rate of energy change in the system is solely determined by the power flows through the external ports.

6.4.2 Modeling locks

The influence of locks is modeled with constraint equations. The lock inputs are represented by $c = (c_1, c_2, c_3)^T$ with $c_i \in \{0, 1\}$ where 1 indicates an active lock and 0 an inactive lock. This results in the following port-Hamiltonian model of the finger concept:

$$\begin{cases} \dot{x} & = J\frac{\partial H_x}{\partial x}(x) + \begin{pmatrix} g(x) & A(c) \end{pmatrix}\begin{pmatrix} \bar{u} \\ \lambda \end{pmatrix} \\ \begin{pmatrix} -\bar{y} \\ 0 \end{pmatrix} & = \begin{pmatrix} g(x)^T \\ A^T(c) \end{pmatrix}\frac{\partial H_x}{\partial x}(x) \end{cases} \tag{6.12}$$

$$A^T(c) = \begin{pmatrix} c_1 & 0 & 0 & 0 & 0 & 0 & 0 & 0 \\ 0 & c_2 & 0 & 0 & 0 & 0 & 0 & 0 \\ 0 & 0 & c_3 & 0 & 0 & 0 & 0 & 0 \end{pmatrix} \tag{6.13}$$

The Lagrangian multipliers λ generate the constraint forces $A(c)\lambda$ for the constraints.

Notice that this is merely a behavioral model of the functionality of conceptual locks. In practice, locks will not generate the required constrained force instantaneously when needed. For the conceptual functional analysis this may be ignored.

6.5 Port-Hamiltonian Analysis

This section uses the port-Hamiltonian model and the mapping properties as discussed in Chapter 5 to analyze and verify existence of the key-features (see Section 6.2) of the finger concept: *controllable (variable) mechanical compliance* (Section 6.5.1) and *configuration reachability* (Section 6.5.2).

6.5.1 Conceptual analysis on finger-tip compliance

The finger compliance (C_f) *without* actuated locks defines the infinitesimal finger-tip displacement δT (i.e. infinitesimal deformation twist) of the finger in response to an externally applied infinitesimal wrench δW_e around an equilibrium configuration:

$$\delta T = C_f \cdot \delta W_e^T \tag{6.14}$$

where $\delta T = T \cdot dt = J_q \cdot \delta q$ and δq is an infinitesimal joint displacement around an equilibrium configuration.

External finger-tip compliance condition Having a finite external finger compliance implies that power can flow from the environment port to the elastic storage $\mathbb{C}_\ell$.

Remark 6.3 (External finger-tip compliance condition)**.** *A necessary condition for the finger compliance to be finite is the ability to let power flow from the environment to* $\mathbb{C}_\ell$*.*

This necessary condition is tested by supplying power $W_e T \neq 0$ from the environment with external wrench $W_e \neq 0$, while no work is done on the controller input ($u = 0$). In this case, equality must hold for:

$$\frac{dH_\ell}{dt} = \left(\frac{\partial H_\ell}{\partial \ell}\right)^T \dot{\ell} = \alpha \cdot W_e T \quad \alpha \in (0, 1]$$

where α indicates that at least a fraction of the total supplied power must flow to the elastic storage element. Naturally, the remaining fraction $(1-\alpha)$ will then flow to H_i (or is dissipated[2]). Applying $u = 0$ and substitutions from Equation 6.9 give:

$$-\dot{q}^T J_a^T \frac{\partial H_\ell}{\partial \ell} \;=\; \alpha \cdot \dot{q}^T J_q^T W_e^T \tag{6.15}$$

Since $\operatorname{im} J_a^T \subset \operatorname{im} J_q^T$, because of underactuation, it can be seen that the condition can be satisfied for at least a limited set $\mathcal{W}_s$, namely:

$$\mathcal{W}_s = \{W \in se^*(3) | J_q^T W^T \in \operatorname{im} J_a^T\} \tag{6.16}$$

In general, because of the pre-multiplication of the row vector $\dot{q}^T$, other solutions that render equality for Equation 6.15 may exist as well. Notice that $\operatorname{im} J_a^T$ represent the torques that are producible through the actuation tendons (and hence can be resisted, as opposed to non-producible torques, see Definition 5.8).

In this case, it is shown that it is possible to fulfill the necessary condition and hence finite external finger compliance *may* exist. This conclusion gives enough ground to continue the compliance analysis.

Variable finger-tip compliance To verify whether the finger compliance can be varied trough the controller port, it is analyzed whether C_f can be a function of u.

To start the analysis, a joint compliance matrix C_q is defined by $\frac{\delta q}{\delta \tau} = -C_q$, such that $\delta q = -C_q \cdot \delta \tau$, with $\delta \tau$ the infinitesimal joint torques around some equilibrium. Pre-multiplying with J_q and substituting $\delta \tau^T = -\delta \tau_e^T = -J_q^T \cdot \delta W_e^T \quad \forall \delta W_e^T \in \mathcal{W}_s$ (Equation 6.7) gives $\delta T = J_q C_q J_q^T \cdot \delta W_e^T$, such that:

$$C_f = J_q C_q J_q^T, \tag{6.17}$$

which is the pull-back of the compliance in joint space to the workspace of the finger-tip ($se^*(3)$), see Definition 5.33. Note that $\delta W_e \in \ker J_q^T$ induces no finger motion, implying zero compliance (i.e. infinite stiffness).

[2]Note: as shown in Figure 6.3, the presented model is dissipation free. Later dissipation is added. Adding dissipation does not change the presented conditional results.

The compliance C_q is inversely related to the joint stiffness K_q, defined by $\frac{\delta \tau^T}{\delta q} = -K_q$. Starting from the linearized force relation of the elastic storage elements

$$\delta f_s^T = \frac{\partial^2 H_\ell}{\partial \ell^2}(\ell) \cdot \delta \ell$$

it follows that (using Equation 6.9):

$$\delta \tau^T = \delta \tau_s^T = J_a^T \cdot \delta f_s^T = J_a^T \cdot \frac{\partial^2 H_\ell}{\partial \ell^2}(\ell) \cdot (-\delta z - J_a \delta q)$$

Hence, using $\delta \tau^T = -K_q \cdot \delta q$, the joint stiffness K_q is found to be:

$$K_q = J_a^T \cdot \frac{\partial^2 H_\ell}{\partial \ell^2}(\ell) \cdot J_a \tag{6.18}$$

which is the pullback of $\frac{\partial^2 H_\ell}{\partial \ell^2}(\ell)$ for the map J_a from q to s.

Thus, to be able to vary joint stiffness K_q through the controller port, the non-linear elastic elements must be designed such that $\frac{\partial^2 H_\ell}{\partial \ell^2}$ is a function of ℓ, where ℓ is known to be a function of the input u (Equation 6.9). In that case, naturally, also the joint compliance C_q depends on u. Therefore it is concluded that the finger-tip compliance C_f (Equation 6.17) is variable through the controller port if $\frac{\partial^2 H_\ell}{\partial \ell^2}$ is a function of ℓ.

Infinite compliance Note that due to the structure of J_a as a result of underactuation, the matrix K_q is not positive definite and has some zero singular values corresponding to some directions, $\dot{q} \in \ker J_a$, of zero stiffness and therefore infinite compliance. In the next section, Section 6.5.2, it is shown that these directions correspond to those directions of equal potential of the elastic energy of the system.

Assume having a metric on $T_q\mathcal{Q}$ and its associated induced inverse metric (see Definition 5.27) on $T_q^*\mathcal{Q}$, which represents a physically sensible norm (Definition 5.22). Then note that the physical dual elements (Definition 5.32) of the motions $\dot{q} \in \ker J_a$ are the torques $\tau \in (\operatorname{im} J_a)^\perp$ (see Remark 5.20). These are indeed the non-producible and hence irresistible torques, which explains infinite compliance in those directions. These torques can be induced by interaction wrenches $W_e \notin \mathcal{W}_s$.

6.5.2 Conceptual analysis on unconstrained finger configuration

This section discusses configuration reachability properties of the finger concept *without* actuated locks for unconstrained (no environment interaction) finger motions.

Configuration reachability Here, reachability refers to what extend the controller port can steer the unconstrained finger configuration q to any $q \in \mathcal{Q}$.

Remark 6.4. *A necessary condition for the configuration of the finger to be altered by the controller, is the ability to transfer power from the controller port to the inertial storage element such that* $\dot{q} \neq 0$.

Requiring (partial) power transfer from the controller port to the inertial storage element, with $y \cdot u \neq 0$, implies requiring:

$$\frac{\partial H_i}{\partial p}^T \cdot \dot{p}^T + \frac{\partial H_i}{\partial q}^T \cdot \dot{q} \;=\; \alpha \cdot y \cdot u \qquad \beta \in (0, 1] \tag{6.19}$$

where $\alpha \in (0, 1]$ indicates that it is required that at least for a fraction of the total supplied power it must be possible to flow to the inertial storage element in order to possibly alter the configuration of the finger. After substitution and rewriting, Equation 6.19 becomes:

$$\begin{aligned} \frac{\partial {H_i}^T}{\partial p} \cdot \left(-\frac{\partial H_i}{\partial q} + J_a^T \cdot y^T \right) + \frac{\partial {H_i}^T}{\partial q} \cdot \frac{\partial H_i}{\partial p} &= \alpha \cdot y \cdot u \\ y \cdot J_a \cdot \frac{\partial H_i}{\partial p} &= \alpha \cdot y \cdot u \end{aligned}$$

Thus, equality can hold for $u \in \operatorname{im} J_a$, such that the resulting force y generates equality. Although environment interactions may induce disturbances or dissipate energy, it shows that for $u \in \operatorname{im} J_a$ at least some portion of the supplied controller energy may be transfered to the inertial storage element in order to alter the finger configuration.

Equilibrium configuration space The unconstrained finger configuration[3] is said to be in static equilibrium if the system has minimal elastic energy with respect to the configuration variables $q \in \mathcal{Q}$, i.e. $\frac{\partial H_\ell}{\partial q}(\ell) = 0$. For some z and $u = 0$, such that $\delta\ell = -J_a \cdot \delta q - \delta z$ (see Equation 6.9 and notice that J_a is constant.), it is found that:

$$\frac{\partial H_\ell}{\partial q}(\ell) = 0 \quad \Rightarrow \quad \left(\frac{\partial H_\ell}{\partial \ell}(\ell) \right)^T \frac{\partial \ell}{\partial q} = 0 \quad \Leftrightarrow \quad -J_a^T \frac{\partial H_\ell}{\partial \ell}(\ell) = 0, \quad \ell \in \mathcal{L}$$

Hence, all states of the elastic elements $\ell \in \mathcal{L}$ that render $\frac{\partial H}{\partial \ell}(\ell) \in \ker J_a^T$ give equilibrium. These equilibrating elastic states define $\mathcal{L}_e \subset \mathcal{L}$:

$$\mathcal{L}_e := \{ \ell \in \mathcal{L} | \frac{\partial H}{\partial \ell}(\ell) \in \ker J_a^T, \ell \geq 0 \}, \tag{6.20}$$

where negative elongations are considered meaningless, due to the unilateral force (and displacement) transmission properties of the tendons. Notice that J_a must be non-surjective (i.e. J_a^T is non-injective: $\ker J_a^T \neq \emptyset$), in order to have an equilibrium other then the trivial $\frac{\partial H_\ell}{\partial \ell}(\ell) = 0$.

Since it holds that, because of linearity of the configuration spaces (see Equation 6.3 and Figure 6.1):

$$\ell = -H_a q - z, \tag{6.21}$$

it is found (see Chapter 5) that for any $\ell_e \in \mathcal{L}_e$ together with any $z \in \mathcal{Z}$, an unconstrained finger equilibrium configuration space $\mathcal{Q}_e$ exists:

$$\mathcal{Q}_e := H_a^{\#} \cdot (-\ell_e + z) + \ker H_a, \qquad \ell_e \in \mathcal{L}_e, z \in \mathcal{Z} \tag{6.22}$$

which implies that *if* the configuration map H_a is a non-injective map (i.e. $\ker H_a \neq \emptyset$) then multiple $q \in Q_e$ map to the same ℓ_e (for given input positions z) and hence produce the same $\frac{\partial H}{\partial \ell}(\ell) \in \ker J_a^T$, such that the equilibrium configuration q is not uniquely determined by the elastic states (ℓ).

Thus:

1. If J_a is non-surjective, then there exists an equilibrium, other than the trivial case $\frac{\partial H_\ell}{\partial \ell}(\ell) = 0$, for every $\ell \in \mathcal{L}_e$.
2. If H_a is non-injective and equilibrium exists, then the equilibrium configuration space Q_e is higher dimensional, $\dim \mathcal{Q}_e = \dim (\ker H_a) > 0$, implying that multiple equilibrating configurations $q \in \mathcal{Q}_e$ exist for one set $z \in \mathcal{Z}, \ell \in \mathcal{L}_e$.

[3] unconstrained finger configuration is the configuration of the finger without any external interactions.

6.5.3 Novel finger example

The presented analyses is applied to the proposed conceptual finger. Equation 6.6 presents J_a for the given coordinate bases of $\mathcal{S}$ and $\mathcal{Q}$. It follows that:

$$\ker J_a = \operatorname{span}\left\{ \begin{pmatrix} \frac{r_2}{r_1} \\ -1 \\ 0 \end{pmatrix}, \begin{pmatrix} \frac{r_2 r_4}{r_1 r_3} \\ 0 \\ -1 \end{pmatrix} \right\} \neq \emptyset, \qquad \operatorname{im} J_a = \operatorname{span}\left\{ \begin{pmatrix} 1 \\ -1 \end{pmatrix} \right\} \subset T_s\mathcal{S},$$

which shows that the map J_a is non-injective and non-surjective, i.e. non-bijective. Hence:

- the finger compliance is infinite (zero stiffness) for some interaction wrenches W_e (Section 6.5.1);
- equilibrium exists $\forall \ell \in \mathcal{L}_e$ (Section 6.5.2);
- the equilibrium configuration space $\mathcal{Q}_e$ is higher dimensional, i.e. $\dim \mathcal{Q}_e = 2$ (Section 6.5.2 and note that $\ker J_a = \ker H_a$);
- inputs: $u \in \operatorname{im} J_a \quad \Rightarrow \quad u^T = \gamma \cdot (1 \quad -1), \quad \gamma \in \mathbb{R}$, i.e. moving the tendon actuation positions in differential mode (move equally in opposite direction), can change configuration (Section 6.5.2);

Furthermore,

$$\ker J_a^T = \operatorname{span}\left\{ \begin{pmatrix} 1 \\ 1 \end{pmatrix} \right\} \subset T_s^*\mathcal{S}$$

shows that:

- dual inputs: $y \in \ker J_a^T \quad \Rightarrow \quad y = \gamma \cdot (1 \quad 1), \quad \gamma \in \mathbb{R}$, i.e. common mode force actuation (pulling both tendons with equal force), induce $\frac{\partial H_\ell}{\partial \ell}(\ell) \in \ker J_a^T$ (recall $y = \frac{\partial H_\ell}{\partial \ell}(\ell) = f_s$), giving *no* configuration change, since it enforces equilibrium (Section 6.5.2).

  Therefore, this common mode actuation changes the state ℓ and hence the finger compliance *if* the elastic storage functions are designed such that $\frac{\partial^2 H_\ell}{\partial \ell^2}$ is a function of ℓ (Section 6.5.1).

  Choosing for example a storage function of the form:

$$H_\ell(\ell) = \begin{cases} \frac{1}{6} k \ell^3 & \forall \ell \geq 0 \\ 0 & \forall \ell < 0 \end{cases},$$

  gives $\frac{\partial^2 H_\ell}{\partial \ell^2}(\ell) = k\ell$, which is clearly a function of ℓ. Note that no energy can be stored in the elastic element for negative elastic states, since the tendons can not push.

- Notice (see Remark 5.20): $y \in \ker J_a^T$ are the M_s-associated dual forces (see Definition 5.26) of the input velocities $u \in (\operatorname{im} J_a)^\perp$, for a metric M_s on $T_z\mathcal{Z}$. Indeed, dual inputs $u \in (\operatorname{im} J_a)^\perp$ do *not* change the finger configuration, since $u \in \operatorname{im} J_a \subset T_z\mathcal{Z}$ *do* change the configuration, see above.

Consider physical dual spaces (see Definition 5.30) for $T_z\mathcal{Z}$ and $T_z^*\mathcal{Z}$, with metric M_s and M_s^{-1} respectively, around some z for some ℓ, s in **equilibrium** with physical dual elements $\delta z \in T_z\mathcal{Z}$ and $\delta y \in T_z^*\mathcal{Z}$, associated by stiffness metric $M_s = \frac{\partial^2 H_\ell}{\partial \ell^2}(\ell)$. Hence, $\delta y = M_s \cdot \delta z$ and $\delta z = M_s^{-1} \cdot \delta y$. Elements $(\operatorname{im} J_a)^\perp \ni \delta z = M_s^{-1} \cdot \delta \tilde{y}$ with $\delta \tilde{y} \in \ker J_a^T$ are dual elements to these $\delta \tilde{y} \in \ker J_a^T$. An applied infinitesimal force $\delta \tilde{y} \in \ker J_a^T$ is in common mode. Hence, for dual common mode displacements $\delta z \in (\operatorname{im} J_a)^\perp$ defined through the given stiffness metric M_s, it holds that $\delta z = \delta \ell \in \mathcal{L}_e$.

The above given explanation clearly shows that it is important to realize that e.g. applying input *motion* $\delta z = (1 \quad 1)^T$ does **not** necessarily induce common mode actuation force $\delta y = (1 \quad 1) \in \ker J_a^T$. This is only true for $M_s = \mathbb{I} \cdot \gamma \quad \forall \gamma \in \mathbb{R}$, which corresponds to usage of equal elastic elements, having equal state ℓ. One must use the exact dual motions $\delta z = M_s^{-1} \cdot \delta \tilde{y}$ with $\delta \tilde{y} = (1 \quad 1) \in \ker J_a^T$. Hence duality shows possible asymmetries in the elastic elements and clearly orthogonality for the not-configuration changing inputs, i.e. $\delta z, u \in (\operatorname{im} J_a)^\perp$, is defined by the metric M_s.

6.5.4 Influence of locks

Without joint locks, the analysis revealed complications of the finger behavior for $\ker J_a \neq \emptyset$. For the proposed underactuated finger, this is the case, which resulted in a higher dimensional equilibrium configuration space $\dim \mathcal{Q}_e = 2$ and infinite compliance for some interaction wrenches W_e. Both symptoms reveal that the finger configuration can not be uniquely determined through the controller port.

Equation 6.13, $A^T(c)$, shows that the dynamics of the locked joints are canceled. Hence, effectively, the dimension of $\ker J_a$ is altered, such that by switching c_i properly, the whole configuration space of the finger can be reached through the controller port, as desired. Chapter 7 presents a controller to utilize the locks for dexterous manipulation of the finger.

6.6 Basic Underactuated Finger Design Parameters

The analysis in Section 6.5.1 indicated that finite compliance is only reflected against a limited set of finger-tip wrenches, i.e. $\delta W_e \in \mathcal{W}_s$ (Equation. 6.16). This section investigates which wrenches actually admit $\delta W_e \in \mathcal{W}_s$ and presents derived design considerations for the basic design parameters.

6.6.1 Finite compliance wrenches

Figure 6.5 shows the kinematics of the situation under investigation. An external wrench δW_e is applied at some contact point on the finger-tip, parameterized by distances x_c and y_c. Expressing δW_e in local coordinates Ψ_c, gives: $\delta W_e^c = (\tau_x \quad \tau_y \quad \tau_z \quad f_x \quad f_y \quad f_z)$, where the first three elements are moments about the coordinate axis of Ψ_c and the remaining three elements represent a force, expressed as vector in Ψ_c. All non-zero moments and forces in δW_e are the moments and forces that are transmitted through the contact and will impose torques on the joints.

To find an expression for the joint torques as a result of W_e, i.e. τ_e, the coordinates of δW_e are changed to those in which the Jacobian mapping (J_q^T) is expressed, e.g. the fixed world

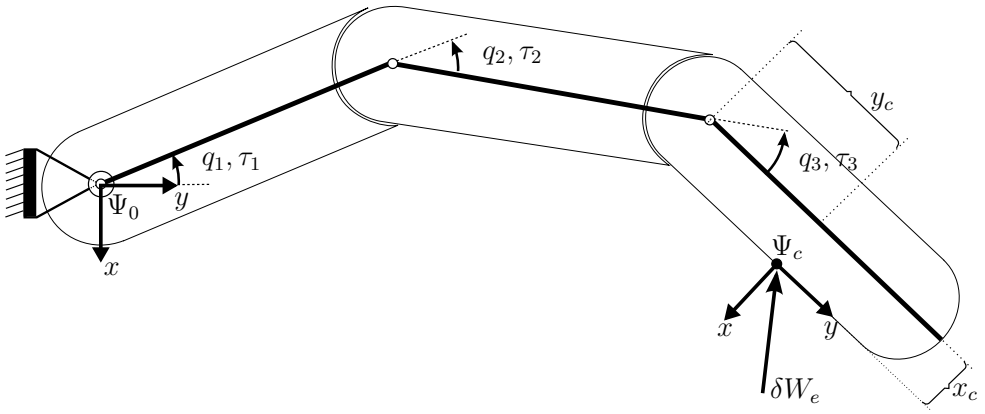

Figure 6.5: External wrench δW_e applied at some contact point on finger-tip. Local coordinates Ψ_c are placed at the contact point. δW_e maps to torques on the joints. This mapping depends on geometric parameters: location of contact point (x_c and y_c) and lengths of the first two phalanges, λ_1 and λ_2.

coordinate frame Ψ_0, by applying the adjoint mapping [88]:

$$\left(\delta W_e^0\right)^T = \left(Ad_{H_0^c}\right)^T \left(\delta W_e^c\right)^T .$$

With Equation 6.4, the torques on the joints as a result of δW_e at a contact point (x_c, y_c) on the finger-tip for a certain configuration q are found to be:

$$\begin{aligned} \tau_e &= J_q^T \delta W_e \\ &= \begin{pmatrix} f_y sq_3\lambda_2 - f_x cq_3\lambda_2 + f_y cq_3 sq_2\lambda_1 - f_x y_c - f_x cq_3 cq_2\lambda_1 + f_x sq_3 sq_2\lambda_1 \\ +f_y sq_3 cq_2\lambda_1 + f_y x_c + \tau_z \\ f_y sq_3\lambda_2 - f_x cq_3\lambda_2 + \tau_z - f_x y_c + f_y x_c \\ \tau_z - f_x y_c + f_y x_c \end{pmatrix} . \end{aligned} \tag{6.23}$$

6.6.2 Finger design trade-off

To have $\delta W_e \in \mathcal{W}_s$ for a certain configuration q, it must hold that $\tau_e \in \operatorname{im} J_a^T$. For the underactuated finger under consideration, shown in Figure 6.1, this implies that the following design trade-off equality must hold:

$$\alpha \cdot \begin{pmatrix} r_1 \\ r_2 \\ \frac{r_2 r_4}{r_3} \end{pmatrix} = \begin{pmatrix} f_y sq_3\lambda_2 - f_x cq_3\lambda_2 + f_y cq_3 sq_2\lambda_1 - f_x y_c \\ -f_x cq_3 cq_2\lambda_1 + f_x sq_3 sq_2\lambda_1 \\ +f_y sq_3 cq_2\lambda_1 + f_y x_c + \tau_z \\ f_y sq_3\lambda_2 - f_x cq_3\lambda_2 + \tau_z - f_x y_c + f_y x_c \\ \tau_z - f_x y_c + f_y x_c \end{pmatrix}, \tag{6.24}$$

with $\alpha \in \mathbb{R}$ some scalar multiplier.

Hence, the design parameters λ_i (phalanx lengths) and r_i (pulley radii) together with the contact point (x_c, y_c) and the applied contact forces (f_x, f_y, τ_z) all together determine whether the applied force meets finite compliance. Note that these forces are also forces that can be transmitted from the actuators to the contact point. Clearly, designing the robotic finger for a specific robotic hand involves considering which forces (in which configurations) have to be generated and need to be resisted with finite compliance.

Example: suppose that for the targeted robotic grasping task it is required to compliantly resist an external force along the x axis of Ψ_0 (i.e. $\delta W_e{}^c = (0,0,0,f_x,0,0)$ at the finger tip ($y_c = \lambda_3$, $x_c = 0$) in a straight finger configuration ($q = 0$). Then the design trade-off equality, Equation 6.24, becomes:

$$\alpha \cdot \begin{pmatrix} r_1 \\ r_2 \\ \frac{r_2 r_4}{r_3} \end{pmatrix} = \begin{pmatrix} -(\lambda_2 + \lambda_3 + \lambda_1) \\ -(\lambda_2 + \lambda_3) \\ -\lambda_3 \end{pmatrix} \cdot f_x, \tag{6.25}$$

which shows that the design must hold:

$$\frac{r_1 r_3}{\lambda_2 + \lambda_3 + \lambda_1} = \frac{r_2 r_3}{\lambda_2 + \lambda_3} = \frac{r_2 r_4}{\lambda_3}.$$

This general design analysis coincides with the equilibrium point observations in [62]. After the design (And hence the design parameters) is fixed, in other configurations, other contact points on the finger-tip and other external wrenches are necessary to admit $\delta W_e \in \mathcal{W}_s$.

6.7 Compliance Analysis of the Underactuated Robotic Finger

The underactuated driving mechanism of the transmission between the series elastic nonlinear elastic elements in the tendons and the joints to be actuated, is modeled by the non-bijective kinematic map J_a. Joint stiffness adjustability was studied for tendon controllable mechanisms in [89]. However, J_a is not full-rank and hence **not** tendon controllable [89] (as expected from underactuation). J_a holds singularities which complicate the compliance analysis of underactuated fingers. Nevertheless, thorough understanding of these properties is crucial to utilize compliance in enhancing grasp robustness. This section contributes by presenting compliance properties of underactuated robotic fingers and in particular the variable compliance properties of the novel underactuated robotic finger.

First, for completeness, the finger-tip compliance under investigation is repeated. Then a geometric space decomposition, as discussed throughout Chapter 5, is used to define the finger-tip compliance. Finally, a physically equivalent metric is proposed to complete the the analysis. In the next section, Section 6.8, the results are validated by simulation experiments.

6.7.1 Finger-tip compliance

The finger-tip compliance matrix (C_f) under investigation is given in Equation 6.14 and repeated here for convenience:

$$\delta T = C_f \cdot \delta W_e^T. \tag{6.26}$$

It defines the infinitesimal finger-tip displacement $\delta T \in se(3)$ of the finger in response to an externally applied infinitesimal wrench $\delta W_e \in se^*(3)$ around an equilibrium. It is noticed that: $\delta T = T \cdot dt = J_q \cdot \delta q$ and $\delta q \in T_q\mathcal{Q}$ is an infinitesimal joint displacement around an equilibrium configuration [90].

For the compliance analysis, the controller inputs remain constant, i.e. $u = 0$, such that, such that $\dot{\ell} = -J_a \cdot \dot{q} = -\dot{s}$ (Equation 6.5 and Equation 6.9).

Variable finger-tip compliance Section 6.5.1 gave an expression for the finger-tip compliance C_f based upon assumed existence of joint compliance C_q, such that (Equation 6.17):

$$C_f = J_q C_q J_q^T. \tag{6.27}$$

The tangent mapping J_a is non-invertible due to underactuation. Hence, as noticed in Section 6.5.1, there is no trivial expression for the joint-compliance C_q.

Alternatively, the inverse relation, the joint stiffness K_q, defined through $\delta\tau^T = -K_q \cdot \delta q$, was found to be the pullback of $\frac{\partial^2 H_\ell}{\partial \ell^2}(\ell)$ for the map $h_s(q)$ (Equation 6.18):

$$K_q = J_a^T \cdot \frac{\partial^2 H_\ell}{\partial \ell^2}(\ell) \cdot J_a, \tag{6.28}$$

where

$$\frac{\partial^2 H_\ell}{\partial \ell^2}(\ell) = \begin{pmatrix} \frac{\partial^2 H_\ell}{\partial \ell_1^2}(\ell_1) & 0 \\ 0 & \frac{\partial^2 H_\ell}{\partial \ell_2^2}(\ell_2) \end{pmatrix}. \tag{6.29}$$

6.7.2 Coordinate transformation

Figure 6.2 clearly shows that both tangent Jacobian mappings (J_q and J_a) have opposite natural preferences for their mapping directions. Clearly, the inverse relation for one of them is needed to resolve the finger-tip compliance. The attached space decomposition (see Chapter 5) of the inverse relation for J_a is used to resolve the finger-tip compliance C_f.

The joint velocities space, $T_q\mathcal{Q}$, is decomposed into two subspaces by introducing new coordinates $\tilde{q}$. These coordinates are defined through coordinate transformation S on $T_q\mathcal{Q}$:

$$\delta q = S \cdot \delta\tilde{q}, \tag{6.30}$$

where $\delta q, \delta\tilde{q} \in T_q\mathcal{Q}$ are expressed in different coordinates; i.e. the original physical joint angle coordinates $q = (q_1, q_2, q_3)$ and new coordinates $\tilde{q} = (\tilde{q}_1, \tilde{q}_2, \tilde{q}_3)$. The columns in S form the new set of base vectors that span $\mathcal{Q}$ expressed as vectors in the joint angle coordinates q. Dually, S^{-T} on $T_q^*\mathcal{Q}$ gives $\delta\tau = S^{-T} \cdot \delta\tilde{\tau}$.

This coordinate transformation results in a joint stiffness $\tilde{K}_q$ in the new coordinates $\tilde{q}$:

$$\tilde{K}_q = S^T \cdot K_q \cdot S, \tag{6.31}$$

such that $\delta\tilde{\tau}^T = \tilde{K}_q \cdot \delta\tilde{q}$. Hence,

$$\delta\tau^T = S^{-T} \cdot \tilde{K}_q \cdot S^{-1} \cdot \delta q. \tag{6.32}$$

6.7.3 Joint space decomposition

In order to choose a useful coordinate transformation, the following understanding is important. Some directions, $\delta q \in \ker J_a$, project through J_a to zero displacement in $\dot{\ell}$, which corresponds to zero stiffness. Other directions ($\delta q \notin \ker J_a$) do impose a change in elongation in the elastic elements, which reflects finite stiffness.

Hence, the mapping J_a is used to decompose $T_q\mathcal{Q}$ into subspace $\mathcal{N}$ and $\mathcal{N}^\perp$, such that $T_q\mathcal{Q} = \mathcal{N} \oplus \mathcal{N}^\perp$. This is visualized in Figure 6.6. Subspace $\mathcal{N}$ is the null-space of J_a:

$$\mathcal{N} = \ker J_a =: \operatorname{span}(n_1, n_2),$$

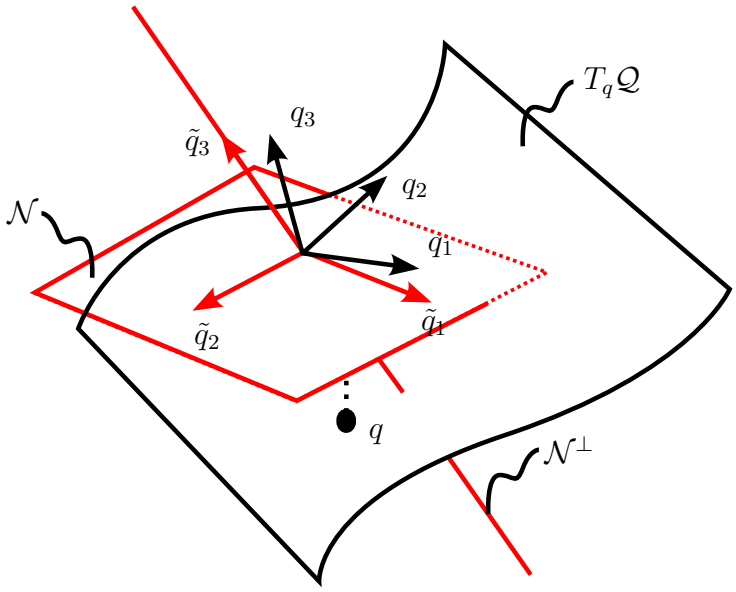

Figure 6.6: Visualization of coordinate change by $\ker J_a$. $T_q\mathcal{Q}$ is decomposed into $\mathcal{N}$ and $\mathcal{N}^\perp$, s.t. $T_q\mathcal{Q} = \mathcal{N} \oplus \mathcal{N}^\perp$. Subspace $\mathcal{N}$ is the null-space of J_a: $\mathcal{N} = \ker J_a$, while $\mathcal{N}^\perp$ is its orthogonal space.

while $\mathcal{N}^\perp = \text{span}(n^\perp)$ is its orthogonal space. The vectors $n_1, n_2, n^\perp \in T_q\mathcal{Q}$ are expressed in the original joint coordinates q. Orthogonality in $T_q\mathcal{Q}$ is defined by the M_q-weighted inner-product on $T_q\mathcal{Q}$ being equal to zero. The M_q-weighted inner-product on $T_q\mathcal{Q}$ is given by (see Definition 5.12):

$$\langle u, w \rangle = u^T M_q w \qquad u, w \in T_q\mathcal{Q},$$

where M_q is a metric to be defined on $T_q\mathcal{Q}$. Using this inner-product definition, $n^\perp$ is found to be (see Theorem 5.2):

$$n^\perp = M_q^{-1} \cdot X_f, \tag{6.33}$$

where X_f is the 3×1 basis matrix of $\text{im}\, J_a^T$ expressed in the original coordinates of $T_q^*\mathcal{Q}$ (the joint torques τ co-aligned with the joint angles q). Thus, S becomes:

$$S = \begin{pmatrix} n_1 & n_2 & n^\perp \end{pmatrix} = \begin{pmatrix} n_1 & n_2 & M_q^{-1} X_f \end{pmatrix}. \tag{6.34}$$

Expressing the infinitesimal finger displacement in the new coordinates ($\delta\tilde{q}$) immediately shows whether there are null-space motions or orthogonal motions:

$$\delta\tilde{q}_{null-space} = \begin{pmatrix} \bullet \\ \bullet \\ 0 \end{pmatrix} \in \mathcal{N}, \quad \delta\tilde{q}_{orthogonal} = \begin{pmatrix} 0 \\ 0 \\ \bullet \end{pmatrix} \in \mathcal{N}^\perp,$$

where $\bullet$ represents some non-zero number.

6.7.4 Finger-tip compliance description

Using the presented coordinate transformation S, $\tilde{K}_q$ is found to be:

$$\begin{aligned} \tilde{K}_q &= S^T \cdot K_q \cdot S \\ &= S^T \cdot J_a^T \cdot \frac{\partial^2 H_\ell}{\partial \ell^2}(\ell) \cdot J_a \cdot S \\ &= \begin{pmatrix} 0 & 0 & 0 \\ 0 & 0 & 0 \\ 0 & 0 & \beta \end{pmatrix}, \end{aligned} \tag{6.35}$$

with

$$\beta = \left(\frac{\partial^2 H_\ell}{\partial \ell_1^2}(\ell_1) + \frac{\partial^2 H_\ell}{\partial \ell_2^2}(\ell_2) \right) \cdot \left(X_f^T M_q^{-1} X_f \right)^2 , \tag{6.36}$$

which clearly shows that stiffness is only reflected in the orthogonal directions, which turns out to be β (Equation 6.35). Whereas, null-space motions experience zero stiffness (Equation 6.35), i.e. infinite compliance.

Calculations for β, Equation 6.36: Equation 6.35 is worked out to verify the given expression for β. Recall S (Equation 6.30) and J_a (Equation 6.6) and consider the following notations:

$$J_{a1}^T := J_a^T \cdot \begin{pmatrix} 1 \\ 0 \end{pmatrix}, \qquad J_{a2}^T := J_a^T \cdot \begin{pmatrix} 0 \\ 1 \end{pmatrix}$$

i.e. J_{ai} is the i^{th} row of J_a. Notice that: $J_{a1} = -J_{a2}$.

By definition $J_a \cdot n_i = 0$, hence:

$$\begin{aligned} J_a \cdot S &= J_a \cdot \begin{pmatrix} n_1 & n_2 & M_q^{-1} X_f \end{pmatrix} \\ &= \begin{pmatrix} 0_{2\times 1} & 0_{2\times 1} & J_a M_q^{-1} X_f, \end{pmatrix} \end{aligned} \tag{6.37}$$

Furthermore, recall $\frac{\partial^2 H_\ell}{\partial \ell^2}(\ell)$ (Equation 6.29) and substitute Equation 6.37 into Equation 6.35:

$$\begin{aligned} \tilde{K}_q &= \begin{pmatrix} 0_{1\times 2} \\ 0_{1\times 2} \\ X_f^T M_q^{-1} J_a^T \end{pmatrix} \cdot \frac{\partial^2 H_\ell}{\partial \ell^2}(\ell) \cdot \begin{pmatrix} 0_{2\times 1} & 0_{2\times 1} & J_a M_q^{-1} X_f \end{pmatrix} \\ &= \begin{pmatrix} 0 & 0 & 0 \\ 0 & 0 & 0 \\ 0 & 0 & \beta \end{pmatrix}, \end{aligned} \tag{6.38}$$

where

$$\begin{aligned} \beta &= X_f^T M_q^{-1} J_a^T \cdot \frac{\partial^2 H_\ell}{\partial \ell^2}(\ell) \cdot J_a M_q^{-1} X_f \\ &= \begin{pmatrix} X_f^T M_q^{-1} J_{a1}^T & X_f^T M_q^{-1} J_{a2}^T \end{pmatrix} \cdot \frac{\partial^2 H_\ell}{\partial \ell^2}(\ell) \cdot \begin{pmatrix} J_{a1} M_q^{-1} X_f \\ J_{a2} M_q^{-1} X_f \end{pmatrix} \end{aligned} \tag{6.39}$$

Recall $\operatorname{span} X_f = \operatorname{im} J_a^T \in T_q^* \mathcal{Q}$, such that X_f can be:

$$X_f := J_{a1}^T = -J_{a2}^T,$$

such that Equation 6.39 becomes:

$$\begin{aligned} \beta &= X_f^T M_q^{-1} X_f \cdot \frac{\partial^2 H_\ell}{\partial \ell_1^2}(\ell_1) \cdot X_f^T M_q^{-1} X_f \\ &\qquad + X_f^T M_q^{-1} X_f \cdot \frac{\partial^2 H_\ell}{\partial \ell_2^2}(\ell_2) \cdot X_f^T M_q^{-1} X_f \\ &= \left(\frac{\partial^2 H_\ell}{\partial \ell_1^2}(\ell_1) + \frac{\partial^2 H_\ell}{\partial \ell_2^2}(\ell_2) \right) \cdot \left(X_f^T M_q^{-1} X_f \right)^2 \qquad \square \end{aligned}$$

Interestingly, the stiffness β is the sum of the parallel linearized stiffnesses of the non-linear elastic elements in the driving tendons multiplied by the square of a weighted transmission.

This is recognized as how generally stiffness is reflected through transmissions. The weighting metric used here is the dual metric of the metric M_q on $T_q\mathcal{Q}$, i.e. M_q^{-1} on the space of torques $T_q^*\mathcal{Q}$.

As noted, torques dual to the null-space motions will excite infinite motions. Hence, infinite compliance is experienced. With Equation 6.35, the joint stiffness relation (Equation 6.32) becomes:

$$\delta\tau^T = S^{-T} \begin{pmatrix} 0 & 0 & 0 \\ 0 & 0 & 0 \\ 0 & 0 & \beta \end{pmatrix} S^{-1} \cdot \delta q.$$

Hence, for the joint compliance, which is inversely related to K_q, the following is concluded:

$$C_q = \begin{cases} S \cdot \frac{1}{\beta} \cdot S^T & \forall \delta\tau^T \in \operatorname{im} J_a^T \\ \infty & \forall \delta\tau^T \in \left(\operatorname{im} J_a^T\right)^\perp \end{cases}, \tag{6.40}$$

such that the finger-tip compliance (Equation 6.27) becomes

$$C_f = \begin{cases} J_q S \cdot \frac{1}{\beta} \cdot S^T J_q^T & \forall J_q^T \delta W_e^T \in \operatorname{im} J_a^T \\ \infty & \forall J_q^T \delta W_e^T \in \left(\operatorname{im} J_a^T\right)^\perp \end{cases}, \tag{6.41}$$

which shows that for $J_q^T \delta W_e$ that have elements in $\left(\operatorname{im} J_a^T\right)^\perp$, which is the M_q- associated dual subspace of $\ker J_a$ (null-space motions) (see Definition 5.29), infinite twists δT will be induced, implying infinite compliance. Hence only finite compliance exists for a limited set of wrenches $\mathcal{W}_s$, as concluded before in Equation 6.16:

$$\mathcal{W}_s = \{\delta W_e \in se^*(3) | J_q^T \delta W_e^T \in \operatorname{im} J_a^T\}. \tag{6.42}$$

Variable compliance Equation 6.36 and Equation 6.41 confirm that if the elastic elements are non-linear, then the finger-tip compliance can be altered by changing their states ℓ.

6.7.5 Physically equivalent metric

The previous section presented the finger-tip compliance analysis. The specific choice of coordinate transformation S on $T_q\mathcal{Q}$ allows to decompose the joint space $\mathcal{Q}$ to describe the finger-tip compliance C_f in Equation 6.41. The new coordinates $\tilde{q}$, span by base vectors n_1, n_2 and $n^\perp$, split the space $T_q\mathcal{Q}$ into two parts, based on the kernel of the tangent mapping J_a ($\mathcal{N}$) and its orthogonal space ($\mathcal{N}^\perp$), see Figure 6.6.

The expression for C_f is given in Equation 6.41, which depends on the choice of metric M_q. Hence, the calculated value of the compliance does change for different metrics. Of course, in reality, only one compliance value exists. In order to use the compliance values for grasping, it is of interest to find physically equivalent compliance values. Therefore, the physically equivalent metric must be used, which has been extensively discussed in Chapter 5.

Candidate metrics Several candidate metrics for different situations have been discussed in Section 5.8. The current situation is induced by an external disturbance δW_e, which causes an interesting combination:

- on configuration space $\mathcal{S}$ and its (co-)tangent mappings, a quasi-static situation appears, where, in the presented model, the elastic energy is the only energy function. Hence, the Hessian of the elastic energy, $\frac{\partial^2 H_\ell}{\partial \ell^2}(\ell)$, is used as metric on $T_s\mathcal{S}$. This is reflected in Equation 6.36, where this Hessian appears in β.

- on configuration space $\mathcal{Q}$ and its tangent mappings, although a quasi static situation (i.e. the compliance analysis) is investigated, there is room for motions independent of the potential energy function in the system. This is reflected in the existence of a higher dimensional equilibrium space $\mathcal{Q}_e$ with $\dim \mathcal{Q}_e = 2$ (see Section 6.5.2). Hence, there exists a situation of free motions for which M_q is to be determined.

Thus, as described in Section 5.8, for the motions on $T_q\mathcal{Q}$ two cases can exist:

1. *undamped* free motions;
2. *damped* free motions;

For both cases, the physically equivalent metric is found and presented. Naturally, in practice, dissipation always exists, which makes the second case more interesting. Nevertheless, it is interesting to present both cases, since it gives illustrative examples of the general presentation in Section 5.8.

Modeling linear damping For the discussion up to here, dissipation was irrelevant and not included in the presented port-Hamiltonian model, Equation 6.10. To include dissipation, linear damping will be considered. Therefore the port-Hamiltonian model is extended with a static resistive structure $R_r^T = R_r \geq 0$ [64], i.e. a 8×8 matrix of the following form:

$$R_r = \begin{pmatrix} B & 0 \\ 0 & 0 \end{pmatrix}, \tag{6.43}$$

where damping matrix B represents linear damping on the joints, giving resistive joint torques $\tau_b = B \cdot \dot{q}$, with:

$$B = \begin{pmatrix} b_1 & 0 & 0 \\ 0 & b_2 & 0 \\ 0 & 0 & b_3 \end{pmatrix}. \tag{6.44}$$

Then, the port-Hamiltonian model is given by:

$$\begin{cases} \dot{x} & = (J - R_r)\frac{\partial H_x}{\partial x}(x) + g(x)\bar{u} \\ -\bar{y} & = g(x)^T \frac{\partial H_x}{\partial x}(x) \end{cases} \tag{6.45}$$

Physically equivalent metrics For both cases, the physically equivalent metric is found:

- *undamped motions*: in accordance with Section 5.8, it may be of no surprise that the mass matrix $M(q)$ is the physically equivalent metric.

  Notice that the according **physical** dual elements are the infinitesimal joint velocity changes $\delta\dot{q}$ and the infinitesimal changes in generalized joint momenta $\delta p(t)$, around a given $q, \dot{q}, p$. Moreover, for the situation under consideration (a disturbance around a static equilibrium, i.e. $\dot{q} = 0$ and $p = 0$, around which C_f is defined), the dual variables resemble the dual variables $\dot{q}, \tau$ as used throughout the chapter: $\delta\dot{q} \approx \dot{q} \in T_q\mathcal{Q}$ and $\delta p \approx \dot{p} = \tau \in T_q^*\mathcal{Q}$.

- *damped motions*: for infinitesimal disturbances $\delta W_e \in \mathcal{W}_s$, only infinitesimal motions are induced, δT. Hence, although the mass matrix $M(q)$ is configuration dependent, it can be considered constant for δq. Therefore, the results obtained for the linear case in Section 5.9 can be applied here. Hence, for damped motions, the physically equivalent metric is the damping matrix, B.

Hence, the following statements summarize the physically equivalent metric for both cases:

Remark 6.5 (C_f without damping)**.** *Any external wrench $\delta W_e \in \mathcal{W}_s$ induces oscillations in the joint motions $\dot{q}$ around an infinitesimal displacement of the equilibrium configuration δq_e. In this case, δq_e is analytically determined by $\delta q_e = C_q \cdot J_q^T \cdot \delta W_e^T$, with C_q described in Equation 6.40 and the metric $M_q = M(q)$, the mass matrix of the finger dynamics.*

Remark 6.6 (C_f with damping)**.** *Any external wrench $\delta W_s \in \mathcal{W}_c$ induces a steady state infinitesimal displacement of the equilibrium configuration δq_e. In this case, δq_e is analytically determined by $\delta q_e = C_q \cdot J_q^T \cdot \delta W_e^T$, with C_q described in Equation 6.40 and the metric $M_q = B$, the damping matrix of the finger dynamics (Equation 6.44).*

6.8 Compliance Validation by Simulation

In this section, the previously derived compliance properties are validated by simulation experiments for both cases. First the validation method is explained, then the results are discussed.

6.8.1 Method

The theoretical results of the previous section are validated by simulation experiments. The goal of the simulation experiments is formulated as follows:

- To investigate the infinitesimal equilibrium displacement δq_e after applying $\delta^c W_e \in \mathcal{W}_s$ for different values of damping (b_1, b_2, b_3), phalanx masses (m_1, m_2, m_3) and phalanx moments of inertia about the out-of-plane axis in the center of mass of each phalanx (I_{z1}, I_{z2}, I_{z3}).
- To verify for each set of parameters, whether the experimentally determined δq_e can be analytically explained by using the metric $M_q = M(q)$ or $M_q = B$, as summarized in Remark 6.5 and 6.6.

Simulation model A dynamic model of the underactuated finger, as sketched in Figure 6.1 and 6.5 and described in Equation 6.45, was simulated with the port-based simulation package 20-sim[4].

Experiment In the simulation experiments, an external 'infinitesimal' wrench is applied: $\delta^c W_e = (0, 0, 0, 0.01, 0, 0) \quad N$ at finger-tip position: $x_c = 0, y_c = \lambda_3 = 0.04 \ m$. The finger configuration is straight $q = 0$ rad., such that the design trade-off equality, as given in Equation 6.25, is satisfied. Hence, $\delta^c W_e \in \mathcal{W}_s$. The external force $\delta^c W_e$ is applied as step-function, induced at $t = 0.1 \ s$.

Two sets of experiments are executed:

Set-1: The first set of experiments use linear springs for the elastic elements with no change of inputs $u = 0$;

Set-2: Thereafter, non-linear elastic elements are used with $u \neq 0$ to vary and verify the variable compliance of the finger.

[4] see http://www.20sim.com

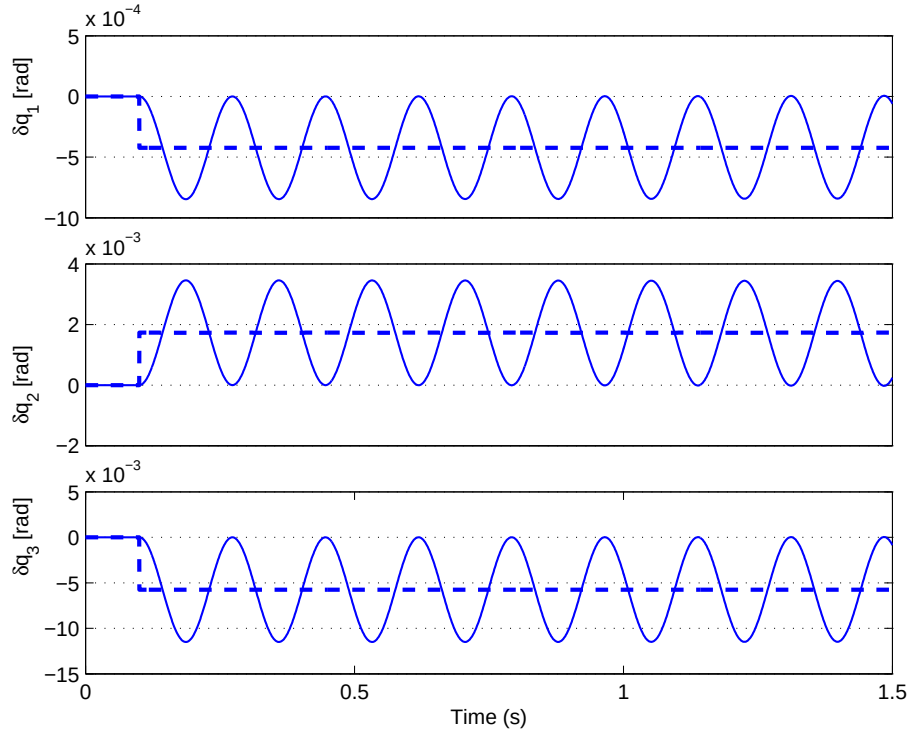

Figure 6.7: Set-1/Case-1: Without damping. Infinitesimal joint displacement δq due to external disturbance δW_e: simulated response [solid line] vs. analytically determined response [dashed line], using metric: $M_q = M(q)$.

Design parameters The following arbitrary human-size design parameters were chosen: $\lambda_1 = \lambda_2 = \lambda_3 = 0.04\ m$, $r_1 = 0.01, r_2 = r_3 = 0.00666, r_4 = 0.00333\ m$. For the first set of experiments, the non-linear elastic elements were simulated with two linear springs with stiffnesses $k_1 = 100\ N/m$, $k_2 = 10,000\ N/m$. The non-linear elastic element for the second set is presented later.

6.8.2 Results

Some representative simulation experiments are discussed.

> **Representative results** Representative means that equal results were obtained for other parameter values and different mass distributions and damping distributions.

For the presented results, the masses of the phalanges were chosen to be $m_1 = 0.1, m_2 = 0.4, m_3 = 0.2\ kg$ and the moments of inertia $I_{z1} = 1e^{-5}, I_{z2} = 4e^{-5}, I_{z3} = 2e^{-5}\ kgm^2$.

For the first set of experiments, the two distinct cases are investigated: without damping (case-1) and with damping (case-2). Also the second set of experiments, varying compliance with non-linear elastic elements, is investigated for both cases.

Experiment Set-1: Fixed linear springs

- **Without damping (case-1):** Figure 6.7 shows the response of the infinitesimal joint displacement for the case without damping in the joints. The plot shows that the oscillations are exactly symmetrically around the analytically determined δq_e, which confirms that the metric to be used should be the mass matrix of the finger dynamics $M(q)$.

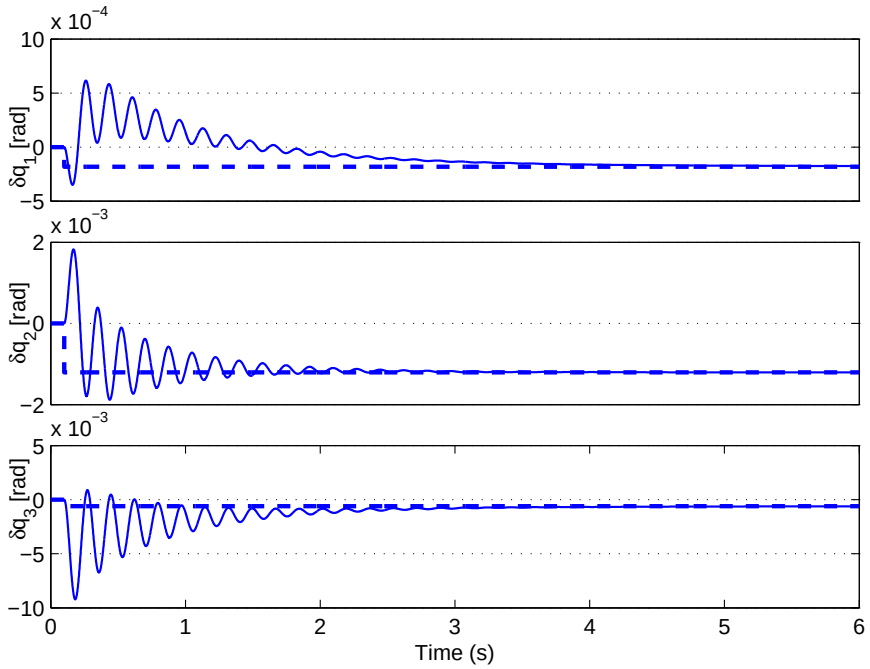

Figure 6.8: Set-1/Case-2: Damping ($b_1 = 0.001, b_2 = 0.0001, b_3 = 0.0001\ Ns/m$). Infinitesimal joint displacement δq: simulated response [solid line] vs. analytically determined response [dashed line], using metric: $M_q = B$.

- **Damping (case-2):** Figure 6.8 shows the response of the infinitesimal joint displacement for the case with damping in the joints. The plot shows that the simulated joint displacements exactly converge to the the analytically determined δq. This confirms that the metric to be used, for this case, should be the joint damping matrix of the finger B.

  Also Figure 6.9 confirms that even for small damping values the metric to be used must be B. The figure also shows that the mass matrix $M(q)$ as a metric gives incorrect results.

Both cases also confirm that the described design trade-off equality from Section 6.6, illustrated in Equation 6.25, is satisfied for the applied wrench, such that equilibrium is truly reached.

Experiment Set-2: Variable compliance (non-linear springs) The results so far have shown the existence of finite compliance and confirmed the analytically determined compliance. In experiment set-2, it was also verified in simulation that the compliance can be varied by changing the input position z if non-linear elastic elements are used, as shown in Figure 6.1.

The two identical non-linear elastic elements were modeled by $f_\ell = k \cdot \ell^2$, with $k = 100\ N/m$ and sufficient pre-tension ($z_1(0) = z_2(0) = 1\ m$) to prevent $\ell \leq 0\ m$ during input changes $u \neq 0$. The input positions z_1, z_2 are driven in common mode and changed in two smooth steps from 1 to 3 and from 3 to $5\ m$.

- **Without damping (case-1):** Figure 6.10 shows the simulation result for no damping on the joints. As expected, the simulated results are analytically described using the metric $M_q = M(q)$.

- **Damping (case-2):** Figure 6.11 shows the simulation result for damping on the joints. As expected, the simulated results are analytically described using the metric $M_q = B$.

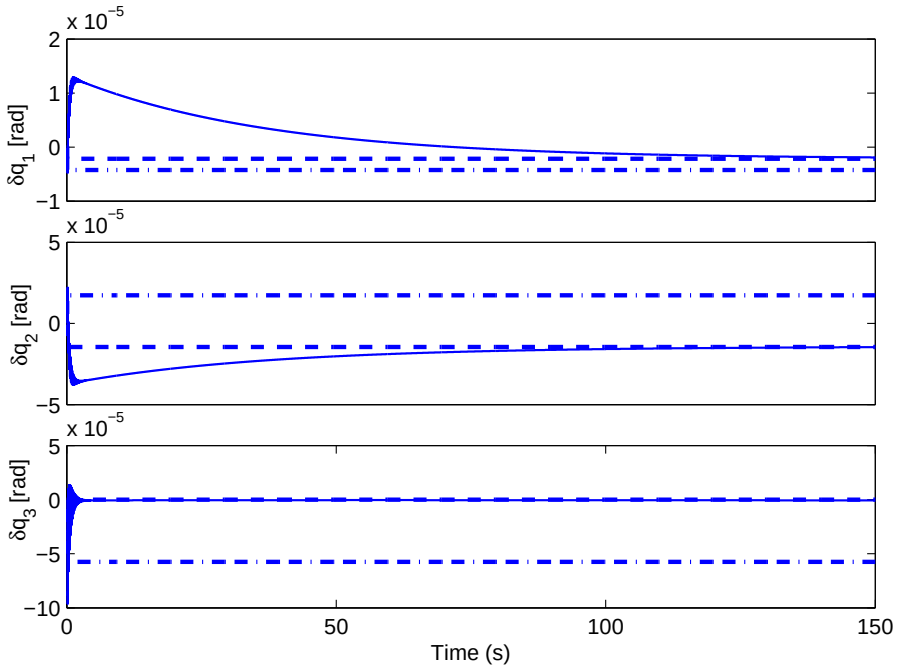

Figure 6.9: Set-1/Case-2: Little Damping ($b_1 = 1e^{-5}, b_2 = 1e^{-6}, b_3 = 1e^{-4}$ Ns/m, $\delta^c W_e = (0, 0, 0, 0.0001 \quad N, 0, 0)$). Infinitesimal joint displacement δq: simulated [solid line] vs. analytically determined response, using metric: $M_q = B$ [dashed line] and $M_q = M(q)$ [dashed-dotted line].

Both Figure 6.10 and Figure 6.11 show that the frequency changes after each input change, which confirms the variation of the compliance. Furthermore, it is confirmed that, also for changing input positions, the analytically determined δq_e indeed corresponds to the simulated response, for both cases.

6.9 Conclusions

Novel robotic finger concept Based upon the derived design consideration of Chapter 3, a novel robotic finger concept was introduced for developing multi-fingered dexterous robotic hands with minimal actuation and variable mechanical compliance.

Port-Hamiltonian analysis The presented port-Hamiltonian model established extensive analysis on the properties of the conceptual finger. Power flow analysis in this port-Hamiltonian framework supported in verifying the properties of the conceptual finger and to establish some basic design considerations. Together with the mapping properties discussed in Chapter 5, the presented port-Hamiltonian analysis method showed an elegant way to quickly verify modeled physical properties, by simply considering energy flows.

The analysis revealed the compliance and reachability properties and showed that the underactuated driving mechanism endangers both properties. Joint locks were introduced to route power from the controller to the right components to improve reachability.

Additionally, a design trade off was formulated to optimize the robotic design for external wrenches which need to be altered with finite compliance.

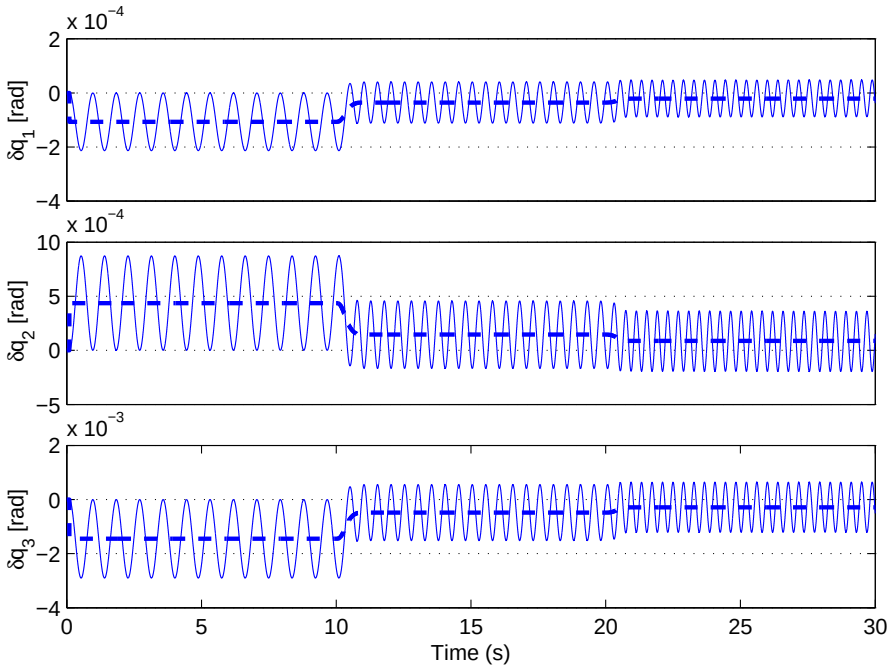

Figure 6.10: Case-1: Without damping. Changing position z alters compliance ($\delta^c W_e = (0, 0, 0, 0.0001 \quad N, 0, 0)$). Infinitesimal joint displacement δq: simulated response [solid line] vs. analytically determined response [dashed line], using metric: $M_q = M(q)$.

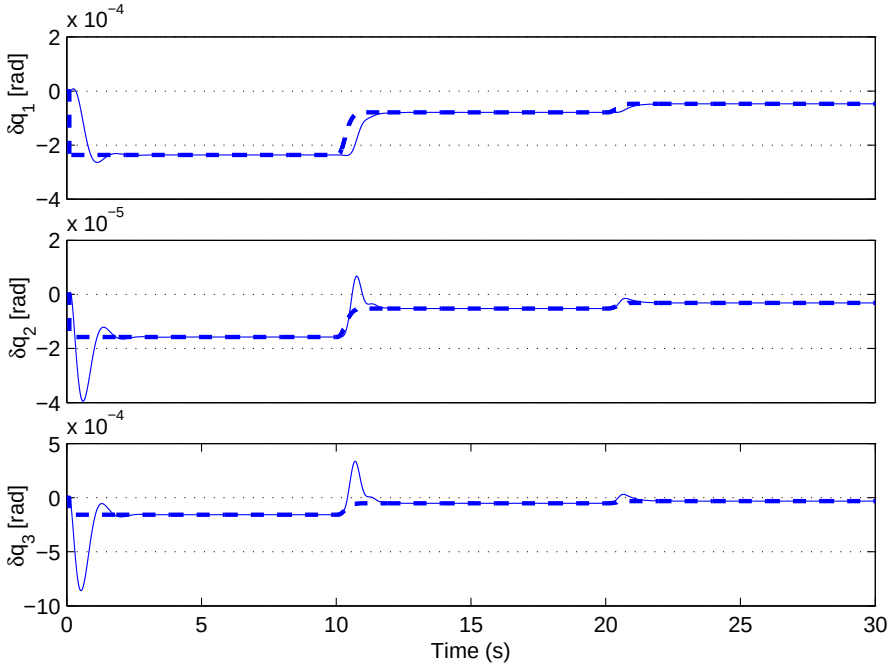

Figure 6.11: Case-2: Damping ($b_1 = 0.001, b_2 = 0.01, b_3 = 0.0005 \; Ns/m$). Changing position z alters compliance ($\delta^c W_e = (0, 0, 0, 0.0001 \quad N, 0, 0)$). Infinitesimal joint displacement δq: simulated response [solid line] vs. analytically determined response [dashed line], using metric: $M_q = B$.

Finger-tip compliance The non-trivial (variable) compliance properties were studied in depth for an underactuated robotic finger mechanism with compliant driving tendons.

The analysis followed the space decompositions as discussed in Chapter 5. Hence, the finger configuration space was decomposed into a subspace of null-space motions (infinite compliance) and its orthogonal space of finite compliance displacements.

In accordance with Chapter 5, the physically equivalent metric was found for two separate cases: dynamics with ($M_q = B$) and without damping ($M_q = M(q)$). The compliance analysis was confirmed by simulation results for both cases. As such, it also presented an application of the results in Chapter 5.

Also the variability property of the compliance for the novel robotic finger was confirmed by simulation and shown to be in accordance with the theoretical results.

Generality Notice that the underactuated analysis results for both the mechanism and the (variable) finger-tip compliance are applicable to the broader class of similar tendon-driven underactuated robot fingers. The general insights and methods developed in Chapter 5 and this chapter can be generally used to analyze kinematics and dynamics.

Robotic hand With this concept, an n-fingered hand will have at most $2n$ large size actuators. Depending on the specific application, the total number of actuators can be reduced by bundling the protagonist and antagonist tendons. Hence, the minimum number of large size actuators for a full dexterous hand would be only two.

Chapter 7

Dexterous Control of Novel Robotic Finger

Chapter 6 presented the novel robotic finger concept, which is reprinted in Figure 7.1. Section 6.1 listed several primary functions for robotic fingers, being dexterous grasping (power grasping, tip grasping), dexterous manipulation, free finger motion (e.g. pre-shaping and gesturing) and interactive finger motion.

For enveloping power grasps and some tip grasps, the underactuated mechanism can be fully utilized to execute these grasps by simply pulling the tendons. Nevertheless, the other tasks require dexterity for which the novel robotic finger concept is equipped with locks.

This chapter presents a low-level controller concept for the novel robotic finger. This low-level controller takes care of lock switching and tendon actuation in such a way that a high-level controller (which takes care of task control) can fully utilize the finger features. The space decomposition and duality concepts (as presented in Chapter 5) are used to synthesize the low-level controller. The controller include lock-switching control and support intuitive usage of the robotic finger for interactive (impedance) control schemes (see Section 3.2.2).

First Section 7.1 gives an overview of classes of interaction control schemes. The robotic finger is most suitable for the controlled mechanical impedance scheme. For this scheme, Section 7.2 sets out the desired behavior for the low-level controller. Before actually introducing the low-level controller, Section 7.3 is needed to analyze and use the underactuated actuation Jacobian (J_a). The analysis relies on insights from Chapter 5. Then, Section 7.4 and Section 7.5 present the conceptual implementation details, which are validated through simulations in Section 7.6. Finally, Section 7.7 demonstrates simulations of usage scenarios of the novel robotic finger, complemented with the presented low-level controller, for high-level controlled robotic finger tasks. Section 7.8 finishes with conclusions and recommendations.

7.1 Interaction Control

The novel robotic finger concept, see Chapter 6 and Figure 7.1, is aimed to be used in interaction control schemes as discussed in Section 3.2.2. Here it was presented that interaction control refers to control schemes that acknowledge that interaction tasks should **not** be seen as a matter of controlling the robot to some setpoint while minimizing the disturbances from the environment. These disturbances can not be minimized, because they have become dependent of the state of the interaction system.

Two interaction control schemes are distinguished from literature, which both acknowledge and implement the above given interaction control paradigm.This section briefly discusses both

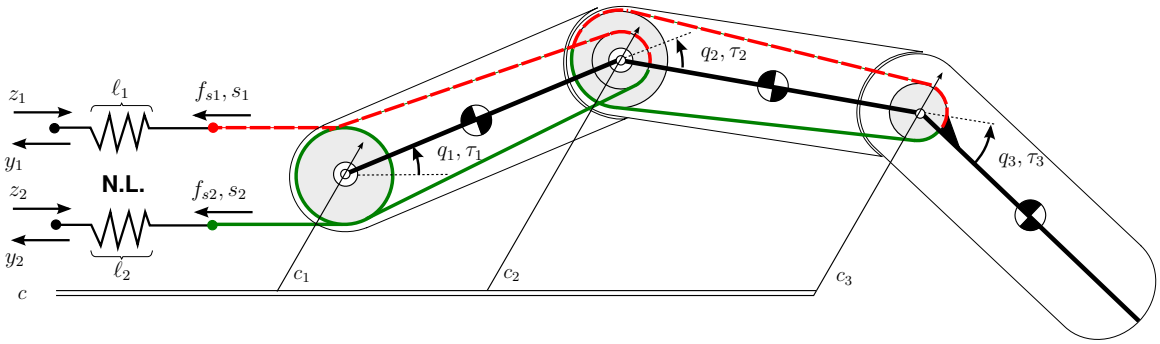

Figure 7.1: Conceptual drawing of novel robotic finger (copied from Figure 6.1): The underactuated 'softgripper' principle is extended with joint locks and non-linear antagonistic elastic elements (denoted by $N.L.$ with length/state $\ell_j, j \in \{1, 2\}$) in series with the driving tendons. Variables $z = (z_1, z_2)^T$ denote the tendon actuation positions, lock switches are denoted with c_i, the relative motion of two attached phalanges is given by $\dot{q}_i$, where q_i is the relative joint angle of joint i and τ_i the torque on joint i. Arrows indicate positive reference directions for attached variables.

distinct interaction schemes, as illustrated in Figure 7.2: *controlled virtual impedance schemes* and *controlled mechanical impedance schemes*. The controlled mechanical impedance scheme is not widely applied yet and has become of interest only recently for the purpose of future robotic applications, as discussed in Chapter 1 and Chapter 3.

It will become clear that the novel robotic finger concept is specifically designed for controlled mechanical impedance schemes. Therefore, the next section, Section 7.2, will introduce the control problem for the low-level controller for usage in this controlled mechanical impedance scheme.

7.1.1 Controlled virtual impedance

Controlled virtual impedance refers to approaches such as reported in e.g. [45, 46, 47]. As illustrated in Figure 7.2(a), a desired task is given to some high-level task controller. The task controller determines a desired position q_d and a desired (impedance) stiffness k_d.

The impedance controller simulates a virtual compliant network of (variable) virtual springs, a virtual mass and damper, which resemble the desired interaction impedance. Based upon a measured (q) and a desired robot position (q_d), the impedance controller calculates the force in the virtual spring k_c as if the virtual network is connected to the robot. This force is then applied to the robot by the actuators of the robot (τ_a). The resulting behavior is a robot displacement towards the virtual (and desired) position $q_v = q_d$. The actual robot displacement depends on the interaction forces and the virtual stiffness.

It is important to realize, that this calculated actuation torque (τ_a) resembles the force from the virtual impedance network. It is *not* the total net force on the robot. The net force also depends on the interaction force, which is externally applied and can not be controlled. Therefore, the net force should not be controlled to some setpoint. Instead, the actuators apply the required actuation force τ_a.

7.1.2 Controlled mechanical impedance

Controlled mechanical impedance refers to approaches such as reported in e.g. [48, 91]. As illustrated in Figure 7.2(b), a desired task is given to some high-level task controller. The task controller determines a desired position q_d and a desired (impedance) stiffness k_d. It is also

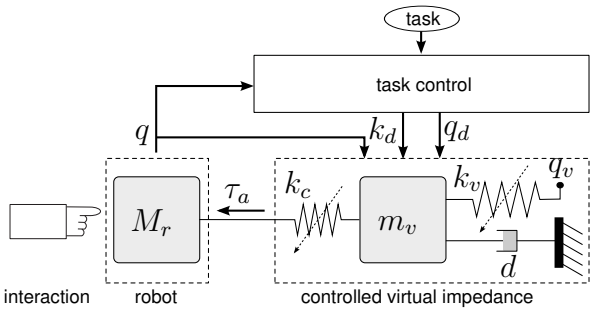

(a) Controlled Virtual Impedance, see also the IPC scheme in [47]: the robot is equipped with a force actuator τ_a. The controlled virtual impedance network calculates the force in spring k_c as if it is connected to the robot, while the virtual position q_v is held equal to the desired position q_d. Hence, the force actuator of the robot (τ_a) must apply this force to the robot.

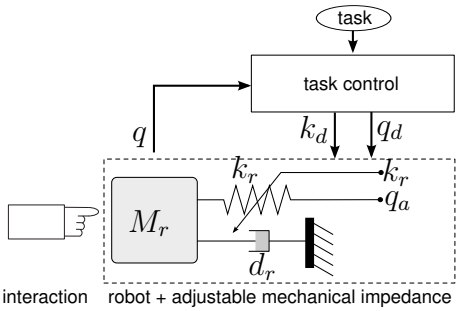

(b) Controlled Mechanical Impedance: the robot itself is equipped with adjustable stiffness k_r and a position actuator q_a. The position actuator of the robot sets the actuator position q_a to the requested position (q_d) and the stiffness k_r is set to the requested stiffness k_d.

Figure 7.2: Two different interaction (impedance) control schemes, sketched as simple 1 DOF examples. M_r refers to the robot mass, q refers to robot position, τ_a is robot actuation force, q_a is the robot actuation position, q_d is desired robot configuration and k_d is the desired stiffness (impedance), k_r is the adjustable mechanical robot stiffness, d_r is the mechanical robot dissipation/friction, k_c, k_v represent virtual (adjustable) stiffness, d virtual damping and m_v represents a virtual mass. A desired task is given to the high-level task controller. The task controller determines a desired position q_d and a desired (impedance) stiffness k_d.

shown that the robot itself contains an adjustable mechanical variable compliance element and a position actuator.

The robot behavior is controlled by steering the compliance attachment position, i.e. the robot actuation position q_a, to some desired position q_d and selecting a desired stiffness k_d for the programmable stiffness component. The position actuator ensures that $q_a = q_d$ is obtained. The resulting behavior is a robot displacement towards the actuator (and desired) position $q_a = q_d$. The actual robot displacement depends on the interaction forces and the virtual stiffness.

This method requires position actuation (q_a). Robot configuration measurements (q) may be needed to observe what the robot is doing, such that k_d and/or q_a can be altered accordingly.

It is important to realize, that this position actuation resembles the position of one end of the series compliant element (q_a), which is compliantly decoupled from the actual robot position q, by a series elastic element. It is *not* the robot position q. The actual robot position q also depends on the interaction force, which is externally applied and can not be controlled. Therefore, the actual robot position can not be controlled directly in interaction tasks.

7.1.3 Controlled mechanical impedance for novel robotic finger

Both approaches are equal with respect to the fact that they both control the interaction behavior by altering impedance and a desired position which is compliantly decoupled from the actual robot position (either mechanically or virtually). The obvious and fundamental difference is the fact that a controlled virtual impedance scheme simulates the interaction impedance, while the controlled mechanical impedance scheme utilizes the intrinsic impedance of the mechanics. Therefore, both approaches require different actuation methods and require different mechanical designs. In principal, the high-level task controller can be the same for both schemes.

Clearly, the novel robotic finger concept encompasses position actuation (on the tendons at actuation position z, see Figure 7.1) and variable mechanical compliance, see Chapter 6. Hence, it is specifically designed for the controlled mechanical impedance scheme for the reasons as given in Chapter 3, such as energy efficiency, robustness and safety.

Therefore, the remainder of this chapter focuses on usage of the novel robotic finger in a controlled mechanical impedance scheme.

Remark 7.1. *Throughout this chapter, equal symbols and variables to describe the robotic finger, as introduced in Section 6.3, are used. New symbols to describe the controller variables are introduced along the discussion.*

7.2 Control Goal - Desired Behavior

The novel robotic finger in mechanical interaction schemes is targeted for usage in mechanical interaction schemes. As illustrated in Figure 7.2(b), a high-level task controller in such schemes expects to control a robot with an input to change the variable mechanical compliance and an input, q_d, to which position actuators are attached (q_a) that are compliantly decoupled from the robot configuration q.

7.2.1 Controller goal

As presented in Chapter 6, the robotic finger concept is actuated by a position actuator at the tendon actuation positions z, see Figure 7.1. The actuator position z is compliantly decoupled from the robotic finger configuration q. Furthermore, tendon force measurements, i.e. $y = f_s$ and joint configuration measurements q are available.

Hence, no direct joint position actuators q_a are available in the robotic finger concept. Also no direct input is available to adjust the mechanical compliance. Nevertheless, Chapter 6 showed that differential tendon displacements $\dot{z} \in \operatorname{im} J_a$ induce finger configuration changes, while common mode tendon forces $f_s = y \in \ker J_a^T$ change the finger compliance. Clearly, without switching the locks, induced finger motions are far from being dexterous motions.

Hence, the robotic finger concept functionally resembles the robot for a mechanical impedance control scheme (Figure 7.2(b)), i.e. it encompasses compliantly decoupled position actuation and it can alter mechanical compliance. However these features are not accessible for the high-level task controller through the usual inputs as illustrated in Figure 7.2(b). Hence, the goal is:

> *to present a low-level finger actuation controller, which supports usage of the novel robotic finger concept in controlled mechanical impedance schemes and which addresses dexterity by means of lock switching control.*

7.2.2 Desired behavior

The low-level finger actuation controller is presented as concept for which the following desired behavior and functional requirements are considered, as schematically pictured in Figure 7.3.

Input/output requirements The low-level actuation controller supports the controlled mechanical impedance scheme (see Figure 7.2(b)), by letting the combination of the presented low-level actuation controller connected to the robotic finger appear as a robotic finger with inputs q_d and s_p and output q with additional outputs f_m, f_p, as shown in Figure 7.3.

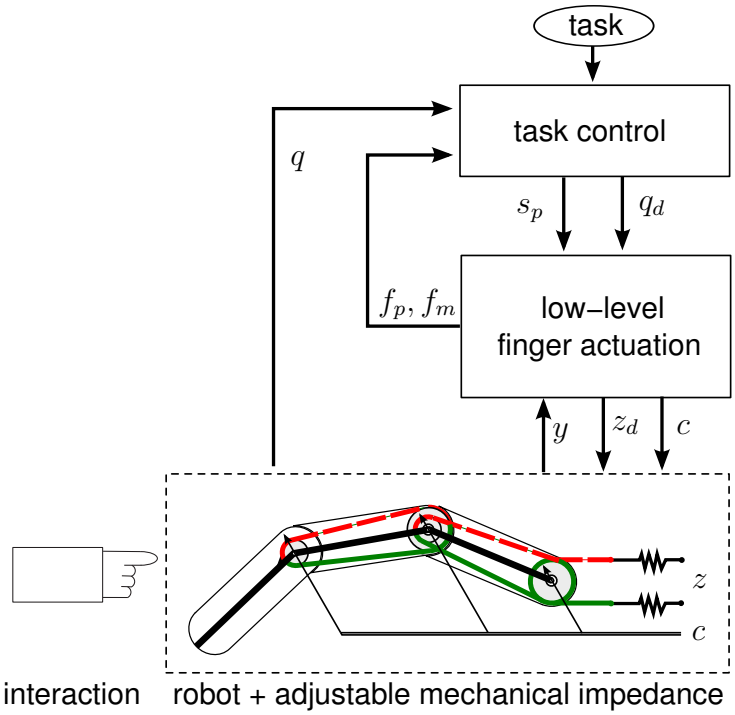

Figure 7.3: Low-level finger actuation controller: maps high-level task controller outputs s_p (a desired pre-load displacement to change mechanical compliance and to resolve the unilateral force transmission property of the tendons) and q_d (desired robot finger configuration) to finger actuation values, i.e. desired tendon actuation positions z_d and lock switch states c. It also maps the measured tendon force $y = f_s$ to f_p (common-mode pre-load force) and f_m (differential-mode tendon force).

A brief overview of these inputs and outputs of the low-level finger actuation controller, as shown in Figure 7.3, is given here. Throughout the chapter, their usage is explained in more detail.

- Inputs:
  - q_d: Desired actuation finger configuration[1];
  - s_p: Desired pre-tension (also called pre-load) displacement, i.e. the displacement of the tendons which induces pre-tensioning of the tendons, without effecting the joint configuration;
  - y: Measured tendon forces, i.e. $y = f_s$;
- Outputs:
  - z_d: Desired tendon actuation positions;
  - f_m: measured differential tendon force, i.e. the differential forces in the tendons, which induce non-zero torques on the joints;
  - f_p: measured pre-tension tendon force, i.e. the common-mode forces in the tendons, which induce no torques on the joints;

[1]Note: this is the configuration to which the position actuator q_a is set. The position actuator can reach this position, however the finger may not reach this configuration (in case of interaction), since q_a is compliantly decoupled from the actual configuration q, as sketched in Figure 7.2(b). Hence, the real actuation position q_a works similar as the virtual position q_v in controlled virtual impedance schemes.

Functional description In addition to Figure 7.3, hereafter a description of the functioning and usage of the low-level actuation controller is given:

- The low-level actuation controller accepts a desired q_d from a high-level task controller and transforms the requested joint actuator positions to desired tendon actuation displacements z_d. Also lock command signals c are generated in order to alter the joint trajectory within the equilibrium space $\mathcal{Q}_e$ (see Equation 6.22). The differential tendon force f_m is given back to the high-level controller, from which it can determine the applied joint torques;

- The input s_p is used to adjust the mechanical compliance of the robotic finger. The low-level actuation controller changes the pre-tension by altering a bias elongation of the series elastic elements according to the input s_p, without interfering with the desired q_d. Hence, this input is used to change the robotic finger compliance as needed;

- Resolving unilateral force transmission property of tendon: Tendons can not transmit negative forces (pushing). The pre-tension inputs can be used to generate a bias force in the tendons, such that pre-tension in the tendons remains positive for external force disturbances within the bias limits.

- Restoring dexterity: The low-level controller takes care of controlling the locks in real-time (i.e. no a priori knowledge on future input commands is used), in accordance with the actuator input commands. Hence, it allows for partial dexterous finger manipulation.

7.2.3 Method

As discussed in Chapter 2, for different applications, different sets of requirement parameters (e.g. speed, accuracy, ...) exist. Specific applications induce specifications for these requirement parameters. And, if the low-level concept is understood well enough, these specifications can be translated to required settings for the various design variables of the low-level controller. No specific applications are treated in this discussion. Hence, no requirements are formulated for the design variables.

The general functional behavior will be evaluated and some examples are shown of executing the primary functions of the finger. These examples present usage scenarios of the robotic finger concept together with the low-level controller concept. Hence functional behavior is verified. These scenarios are also used to investigate and explain the influence of the design variables with respect to requirement parameters.

Note: from now on, the low-level finger actuation controller will be called low-level controller for reasons of shortness of notation.

Remark 7.2. *For the remaining presentation, the novel robotic finger concept is assumed to have linear damping on the joints. Hence, for the analysis and simulations, the model of the novel robotic concept includes dissipation structure R_r, as shown in Equation 6.43, with damping matrix B, see Equation 6.44.*

7.3 Actuation Jacobian (J_a) Analysis

The design of the low-level controller relies on space decompositions attached to the mapping properties of the actuation Jacobian, J_a (Equation 6.5). Hence, before describing the

implementation details of the controller, this section describes the analysis of the space decomposition and the attached variables and mappings used for the low-level controller. These are complementary to the previously described variables for the model of the robotic finger concept, see Section 6.3. The analysis is based on insights from Chapter 5.

7.3.1 Full-rank decomposition of actuation Jacobian (J_a)

As discussed in Chapter 6, the actuation Jacobian is a non-surjective and non-injective map. Following Section 5.4, consider the full-rank decomposition of J_a:

$$J_a := FC \tag{7.1}$$

with F and C being matrix representations of the tangent maps, given by:

$$\begin{aligned} C &: T_q\mathcal{Q} \mapsto T_m\mathcal{M} \\ F &: T_m\mathcal{M} \mapsto T_s\mathcal{S}, \end{aligned}$$

where $\mathcal{M}$ ($\dim \mathcal{M} = 1$) is called the space of differential tendon displacements and $T_m\mathcal{M}$ is its tangent space[2]. For the dual spaces, one finds the dual mappings, being the co-tangent maps:

$$\begin{aligned} C^T &: T_s^*\mathcal{S} \mapsto T_m^*\mathcal{M} \\ F^T &: T_m^*\mathcal{M} \mapsto T_q^*\mathcal{Q}, \end{aligned}$$

with $T_m^*\mathcal{M}$ the co-tangent space of $\mathcal{M}$. Let the physical quantities attached to the variables denoted in the schematic of the robotic finger, Figure 7.1, be the original coordinates of the spaces (see Section 5.5.1). Hence, the original coordinates are chosen to coincide with the modeled physical forces and displacements in the robotic finger:

- **Original coordinates of $T_s^*\mathcal{S}$:** the coordinates of $T_s^*\mathcal{S}$ of which the bases coincide with the actual tendon forces $f_s \in T_s^*\mathcal{S}$ in the robotic finger, see Figure 7.1.
- **Original coordinates of $T_s\mathcal{S}$:** the coordinates of $T_s\mathcal{S}$ of which the bases coincide with the actual tendon displacements $\dot{s} \in T_s\mathcal{S}$ in the robotic finger, see Figure 7.1.

The matrix representation of the Jacobian J_a for the chosen original coordinates is already given in Equation 6.6. Hence the matrices F and C are found to be:

$$\begin{aligned} F &:= \begin{pmatrix} 1 \\ -1 \end{pmatrix} \\ C &:= \begin{pmatrix} r_1 & r_2 & \frac{r_2 r4}{r_3} \end{pmatrix}. \end{aligned} \tag{7.2}$$

7.3.2 Dual variables

For the controller design, it is useful to consider quasi-static situations on spaces $\mathcal{M}$ and $\mathcal{S}$, where the equilibrium is determined by the forces of the non-linear elastic elements in the

[2]Note: the mapping properties of F and C correspond to the equivalently named maps in the general discussion of Chapter 5, i.e. F is injective and non-surjective and C is surjective and non-injective.

driving tendons. Hence, physical dual spaces are defined through the metric M_s on $T_s\mathcal{S}$, given by the local stiffness matrix (see Equation 6.29):

$$M_s = \frac{\partial^2 H_\ell}{\partial \ell^2}(\ell) = \begin{pmatrix} \frac{\partial^2 H_\ell}{\partial \ell_1^2}(\ell_1) & 0 \\ 0 & \frac{\partial^2 H_\ell}{\partial \ell_2^2}(\ell_2) \end{pmatrix}, \tag{7.3}$$

and naturally, the metric on $T_s^*\mathcal{S}$ is the inverse metric, i.e. M_s^{-1}.

The according variables on the physical dual spaces represent infinitesimal variations around a local equilibrium point, determined by $\ell \in \mathcal{L}_e$ (see Equation 6.20). For the description of the controller, the following variables are used, as illustrated in Figure 7.4:

- $\delta f_t \in T_s^*\mathcal{S}$**:** required tendon forces, expressed in the original coordinates of $T_s^*\mathcal{S}$, denoted as co-vector.
- $\delta f_m \in T_m^*\mathcal{M}$**:** measured differential tendon force.
- $\delta s_t \in T_s\mathcal{S}$**:** required tendon displacements expressed in the original coordinates of $T_s\mathcal{S}$.
- $\delta s_m \in T_m\mathcal{M}$**:** desired differential tendon displacement.
- $\delta q_d \in T_q\mathcal{Q}$**:** desired joint displacement.

Notice that the dual variables are induced by the associated isomorphism for the M_s- and M_m-weighted inner-products on $T_s\mathcal{S}$ and $T_m\mathcal{M}$ respectively:

$$\begin{aligned} \delta f_m &= M_m \cdot \delta s_m = F^T M_s F \cdot \delta s_m \\ \delta f_t^T &= M_s \cdot \delta s_t, \end{aligned}$$

where $M_m = F^T M_s F$ is recognized as the pull-back of M_s onto $T_m\mathcal{M}$ and used as metric on $T_m\mathcal{M}$, see Definition 5.33.

The dual maps F and F^T are non-bijective. Hence, some redundancy ($\delta f_t \in \ker F^T$) exists on $T_s^*\mathcal{S}$ and some $\delta s_t \notin \operatorname{im} F$ are examined on $T_s\mathcal{S}$. For the design of the low-level controller, the properties of F^T and F are discussed in the following section.

7.3.3 Surjective and non-injective map F^T:

Consider co-tangent space $T_s^*\mathcal{S}$ and notice that F^T being a non-injective map implies $\ker F^T \neq \emptyset$, $\dim\left(\ker F^T\right) = 1$. Let subspace $\mathcal{F}_p$ be defined as:

$$\mathcal{F}_p := \ker F^T \subset T_s^*\mathcal{S},$$

Let the 2×1 matrix F_p be the basis matrix of $\mathcal{F}_p$, expressed in the original coordinates, such that it represents a coordinate transformation map: $F_p : T_s^*\mathcal{S} \mapsto T_s^*\mathcal{S}$. Then, define the following coordinate:

- $\delta f_p \in \mathcal{F}_p$**:** (defined along the base of $\mathcal{F}_p$) represents the measured infinitesimal change in pre-tension in the tendons.

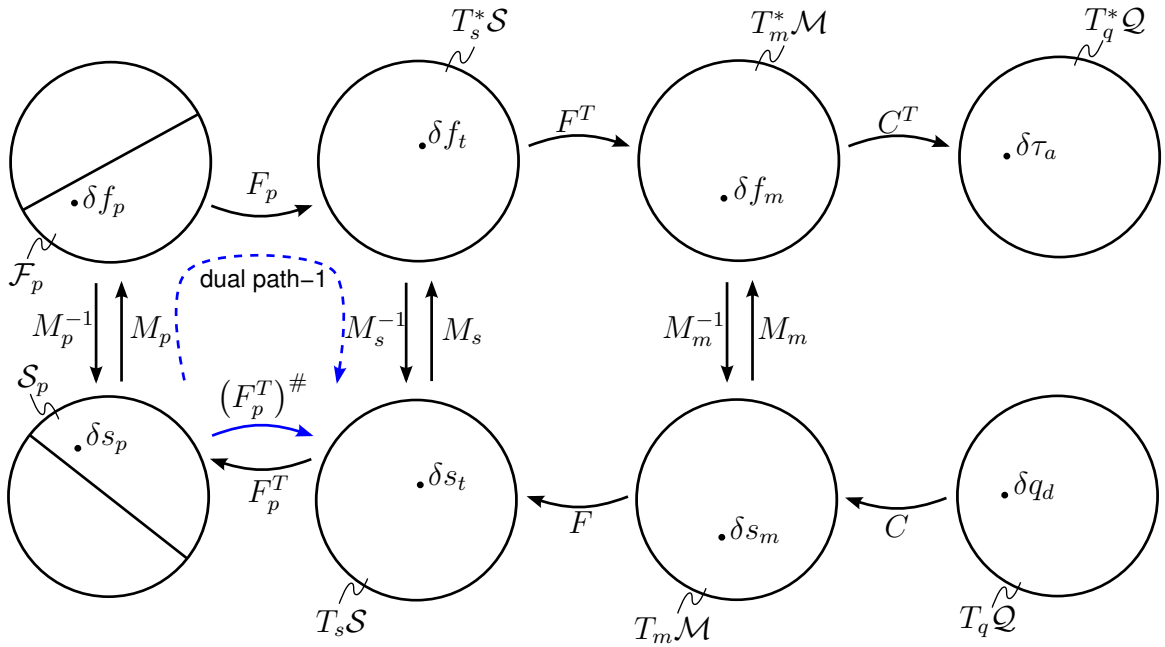

Figure 7.4: Physical dual spaces, dual variables and dual maps used for the low-level controller design. The metric on $T_s\mathcal{S}$ is given by $M_s = \frac{\partial^2 H_\ell}{\partial \ell^2}(\ell)$. The pull-back of this metric onto $T_m\mathcal{M}$ is used as metric on $T_m\mathcal{M}$, given by $M_m = F^T M_s F$ and the inverse of the pull-back of M_s onto $\mathcal{F}_p$ is used as metric on $\mathcal{S}_p$, given by $M_p = \left(F_p^T M_s^{-1} F_p\right)^{-1}$. Dual path-1 shows the minimum M_s-norm solution for $\left(F_p^T\right)^\# = M_s^{-1} F_p M_p = M_s^{-1} F_p \cdot \left(F_p^T M_s^{-1} F_p\right)^{-1}$.

This pre-tension δf_p resembles the set of forces that induce equal loads on both tendons. Hence, the pre-tension force elongates the elastic elements but does not induce any torques on the joints.

Remark 7.3 (Metric M_p^{-1})**.** *Consider the metric M_p^{-1} on $\mathcal{F}_p$ and notice that the pull-back of metric M_s^{-1} on $T_s^*\mathcal{S}$ onto $\mathcal{F}_p$ is a suitable choice for the metric M_p^{-1}:*

$$M_p = F_p^T M_s^{-1} F_p.$$

It may be noticed that the pre-tension $f_p \in \mathcal{F}_p$ behaves similar to the internal force f_i in the grasp example, Section 5.6.1.

7.3.4 Non-surjective and injective map F:

Consider tangent space $T_s\mathcal{S}$ which holds displacements, and notice that F being a non-surjective map implies $(\operatorname{im} F)^\perp \neq \emptyset$, $\dim (\operatorname{im} F)^\perp = 1$. Let subspace $\mathcal{S}_p$ be the physical dual space of $\mathcal{F}_p$, defined as:

$$\mathcal{S}_p := (\operatorname{im} F)^\perp \subset T_s\mathcal{S},$$

where the orthogonal complement is given by the inner-product induced by the metric M_s on $T_s\mathcal{S}$. Furthermore, define the following coordinate:

- $\delta s_p \in \mathcal{S}_p$**:** (defined along the base of $\mathcal{S}_p$) represents the desired infinitesimal pre-tensioning displacement changes in the tendons.

Note that the metric M_p^{-1}, as given in Remark 7.3, is the isomorphism for the dual elements:

$$\delta s_p = M_p^{-1} \cdot \delta f_p \tag{7.4}$$

Blocked motions Since $\mathcal{S}_p = (\operatorname{im} F)^{\perp}$, these pre-tension displacements can not be induced by any joint displacements. Moreover, coordinate $\delta s_p \neq 0 \in \mathcal{S}_p$ may seem to represent blocked motions in δs_t, see Definition 5.7. However, it is important to realize that the *required* tendon displacements δs_t *can* include these seemingly blocked (common mode) displacements. This is physically possible, since the controller applies these required tendon displacements (δs_t) at the actuation position z, which is compliantly decoupled from the tendon positions s, see Figure 7.1.

For the actual tendon positions s_1, s_2, see Figure 6.1, it can be verified that $\delta s \in (\operatorname{im} F)^{\perp}$ (moving in common mode) can not exist. It would violate the modeled kinematic constraints of the tendons (modeled by the actuation Jacobian J_a and assuming rigid tendons).

The blocked tendon displacements are resolved due to the series elastic elements in the tendons and actuating z instead of position s. Similarly, Section 5.7.8 showed how compliance resolved blocked contact motions for the modeled grasping system.

Pre-tension displacements let the 2×1 matrix S_p be the basis matrix of $\mathcal{S}_p$, expressed in the original coordinates, such that it represents a coordinate transformation map: $S_p : T_s\mathcal{S} \mapsto T_s\mathcal{S}$. However, since $\mathcal{F}_p$ and $\mathcal{S}_p$ are required to be physical dual spaces, the previously defined map F_p already imposes a physical dual map $F_p^T : T_s\mathcal{S} \mapsto T_s\mathcal{S}$. Thus, in coordinates, the map gives:

$$\delta s_p \;=\; F_p^T \cdot \delta s_t \qquad \delta s_t \in T_s\mathcal{S}, \delta s_p \in \mathcal{S}_p \tag{7.5}$$

which expresses the pre-tension (common-mode) displacement coordinate contained in a required tendon displacement $\delta s_t \in T_s\mathcal{S}$.

Clearly, it must hold that $S_p = \left(F_p^T\right)^{\#}$, which defines the projection of any $\delta s_p \in \mathcal{S}_p$ on the original basis of $T_s\mathcal{S}$, being the minimum M_s-norm inverse. Notice that F_p^T is a surjective and non-injective map. Therefore, using results from Section 5.5.2 and recalling that the metric on $T_s\mathcal{S}$ is given by M_s, it is found that:

$$\left(F_p^T\right)^{\#} \;=\; M_s^{-1}F_p \cdot \left(F_p^T M_s^{-1} F_p\right)^{-1}, \tag{7.6}$$

such that for any desired pre-tension displacement δs_p and any desired differential displacement δs_m, the total required tendon displacement to be applied to the finger tendon actuation positions z, is found to be:

$$\delta s_t = F \cdot \delta s_m + M_s^{-1}F_p \cdot \left(F_p^T M_s^{-1} F_p\right)^{-1} \cdot \delta s_p \qquad \delta s_m \in T_m\mathcal{M}, \delta s_p \in \mathcal{S}_p, \tag{7.7}$$

7.3.5 Details on usage of metric M_s

For the presented space decompositions, orhtogonal complementary spaces are chosen, which are defined by the metric M_s. Hence, proper usage of the metric M_s is needed. Some intuition is given here, and a useful properties are presented.

Some intuition Consider to induce a desired pre-tensioning displacement δs_p. Intuitively, this implies that one wants to move both tendon actuation positions z in such a way that the displacement induces elongations $\delta\ell$ of the elastic elements, without changing the configuration of the finger. Hence, no torques on the joints may be induced, i.e. $\tau = 0$. In order to do so, Section 6.5.2 learned that the induced tendon elongations must comply to $\delta\ell \in \mathcal{L}_e$ (Equation 6.20). This result shows that the elongations of the elastic elements must induce equal tendon forces f_s in both tendons, i.e. $f_s^T \in \ker F^T = \text{span}\{\begin{pmatrix}1 & 1\end{pmatrix}^T\}$, such that indeed $\tau^T = J_a^T \cdot f_s^T = 0 \quad \forall f_s \in \ker F^T$.

It is easily understood that if both tendons have equal elastic energy storage functions, then equal tendon actuation displacements δz induce the required equilibrating tendon forces. Obviously, if the elastic energy storage functions of both tendons are **not** equal, then also different tendon displacements on both tendons are needed to induce equilibrating forces.

Dual path explanation The stiffness metric M_s in the dual path-1 (see Figure 7.4) corrects the tendon displacements for possible unequal elastic elements. Following the dual path shows: Metric M_m takes the desired pre-tension displacement to the equivalent pre-tension force, $\delta f_p = M_p \cdot \delta s_p$. Then the basis matrix F_p maps the desired pre-tension force to the required equal tendon forces, $\delta f_t^T = F_p \cdot \delta f_p = \begin{pmatrix}1 & 1\end{pmatrix}^T \cdot \delta f_p$. And finally, the stiffness metric maps the required tendon forces to the required tendon displacements, $\delta s_t = M_s^{-1} \cdot \delta f_t^T$, such that the possible difference in the tendon stiffness is accounted for.

Practical implications Hence, usage of an incorrect metric leads to a physically incorrect space decomposition. The practical effect would be, that desired pre-tension displacements lead to unintended finger configuration changes, see also Section 7.6.3.

Constant projection condition The stiffness metric M_s has shown to be important in defining the physical dual spaces for the controller variables. Equation 7.3 shows that the metric M_s depends on ℓ for non-linear elastic elements. Therefore, it should be used locally around a given ℓ. So far, because of this local property, infinitesimal deviations (denoted by δ) have been used for the variables.

However, for the controller it is useful to use absolute values, instead of relative infinitesimal values for the variables.

However, for the controller it is useful not to use relative infinitesimal values for the variables. The following two theorems give useful properties for a broad class of force functions, $f_\ell(\ell)$ of the elastic elements. These force functions of the elastic elements are called the **constitutive relations** of the elastic elements. These properties allow to use global values for some variables, as discussed later (Section 7.5).

Theorem 7.1 (Constant projection condition for finger)**.** *Consider the following class of constitutive relations of the elastic elements:*

$$f_i(\ell_i) = k_i \cdot (\ell_i)^x \quad \ell \in \mathcal{L}, k_i \in \{k \in \mathbb{R} | k > 0\}, x \in \{x \in \mathbb{R} | x \geq 1\}$$

which represent the external force across the series elastic element of driving tendon $i \in \{1, 2\}$, with k_i some positive constant and x a constant power greater than (or equal to[3]) one. Then

[3]Note: the theorem also holds for $x = 1$. However, it represents the case for which the elastic elements are linear springs. This would eliminate the variable mechanical compliance property of the robotic finger concept.

the metric $M_s(\ell)$ is given by:

$$M_s(\ell) = \begin{pmatrix} k_1 \cdot x \cdot (\ell_1)^{x-1} & 0 \\ 0 & k_2 \cdot x \cdot (\ell_2)^{x-1} \end{pmatrix}$$

and the projection $(M_s(\ell))^{-1} F_p \cdot \left(F_p^T (M_s(\ell))^{-1} F_p\right)^{-1}$ (Equation 7.7) is **constant** *for all $\ell \in \mathcal{L}_e$:*

$$(M_s(\ell))^{-1} F_p \cdot \left(F_p^T (M_s(\ell))^{-1} F_p\right)^{-1} = \begin{pmatrix} \frac{1}{1+\frac{k_1}{k_2}\left(\frac{k_1}{k_2}\right)^{\frac{1-x}{x}}} \\ \frac{1}{1+\frac{k_2}{k_1}\left(\frac{k_2}{k_1}\right)^{\frac{1-x}{x}}} \end{pmatrix} \qquad \forall \ell \in \mathcal{L}_e.$$

Proof. For $\ell \in \mathcal{L}_e$ it holds that: $f(\ell) \in \ker F^T$ (see Equation 6.20, notice that $\ker F^T = \ker J_a^T$). Hence, it is given that for any α it must hold that:

$$\begin{pmatrix} f_1(\ell) \\ f_2(\ell) \end{pmatrix} \ni \operatorname{span}\{\begin{pmatrix} 1 \\ 1 \end{pmatrix}\} \Rightarrow \exists \alpha \quad s.t. \begin{pmatrix} f_1(\ell) \\ f_2(\ell) \end{pmatrix} = \alpha \begin{pmatrix} 1 \\ 1 \end{pmatrix} \qquad \forall \ell \in \mathcal{L}_e, \forall \alpha \in \mathbb{R}, \tag{7.8}$$

where α is any scaling factor. Solving the equations for ℓ gives **all** $\ell \in \mathcal{L}_e$. These are **all** $\ell \in \mathcal{L}_e$, since the expression depends on $\alpha \in \mathbb{R}$, which can be arbitrarily chosen:

$$\mathcal{L}_e \ni \ell = \begin{pmatrix} \left(\frac{\alpha}{k_1}\right)^{\frac{1}{x}} \\ \left(\frac{\alpha}{k_2}\right)^{\frac{1}{x}} \end{pmatrix} \quad \forall \alpha \in \mathbb{R},$$

such that:

$$M_s(\ell) = \begin{pmatrix} k_1 x \cdot \left(\frac{\alpha}{k_1}\right)^{\frac{x-1}{x}} & 0 \\ 0 & k_2 x \cdot \left(\frac{\alpha}{k_2}\right)^{\frac{x-1}{x}} \end{pmatrix} \qquad \ell \in \mathcal{L}_e \quad \forall \alpha \in \mathbb{R}$$

Working out $(M_s(\ell))^{-1} F_p \cdot \left(F_p^T (M_s(\ell))^{-1} F_p\right)^{-1}$ gives, after fractioning for $\alpha^{\frac{1-x}{x}}$ and rewriting:

$$\begin{aligned} &(M_s(\ell))^{-1} F_p \cdot \left(F_p^T (M_s(\ell))^{-1} F_p\right)^{-1} = \\ &= \begin{pmatrix} \frac{1}{k_1 x} \alpha^{\frac{1-x}{x}} \cdot \left(\frac{1}{k_1}\right)^{\frac{x-1}{x}} \\ \frac{1}{k_2 x} \alpha^{\frac{1-x}{x}} \cdot \left(\frac{1}{k_2}\right)^{\frac{x-1}{x}} \end{pmatrix} \cdot \left(\left(\frac{1}{k_1 x} \cdot \left(\frac{1}{k_1}\right)^{\frac{x-1}{x}} + \frac{1}{k_2 x} \cdot \left(\frac{1}{k_2}\right)^{\frac{x-1}{x}} \right) \alpha^{\frac{1-x}{x}} \right)^{-1} \\ &= \begin{pmatrix} \frac{1}{1+\frac{k_1}{k_2}\left(\frac{k_1}{k_2}\right)^{\frac{1-x}{x}}} \\ \frac{1}{1+\frac{k_2}{k_1}\left(\frac{k_2}{k_1}\right)^{\frac{1-x}{x}}} \end{pmatrix} \qquad \forall \ell \in \mathcal{L}_e. \end{aligned} \tag{7.9}$$

□

Theorem 7.2 (Constant projection condition for finger)**.** *Consider the following class of constitutive relations of the elastic elements:*

$$f_i(\ell_i) = x_i \cdot e^{\ell_i \cdot k_i} - 1 \qquad \ell \in \mathcal{L}, x_i, k_i \in \{k \in \mathbb{R} | k > 0\}$$

which represent the external force across the series elastic element of driving tendon $i \in \{1, 2\}$, with x_i and k_i some positive constant. Then the metric $M_s(\ell)$ is given by:

$$M_s(\ell) = \begin{pmatrix} k_1 x_1 \cdot e^{\ell_1 \cdot k_1} & 0 \\ 0 & k_2 x_2 \cdot e^{\ell_2 \cdot k_2} \end{pmatrix}$$

and the projection $(M_s(\ell))^{-1} F_p \cdot \left(F_p^T (M_s(\ell))^{-1} F_p\right)^{-1}$ (Equation 7.7) is **constant** *for all $\ell \in \mathcal{L}_e$:*

$$(M_s(\ell))^{-1} F_p \cdot \left(F_p^T (M_s(\ell))^{-1} F_p\right)^{-1} = \begin{pmatrix} \frac{k_2}{k_1+k_2} \\ \frac{k_1}{k_1+k_2} \end{pmatrix} \qquad \forall \ell \in \mathcal{L}_e.$$

Proof. Similar to the proof of Theorem 7.1. For $\ell \in \mathcal{L}_e$ it holds that: $f(\ell) \in \ker F^T$. Hence, Equation 7.8 must hold for **any** $\alpha \in \mathbb{R}$. Solving these equations for ℓ and the given force functions, shows:

$$\mathcal{L}_e \ni \ell = \begin{pmatrix} \frac{1}{k_1} \ln\left(\frac{\alpha+1}{x_1}\right) \\ \frac{1}{k_2} \ln\left(\frac{\alpha+1}{x_2}\right) \end{pmatrix} \qquad \forall \alpha \in \mathbb{R},$$

such that:

$$M_s(\ell) = \begin{pmatrix} k_1 x_1 \cdot e^{\ln\left(\frac{\alpha+1}{x_1}\right)} & 0 \\ 0 & k_2 x_2 \cdot e^{\ln\left(\frac{\alpha+1}{x_2}\right)} \end{pmatrix} = \begin{pmatrix} k_1 (\alpha+1) & 0 \\ 0 & k_2 (\alpha+1) \end{pmatrix} \quad \forall \ell \in \mathcal{L}_e, \forall \alpha \in \mathbb{R}.$$

Working out $(M_s(\ell))^{-1} F_p \cdot \left(F_p^T (M_s(\ell))^{-1} F_p\right)^{-1}$ proves the theorem. □

7.3.6 Surjective and non-injective map C:

Consider any given joint displacement $\delta q \in T_q\mathcal{Q}$. The map C, maps this displacement to the corresponding tendon differential displacement δs_m:

$$\delta s_m = C \cdot \delta q. \tag{7.10}$$

However, since C is a surjective and non-injective map, the corresponding δs_m holds for multiple δq, i.e. it holds for all $\delta q \in \mathcal{Q}_e \subset T_q\mathcal{Q}$. Vice versa, for any $\delta s_m \in T_m\mathcal{M}$, the corresponding space of according joint displacements is given by (see Section 5.5.2):

$$\begin{aligned} \mathcal{Q}_e &:= \delta\hat{q} + \ker C = C^{\#} \cdot \delta s_m + \ker C \qquad \delta s_m \in T_m\mathcal{M}, \\ &= M_q^{-1} C^T \cdot \left(C M_q^{-1} C^T\right)^{-1} \cdot \delta s_m + \ker C \end{aligned} \tag{7.11}$$

with M_q the metric on $T_q\mathcal{Q}$ and $\delta\hat{q} \in \mathcal{Q}_e$ the minimum M_q-norm joint displacement for any δs_m (see Section 5.5.2).

Applying differential tendon displacement δs_mon the tendons (assuming no disturbances), induces a joint displacement in the physical system (the robotic finger), which is described by the physically equivalent solution for the pseudo-inverse map $C^{\#}$. Thus, if M_q is the physically equivalent metric, $\delta\hat{q} = C^{\#} \cdot \delta s_m$ represents this physically equivalent solution.

Hence, for any desired joint displacement δq_d, assuming usage of the physically equivalent metric for M_q, applying the differential tendon displacement $\delta s_m = C \cdot \delta q_d$ is expected to induce joint displacement $\delta\hat{q}_d$, given by:

$$\delta\hat{q}_d = C^{\#} C \cdot \delta q_d. \tag{7.12}$$

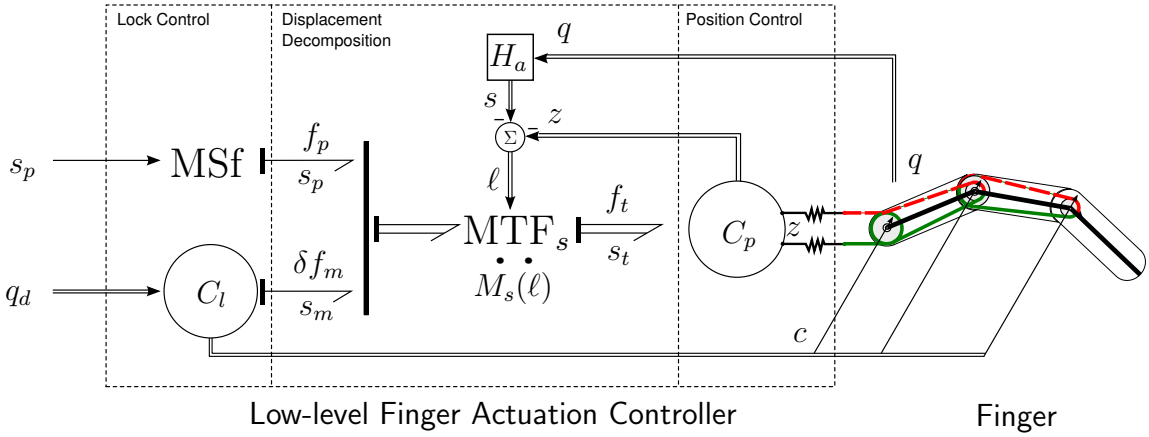

Figure 7.5: Pseudo bond-graph representation of low-level controlled novel robotic finger concept. Standard bond-graph notations are used: MSf denotes a modulated source of (infinitesimal) displacements, the vertical bar represents a multiplexer, which splits the multi-bond into single bonds and MTF denotes a modulated coordinate transformation, which is modulated by the elongations (ℓ) of the elastic elements. These elongations are calculated from the measured joint angles q and actuation positions z. C_p and C_l represent a position controller for the actuation port and a lock switching controller respectively. H_a is the configuration map, as given in Equation 6.3.

Remark 7.4. *The given induced joint angles $\delta\hat{q}_d$ (Equation 7.12) can only be expected not controlled nor enforced through tendon actuation, since any external disturbance may induce additional joint displacements that are in the kernel of C, see Section 6.5.1, such that the resulting joint displacement is still in $\mathcal{Q}_e$, but not equal to the expected $\delta\hat{q}_d$.*

Remark 7.5. *Note that $\delta\hat{q}_d \in (\ker C)^\perp \subset T_q\mathcal{Q}$ is the projection of the desired δq_d along the kernel of C onto the orthogonal complement (defined through M_q) of the kernel of C.*

7.4 Low-level Controller Implementation Overview

Before presenting the implementation details of the low-level controller, this section shortly gives a general description and intuition on the implementations of the low-level controller. The low-level controller is illustrated in a pseudo bond-graph model in Figure 7.5.

7.4.1 Bond-graph usage

The bond-graph representation gives a powerful compact way to describe the working principle of the low-level controllers. Also, being able to represent the controller in bond-graph representation, shows that the low-level controllers are energetically consistent.

Remark 7.6. *Regular bonds in bond-graphs represent power flows ($\frac{d\mathbb{E}}{dt}$), for which, in mechanics, the power conjugate dual variables are forces and velocities [64]. Here the physical dualism for quasi-static situations is used (see Section 5.8.2). Hence the dual variables in the low-level controllers are (infinitesimal) forces and (infinitesimal) displacements. The bonds of the bond-graph represent the relations between these controllers variables. Hence, the bonds represent change in elastic energy, $\delta\mathbb{E}$, and passive elements (e.g. the transformer, MTF) preserve conservation of $\delta\mathbb{E}$.*

Remark 7.7. *Both the power conjugate variables (velocity and force) and the here used physical dual variables for quasi-static situations (infinitesimal displacements and forces around*

an equilibrium) are elements of the tangent and co-tangent spaces, as presented in Section 7.3. In fact, the difference between these sets of variables and the attached physical quantity is just a scaling factor, i.e. infinitesimal time changes, i.e. dt.

Infinitesimal versus absolute variables for the low-level controller As said, the bond-graph presentation is used to give an intuition on the design of the low-level controller. As clarified in the given remarks, in principle, the variables in the controller represent infinitesimal quantities.

However, these infinitesimal quantities are relative quantities around some local point. For control purposes, it is useful to be able to use absolute (globally valid) values as well. As shown in Figure 7.5, some variables are used as absolute values (i.e. f_p, s_t, s_m, s_p, q_d) whereas others are used as infinitesimal variations (i.e. δf_m).

The next section, Section 7.5, will present the details of each of the sub-parts of the controller. There, it is also explained which variables must be infinitesimal and which are used as absolute values.

7.4.2 Implementation overview

The working principle of the low-level controller for the controlled mechanical impedance scheme is illustrated in Figure 7.5. It encompasses three sub-parts. *Lock control*, *Displacement decomposition* and *Position control*. A summarizing intuitive description is given for each of the sub-parts. Detailed descriptions are given in the subsequent section (Section 7.5).

- *Lock control (*C_l*)*: The lock controller, C_l, takes the desired joint actuator positions q_d. It selects an appropriate set of active locks (signal c) and it calculates the corresponding differential tendon displacement, s_m. The activated locks change the degrees of freedom in the equilibrium space $\mathcal{Q}_e$, such that applying s_m and c, produces a joint actuation displacement closest to the desired q_d.

- *Displacement decomposition (*MTF_s*)*: The multiplexer combines the requested pre-tension common mode motion s_p and the differential tendon motion, s_m, into one vector $(s_p \quad s_m)^T$. Then the modulated transformation element (MTF_s) changes coordinates, such that $(s_p \quad s_m)^T$ is transformed into a set of required tendon displacements s_t.

- *Position control (*C_p*)*: The position controller, C_p, steers the input actuation position of the robotic finger (z) in accordance with the required tendon displacement s_t. Furthermore, it measures the resulting tendon forces $y = f_s$.

7.5 Low-level Controller Details

The sub-parts of the low-level controller are presented in detail. Also, in accordance with this presentation, it is explained how the controller variables are used (local or global values). Thereafter, a summarizing block-diagram is presented, which shows the flow of the low-level controller calculations and measurements (in accordance with the given causality in the bond-graph, Figure 7.5). In the next section, Section 7.6, some simulation experiments are shown to validate the decompositions.

7.5.1 Displacement decomposition (MTF_s)

The modulated transformer (MTF) performs an energetically consistent change of coordinates. This coordinate change takes care of the physically equivalent space decompositions as discussed in Section 7.3.

Equation 7.7 gives the coordinate transformation for the desired causality, i.e.: the required tendon positions (s_t) are calculated for a desired pre-tensioning positions (s_p) and a desired differential tendon positions (s_m). It is rewritten into:

$$\begin{aligned} s_t &= T(\ell) \cdot \begin{pmatrix} s_m \\ s_p \end{pmatrix} \\ &= \begin{pmatrix} F & (M_s(\ell))^{-1} F_p \cdot \left(F_p^T \left(M_s(\ell)\right)^{-1} F_p\right)^{-1} \end{pmatrix} \cdot \begin{pmatrix} s_m \\ s_p \end{pmatrix} \end{aligned} \tag{7.13}$$

Furthermore, the physical dual map gives the dual forces for each of the desired input variables as a function of the measured resulting actual tendon forces $f_s = y$:

$$\begin{aligned} \begin{pmatrix} f_m \\ f_p \end{pmatrix} &= (T(\ell))^T \cdot y^T \\ &= \begin{pmatrix} F^T \\ \left(F_p^T \left(M_s(\ell)\right)^{-1} F_p\right)^{-1} \cdot F_p^T \left(M_s(\ell)\right)^{-1} \end{pmatrix} \cdot y^T \end{aligned} \tag{7.14}$$

Hence, the displacement decomposition (MTF_s) module calculates required tendon positions s_t for the desired input values, while giving back the measured pre-tension f_p and measured differential tendon force f_m.

The decomposition uses the elongations of the elastic elements (ℓ). These are available from straight forward position measurements of the joints angles q and the tendon actuation positions z, see also Figure 7.5. From the model of the robotic finger concept, it follows that (Equation 6.21):

$$\ell = -H_a \cdot q - z \tag{7.15}$$

Remark 7.8. *For s_t, s_m and s_p absolute displacement positions are used, instead of relative infinitesimal displacements. This allowed, due to the fact that $T(\ell)$ is constant, i.e. both map F and $(M_s(\ell))^{-1} F_p \cdot \left(F_p^T \left(M_s(\ell)\right)^{-1} F_p\right)^{-1}$ are constant, assuming:*

1. *usage of any of the elastic force functions given in Theorem 7.1 and 7.2;*
2. *small changes in elongations around the equilibrium for finger-environment interactions (for free finger motions, elastic elongations naturally reside to $\ell \in \mathcal{L}_e$). Clearly, interaction is mechanically resolved by the compliant decoupling of the actuation position and the joint angles. In that case, the finger will not reach its equilibrium configuration. Therefore some non-zero external force arises, see Section 7.7.4, which is naturally used for grasping;*

Explanation. Clearly F is constant. For $(M_s(\ell))^{-1} F_p \cdot \left(F_p^T \left(M_s(\ell)\right)^{-1} F_p\right)^{-1}$, the first assumption implies that $(M_s(\ell))^{-1} F_p \cdot \left(F_p^T \left(M_s(\ell)\right)^{-1} F_p\right)^{-1}$ is constant $\forall \ell \in \mathcal{L}_e$. The second assumption assures that the robotic finger can and will move to an equilibrium for any applied actuation position z. In equilibrium, it holds that $\ell \in \mathcal{L}_e$. Then, for a desired $s_p \neq 0$, it holds that by controlling the actuation position z to the according required tendon position s_t, i.e. $z = s_t$, again $\ell \in \mathcal{L}_e$ is induced, such that indeed ℓ remains in $\mathcal{L}_e$. Hence, $(M_s(\ell))^{-1} F_p \cdot \left(F_p^T \left(M_s(\ell)\right)^{-1} F_p\right)^{-1}$ is constant. The same holds for the resulting dual forces (Equation 7.14). Hence, these also represent absolute values. □

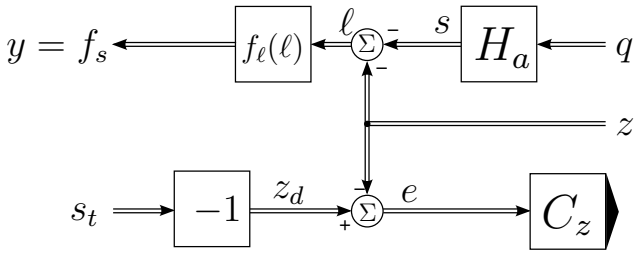

Figure 7.6: C_p inter-connection implementation: controller C_z implements the position control for tendon actuation position z, such that the actual tendon actuation position z is controlled to the desired tendon position s_t. Hence, it makes sure that the tendon actuation positions reach the desired position z_d, such that the error e is minimized. The measured tendon force y is calculated based on measured q and z and on (estimated) constitutive relations $f_\ell(\ell)$ of the elastic elements in the tendon drive. The negation of s_t is explained in Remark 7.9.

Note that the above used assumption implies that it is supposed that non-linear elastic elements which approximate the functions in Theorem 7.1 and 7.2 can be manufactured. If this turns out to be to non-feasible, then infinitesimal quantities should be used. This would not effect the design of the proposed low-level controller. It rather requires different input values from the high-level task controller. Instead of generating a global desired position, it should generate infinitesimal displacement steps, which can be obtained by using feedback control (on the difference between the desired and measured finger configuration) in the high-level task controller. This is in fact used in the demonstrations in Section 7.7.

7.5.2 Position control (C_p)

The position controller C_p creates the inter-connection on the controller port, between the low-level controller and the robotic finger. Recall that the finger is designed for position control at the finger actuation position z (See Figure 6.1).

As illustrated in Figure 7.5 and presented in Equation 7.13, controller C_p receives the required tendon actuation positions s_t from the displacement decomposition (MTF_s) and it sends back the measured tendon forces, y. A block diagram of the implementation is shown in Figure 7.6. A position controller C_z controls the actual tendon actuation position z to the required tendon actuation position $z_d = -s_t$ (the minus sign is just a modeling choice, see Remark 7.9 below), such that the error e is minimized. Hence, the position controller C_z reflects the behavior of a position actuator on tendon actuation positions z.

Remark 7.9. *As noted in Remark 6.2, variables s and z are modeled with opposite reference directions. Hence, as shown in Figure 7.6, for the desired tendon actuation position z_d it holds that: $z_d = -s_t$, such that it is assured that the control action of C_z co-aligns the required tendon positions s_t and the actual tendon positions s. This is merely a consequence of modeling choices, and does not effect the conceptual discussion whatsoever.*

Some comments:

- C_z represents any position actuation drive. Hence, various implementations can be used. Nevertheless, it is preferred to use non-backdrivable servo-drives, such that energy usage reduces to (almost) zero for steady state situations, i.e. $e = 0$. These situation will occur often in grasping.

- The measured tendon force y is calculated based on measured q and z and on (estimated) constitutive relations $f_\ell(\ell)$ of the elastic elements in the tendon drive, where ℓ follows from Equation 7.15 with position measurements for z and q from the robotic finger.

- As noted in Section 7.3.4, the tendon actuation positions z are compliantly decoupled from the tendon positions s. Hence, there are no blocked displacements for z, while there are blocked displacements for s, see Section 7.3.4. Therefore, it is physically plausible to require any tendon displacement $s_t \in \mathcal{S}$.

- Clearly, in many (almost all) robot finger tasks, interaction is important. Contact and interaction forces arise when the finger does not reach $\mathcal{Q}_e \ni q_d$. Hence, the high-level controller should use the desired configuration q_d and the pre-tension s_p in order to define how the finger behaves in this interaction.

  Nevertheless, the low-level controller performs its calculations to determine the compliantly decoupled actuation positions s_t (for a given desired q_d), by assuming no interaction, such that the finger indeed moves to a $q \in \mathcal{Q}_e$ for a given q_d if there is no interaction.

  Thus:

  - for a desired configuration change Δq_d and assuming that the elastic elongation do not change, gives $\Delta z = -\Delta s_t = J_a \Delta q_d$;
  - for any s_p, indeed the finger will not move and thus a change in elastic elongations is equal to a change in actuation position: $\Delta \ell = \Delta z$;

  Both examples show usability of position control for z.

7.5.3 Lock control (C_l)

This section presents the lock control element, which receives the low-level controller inputs, i.e. the desired joint position q_d, and translates these into suitable inputs for the decomposition element (MTF_s), i.e s_m, as illustrated in Figure 7.5 and discussed in Section 7.5.1. Furthermore, the states of the lock switches c are controlled.

Lock control problem The following control problem for C_l is stated for infinitesimal displacements on $T_q\mathcal{Q}$. Thereafter, as shown in the implementation, the results are applied for absolute displacements, as explained in Remark 7.8.

Assuming no disturbances or interactions, then the induced joint displacement δq on the finger is a function of the control values, i.e. δs_m and lock switch state c, denoted by:

$$\delta q = f_q(\delta s_m, c) \qquad \delta s_m \in T_s\mathcal{M}, c \in 2^3, \tag{7.16}$$

where $c \in 2^3$ denotes $c = (c_1 \quad c_2 \quad c_3)$ with each $c_i \in \{1, 0\}$.

The purpose of the lock control element (C_l) is to select a set of control values $(\delta s_m, c)$, such that the induced joint displacement δq is closest to the desired δq_d for all possible control values. Hence, the control problem for C_l is given as follows:

Let the M_J-norm measure the M_J-distance between the desired δq_d and any induced $\delta q = f_q(\delta s_m, c)$ on $T_q\mathcal{Q}$, such that a criterion J is given by:

$$\begin{aligned} J(\delta s_m, c) &:= ||\delta q_d - f_q(\delta s_m, c)||_J^2 \\ &= (\delta q_d - f_q(\delta s_m, c))^T \cdot M_J \cdot (\delta q_d - f_q(\delta s_m, c)), \end{aligned} \tag{7.17}$$

where M_J is the metric of a M_J-weighted inner-product on $T_q\mathcal{Q}$, which in coordinates is represented by the matrix M_J .

Then the control outputs $(\delta s_m, c)$ are chosen such that J is minimized:

$$(\delta s_m, c) = \arg \begin{pmatrix} \min \\ \delta s_m \in T_m\mathcal{M} \\ c \in 2^3 \end{pmatrix} (J) \tag{7.18}$$

Note that there is no intrinsic inner-product on $T_q\mathcal{Q}$. In the above defined criterion it is chosen to use the M_J-weighted inner-product to measure distance on $T_q\mathcal{Q}$ for this control problem. Clearly, the control problem must be coordinate invariant. Hence, the representing matrix M_J changes for changing coordinates, in such a way that the M_J-norm is invariant under coordinate changes, i.e. the measured distance does not change for different coordinates.

Expected induced joint displacements As discussed in Section 7.3.6, for $c = 0$, i.e. no lock activation and any δs_m, the expected induced joint displacement is given by: $\delta\hat{q} = C^{\#} \cdot \delta s_m$, where $C^{\#}$ depends on the metric M_q on $T_q\mathcal{Q}$. Hence, $C^{\#}$ generates the physically equivalent inverse map, if M_q is the physically equivalent metric for the given situation. Therefore, assuming usage of a physically equivalent metric and having $c = 0$, the expected joint displacement function $f_q(\delta s_m, 0)$ is given by:

$$\delta q = f_q(\delta s_m, 0) = C^{\#} \cdot \delta s_m, \qquad \delta s_m \in T_s\mathcal{M} \tag{7.19}$$

As shown in Equation 7.11 and noted in Remark 7.5, the producible joint displacements $f_q(\delta s_m, c)$ are bound to $\mathcal{X}_v = (\ker C)^{\perp} \subset T_q\mathcal{Q}$, i.e. elements in the orthogonal complement of the kernel of C. This orthogonal complement is defined through the metric M_q on $T_q\mathcal{Q}$. Note that M_q should be the physically equivalent metric for this case in order to let Equation 7.19 produce the physically equivalent induced δq for a given δs_m.

As shown in Section 5.9 and Section 6.7.5, if damping is relatively large with respect to inertia, then the physically equivalent metric is found to be represented by the linear damping matrix on the joints, given by B (e.g. Equation 6.44). Due to pre-tension forces in the tendons, tendon driven mechanisms posses substantial amounts of friction in the joints, see e.g. [62]. Hence, $M_q = B$ is considered an appropriate metric to approximate expected induced displacements.

Modulated damping Now, in order to include the lock actions into the control problem, instead of considering infinite stiff locks, for the time being, the locks are considered to modulate the damping on the joints. Hence, also the damping matrix is affected by the lock actions,

which is represented by the following (modulated) inverse damping matrix:

$$B^{-1}(\eta) = \begin{pmatrix} \frac{\eta_1}{b_1} & 0 & 0 \\ 0 & \frac{\eta_2}{b_2} & 0 \\ 0 & 0 & \frac{\eta_3}{b_3} \end{pmatrix} \qquad \eta \in \mathcal{B}, \tag{7.20}$$

where $\mathcal{B} = \{(\eta_1, \eta_2, \eta_3) \in \mathbb{R}^3 | 0 < \eta_i \leq 1\}$. The elements η_i represent the damping modulation induced by lock c_i, such that $\eta_i = 1$ represents an in-active lock, i.e. $c_i = 0$, while $\lim \eta_i \to 0$ represents a fully blocked lock, i.e. $c_i = 1$, since it renders zero for the inverse damping of the corresponding joint q_i.

Hence, the metric is changed to $M_q^{-1} = B^{-1}(\eta)$, which represents the actual damping on the joints including the effects of the locks, see Equation 7.20. Thus, the effect of locking is modeled as changing the orthogonal complementary space $\mathcal{X}_v$. The expected joint displacement function, Equation 7.19, is extended for any lock state $\eta \in \mathcal{B}$:

$$\begin{aligned} \delta q &= f_q(\delta s_m, \eta) = C^{\#} \cdot \delta s_m, \qquad \delta s_m \in T_s\mathcal{M}, \eta \in \mathcal{B} \\ &= M_q^{-1} C^T \cdot \left(C M_q^{-1} C^T\right)^{-1} \cdot \delta s_m \\ &= B(\eta)^{-1} C^T \cdot \left(C B(\eta)^{-1} C^T\right)^{-1} \cdot \delta s_m, \end{aligned} \tag{7.21}$$

Clearly, $\delta q = f_q(\delta s_m, \eta) \in \mathcal{X}_v$ and subspace $\mathcal{X}_v$ is span by the image of the basis matrix $X_v(\eta)$ (as generally explained by Theorem 5.2):

$$X_v(\eta) = M_q^{-1} C^T = B(\eta)^{-1} C^T, \tag{7.22}$$

where $X_v(\eta)$ is expressed in the original coordinates[4] of $T_q\mathcal{Q}$. Thus, the orthogonal complementary space $\mathcal{X}_v(\eta)$, and hence the basis matrix $X_v(\eta)$, depend on η.

Lock control solution From optimization theory the following implication is known. Let $(\delta\bar{s}_m, \bar{c})$ be the solution to the optimization problem as given above, then:

$$(\delta\bar{s}_m, \bar{c}) = \arg\left(\min_{\substack{\delta s_m \in T_m\mathcal{M} \\ c \in 2^3}} (J) \right) \Rightarrow \frac{\partial J}{\partial \delta s_m}(\delta\bar{s}_m, c) = 0 \text{ AND } \frac{\partial J}{\partial c}(\delta s_m, \bar{c}) = 0$$

Hence, candidate solutions can be found by first assuming input c fixed and searching candidate solution $\delta\bar{s}_m$, and then, if any candidate is found, searching for candidate solution $\bar{c}$ and taking $\delta\bar{s}_m$ fixed. This procedure is followed.

Recall Equation 7.21 and note that for any δs_m and a given fixed lock state c (and hence also η fixed), the expected induced $\delta q = f_q(\delta s_m, \eta)$ is an element of $\mathcal{X}_v(\eta)$. Thus, to solve the control problem, for any δs_m and fixed η, δs_m must be chosen such that J is minimized, i.e.: the M_J-distance between the according $\delta q = f(\delta s_m, \eta) \in \mathcal{X}_v(\eta)$ and the desired δq_d is minimized. From projection theory (see also Theorem 5.6), it is known that this minimized δq is found to be the orthogonal projection of δq_d on $\mathcal{X}_v(\eta)$, denoted by $\delta q_p(\eta)$, see Figure 7.7. Note that for this minimum M_J-distance, orthogonality is determined by the metric M_J, called M_J-orthogonality.

[4] Recall that the original coordinates are defined for the bases on $T_q\mathcal{Q}$, which are co-aligned with the actual joint axes in the robotic finger. Also δq and δq_d are expressed in these original coordinates.

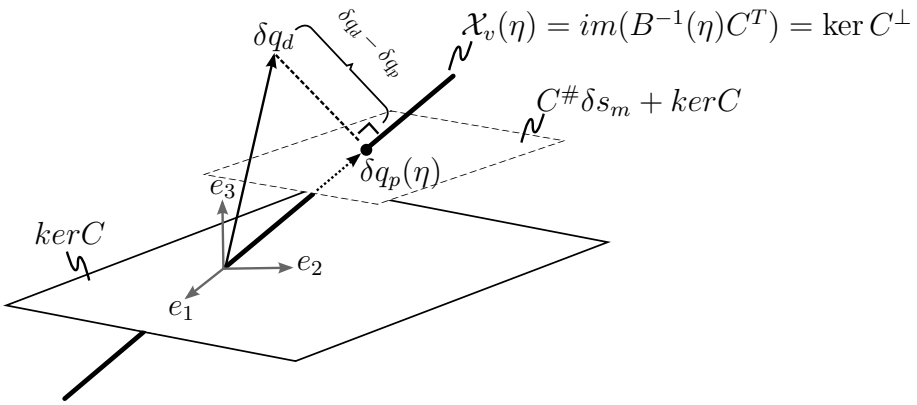

Figure 7.7: Illustration of minimizing control solution: for a given η, the orthogonal complement of $\ker C$ is given by $\ker C^\perp = \mathrm{im}(B^{-1}(\eta)C^T)$, where it is used that the physically equivalent metric to decompose the infinitesimal joint displacements is given by $M_q = B^{-1}(\eta)$. For the given η, any δs_m produces a $\delta q \in \mathcal{X}_v(\eta)$. The control problem specifies that the $\delta q \in \mathcal{X}_v(\eta)$ which is M_J-closest to δq_d, is considered the δq to be activated, which is found by taking the M_J-orthogonal projection of δq_d onto $\mathcal{X}_v(\eta)$, which gives $\delta q_p(\eta)$.

Hence, the $M)J$-projection of δq_d onto $\mathcal{X}_v(\eta) = \mathrm{im}\, X_v(\eta)$ is given by:

$$\delta q_p(\eta) = X_v(\eta)\left(X_v(\eta)^T M_J X_v(\eta)\right)^{-1} X_v(\eta)^T M_J \cdot \delta q_d = E_p(\eta)\cdot \delta q_d, \tag{7.23}$$

where the projection matrix, denoted by $E_p(\eta) := X_v(\eta)\left(X_v(\eta)^T M_J X_v(\eta)\right)^{-1} X_v(\eta)^T M_J$, follows from well-known linear algebra and also from the discussion in Section 5.5.3 (with the metric M_J to define $(\mathrm{im}\, X_v(\eta))^\perp$). Thus, for a given η and a desired δq_d, the candidate J-minimizing control δs_m is given by:

$$\begin{aligned} \delta \bar{s}_m = C\cdot \delta q_p(\eta) &= CE_p(\eta)\cdot \delta q_d \\ &= C\cdot X_v(\eta)\left(X_v(\eta)^T M_J X_v(\eta)\right)^{-1} X_v(\eta)^T M_J \cdot \delta q_d. \end{aligned} \tag{7.24}$$

As shown in Equation 7.11, applying $\delta \bar{s}_m$ induces subspace $\mathcal{Q}_e$ representing all possible displacements belonging to $\delta \bar{s}_m$, in which $\delta q_p(\eta)$ is the minimum M_q-norm physically equivalent solution. Hence, for $\delta \bar{s}_m$ and a given η, $f_q(\delta \bar{s}_m, \eta) = \delta q_p(\eta)$ is expected to be induced, which is the joint displacement with smallest M_J-distance to the desired δq_d, see also Figure 7.7.

For the given candidate $\delta \bar{s}_m$, which produces $f_q(\delta \bar{s}_m, \eta) = q_p(\eta)$, the J-minimizing control problem is reduced to finding the lock state c, modeled by η in the metric $M_q^{-1} = B(\eta)^{-1}$, which minimizes J for the given candidate $\delta \bar{s}_m$, i.e.:

$$\bar{\eta} = \arg\left(\min_{\eta\in\mathcal{B}}\left(J(\delta \bar{s}_m, \eta)\right)\right) \tag{7.25}$$

with

$$J(\delta \bar{s}_m, \eta) = ||\delta q_d - f_q(\delta \bar{s}_m, \eta)||_J^2 = ||\delta q_d - \delta q_p(\eta)||_J^2 = ||(\mathbb{I}_3 - E_p(\eta))\cdot \delta q_d||_J^2,$$

where $||\bullet||_J^2$ still represents the M_J-norm as given in the control problem and $\mathbb{I}_3$ is the 3×3 identity matrix. Hence, a $\eta \in \mathcal{B}$ needs to be found, which alters the space of producible δq, given by subspace $\mathcal{X}_v(\eta)$, such that the distance between $\delta q_p(\eta) \in \mathcal{X}_v(\eta)$ and δq_d is minimized[5]. The minimization can be changed into a maximization problem:

$$\bar{\eta} = \arg\left(\max_{\eta\in\mathcal{B}}\left(||\delta q_p(\eta)||_J^2\right)\right), \tag{7.26}$$

[5]Remember: for every η, $\delta q_p(\eta) \in \mathcal{X}_v(\eta)$ represents the producible infinitesimal joint displacement closest to δq_d.

which is shown by writing out the argument ($E_p(\eta)$ is given in Equation 7.23 and use $E_p(\eta)^T M_J E_p(\eta) = M_J E_p(\eta)$ and $E_p(\eta)^T M_J = M_J E_p(\eta)$):

$$\begin{aligned}
\bar{\eta} &= \arg\left(\min_{\eta\in\mathcal{B}}\left(||(\mathbb{I}_3 - E_p(\eta))\cdot\delta q_d||_J^2\right)\right) \\
&= \arg\left(\min_{\eta\in\mathcal{B}}\left(\delta q_d^T\cdot(\mathbb{I}_3 - E_p(\eta))^T\cdot M_J\cdot(\mathbb{I}_3 - E_p(\eta))\cdot\delta q_d\right)\right) \\
&= \arg\left(\min_{\eta\in\mathcal{B}}\left(\delta q_d^T\cdot M_J\cdot\delta q_d - \delta q_d^T\cdot M_J E_p(\eta)\cdot\delta q_d\right)\right) \\
&= \arg\left(\min_{\eta\in\mathcal{B}}\left(-\delta q_d^T\cdot M_J E_p(\eta)\cdot\delta q_d\right)\right) \\
&= \arg\left(\max_{\eta\in\mathcal{B}}\left(\delta q_d^T\cdot M_J E_p(\eta)\cdot\delta q_d\right)\right) = \arg\left(\max_{\eta\in\mathcal{B}}\left(||\delta q_p(\eta)||_J^2\right)\right),
\end{aligned}$$

which shows that the maximization of the M_J-norm of the M_J-projection of δq_d onto $\mathcal{X}_v(\eta)$ is equal to the minimization of the smallest M_J-distance between $\delta q_p(\eta) \in \mathcal{X}_v(\eta)$ and δq_d.

This maximization problem is a non-linear constrained (i.e. η is bound, i.e. $0 < \eta_i \leq 1$) optimization problem, with no trivial analytical solution for η. Naturally, the *un*bounded optimal solution $\bar{\eta}$ produces $\mathcal{X}_v(\bar{\eta})$, such that $\delta q_d \in \mathcal{X}_v(\bar{\eta})$.

Nevertheless, considering the locks again to be the original stiff switching locks, the solution can be found by calculating $||\delta q_p(\eta)||_J^2$ (to solve maximization in Equation 7.26) for the limited set of possible combinations of lock states. This will be used in the lock-controller. Therefore, the following definitions are used and the solution is given thereafter.

Definition 7.1 (selection index κ)**.** *The index number $\kappa \in K_s$ is called the selection index, which can take any value from the integer set $K_s = \{1, 2, 3, 4, 5, 6, 7\}$.*

Definition 7.2 (Lock-switch matrix (LS))**.** *Let the lock-switch matrix LS be given by:*

$$LS = \begin{pmatrix} 0 & 0 & 0 \\ 1 & 0 & 0 \\ 0 & 1 & 0 \\ 0 & 0 & 1 \\ 1 & 1 & 0 \\ 0 & 1 & 1 \\ 1 & 0 & 1 \end{pmatrix},$$

where column $LS_c(j) \quad j \in \{1, 2, 3\}$ corresponds to the on/off state of lock c_j (and j refers to the corresponding joint number). Hence, each row $LS_r(\kappa) \quad \kappa \in K_s$ represents to state c of all three lock switches (recall that $c_j = 1$ corresponds to an active lock on joint j, while $c_j = 0$ represents an inactive lock, see Section 6.4.2).

For this discrete set of lock switch states, also the possible damping modulation values η reduce to two options for each joint:

$$\begin{array}{lcll} c_i = 0 & \Leftrightarrow & \eta_i = 1 & \text{inactive lock} \\ c_i = 1 & \Leftrightarrow & \lim\eta_i \to 0 & \text{active lock} \end{array} \tag{7.27}$$

where in practice $\lim\eta_i \to 0$ can be numerically represented by $\eta_i = 0$.

Thus, Equation 7.26 is solved by calculating the M_J-norm, $||\delta q_p(\eta)||_J^2$, for the seven possible lock combinations given by LS and using that specific lock combination that gives the maximum norm, which is summarized by rewriting Equation 7.26 into:

$$\kappa \;=\; \arg\left(\max_{\kappa\in K_s}(J_\kappa)\right), \tag{7.28}$$

which gives the selection index κ that selects the specific lock switch state $LS_r(\kappa)$ that maximizes J_κ, with:

$$\begin{aligned} J_\kappa := ||\delta q_p(\eta_\kappa)||_J^2 &= ||E_p(\eta_\kappa)\cdot\delta q_d||_J^2 = \delta q_d^T\cdot M_J E_p(\eta_\kappa)\cdot\delta q_d \\ &= \delta q_d^T\cdot M_J X_v(\eta_\kappa)\left(X_v(\eta_\kappa)^T M_J X_v(\eta_\kappa)\right)^{-1} X_v(\eta_\kappa)^T M_J\cdot\delta q_d \end{aligned} \tag{7.29}$$

and $X_v(\eta_\kappa)$ is given in Equation 7.22, where η_κ is the damping modulation state which corresponds to switch state $c = LS_r(\kappa)$, as defined in Equation 7.27.

Hence, for the given discrete problem, the control solution is given by $\bar\eta = \eta_\kappa$ and the corresponding differential tendon displacement $\delta\bar s_m$, given in Equation 7.24, becomes:

$$\delta\bar s_m = CE_p(\eta_\kappa)\cdot\delta q_d = C\cdot X_v(\eta_\kappa)\left(X_v(\eta_\kappa)^T M_J X_v(\eta_\kappa)\right)^{-1} X_v(\eta_\kappa)^T M_J\cdot\delta q_d. \tag{7.30}$$

For reasons given in Remark 7.8, the infinitesimal quantities can be enlarged to absolute values, i.e. q_d and s_m.

Remark 7.10 (choice of metric M_J)**.** *For this control problem, described in the original coordinates for which the bases of $T_q\mathcal{Q}$ are co-aligned with the actual joint axes in the robotic finger, the chosen metric M_J is represented by the identity matrix, i.e. $M_J = \mathbb{I}_3$. Hence, the M_J-norm measures the sum of the squared angular errors with respect to the desired (infinitesimal) change in finger shape. Thus, for this choice, the control problem tries to minimize errors of the desired (infinitesimal) change in finger shape.*

C_l-action algorithm implementation The given solution in Equation 7.28 produces a selection index κ for each q_d such that the lock switch state is found to be $c = LS_r(\kappa)$. In practice, the desired q_d may change over time, i.e. $q_d(t)$ is a function of time. Hence, Equation 7.28 needs to be evaluated at each instant of time. Hence, the selection index becomes a function of time $\kappa(t)$:

$$\kappa(t) = \arg\left(\max_{\kappa\in K_s}\left(||\delta q_p(\eta_\kappa)(t)||_J^2\right)\right) = \arg\left(\max_{\kappa\in K_s}\left(||E_p(\eta_\kappa)\cdot\delta q_d(t)||_J^2\right)\right), \tag{7.31}$$

To implement the algorithm for practical use, two issues must be accounted for:

1. The algorithm is implemented in a digital controller. Hence, continuous time t, changes to discrete intervals, with counter k and sample-time T_s, such that $t = T_s\cdot k$.

2. The selection index κ (Equation 7.31) may change frequently (even if $q_d(t)$ changes relatively slow) in cases where multiple projections of the desired q_d have almost equal norms. Hence, also the lock states $c = LS_r(\kappa)$ change frequently. Any mechanical implementation of the lock is expected to have limited switching times. Therefore, an index switching delay factor $\gamma \in \{\gamma\in\mathbb{R}|\gamma\geq 0\}$ is used.

Furthermore, the allowable frequency content of the signal $q_d(t)$ is limited to the range for which the damping metric is the appropriate physically equivalent metric (which depends on the actual damping and inertia of the finger, as found in Section 5.9).

For time step k, $\kappa(k)$ denotes the used selection index κ at time instant k and hence $\eta_{\kappa(k)}$ corresponds to switch state $c = LS_r(\kappa(k))$, as defined in Equation 7.27. This notation is used in the presentation of the complete implementation, which is shown in Figure 7.8.

Figure 7.8 also shows the usage of the index switching delay factor γ. Using $\gamma > 0$ results in delayed switching behavior: the M_J-norm of the projection of $q_d(k)$ onto $\mathcal{X}_v(\eta_{\kappa(k)})$ for the updated (hence optimized) index $\kappa(k)$ (which maximizes the norm of this projection) at current time instant k, is compared to the norm of the projection of $q_d(k)$ onto the previously selected subspace $\mathcal{X}_v$, denoted by $\mathcal{X}_v(\eta_{\kappa(k-1)})$ with $\kappa(k-1)$ the previous selection index:

$$||E_p(\eta_{\kappa(k)}) \cdot \delta q_d(k)||_J^2 > (1+\gamma) \cdot ||E_p(\eta_{\kappa(k-1)}) \cdot \delta q_d(k)||_J^2,$$

If the statement is true, the updated selection index $\kappa(k)$ is accepted and the lock state is set accordingly. If not, then the previous selection index, $\kappa(k-1)$ is used to select the lock state c. The inequality enforces that the selection index (and hence the switch state) only changes when the maximized norm of the projection of q_d is larger than $(1+\gamma)$ times the norm of the projection onto the previously selected complementary space $\mathcal{X}_v(\eta_{\kappa(k-1)})$.

Thus, with parameter γ, the lock switch selection can be influenced: either (for smaller γ) switching more often and hence selecting more often the closest realizable joint displacement, or (for larger γ) switching less and hence inducing some joint displacement, which is not always closest to the desired[6] q_d.

7.5.4 Complete low-level controller block scheme

All sub-parts of the low-level controllers have been presented. A complete inter-connecting block scheme for each of the low-level controllers is given in Figure 7.9. In addition to Figure 7.5, the block scheme gives an overview of the causal path of calculations from inputs to outputs.

Remark 7.11 (basic action)**.** *For enveloping grasp tasks, dexterity is not needed, and the natural closing properties of the underactuated tendon drive mechanism can be controlled with the so called basic action, i.e. $\delta s_m = C \cdot \delta q_d$ (Equation 7.10), without lock actuation. Hence, the presented low-level controller is useful for a broader class of underactuated robotic finger concepts. As presented in Equation 7.12, the basic action induces: $\delta \hat{q}_d = C^{\#} C \cdot \delta q_d$ (see also Remark 7.5).*

7.6 Low-level Controller Validation Sim. Experiments

The design of the low-level controller is based on the decomposition analysis as presented in Section 7.3. This section validates the proposed low-level controller implementation through simulation experiments that verify the designed properties of the decomposition element and the basic action of the C_l element, see Remark 7.11.

[6] In fact, $\gamma \neq 0$ lets the algorithm have a preference to stick to the current lock state.

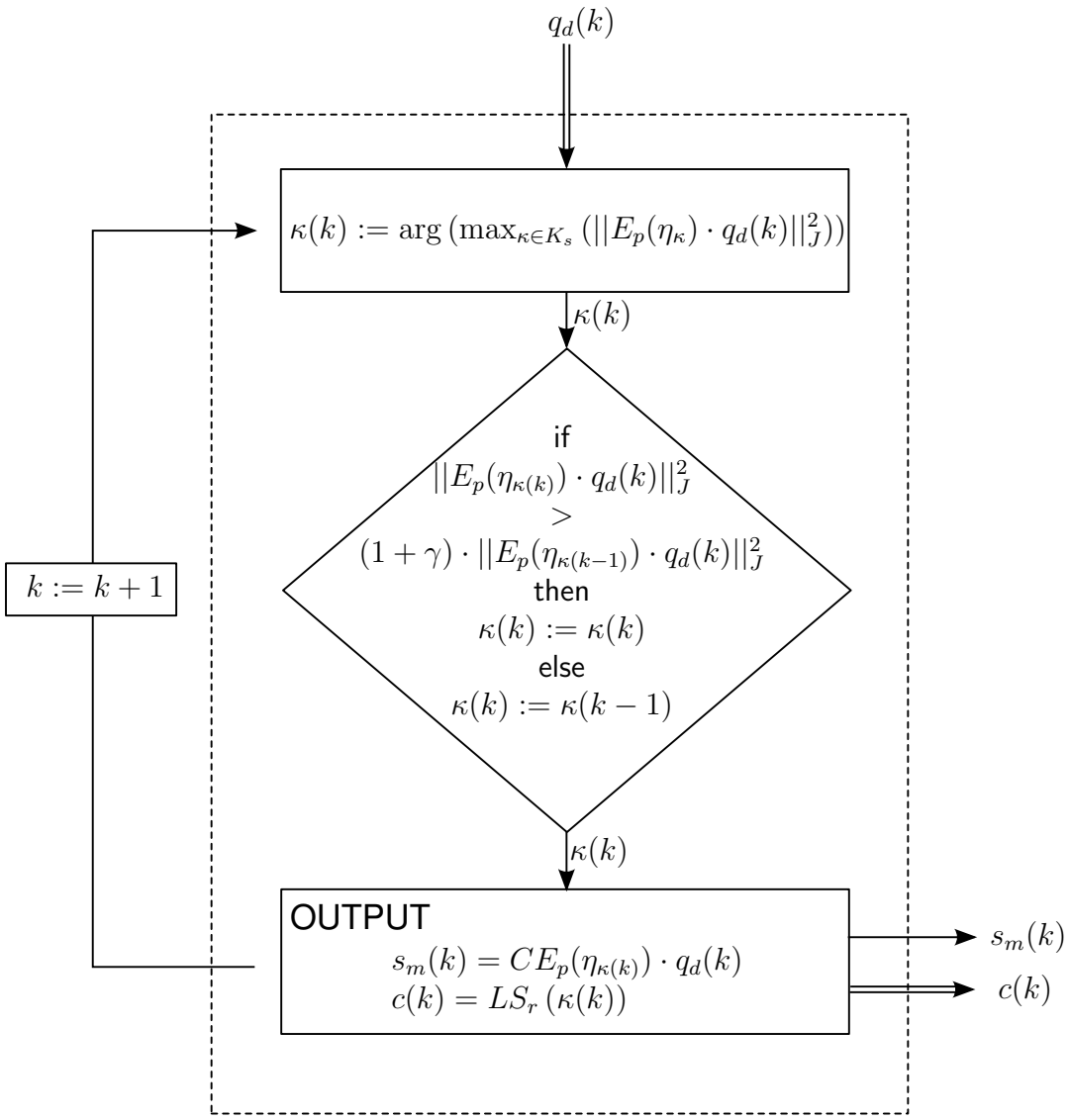

Figure 7.8: C_l-action algorithm implementation. At time index k, the desired joint displacement $q_d(k)$ enters and the new selection index $\kappa(k)$ is determined. Next, the M_J-norm of the projection of $q_d(k)$ for the new index $\kappa(k)$ is compared to the norm of the projection of $q_d(k)$ for the previous selection index, $\kappa(k-1)$. The result of the comparison determines whether the selection index remains to be the old index ($\kappa(k-1)$) or it changes to the new index $\kappa(k)$. Finally, the according outputs are selected. If the selection index does not change with respect to the previous times instant k, then also the lock switch state remains unchanged.

7.6.1 Validation goals

Validity of the conceptual design is checked by verifying the following properties:

1. a required pre-tension bias s_p is applied, without effecting the joint positions q or applied joint torques $\delta\tau$;
2. constant projection condition (Theorem 7.1 and 7.2), which allows for using global absolute variable values in low-level controller;
3. meaningful dual measurements f_p;
4. validity of expected induced joint displacement $\hat{q}_d$ (Equation 7.12) after applying the basic action, see Remark 7.11 of the C_l element (Equation 7.10) for a desired q_d and

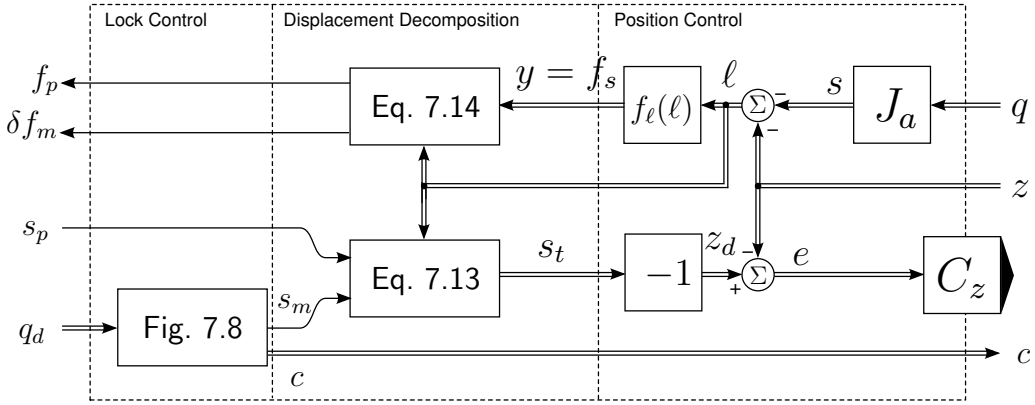

Figure 7.9: Complete block scheme of the presented low-level controller. In addition to Figure 7.5, the block scheme gives an overview of the causal path of calculations from inputs to outputs. The desired tendon actuation position is denoted by z_d and e denotes the error between z_d and z.

using the physically equivalent metric for M_q, without lock activation (lock activation is evaluated later);

The presented experiments aim to verify the functional behavior of the controller concept. Therefore, ideal circumstances are used, such that focus is given to the functional behavior. Clearly, implementing in practice requires to handle non-idealities.

7.6.2 Validation method

Simulation experiments are executed with the dynamic simulation package 20-sim[7]. To illustrate the results, some representative simulation experiments are discussed in the subsequent sections.

> **Representative results** Representative means that equal results were obtained for other parameter values such as different non-linear functions for the elastic elements (within the given class of functions given in Theorem 7.1 and 7.2, different mass distributions and damping distributions.

Simulation Model

- The novel robotic finger concept is modeled and simulated as presented in Chapter 6.
- The low-level controller is implemented as presented in this chapter, see e.g. Figure 7.9, where the lock control element is not actuating the locks, $c = 0$, (C_l is implemented with basic action, Equation 7.10). Hence, actual lock control is not tested. However, the underlying design principles are verified, see validation goals 4 (Section 7.6.1). Lock control is used and tested in the next section, Section 7.7.
- Ideal measurements are assumed for the joints q and tendon actuation position z.
- The position controller C_z is implemented by two straight forward single-input-single-output proportional gain (K_p) feedback controllers. The controllers feed ideal velocity actuator, which realize any desired actuation position velocity, $u = K_p \cdot (z_d - z)$. Hence,

[7] See Controllab Products B.V., The Netherlands `http://www.20sim.com/`.

the closed-loop transfer function for the actual tendon actuator position (z) over the desired tendon actuation position (z_d) is given by:

$$\frac{z(s)}{z_d(s)} = \frac{1}{\frac{1}{K_p}s + 1} \qquad s \in \mathbb{C}$$

Naturally, in practice, the actuator and according hardware impose bandwidth limitations for the closed-loop position controller C_z. Limited bandwidth can be simulated by choosing K_p accordingly.

Parameters The following arbitrary human-size design parameters are used for presenting the results (unless otherwise stated): $\lambda_1 = \lambda_2 = \lambda_3 = 0.04\ m$, $r_1 = 0.01, r_2 = r_3 = 0.00666, r_4 = 0.00333\ m$.

An arbitrary mass distribution is used for the masses of the phalanges: $m_1 = 0.1, m_2 = 0.4, m_3 = 0.2\ kg$ and the moments of inertia $I_{z1} = 1e^{-5}, I_{z2} = 4e^{-5}, I_{z3} = 2e^{-5}\ kgm^2$. The linear damping coefficients on the joints are set to: $b_1 = b_2 = b_3 = 1\ Ns/m$.

Theorem 7.1 is followed for the non-linear spring elements, such that:

$$f_\ell(\ell) = \begin{cases} \begin{pmatrix} k_1 \cdot \ell^2 \\ k_2 \cdot \ell^2 \end{pmatrix} & \forall \ell \geq 0 \\ 0 & \forall \ell < 0 \end{cases},$$

with $k_1 = 10.000$ and $k_2 = 30.000$, such that the elastic elements are different to avoid arbitrary results for equal elastic elements[8].

The proportional gain of the position controller C_z is set to $K_p = 1000$.

Experiment descriptions for low-level controller Two experiments are presented for the low-level controller. Each experiment is briefly described together with a set of desired (and expected) results that correspond to the desired behavior of the low-level controller, Section 7.2. The results are presented in the following section.

1. **Experiment-1, displacement decomposition test:**
   - Goal: establish validation goals 1,2 and 3 (Section 7.6.1).
   - Input:
     - desired pre-tension displacement: $s_p = 0.15$;
     - no desired joint displacement: $q_d = 0.0$;
   - Expected results/output:
     - constant projection $P_s = (\mathrm{MTF}_s[1:2,2]$ (Theorem 7.1) for $M_s = \frac{\partial^2 H_\ell}{\partial \ell^2}(\ell)$ (Equation 7.3):

$$\begin{aligned} P_s &= M_s^{-1} F_p \cdot \left(F_p^T M_s^{-1} F_p\right)^{-1} = \begin{pmatrix} \frac{1}{1+\frac{k_1}{k_2}\left(\frac{k_1}{k_2}\right)^{\frac{1-x}{x}}} \\ \frac{1}{1+\frac{k_2}{k_1}\left(\frac{k_2}{k_1}\right)^{\frac{1-x}{x}}} \end{pmatrix} \quad \forall t. \\ &= \begin{pmatrix} 0.634 \\ 0.366 \end{pmatrix} \end{aligned} \tag{7.32}$$

[8] The experiments are started with a small pre-tension of $10^{-6}\ N$ in both elastic elements, such that the system is initialized in equilibrium with pre-tension, $f_\ell = f_s = \ker F^T$. This pre-tension is merely used to avoid numerical errors (division by zero) at simulation start up. Of course, in practice, this can easily be avoided otherwise

– induced tendon displacements z (Equation 7.7, Theorem 7.1):

$$z = s_t = M_s^{-1} F_p \cdot \left(F_p^T M_s^{-1} F_p\right)^{-1} \cdot s_p = P_s \cdot s_p = \begin{pmatrix} 0.0951 \\ 0.0549 \end{pmatrix}, \qquad (7.33)$$

such that indeed: $s_p = 0.15 = F_p \cdot z = z_1 + z_2$ (Equation 7.5);

– no joint displacement: $q(t) = q(0) \quad \forall t$, no joint torques: $\tau(t) = \tau(0) \quad \forall t$;

– measured pre-tension force $f_p = P_s \cdot y^T$ (Equation 7.14), for which $f_p = y_1 = y_2 = f_{\ell 1}(z) = k_1 \cdot z_1^2 = 90.45\ N$ must hold, since all induced tendon displacements are expected to elongate the elastic elements and hence induce pre-tension forces.

2. **Experiment-2, induced finger displacement test:**

- Goal: establish validation goal 4 (Section 7.6.1).
- Input:
  – desired pre-tension displacement: $s_p = 0.15$;
  – desired joint displacement: $q_d = (-0.3 \quad -0.2 \quad -0.1)^T$;
  – no active locks, use basic action for C_l-element (Equation 7.10:$s_m = C \cdot q_d$);
- Expected results/output:
  – induced steady state joint displacement (Equation 7.12):

$$\hat{q}_d = M_q^{-1} C^T \cdot \left(C M_q^{-1} C^T\right)^{-1} C \cdot q_d,$$

where $r_2 = r_3$ is used and damping matrix B is used as the physically equivalent metric for the steady state solution ($M_q = B$);

  – Tested for two sets of damping coefficients in the joints (and the metric is adapted accordingly):
    (a) for $b_1 = b_2 = b_3 = 1\ Ns/m$, the expected joint displacement is $\hat{q}_d = q_d$;
    (b) for $b_1 = 3, b_2 = 2, b_1 = 1\ Ns/m$, the expected joint displacement is $\hat{q}_d = (-0.2334 \quad -0.2334 \quad -0.2334)^T$;

7.6.3 Validation results

1. **Experiment-1, displacement decomposition:** Figure 7.10 shows results of the displacement decomposition tests for two different metrics used in the MTF_s element: the correct metric $M_s = \frac{\partial^2 H_\ell}{\partial \ell^2}(\ell)$ (Equation 7.3) and some arbitrary metric $M_s = \mathbb{I}_2$ (identity).

   It is observed that for $M_s = \frac{\partial^2 H_\ell}{\partial \ell^2}(\ell)$, the expected results (Section 7.6.2) are found:

- induced steady state tendon displacements z:

$$z = s_t = \begin{pmatrix} 0.0951 \\ 0.0549 \end{pmatrix},$$

such that indeed: $s_p = 0.15 = F_p \cdot z = z_1 + z_2$;

- no joint displacement: $q(t) = q(0) \quad \forall t$, no joint torques: $\tau(t) = \tau(0) \quad \forall t$;

- measured steady state pre-tension force $f_p = y_1 = y_2 = 90.45\ N$ and indeed $f_t = y \in \ker F^T$, confirming no induced joint torques.
- $P_s = \begin{pmatrix} 0.634 \\ 0.366 \end{pmatrix} \quad \forall t$ for $M_s = \frac{\partial^2 H_\ell}{\partial \ell^2}(\ell)$, see Figure 7.10(c), i.e. P_s is constant.

Figure 7.10 shows that usage of an incorrect metric, such as $M_s = \mathbb{I}_s$, results in undesired behavior: the joints are displaced, while s_p is running from 0 to 0.15, due to non-zero induced torques on the joints.

2. **Experiment-2, induced finger displacement:** Figure 7.11 shows results of the induced finger displacement tests for $q_d = (-0.3 \quad -0.2 \quad -0.1)^T$. It is observed that the measured steady state joint displacements q agree with the expected induced joint displacements $\hat{q}_d$ (Section 7.6.2):

   - Indeed, as expected, for $b_1 = b_2 = b_3 = 1\ Ns/m$, the measured joint displacement is $q = \hat{q}_d = q_d \in (\ker C)^\perp = B^{-1} \operatorname{im} C^T = \operatorname{span}\{(r_1 \quad r_2 \quad r_4)^T\}$ with $B = \operatorname{blockdiag}(b_1, b_2, b_3)$. Which shows that the axis of not-kernel displacements (i.e. the minimum M_q-norm displacements) is co-aligned with the desired q_d;
   - Indeed, as expected, for $b_1 = 3, b_2 = 2, b_1 = 1\ Ns/m$, the measured joint displacement is $q = \hat{q}_d = (-0.2334 \quad -0.2334 \quad -0.2334)^T \in (\ker C)^\perp = B^{-1} \operatorname{im} C^T = \operatorname{span}\{(1 \quad 1 \quad 1)^T\}$ with $B = \operatorname{blockdiag}(b_1, b_2, b_3)$. Which shows that the axis of not-kernel displacements (i.e. the minimum M_q-norm displacements) is not co-aligned with the desired q_d. Hence, $q \neq q_d$;

   Thus, if no external disturbances are applied, indeed the given expected induced displacement $\hat{q}_d$ corresponds to the actual measured steady state displacements. Again, usage of the damping metric ($M_q = B$) is confirmed to be correct for physically equivalent results, see also Section 5.9 and Section 6.8. Hence, the C_l controller design is yet another example of applying physically equivalent metrics (Chapter 5).

Conclusions for low-level controller validation:

- The desired functional behavior is verified and the importance of using the correct metric $M_s = \frac{\partial^2 H_\ell}{\partial \ell^2}(\ell)$ for the MTF_s is shown.
- Applying the calculated tendon displacement for the desired joint displacement indeed induces expected $\hat{q}_d$, if no disturbances are applied, as stated in Remark 7.4.
- This expected $\hat{q}_d$ must be calculated by using for M_q the physically equivalent metric for the situation at hand.
- Since the tendon displacements can not enforce the exact joint displacement, if no information is available on disturbances, the expected $\hat{q}_d$ is the only available estimate, and hence used for the lock controller.

7.7 Primary Functions Examples - Sim. Experiments

The previous section validated the general low-level controller properties. This section presents some results of various simulation experiments to show applications of the low-level controller in combination with high-level task controllers to render primary functions of the robotic finger.

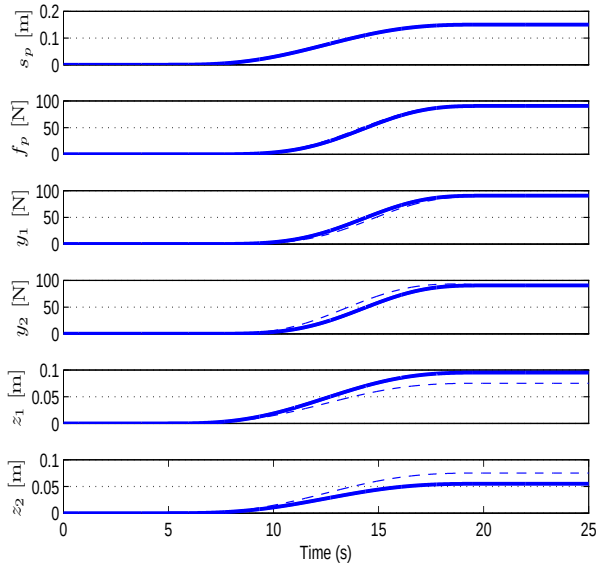

(a) Input profile for s_p and measured controller variables: f_p, y_1, y_2, z_1, z_2.

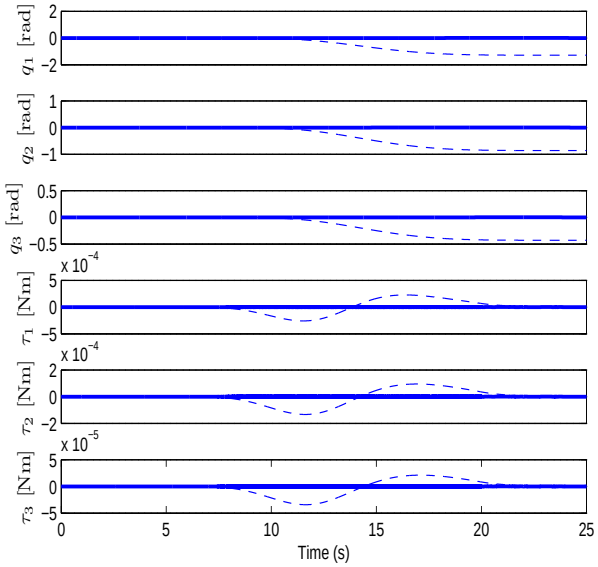

(b) Measured finger variables: q and τ. Using metric $M_s = \mathbb{I}_2$ (dashed line) shows non-zero torques, which should not happen if only pre-tensioning displacements are asked ($s_p \neq 0$ and $s_m = 0$). Solid line shows correct behavior.

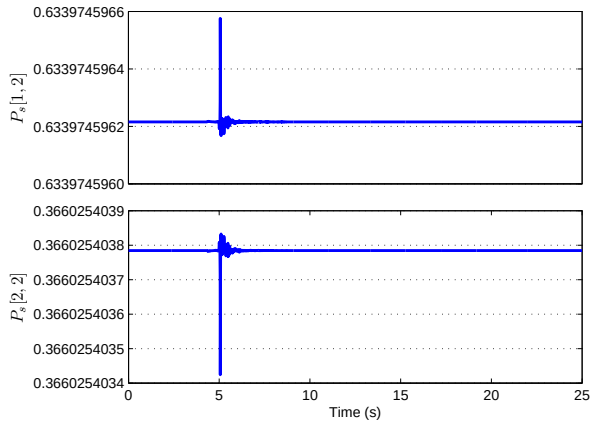

(c) Elements of P_s for $M_s = \frac{\partial^2 H_\ell}{\partial \ell^2}(\ell)$ are constant (plotted deviations are numerical simulation errors and depend on the integration time-step of the simulation method.)

Figure 7.10: Experiment-1, displacement decomposition: plots show results for two different metrics used in the MTF_s element for inputs $s_p \neq 0$ and $s_m = 0$: (**solid line**) the correct metric $M_s = \frac{\partial^2 H_\ell}{\partial \ell^2}(\ell)$ (Equation 7.3) and (**dashed line**) some arbitrary metric $M_s = \mathbb{I}_2$. With incorrect metric, non-zero torques are induced, while only pre-tensioning displacements are supposed to be induced.

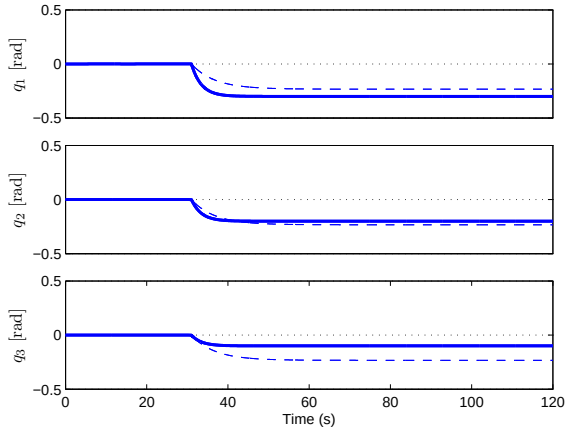

Figure 7.11: Experiment-2, induced finger displacement for basic action: plots show results for desired displacement $q_d = (-0.3 \quad -0.2 \quad -0.1)^T$ with different damping sets. **Solid line**: $b_1 = b_2 = b_3 = 1$ Ns/m, measured displacement $q = (-0.3 \quad -0.2 \quad -0.1)^T$, **Dashed line**: $b_1 = 3, b_2 = 2, b_1 = 1$ Ns/m, measured displacement $q = (-0.233 \quad -0.233 \quad -0.233)^T$. The applied basic action is equal ofr both experiments. As expected damping on the joints changes the expected induced joint displacement. Both results match the expected results, see Section 7.6.2.

Finger motions are shown by presenting control of circular finger-tip motions (Section 7.7.2). Dexterous grasping functions (power grasping, tip grasping) are illustrated by showing execution of dexterous pre-shape motions (Section 7.7.3) and power-grasps (Section 7.7.4).

The chosen high-level controllers are not subject to evaluation. The presentation is merely intended to illustrate usage of the robotic finger in combination with the low-level controllers for various finger tasks. The discussion gives an intuitive evaluation of the influence of pre-tension and the low-level design parameter γ for disturbance rejection and motion tracking accuracy.

7.7.1 Simulation model

The simulation model of the robotic finger and low-level controller are equal to the model and parameters settings used in Section 7.6.2.

The simulation model includes modeled locks. Each lock is modeled as a stiff parallel torsional spring-damper combination acting on the joint. The combined modeled element has two attachment points on both sides of the spring-damper. One point is fixed to one of the two phalanges on the joint. The other point is fixed to the other phalanx **if** the lock is activated, while it is released (and hence kept free) when the lock is switched off[9]. Hence, the lock torque τ_c is modeled by:

$$\tau_c = \begin{cases} 0 & c = 0 \\ k_c \cdot (q - q_c) + b_c \cdot (q - q_c)\dot{q} & c = 1 \end{cases}, \tag{7.34}$$

where q_c is the desired lock angle (the position of the joint at the moment of activating the lock) and q is the actual joint angle ($\cdot q$ is the joint velocity), hence $q - q_c$ represents lock deflection. In order to avoid discontinuous peak torques, the linear damping constant b_c is modulated with the lock deflection, $(q - q_c)$, which in fact uses the concept of the Hunt-Crossley contact model, see e.g. [93]. The locks are simulated with high stiffness ($k_c = 10,000$ Nm/rad) and damping ($d_c = 100$ Nms/rad) in order to simulate ideal locks. Ideal locks are used to verify conceptual behavior.

[9] In bond-graph modeling, this is modeled with a switched zero-junction, denoted as $X0$, see e.g. [92].

Notice that there should always be positive pre-tension, in order to be able to induce positive and negative differential tendon forces around this positive pre-tension, since negative forces can not be transmitted through the tendons.

Each of the three subsequent experiments give a short list of settings and a description of the used high-level controller. Thereafter, the representative simulation results are discussed.

7.7.2 Dexterous finger motions

The low-level controller enable dexterous finger manipulation through the C_l action algorithm, see Figure 7.8. A circular path motion for the finger-tip is considered a highly dexterous finger motion.

Simulation goal: Give an illustrative example of generating dexterous finger motion by using the low-level controller for the novel robotic finger concept.

High-level controller description: A mechanical impedance scheme is used (a 1DOF example is shown in Figure 7.2(b)). The scheme uses feedback of the measured finger configuration $q(t)$ in order to observe the finger displacement path and adapt the desired actuation position q_d.

> *high-level control-law:* consider a desired path $q_c(t)$, which corresponds to a circular path for the finger-tip. The high-level control-law produces a desired $q_d(t)$ which is fed to the low-level controller, given by:
>
> $$q_d(t) = K_{hl} \cdot (q_c(t) - q(t)),$$
>
> where $q(t)$ is the measured actual joint configuration and $K_{hl} = \mathrm{blockdiag}(100, 100, 100)$ represents some arbitrary proportional feedback gain.

The circular path $q_c(t)$ describes a circle with radius $0.02\ [m]$ for time $20 \leq t \leq 40$.

Low-level controller Figures 7.12 shows the (undesired) tracking result when the locks are **not** used and C_l is implemented with just the basic action (Remark 7.11, Equation 7.10). Naturally, the underactuated finger can only be steered along a line.

Clearly, for this dexterous motion application, the low-level controller must use the algorithms for the lock controllers (C_l), where sample time is arbitrarily chosen to be: $T_s = 0.01\ sec.$

Discussion Figures 7.13 - 7.15 illustrate experiments for various parameter settings and scenarios. It is shown that, with the extended lock control action, the finger-tip indeed follows the desired circular trajectory, which verifies that the presented low-level controller enables dexterous finger manipulation for mechanical impedance schemes.

The plotted error $\hat{e}(t)$ is defined as the cumulative squared tracking error:

$$\hat{e}(t) = \int_0^t e(t)^T \cdot e(t) dt,$$

where the error signal $e(t)$ represents the deviation of the actual finger tip position (x_{tip}, y_{tip}) with respect to the desired finger-tip position.

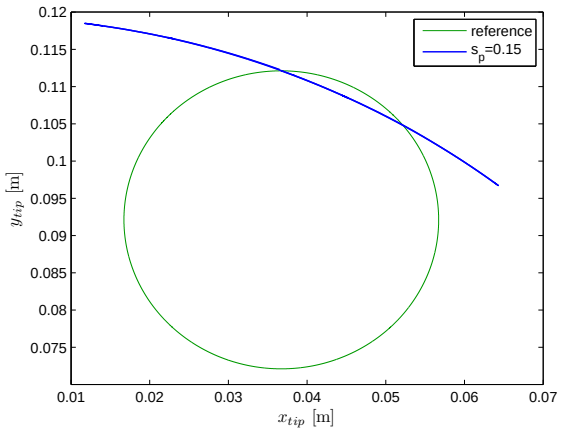

Figure 7.12: Finger-tip motion profile for basic C_l action, i.e. **no** lock actuation ($s_p = 0.15\ [m]$). The desired circular reference trajectory is badly tracked, i.e. no dexterous finger motions due to underactuation.

The results are interpreted as follows:

- Parameter γ: Figure 7.13 shows results for various settings of γ. As expected, increasing γ reduces the number of lock switching moments at the cost of tracking accuracy, i.e. the average trajectory remains unaffected, however the variation around the average trajectory increases.

- Sample-time T_s: For $\gamma = 0$, reducing the sample-time increases tracking accuracy and reduces variation around the average path. This effect is caused due to faster updates of the evaluation of the largest projection in the lock switching algorithm. Faster re-evaluations also lead to an increased number of switching moments. Increasing T_s leads to the opposite effect. For $\gamma > 0$, the influence of altering T_s is limited, since γ now determines and limits switching moments independent of time.

- Pre-tension s_p: Figure 7.14 and Figure 7.15 show results for various settings of pre-tension s_p:

  1. Tracking error: Figure 7.14 shows reduction of the tracking error for increased pre-tension values. This is expected behavior, since increased pre-tension increases the stiffness of the finger (see also Section 6.8).
  2. Disturbance rejection: Figure 7.14 shows the disturbed finger-tip trajectory for different pre-tension settings. As expected, the force disturbance induces smaller position errors for larger pre-tension (i.e. larger stiffness) values.

- Proportional gain K_{hl}: The feedback gain K_{hl} of the high-level controller acts similar to stiffness elements in parallel with the elastic elements of the driving train. Hence, disturbance rejection and tracking accuracy are increased for larger K_{hl}. Nevertheless, larger gains require faster and more aggressive actuator responses, which are limited in practice. Hence, it is considered preferable to use the mechanical disturbance rejection of the finger, by altering the pre-tension instead of tuning high-level control parameters.

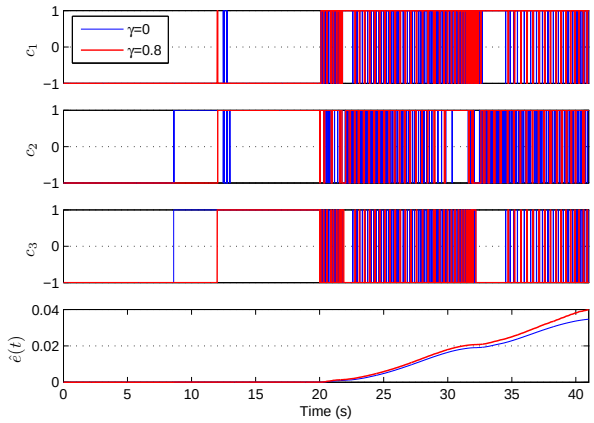

(a) Lock switches c and finger-tip cumulative tracking error $\hat{e}(t)$ for different γ settings.

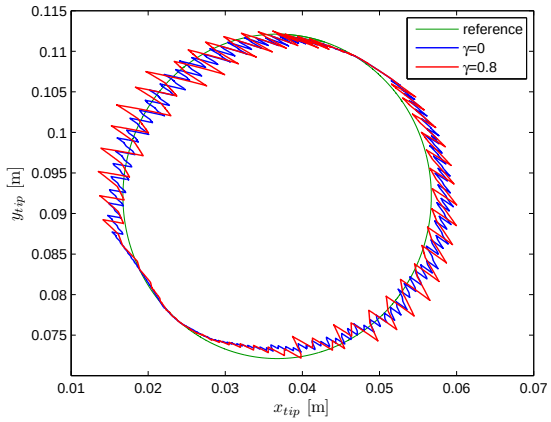

(b) Finger-tip motion profile for different γ settings.

Figure 7.13: Experiment: dexterous finger manipulation, circular path motion. Increasing γ decreases tracking accuracy and number of lock switching moments (fixed pre-tension, $s_p = 0.15\ [m]$).

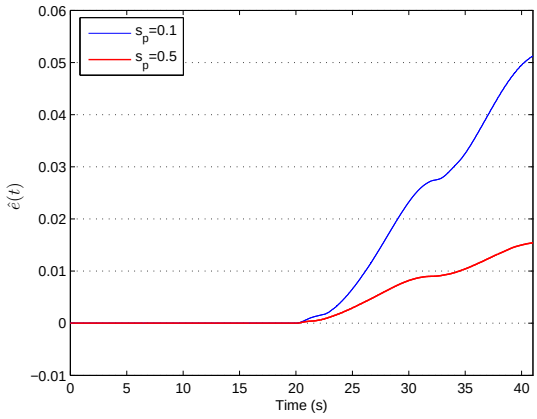

(a) Finger-tip cumulative tracking error $\hat{e}(t)$ for different pre-tension s_p settings.

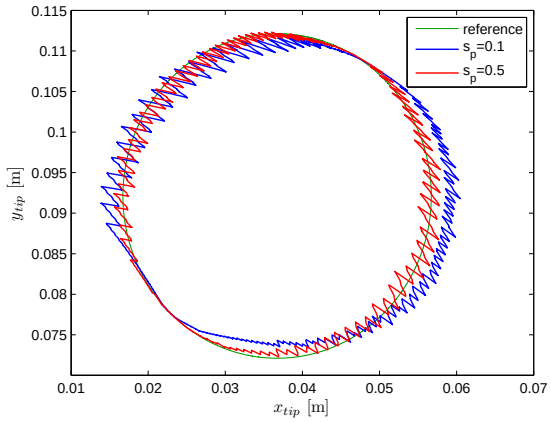

(b) Finger-tip motion profile for different pre-tension s_p settings.

Figure 7.14: Experiment: dexterous finger manipulation, circular path motion. Increasing pre-tension (s_p), increases tracking accuracy, due to increased finger stiffness (fixed $\gamma = 0$).

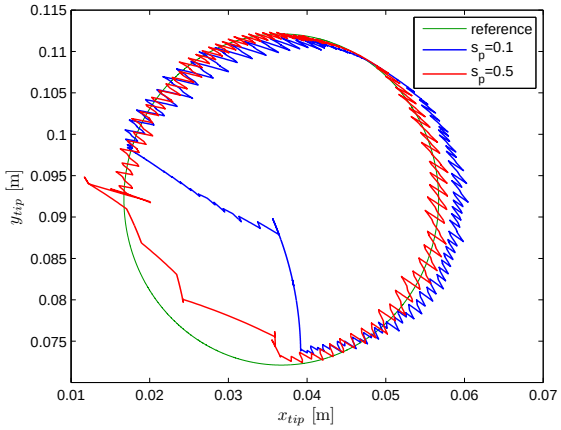

Figure 7.15: Experiment: dexterous finger manipulation, circular path motion exposed to joint torque disturbance $\tau_d \in \operatorname{im} C^T$:

$$\tau_d = \begin{cases} 0 & 0 \leq t \leq 30, t > 40 \\ (3 \quad 2 \quad 1) \in \operatorname{im} C^T & 30 \leq t \leq 40 \end{cases}$$

Increasing pre-tension s_p, increases finger stiffness and hence disturbance rejection (fixed $\gamma = 0$).

7.7.3 Dexterous pre-shaping

To execute grasps, and in particular tip-grasps, it is necessary to be able to impose a desired pre-shape to the finger configuration.

Simulation goal: Give an illustrative example of generating a pre-shape by inducing dexterous finger motion and using the low-level controller for the novel robotic finger concept.

High-level controller description: The scheme uses feedback of the measured finger configuration $q(t)$ in order to observe the finger displacement path and to adapt the desired actuation position q_d.

> *high-level control-law:* Consider a desired pre-shape configuration q_{dp}. The high-level control-law for the mechanical impedance scheme produces a desired q_d which is fed to the low-level controller, given by:
>
> $$q_d(t) = K_{hl} \cdot (q_{dp} - q(t)),$$
>
> with $K_{hl} = \operatorname{blockdiag}(25, 25, 25)$. Using no feedback and just setting $q_d = q_{dp}$ would result in a constant q_{dp}, for which the lock algorithm choses a constant lock state c which produces the closest joint angles. The high-level controller uses feedback to steer the joint angles to the desired pre-shape and switching the locks accordingly along the trajectory, such that the desired pre-shape is actually reached.

Low-level controller Clearly, for this dexterous displacement application, the low-level controller must use the extended algorithm for the lock controller (C_l), where sample time is arbitrarily chosen to be: $T_s = 0.01\ sec$. Unless stated otherwise, pre-tension is set to: $s_p = 0.15$ (i.e. $f_p = 90.45\ N$).

At simulation start-up, the finger starts in configuration $q(0) = (-0.1 \quad -0.2 \quad -0.25)^T$. The desired pre-shape for the presented representative result is set to: $q_d = (-0.3 \quad 0.1 \quad -$

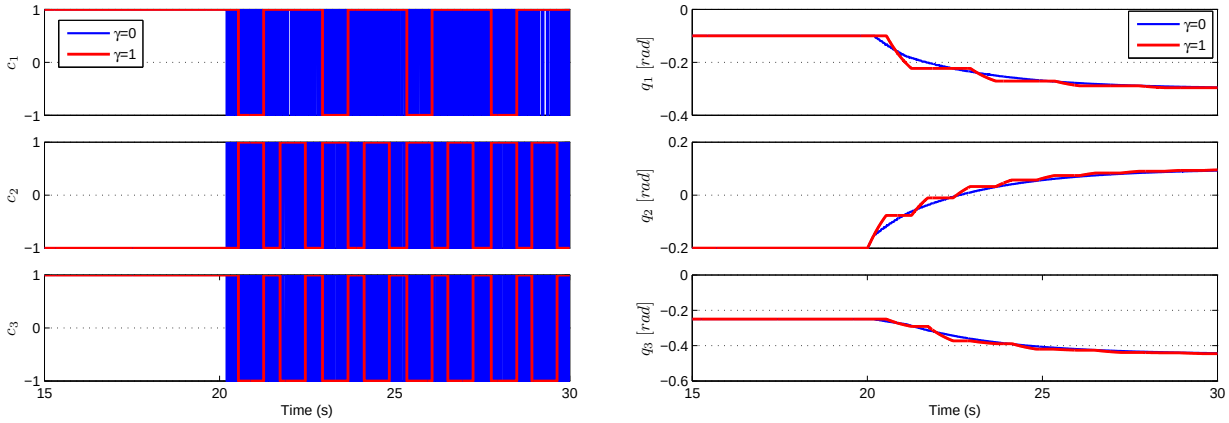

(a) Lock switch states c for different settings of parameter γ. Larger γ shows less switching moments.

(b) Joint positions $q(t)$ for different settings of parameter γ.

Figure 7.16: Experiment: dexterous pre-shape displacement for mechanical impedance scheme with $k_{hl} = 10$. Increasing γ decreases number of lock switching moments, but creates less smooth motion profile (fixed pre-tension, $s_p = 0.15$ $[m]$).

$0.45)^T$. Note that this desired pre-shape partially resides in the null-space of the finger motions. Furthermore, the joints have to move in opposite direction to reach the pre-shape. Clearly, without lock control, this configuration can not be reached with an underactuated finger.

Discussion Figures 7.16 - 7.17 illustrate experiments for some parameter settings and scenarios. It is shown that, with the extended lock control action, the finger-tip indeed reaches the desired pre-shape, which verifies that the presented low-level controller enables dexterous pre-shaping and hence finger-tip grasping for mechanical impedance schemes.

The results coincide with the discussion given for the previously demonstrated experiment (Section 7.7.2):

- Parameter γ: Figure 7.16(a) shows results for various settings of γ. Again, increasing γ reduces the number of lock switching moments. at the cost of tracking accuracy, i.e. the average trajectory remains unaffected, however the variation around the average trajectory increases.

- Accuracy: Figure 7.16(b) shows that the steady state error of the reached configuration is zero for $\gamma = 0$. In this particular demonstration, also for $\gamma \neq 0$, the steady state error vanishes. In general, $\gamma \neq 0$ may lead to a steady state error, since for $\gamma \neq 0$ the lock switches can reside in a final state c.

- Convergence speed: Figure 7.17 shows the influence of the finger stiffness. As seen in Section 7.7.2, the finger reaches the desired pre-shape faster for larger pre-load settings s_p, i.e. larger mechanical stiffness.

- Disturbance rejection: Figure 7.17 shows a disturbance response as a result of an external disturbance. As expected, the disturbance response is largely determined by the mechanical stiffness, altered by the pre-tension displacement s_p. Again (see Section 7.7.2), increased pre-tension s_p, increases disturbance rejection (i.e. less position displacement under force disturbance).

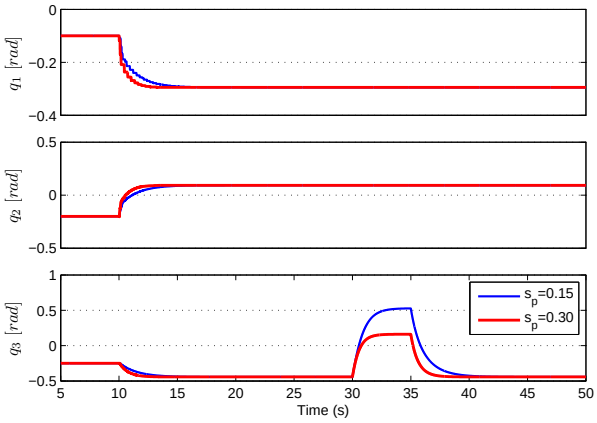

Figure 7.17: Experiment: dexterous pre-shape displacement for virtual impedance scheme for mechanical impedance scheme ($\gamma = 0$). Plotted: joint positions $q(t)$ for mechanical impedance scheme and different settings for pre-tension s_p. Some external disturbance is applied to the joint torques, τ_d, as described in caption of Figure 7.15. Increased pre-tension (i.e. larger stiffness) gives improved disturbance rejection (i.e. less position displacement under force disturbance).

7.7.4 Power-grasp

The low-level controller which uses the basic action for C_l, see Remark 7.11, enables for simple and intuitive control of power grasps (enveloping the object with the robotic fingers), without joint actuation.

Since, it involves a grasp, multiple fingers of the robotic finger concept are plugged together on a robotic hand. Each has its own low-level controller. This section will present the behavior of one finger as part of a whole-hand grasp.

Simulation goal: Give an illustrative example of generating a simple yet powerful power grasp by using the low-level controller for the novel robotic finger concept.

Power-grasp description: The presented example utilizes the low-level controller in a mechanical impedance scheme is used (a 1DOF example is shown in Figure 7.2(b)).

As given in Equation 7.11, any differential tendon displacement s_m defines a space of possible corresponding joint displacements for which equilibrium[10] holds:

$$\mathcal{Q}_e \quad := \quad C^{\#} \cdot s_m + \ker C = \hat{q}_d + \ker C. \tag{7.35}$$

This is used to generate a simple, yet sophisticated, power grasp. It is assumed that a suitable initial configuration of the robotic fingers (i.e. the pre-shape) is established and that the robotic hand (to which the fingers belong) is close enough to the object. Then, the power grasp is simply generated as follows:

1. select a desired finger stiffness (for each finger) by sending an appropriate pre-tension displacement s_p to the low-level controller;

2. the low-level controller calculates the desired tendon displacements s_t and controls the actuator positions accordingly, i.e. $z = s_t$ such that equilibrium elongations $\ell_e \in \mathcal{L}_e$ are established ($z = s_t = \ell_e$);

[10] Note: recall that in equilibrium (see Equation 6.22), the joint configuration q and tendon actuator positions z are such that for the elongations of the elastic elements ($\ell = -z - H_a \cdot q$), it holds that $\ell \in \mathcal{L}_e$, such that the tendon forces are equal, and hence the joint torques zero, i.e. $\frac{\partial H}{\partial \ell}(\ell) \in \ker J_a^T = \ker F^T$.

3. send a desired s_m to the low-level controller, such that a specific equilibrium space is chosen (for each finger);
4. the low-level controller calculates the desired tendon displacements s_t (added to the pre-tension displacements) and controls the actuator positions accordingly, i.e. $z = s_t$;
5. the joints start to move towards some configuration in $\mathcal{Q}_e$;
6. at some point, the finger is constrained at finger configuration q_c, due to finger-object-contact. The finger naturally envelopes the object (see underactuated design parameters in e.g. Section 6.6 and [62]). Hence, a grasp is established, while a $q \in \mathcal{Q}_e$ is not reached;
7. since, $q \notin \mathcal{Q}_e$, it is found that $\ell \notin \mathcal{L}_e$ such that the joint torques are non-zero, which gives rise to non-zero contact forces.

Mathematical description of constrained finger situation For the constrained grasp situation, the difference vector between the desired configuration space $\mathcal{Q}_e$, and the constrained configuration q_c, is given by the difference between the projection of $q \in \mathcal{Q}_e$ onto $(\ker C)^\perp$ and q_c onto $(\ker C)^\perp$, i.e.

$$\delta q = \hat{q}_d - C^{\#} C \cdot q_c = \hat{q}_d - M_q^{-1} C^T \cdot \left(C M_q^{-1} C^T\right)^{-1} C \cdot q_c.$$

This δq causes a change in elongations ($\delta \ell$) around the equilibrium elongations induced by the pre-tension. This is verified by recalling that for any $q_e \in \mathcal{Q}_e$ and actuator position z, the (unconstrained) equilibrium elongations are given by (see also Equation 6.22):

$$\ell_e = -z - H_a \cdot q_e = -z - H_a \cdot \hat{q}_d,$$

while for the constrained configuration, the elongations are given by:

$$\ell = -z - H_a \cdot q_c,$$

such that the change in elongations, with respect to the desired equilibrium is given by:

$$\delta \ell = \ell - \ell_e = H_a(\hat{q}_d - q_c) = J_a \cdot \delta q, \tag{7.36}$$

with $\delta \ell \notin \mathcal{L}_e$ and numerically $J_a = H_a$ represent the same transformation. Hence, for small changes around the desired equilibrium, the corresponding changes in the (dual) tendon forces are given by:

$$\delta f_s = M_s(\ell_e) \cdot \delta \ell, \tag{7.37}$$

for which it holds that $\delta f_s \in (\ker F^T)^\perp = \delta f_s \in (\ker J_a^T)^\perp$, which are the dual forces, for metric $M_s(\ell_e)$, of $\delta \ell \in \operatorname{im} J_a$ (see Remark 5.20).

Low-level controller The low-level controller measures this $\delta y = \delta f_s$, which corresponds to a differential tendon force $f_m = \delta f_m = F^T \cdot \delta f_s$ around the desired equilibrium. And, most useful, inside the low-level controller, this differential tendon force is actually calculated automatically by the MTF_s element as a function of the measured forces y, see Equation 7.14. Thus, the low-level controller with MTF_s element, gives back a $f_m \neq 0$ measurement for any constrained finger situation for which $q_c \notin \mathcal{Q}_e$.

Finally, notice that the induced joint torques, due to the contact constraints and $q_c \notin \mathcal{Q}_e$ are given by:

$$\tau = C^T \cdot f_m,$$

which enables the high-level power grasp controller to directly use the given f_m to determine the joint torques, without any force sensor. If contact positions are known, these joint torques can be used to estimate contact forces. Furthermore, changing the stiffness (by altering pre-tension s_p) will of course change $\ell_e \in \mathcal{L}_e$ such that the mechanical finger stiffness changes (given by $M_s(\ell_e)$, see Equation 7.3) and hence the differential tendon force (Equation 7.37) and therefore also the joint torques.

Conclusively, the above given power-grasp method utilizes all features of the robotic finger concept that are intuitively enabled by the low-level controller. It is used in a straight forward manner to establish power-grasps and steer the mechanical stiffness and contact forces mechanically.

Discussion of establishing a grasp Figures 7.18 illustrates the given power-grasp method by showing the results of a dynamic simulation of an example power-grasp experiment for one finger.

The power-grasp method is explained and verified by briefly discussing the subsequent actions (as shown in the plots) in chronological order:

- $5 \leq t \leq 10\ sec.$: pre-tension displacement $s_p = 0.15\ [m]$ induces $y_1 = u_2 = f_p = 90.45\ [N]$.
  - no joint displacement (finger remains at $q(0) = 0 \quad 0 \quad 0)^T$, no joint torques, $\tau = 0\ [Nm]$;
  - resulting equilibrating elastic elongations ℓ_e are given by: $\ell = z = s_t = P_s \cdot s_p = (0.0951 \quad 0.0549)^T\ [m]$, see Equation 7.33.
- $t > 10\ sec.$: $s_m = -0.00933\ [m]$ induced, corresponding to $\hat{q}_d = (-0.6 \quad -0.4 \quad -0.2)^T$.
  - fingers move until constraint configuration, $q_c = (-0.5 \quad -0.3 \quad -0.1)^T \notin \mathcal{Q}_e$, hence $f_m = -10.448 \neq 0\ [N]$ is measured and non-zero joint torques arise, $\tau = (-0.1 \quad -0.07 \quad -0.03)\ [Nm]$;
  - measured $f_m = -10.448\ [N]$ corresponds to measured joint torques, i.e. $\tau = C^T \cdot f_m$ gives actual joint torques;
  - measured $f_m = -10.448\ [N]$ is manually verified by applying Equation 7.3, Equation 7.36 and using the linear approximation given in Equation 7.37 around the given equilibrium elongation ℓ_e. The estimated expected differential tendon force $\tilde{f}_m$ is found to be:

$$\begin{aligned}
\tilde{f}_m &= F^T \cdot \delta f_s = F^T M_s(\ell_e) \cdot \delta\ell \\
&= F^T \cdot \begin{pmatrix} 2 \cdot k_1\ell_1 & 0 \\ 0 & 2 \cdot k_2\ell_2 \end{pmatrix} (J_a(\hat{q}_d - q_c)) \\
&= F^T \cdot \begin{pmatrix} 2 \cdot k_1\ell_1 & 0 \\ 0 & 2 \cdot k_2\ell_2 \end{pmatrix} (F \cdot s_m - J_a \cdot q_c) \\
&= -10.387 \approx -10.448 = f_m \quad [N].
\end{aligned}$$

- $20 \leq t \leq 25$ $sec.$: additional pre-tension displacement, such that total pre-tension displacement increases to $s_p = 0.25$ $[m]$;
  - joint configuration remains in constrained configuration.
  - since joints do not move, elongations change to $\ell = z = s_t = P_s \cdot 0.25 = (0.1585 \quad 0.0915)^T$ $[m]$, and hence stiffness has increased.
  - indeed, due to increased stiffness, also measured differential tendon force $f_m = -17.337$ $[N]$ and the joint torques have increased accordingly.
  - Manual verification of f_m leads again to a close approximate of the actually measured differential tendon force: $\tilde{f}_m = -17.311 \approx -17.337 = f_m$ $[N]$.

Conclusively, the demonstration of the presented power-grasp method illustrated the following features:

- The low-level controller enables to fully use the mechanical features of the novel robotic finger concept for a simple yet sophisticated power-grasp method;
- A power-grasp is easily established by simply defining some equilibrium configuration space Q_e by setting some s_m and selecting a desired pre-tension s_p.
- The pre-tension s_p adjusts the stiffness of the robotic finger.
- The difference between the actual resulting finger configuration (due to object interaction) and the pre-set equilibrium configuration space Q_e, together with the mechanical finger stiffness, determine the resulting joint torques and hence the established contact forces.
- Joint torques can be measured directly from the measured f_m delivered by the low-level controller C_m.
- Clearly, the resulting mechanical finger-stiffness also supports (adjustable) disturbance rejection without any high-level (or low-level) control action.

7.8 Conclusions and Discussion

The chapter is finished by summarizing conclusions and discussing limitations and possible directions for future work.

7.8.1 Conclusions

Two classes of impedance control schemes were distinguished: *controlled virtual impedance* and *controlled mechanical impedance*. The proposed novel robotic finger concept, see Chapter 6, is specifically meant to be used in controlled mechanical impedance schemes, as desired in Section 3.3.

A conceptual low-level controller is presented which takes care of actuating the basic features of the robotic finger; adjustable mechanical compliance and dexterous finger manipulation. Hence, the low-level controller avails the finger features to be used by high-level task controllers in controlled mechanical impedance schemes. The low-level controller basically consists of two main building blocks:

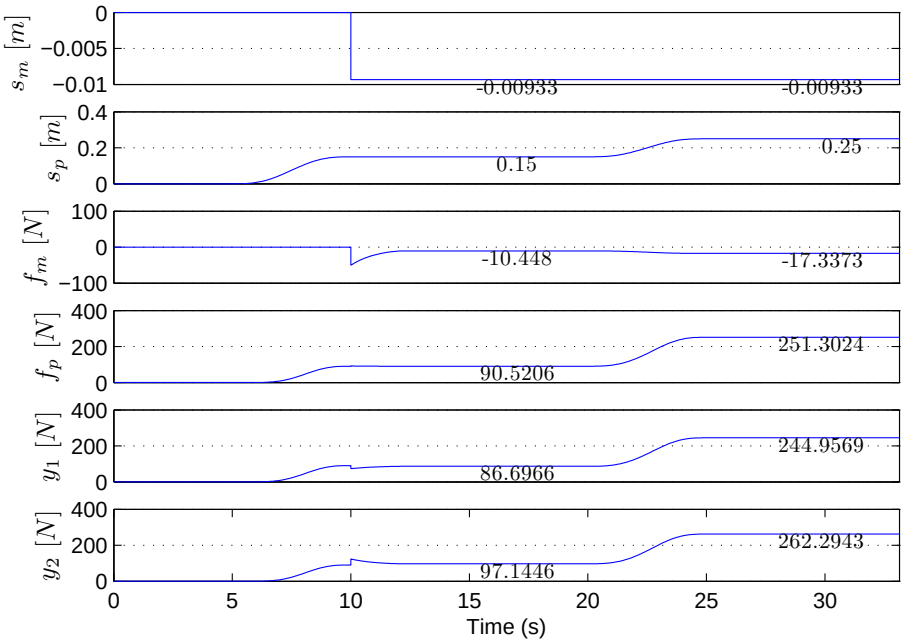

(a) Low-level controller variables and measurements.

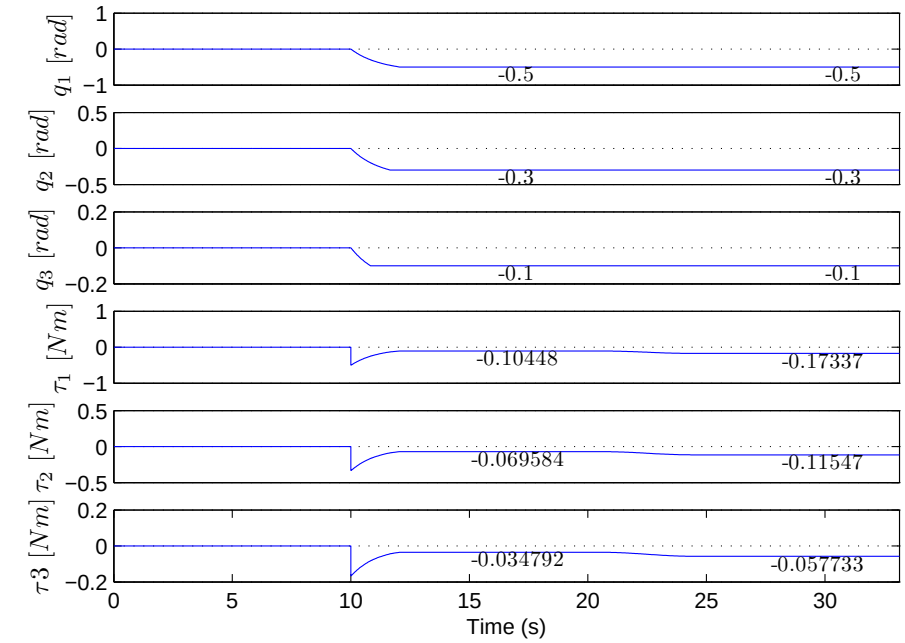

(b) Joint displacements and joint torques. Finger-object interaction is modeled by angular constraints on the expected power-grasp finger configuration, i.e. $q_c = (-0.5 \quad -0.3 \quad -0.1)^T$.

Figure 7.18: Experiment: demonstration of power-grasp method with mechanical impedance scheme, utilizing the low-level controller with the basic action for C_l, i.e without lock switching algorithm.

1. Coordinate transformation; transforms the tendon input actuator positions into two separate input coordinates:

   (a) common mode actuation: to adjust finger compliance and tendon pre-load[11];

   (b) differential mode actuation: to adjust the desired finger equilibrium configuration;

   These inputs are used by a high-level controller, such that it can directly and intuitively utilize the finger features.

2. Lock controller: a lock switching algorithm is presented to address dexterous finger manipulation in the underactuated mechanism. The algorithm translates a desired joint displacement to proper differential mode actuation inputs and discrete lock switch states. The algorithm uses joint damping as physically equivalent metric, M_q, to define the producible joint displacements. An optimization criterion is defined, which measures the distance (for a chosen metric M_J) between a desired and actual finger displacement. To solve the optimization control problem and select an optimized control input, active joint locks are modeled as infinite dampers in the physically equivalent metric. As such, the locks are modeled to change the space of producible joint displacements, from which the optimized displacement is selected by considering orthogonal projections for metric M_J.

   It is deliberately chosen to never activate all locks at the same time, since that would kill the compliance properties.

   Because of expected limited switching frequencies of mechanical locks, a delay-parameter γ is included in the lock controller, which can be tuned to balance between accuracy and the switching frequency.

The coordinate transformation relies on proper usage of a physically equivalent metric, M_s, which is induced by the elastic elements in the tendons. Physical duality is utilized to use the dual of the coordinate transformation to get force measurements along the common mode and differential mode coordinates. Also the lock controller utilizes metrics and space decompositions. Clearly, the understanding of metrics and decompositions, as presented in Chapter 5, is extensively used in the low-level controller.

Validation simulation experiments have verified the conceptual behavior of the low-level controller. Also the choices of metrics were validated.

Furthermore some demonstrations were presented, which showed usage of the low-level controller and the proposed finger concept in combination with simple high-level task controllers. Power grasping with variable compliance was demonstrated and the results were analytically verified Dexterous pre-shaping and finger-manipulation scenarios demonstrated usage and validity of the lock controller. Position feedback in the high-level controller lets the finger configuration converge to the desired configuration up-until the accuracy of the feedback loop.

In all demonstrations, the adjustable mechanical compliance showed adjustable disturbance rejection properties.

Conclusively, the presented low-level controller enables full utilization of the novel robotic finger concept and it was conceptually shown how to execute primary functions for robotic fingers (power grasping, tip grasping, free finger motion).

[11] Tendon pre-load is needed to avoid un-transmittable negative tendon forces.

7.8.2 Discussion and future work

Some limitations and corresponding recommendations for future work are discussed hereafter.

(Relative) infinitesimal versus absolute controller variables In the design, absolute values are used for the controller variables, based on the assumption of constant projections. This assumption does not hold for elastic elements that do not fit in model of Theorem 7.1 or Theorem 7.2. Nevertheless, the complete analysis (for both the coordinate transformation and the lock controller) was done for infinitesimal variables. Hence, for non-linear elastic elements with arbitrary constitutive force relations, the low-level controller can be used for infinitesimal inputs. In practice, the low-level controller can easily generate such inputs by using for example position feedback and letting the position error be the desired infinitesimal change.

It should be noted that these infinitesimal values represent *changes* with respect to some current (equilibrium) state. Hence, as long as an infinitesimal variable is non-zero, it indicates that the state of the mechanism should change. Therefore, in this case, the position actuators for the tendon actuation positions z should change to velocity actuators. These actuators can still be implemented as non-backdrivable actuators, such that maintaining a constant state (desired infinitesimal change is zero) does not consume power.

Recommendation:

- For future research towards implementing the proposed concepts, it is recommended to let the actual implementation of the non-elastic elements (or any other variable mechanical compliance structure, see below) be leading on deciding which variables to use in the low-level controller. As discussed, the presented low-level controller is suitable for both options.

Elastic elements Usage of antagonistic non-linear elastic elements to create variable mechanical compliance may require relatively large pre-tension forces, see also e.g. [94]. Instead of implementing such an antagonistic drive (either with or without constitutive force relations as given in Theorem 7.1 or Theorem 7.2, see previous discussion on infinitesimal variables), one can consider using other variable compliance actuator mechanisms, generally called Variable Impedance Actuators (VIAs), see e.g. [91, 94].

Any such VIA, which has a position input and a stiffness changing input, could be used to replace the coordinate transformation plus antagonistic non-linear elements in the proposed concept. Such VIA should then be connected to the tendon positions s (s is depicted in Figure 7.1). An example could be to connect a rotational VIA to a pulley to which tendon positions s_1 and s_2 are attached.

The presented lock controller can still be used in combination with such VIA.

Recommendation:

- For future research towards implementing the proposed concepts, it is recommended to consider which non-linear elastic constitutive force relations can be actually implemented. Parallel to this search, one should consider and compare upcoming novel results from research on VIAs. Comparison should be evaluated for several design criteria, such as size, weight and also on achievable forces and compliance range, as well as considering the fact that large tendon pre-tension induces friction on the pulleys.

Lock switching In the simulations and for the control solution of the lock controller optimization criterion, the locks were simulated and assumed to be (almost) ideal locks, which instantaneously block the motion of a joint when activated. Clearly, in practice such locks will not exist, since it would e.g. require to generate large peak forces.

Therefore it is noted that switching lock states should be done in stand-still quasi-static situations or at relative slow angular speeds. Relative slow speeds suggest speeds for which the implemented lock can build up blocking forces. Furthermore, even if a lock is not yet fully blocked, still the increased resistance may alter the joint motions (close to) the desired direction.

Most robotic finger tasks are expected to admit to these speed restrictions. Therefore, the optimized control solution is considered a useful (approximate) solution for practical situations to generate dexterous motions.

Recommendation:

- For future research, it is interesting to study the (bounded) continuous optimization problem as stated in Equation 7.26, and solve for any $\eta \in \mathcal{B}$. Such a solution would require the locks to be implemented as variable damping elements and may generate a more smooth function for the lock states η (assuming smooth inputs). It should be evaluated whether in practice, the cost of needing a variable damping element (instead of a 2-state element) and the according electronic hardware and lock controller implications balances with respect to having an approximate discrete solution.

Other future work

- High-level controller for object manipulation: the simulated demonstrations of finger tasks showed examples of high-level controllers that implement three of the four primary finger functions: pre-shaping (used for tip-grasping), power-grasping and dexterous finger manipulation. For dexterous object manipulation the presented low-level controller can be used for each of a set of fingers that together compose a robotic hand. Nevertheless, a high-level object manipulation task controller is needed to generate desired inputs for each of the low-level controllers, such that the object is manipulated by using the compliance properties and lock controllers of the fingers (in a controlled mechanical impedance scheme).

- If feedback is used for the design of high-level task controllers, clearly stability of the total system should be inspected. For the basic action (see Remark 7.11) the low-level controller applies some scaling of the inputs. It should be noted that the lock controller imposes discrete states, which for some feedback control could give rise to unwanted limit cycles.

Chapter 8

Conclusions and Future Work

Conclusions and recommendations for future work are summarized in this chapter.

8.1 Conclusions

The goals of this thesis, as formulated in Section 1.3, were (1) to reflect on challenges in application driven research projects, (2) to develop a novel robotic finger concept for dexterous robotic hands, (3) to present theory on natural vector space decompositions for the analysis of physical systems and (4) to present specific low-level controller synthesis to utilize the features of the novel robotic finger concept. The first goal and the last three goals are grouped together and discussed in two distinct subsections hereafter.

8.1.1 Conclusions on challenges in application driven research projects

Chapter 1 and 2 presented the project plan and project contents of the Falcon project. The project has greatly pushed forward technology development in multiple diverse research areas. Nevertheless, as a project member in the Falcon project, the author observed that the aim to follow a coherent systems engineering approach and to deliver integrated research results for the targeted application did not achieve its full potential.

The government and commercial companies (such as, in the case of the Falcon project, Vanderlande Industries BV) stress the economic need for these integrated application driven research results in order to stimulate knowledge diffusion from academia to industry. The author has named these projects 'application driven research projects'. Because of the economic needs, the government strives to stimulate application driven research projects and knowledge diffusion. Hence, in this thesis reflections and lessons learned were analyzed for future application driven research projects, which resulted in the following conclusions (Chapter 2):

- Top-down systems architecting approaches, as commonly successfully followed for application driven projects in industry, are obstructed by technology gaps. Hence research activities are needed: application driven research projects.

- A top-down-bottom-up application analysis framework was presented as analysis model for deriving research areas in application driven research projects. As soon as bottom-up selection of research areas starts[1], there is a risk of letting the research areas diverge

[1] This may start due to lacking a fixed system architecture. As a consequence, people start defining research directions in order to avoid being dependent of the not yet existing architecture.

from the targeted application. Hence the framework is proposed to be used to make this process of filling technology gaps explicit, such that coherent project wide choices are made. The framework also served as a base for project reflections.

- Project members (people) have different roles, interests and act upon different reward mechanisms, depending on their own interest and the interest of their affiliation. For example, a Ph.D. student is rewarded for individual achievements in novel research contributions, whereas a systems engineer in industry is rewarded for integrating (proven) technology through a cost effective, low risk approach.

- The application driven research projects have been modeled as a mix of objectives, strategy and people (plus affiliations). It was argued that it is important to match these three. For the choice on people (and affiliations) the previous conclusion should be considered, while the strategy involves basic choices on type of activities (fundamental/applied research, (systems) engineering) and exploration extensiveness (limited, broad, deep or full coverage exploration).

- Underestimating the differences in reward mechanisms, especially between academia and industry, seems to be a pitfall and should be carefully assessed when formulating a project strategy.

8.1.2 Conclusions on novel robotic finger concept

The goals of this thesis were to develop a novel robotic finger concept and accompanying theory.

- The proposed top-down-bottom-up analysis framework (Chapter 2) was followed to allow to generate a novel idea for a robotic dexterous finger concept. For such conceptual exploration (i.e. research to generate novel technology options), strict design requirements are not needed and even difficult to formulate since no application architecture is attached. Instead, a qualitative research direction was formulated by (1) distinguishing four primary functions for a human-like dexterous robotic hand (dexterous grasping, dexterous manipulation, free motion and interactive motion) and (2) by selecting (based on literature review) design goals for a set of critical requirement parameters: weight reduction, energy efficiency improvement, increasing task and operational robustness, reducing dimensions and lowering costs. In order to generate novel concepts within this research direction, it was concluded that the following design considerations should be followed: aim for minimal component design, especially a minimal number of power actuators, through *underactuation* and *variable compliance* actuation.

- Grasping is an interactive unstructured task. Robustness threats were analyzed to stem from three disturbance types: constant position disturbance, constant force disturbance and (less important) dynamic force disturbances. Through a series of simple 1DOF and dexterous 3DOF task robustness scenario analysis, it was shown that using variable compliance to adjust grasping compliance (i.e. high and low compliance settings) for different tasks can improve task robustness in grasping. Hence it justifies the design consideration of aiming for variable compliance actuation.

- In underactuated robotic fingers, as well as in the model representation of grasp-systems and in many other model representations of physical systems, non-bijective maps (i.e.

non-invertible maps) are used. Pseudo-inverse maps describe the (pseudo-) inverse relations. Chapter 5 showed properties of the commonly known generalized weighted pseudo-inverse. Mathematically speaking, there is not a unique pseudo-inverse map. It was explained to rely on the choice of inner-products, being represented by metrics. However, in this case, these maps are modeling physical behavior, which is uniquely determined by nature. Hence, the one pseudo-inverse map which resembles that physical behavior is called the physically equivalent pseudo-inverse map. The according metric is called the physically equivalent metric.

- Chapter 5 shows that the pseudo-inverse map can be understood from projection theory, where the metric defines the orthogonal complementary space along which the physical quantities are projected. Also dual spaces were used to understand that the pseudo-inverse map, for a chosen inner-product (metric) and associated isomorphisms, describe a pull-back function, named dual path. The dual-path easily verifies whether a metric can be a candidate physically equivalent metric, since it relates physical dual elements, which should be meaningful for the modeled situation. Furthermore, it was discussed that a candidate physically equivalent metric is coordinate invariant and defines a physical function for which the system is minimizing.

- For the particular case of (linearly) damped motions in a linear system, a time dependent physically equivalent metric was derived. It was concluded that for steady state motions, the norm that describes power losses in the system determines the physically equivalent metric, i.e. a linear damping matrix, called damping metric. Before a system reaches steady state motions, a transition phase was observed where the physically equivalent metric changes from being the mass matrix (at the start of a transition, when steady state motions start to change by inducing accelerations) to being the damping metric (at the end of a transition, when arriving at steady state motions).

- Based upon the derived design consideration of Chapter 3, a novel robotic finger concept was introduced (Chapter 6) for developing multi-fingered dexterous robotic hands with variable mechanical compliance and minimal actuation. The concept uses the underactuated softgripper mechanism to reduce the number of actuators. Variable mechanical compliance is implemented by using non-linear elastic elements in the antagonistic driving tendons. The underactuated tendon drive deteriorates dexterity, which is proposed to be restored by utilizing low-power locks on the joints (theoretically, such locks do not consume power).

- The thesis presents a conceptual port-Hamiltonian analysis in order to verify and understand the expected behavior of the proposed robotic finger. From the presented analysis it was concluded that variable finite compliance can be expected for a subset of possible disturbance wrenches. Infinite compliance (zero stiffness) is experienced for remaining disturbance wrenches.

- The variable compliance properties of the novel robotic finger concept (as well as for generally any comparable underactuated finger with compliant tendons), were analytically described and verified by simulation experiments. In accordance with Chapter 5, the required physically equivalent metric was found for two separate cases: dynamics with ($M_q = B$) and without damping ($M_q = M(q)$). The compliance analysis was confirmed by simulation results for both cases. As such, it also presented an application of the results in Chapter 5.

- The proposed novel robotic finger concept was complemented with a low-level controller that makes the finger features available for high-level task controllers in controlled mechanical impedance schemes (Chapter 7). The low-level controller presents separate inputs for selecting a desired finger configuration and adjusting the finger compliance properties. The low-level controller includes a lock controller, which activates the locks to let the underactuated finger position converge to the desired finger-position. The design of the low-level controller used the understanding of metrics and decompositions, as presented in Chapter 5,

  Controlled mechanical impedance schemes allow for a deviation between the actual finger configuration and the desired configuration, during interaction tasks. Due to compliant mechanical decoupling of the finger configuration and the actuated position, the mechanics determine the interaction behavior and hence the occurring contact forces. This behavior is influenced by adjusting the mechanical compliance. Application of the controlled mechanical impedance scheme for the novel robotic finger concept in combination with the presented low-level controller was successfully demonstrated in simulation experiments of various usage scenarios. Conclusively, the presented low-level controller enables full utilization of the novel robotic finger concept and it was conceptually shown how to execute primary robotic finger functions (power grasping, tip grasping, free finger motion).

8.2 Recommendations for Future Work

The presented research in this thesis left open some considerations for future work. Hence several directions for future research and continuation of this work are discussed. Again organized in two parts.

8.2.1 Recommendations for application driven research projects

Based on the conclusions on application driven research projects, where academia and industry are collaborating to stimulate knowledge generation and diffusion towards industry, the following recommendations are formulated:

- The author believes that aiming to integrate research results greatly stimulates knowledge diffusion. If knowledge is supposed to be diffused from academia towards industry, then integrating activities are recommended to be executed by industrial affiliations. It is then important to adapt the reward mechanisms such that the integration activities are rewarded different from standard commercial activities. This reward mechanism should encourage early acceptance of 'risky' novel technology.

- In order to stimulate knowledge diffusion, it is recommended that researchers involve industrial partners in the process of selecting bottom-up research directions. This is expected to enhance acceptance of novel technologies.

- It is recommended to be careful with planning multidisciplinary integration activities for academic Ph.D. students, if the results to be integrated are not yet accomplished. The academic reward mechanism requires an individual achievement of Ph.D. students and above all, integration activities depend on outcomes of other activities. These outcomes may not be satisfactory, such that integration can not be started. This may cause an unacceptable dependency for the Ph.D. student.

8.2.2 Recommendations for novel robotic finger concept

Directions for future work and research considerations for the work on dexterous robotic hands are given hereafter and grouped in several themes.

From theory to practice This thesis presented conceptual ideas and theoretical analysis for a novel robotic finger concept. The author believes that it is important to have a solid theoretical understanding of such concept before implementing actual realizations in practice. Nevertheless, practical feasibility of theoretical concepts is at least equally important for the actual realization of novel ideas. The robotic finger concept was concluded to encompass the basic desired features and corresponding enabling control was demonstrated. Hence, the following recommendations are given to pursue research towards actual realization of the concept.

- **Lock development:** The implementation of locks is non-trivial and demands careful attention. The author supervised a brief preliminary study on several mechanical designs [95]. Several disc brake mechanisms were evaluated in theory. It is recommended to develop prototypes and test feasibility of several options. Also, regarding the fact that an alternative would be to implement friction-modulating locks (see Chapter 7), it would be interesting to look into e.g. bearings with electro-rheonomic fluids. Note that, whether or not it is necessary to fully block joints for tip-grasping (which may not be possible with such fluids), depends heavily on the design (pulley radii, phalanx lengths, etc) of the finger, see Chapter 6 and e.g. [62].

- **Variable compliance:** The antagonistic tendons with non-linear elastic elements implement variable compliance. It is recommended to consider which non-linear elastic constitutive force relations can be actually implemented for use in the elastic elements. Parallel to this search, one should consider and compare upcoming novel results from research on variable impedance actuators (see e.g. [91, 94]). These can be incorporated in the concept as well, as long as it serves the purpose of actuation the antagonistic tendons and inducing a variable compliant decoupling of the tendon and the actuator positions. The comparison should be evaluated for several design criteria, such as size, weight and also on achievable forces and compliance range, as well as considering the fact that large tendon pre-tension induces friction on the pulleys, see also Chapter 7.

- **Compliance range:** It is recommended to test and analyze a desired range of compliance values for the robotic finger concept for different sets of task and application scenarios. This should result in application specific knowledge, which is used to determine which stiffness ranges suit which applications. Rough first estimates could be found by e.g. comparing with human body properties and by considering different desired disturbance rejection values for 1 DOF gripper scenarios, as presented in Chapter 4.

  Although it does not implement the proposed robotic finger concept, it could be useful to use a full dexterous robot hand (without locks) to test and validate various compliance ranges, which then may be translated to a suitable range for the novel robotic concept under consideration. As such, the general planar two fingered grasping test-setup for full dexterous grasping experiments may be used, which was developed in collaboration with the Dutch company Demcon B.V., the author and various students supervised by the author [96, 97].

- **Finger proof of principle setup:** Using the results from the above given recommendations it is recommended to try to combine them into a realization of a proof of principle

test setup, which implements a full realization of the novel robotic finger concept.

From robotic finger to robotic hand With the proposed novel robotic finger concept, an n-fingered hand will have at most $2n$ large size actuators. Depending on the specific application, the total number of actuators can be reduced by bundling the protagonist and antagonist tendons through differential drives. The differential drives allow differential finger actuation, such that the locks on each of the fingers can be used to change individual finger configurations. Hence, the minimum number of large size actuators for a full dexterous hand would be only two.

Further conceptual work Also conceptually some interesting future research is found, as listed hereafter.

- **Object compliance:** The work on the compliance analysis of the underactuated finger should be extended to finding a stiffness matrix for grasped objects, that are grasped by multiple robotic fingers of the novel robotic finger concept. A single finger was shown to have some zero compliance directions. For a grasping system, it is expected that, considering the fingers to be constrained by the grasp in non-equilibrium finger configurations, the set of zero compliance directions is reduced.

- **Dexterous object manipulation:** Chapter 7 presented some rudimentary high-level task controllers for the identified primary functions, excluded dexterous object manipulation. Dexterous object manipulation involves controlling multiple fingers to cooperate simultaneously. For controlled virtual impedance schemes, several methods exist, such as e.g. the IPC concept applied to grasping control in [47]. However, for the novel robotic finger concept, it is desired to use a controlled mechanical impedance scheme which calculates desired joint configurations, instead of joint torques. Hence, it is needed to find an elegant[2] way to transform a desired object displacement into desired joint displacements for all fingers involved in the manipulation task.

- **Smooth lock control:** Chapter 7 presented a general optimization control problem for the lock controller, where the locks are modeled as elements that modulate the damping (friction) of the joints. In the thesis the control problem is solved by considering a limited set of possible lock states. However, for more dynamic manipulation tasks (which possibly may generate too large impact forces for discrete locks), it may be advantageous to have more smooth activation functions for controlling the locks. Hence, it seems interesting to investigate optimization solutions that consider a continuous range of possible lock states instead of a discrete set.

Grasp simulation Although not used in this thesis, the author likes to mention some research efforts on contact modeling for simulating grasp systems.

Modeling and simulation techniques were used to analyze and evaluate novel concepts, without having to actually implement them. For future grasping simulations, when whole hand grasps are simulated (e.g. for the object stiffness analysis), it inevitably involves modeling of contact dynamics and shape geometry of grasped objects. The author has worked with the port-based visco-elastic contact model as presented in [67], which incorporates contact surface

[2] It would be nice to avoid pseudo-inversion of the (concatenated) geometric Jacobian of multiple contact points for each of the fingers, since a proper metric may not be obvious to find.

geometry in an analytic way. However, this existing compliant contact model requires an analytic parametrization of the surfaces involved in the interaction. For simple object shapes, this model can be used for simulation. Nevertheless, oftentimes, objects in human environments have irregular shapes. Incorporating irregular surfaces in this port-based contact model is still challenging. Following the recommendations in [63], the author, together with the co-authors, presented a first step towards incorporating these irregular surfaces in the port-based contact model by using global contact point detection approaches from the field of computer graphics, see [98].

In order to support future grasping research, it is recommended to continue this work by enhancing port-based simulation capabilities for dexterous grasping. The presented method in [98] should be generalized to interpolation methods for the reconstruction of 3D surfaces of (closed) objects generated with e.g. CAD software, such as tried in [99].

Appendix A

Dexterous Hand Task Threats

Task robustness is endangered by threats during task operation. In this appendix some threats are identified for the human-like dexterous hand primary functions (see Section 3.1.2). The threat identification is used to give some use-case scenarios from which general disturbances are derived.

First, Section A.1 discusses threats in general and presents some failure modes. Then, Section A.2 gives threats for each of the primary functions. Finally, Section A.3 generalizes these threats to a small set of physical disturbances.

A.1 Failure Modes

For each action, different threats can be identified by reasoning about different use cases and scenarios for each action. A threats is seen as identified behavior that endangers normal operation, possibly causing task failure and requiring a retry of the task. Hence, threats endanger task robustness. Some failures-modes are:

1. Prehension
   (a) Dexterous grasping:
      - not grasping/releasing (in time);
      - loosing the item;
      - damaging the item, the hand or the environment;
   (b) Dexterous manipulation:
      - loosing the item;
      - damaging the item, the hand or the environment;
2. Non-prehensile skilled movements
   (a) Free motion:
      - poor finger motion trajectory tracking;
   (b) Interactive motion:
      - damaging the hand or the environment;

A.2 Primary Function Specific Threats

For each of the failure modes, different threats exist. These are listed per primary function. The list of threats is not even close to complete. It merely serves to give some intuition behind different disturbances that can arise during task operation.

A.2.1 Dexterous Grasping

Grasp threats (GT)

1. Object dimension is different than expected, contact forces can be too low/high;
2. Object position is different from ideal grasp position, contact forces can be too low/high;
3. Finger unexpectedly slides over surface, changes finger configuration or induces change of contact force;
4. Force on object changes when it is lifted from support to free space, contact forces are changed;
5. Fingers are blocked by obstacle in environment, fingers can not grasp, other grasp needs to be planned;

Hold Threats (HT)

1. Hand is accelerating, induces force on object, leading to different contact forces;
2. Hand is vibrated, induces force on object, leading to different contact forces and might cause the fingers to vibrate, such that contact is lost;
3. Object shape changes (deformation), contact forces change;
4. Fingers hit environment, contact forces change;
5. Object hits environment, contact forces change;
6. Door(handle)/drawer opens lots of friction, changing forces on fingers, maybe causing them to loose their configuration and hence loose hold on the handle;
7. Object's mass and mass distribution changes due to eg. zipping in a drink, changing contact forces, changing configuration of fingers, s.t. object maybe lost;

Release Threats (RT)

1. Fingers are blocked by obstacle in environment, fingers can not grasp, other release needs to be planned;
2. Fingers are subject to large amount of friction due to interaction with environment, changes finger configuration or induces change of contact force, such that object is not released, or released too early;
3. Object deforms, such that fingers need to quickly reconfigure in order not to drop it too fast, or to be able to still release it;

4. Object position is different from ideal release position, object released from too large distance (too high deceleration) and/or released at wrong location (e.g. just besides table, instead of on table);

A.2.2 Dexterous Manipulation Threats (MT)

1. Erroneous finger manipulation control, leading to not generating the desired end-position;
2. Over-/undershoot in control: Object is dropped, due to loss of contact force during manipulating;
3. Hitting obstacles, leading to damage or to task abortion due to obstruction;

A.2.3 Free Motion Threats (FMT)

1. Erroneous finger control, leading to miscommunication due to not generating desired gestures.
2. Undesired environment interaction (hitting something) during gesturing.

A.2.4 Interactive Motion Threats (IMT)

1. Overshoot of fingers in case of sudden interaction changes (e.g. friction force changes, during wiping a surface), accidentally leading to hit other environment parts;
2. Hitting obstacles, leading to damage or to task abortion due to obstruction;

A.3 Physical Disturbances

The identified threats arise from either poor design (e.g. wrong controller action or set-point generation) or a limited set of physical disturbances. Design issues must 'simply' be avoided, however disturbances will always exist. Hence, novel dexterous hand technologies should be evaluated with respect to these disturbances.

After careful inspection of the threats, one recognizes a limited set of physical causes behind each of these threats, as shown in the following threat-disturbance map[1]:

disturbance	**physics**	**threat**
constant (or step function)	position	GT.1, GT.2, HT.3, HT.4, HT.5, RT.3, MT.3, FMT.2, IMT.2
	force	GT.3, GT.4, HT.1, HT.6, HT.7, RT.2, MT.3, FMT.2, IMT.1
dynamic	force	HT.2

Environment interactions that obstruct motion, are considered to impose position disturbances. No dynamic position disturbances were found.

Note that RT.1, GT.5, MT.1, MT.2 and FMT.1 require re-planning or design improvements for the requested action. Hence these threats are considered to have no causal relation with any

[1]Threat reference (XXX.i); *XXX* refers to threat type acronym, *i* refers to listed numbering of the selected threat type.

of the physical disturbance. Of course, control errors can also arise from (internal) measurement disturbances. That would lead to position or force disturbances.

The disturbances can be either internal or external. Internal could be caused by e.g. measurement errors, external could come from e.g. environment interaction. In any case, this distinction does not change the disturbance and is not relevant for a general disturbance and effect analysis. Of course, when searching for counteracting solutions, the source of error is relevant.

A.4 Conclusions

It was shown that three different physical disturbances impose threats on successful execution of the dexterous hand tasks: *constant position* and *force* disturbances and *dynamic* force disturbances. The identification of threats supports the intuition behind these disturbances.

Bibliography

[1] *Executive Summary of World Robotics 2009 Industrial and Service Robots*. IFR Statistical Department, 2009. [Online]. Available: http://www.worldrobotics.org

[2] R. Bisschoff and T. Guhl, Eds., *Robotic Visions - To 2020 and Beyond - The Strategic Research Agenda for Robotics in Europe*. European Robotics Technology Platform, Jul. 2009. [Online]. Available: http://www.robotics-platform.eu

[3] *Summary Report on Technology Strategy for Creating a "Robot Society" in the* 21^{st} *Century*. Japan Robot Association, 2001.

[4] M. van den Brandt, "U.S. technological innovation systems for service robotics," Master's thesis, University of Twente, Jun. 2010.

[5] G. Bekey, R. Ambrose, V. Kumar, A. Sanderson, B. Wilcox, and Y. Zheng, "International assessment of research and development in robotics - final report," World Technology Evaluation Center, Inc., Tech. Rep., Jan. 2006.

[6] H. Christensen, *A Roadmap for US Robotics - From Internet to Robotics*. Computing Community Consortium / Computing Research Association, May 2009. [Online]. Available: http://www.us-robotics.us/

[7] A. Bicchi, "Hands for dexterous manipulation and robust grasping: A difficult road toward simplicity," *IEEE Transactions on Robotics and Automation*, vol. 16, no. 6, pp. 652–662, Dec. 2000.

[8] B. Verlaan, R. in 't Veld, H. van der Veen, V. van Rij, P. Morin, and H. M. van den Brink, *Horizon Scan Report 2007 - Towards a Future Oriented Policy and Knowledge Agenda*. The Hague, 2007. [Online]. Available: http://www.horizonscan.nl/publicaties/

[9] "World robotics 2004," Press Release ECE/STAT/04/P01, Oct. 2004, executive Summary of in depth analysis. [Online]. Available: http://www.unece.org/press/pr2004/

[10] B. Gates, "A robot in every home," *Scientific American Magazine*, pp. 58–65, Jan. 2007.

[11] T. Asfour, K. Regenstein, P. Azad, J. Schröder, A. Bierbaum, N. Vahrenkamp, and R. Dillmann, "ARMAR-III: An integrated humanoid platform for sensory-motor control," in *Proceedings of IEEE-RAS International Conference on Humanoid Robots*, Dec. 2006.

[12] Y. Sakagami, R. Watanabe, C. Aoyama, S. Matsunaga, N. Higaki, and K. Fujimura, "The intelligent ASIMO: system overview and integration," in *Proceedings of IEEE/RSJ International Conference on Intelligent Robots and System*, vol. 3, 2002, pp. 2478–2483.

[13] T. Odashima, M. Onishi, K. Tahara, K. Takagi, F. Asano, Y. Kato, H. Nakashima, Y. Kobayashi, T. Mukai, Z. Luo, and S. Hosoe, "A soft human-interactive robot RI-MAN," in *Proceedings of IEEE/RSJ International Conference on Intelligent Robots and Systems*, Oct. 2006.

[14] J. J. Bartholdi and S. T. Hackman, *Warehouse and Distribution Science (release 0.89)*. The Supply Chain and Logistics Institute - Georgia Institute of Technology, 2008. [Online]. Available: http://www2.isye.gatech.edu/~jjb/wh/book/editions/history.html

[15] S. Hirose and Y. Umetani, "The development of soft gripper for the versatile robot hand," *Mechanism and Machine Theory*, vol. 13, pp. 351–359, 1978.

[16] J. K. Salisbury and J. J. Craig, "Articulated hands - force control and kinematic issues," *The International Journal of Robotics Research*, vol. 1, no. 1, pp. 4–17, 1982.

[17] S. C. Jacobsen, E. K. Iversen, D. Knutti, R. Johnson, and K. Biggers, "Design of the Utah/M.I.T. dextrous hand," in *Proceedings of IEEE International Conference on Robotics and Automation*, vol. 3, Apr. 1986, pp. 1520–1532.

[18] T. Mouri, H. Kawasaki, K. Yoshikawa, J. Takai, and S. Ito, "Anthropomorphic robot hand: Gifu Hand III," in *Proceedings of International Conference on Control, Automation and Systems*, 2002, pp. 1288–1293.

[19] F. Lotti, P. Tiezzi, G. Vassura, L. Biagiotti, C. Melchiorri, and G. Palli, "UBH 3: A biologically inspired robotic hand," in *Proceedings of IEEE International Conference on Intelligent Manipulation and Grasping*, Jul. 2004.

[20] A. Kargov, T. Asfour, R. Oberle, H. Klosek, S. Schulz, K. Regenstein, G. Bretthauer, and R. Dillmann, "Development of an anthropomorphic hand for a mobile assistive robot," in *Proceedings of IEEE 9th International Conference on Rehabilitation Robotics*, Jun. 2005, pp. 182–186.

[21] J. Butterfaß, M. Grebenstein, H. Liu, and G. Hirzinger, "DLR-Hand II: Next generation of a dextrous robot hand," in *Proceedings of IEEE International Conference on Robotics and Automation*, 2001, pp. 109–114.

[22] G. Muller, "CAFCR: A multi-view method for embedded systems architecting," Ph.D. dissertation, Delft University of Technology, The Netherlands, 2004.

[23] R. Andriansyah, L. F. P. Etman, and J. E. Rooda, "Flow time prediction for a single-server order picking workstation using aggregate process times," *International Journal on Advances of Systems and Measurements*, 2010.

[24] M. Rudinac, B. Lenseigne, and P. Jonker, "Keypoint extraction and selection for object recognition," in *Proceedings of IAPR Conference on Machine Vision Applications*, 2009.

[25] O. Akman and P. Jonker, "Exploitation of 3D information for directing visual attention and object recognition," in *Proceedings of IAPR Conference on Machine Vision Applications*, 2009, pp. 50–53.

[26] S. Adinandra, J. Caarls, D. Kostic, and H. Nijmeijer, "Performance of high-level and low-level control for coordination of mobile robots," in *Proceedings of 7th International Conference on Informatics in Control, Automation and Robotics (ICINCO)*, 2010.

[27] B. Cleves and R. Bruns, "Neues greiferprinzip für die logistik - untersuchungen an einem toroid greifer," *Hebezeuge Fördermittel*, vol. 48, no. 1-2, pp. 66–67, 2008. [Online]. Available: http://hf.hussmedien.de/hf_magazin/03_fachbeitraege/index.htm

[28] G. Kragten and J. Herder, "A platform for grasp performance assessment in compliant or underactuated hands," *Journal of Mechanical Design*, vol. 132, no. 2, 2010.

[29] L. A. Jones and S. J. Lederman, *Human Hand Function*. New York: Oxford University Press, 2006.

[30] H. Gray, *Anatomy of the Human Body*, 20th ed. Philadelphia: Lea & Febiger, 1918. [Online]. Available: http://www.bartleby.com/107/

[31] P. H. Veltink, "Sensory feedback in artificial control of human mobility," *Technology and Health Care*, vol. 7, no. 6, pp. 383–391, 1999.

[32] F. C. T. van der Helm, A. C. Schouten, E. de Vlugt, and G. G. Brouwn, "Identification of intrinsic and reflexive components of human arm dynamics during postural control," *Journal of Neuroscience Methods*, vol. 119, no. 1, pp. 1–14, 2002.

[33] E. de Vlugt, F. C. T. van der Helm, A. C. Schouten, and G. G. Brouwn, "Analysis of the reflexive feedback control loop during posture maintenance," *Biological Cybernetics*, vol. 84, no. 2, pp. 133–141, 2001.

[34] N. Hogan, "Adaptive control of mechanical impedance by coactivation of antagonist muscles," *IEEE Transactions on Automatic Control*, vol. 29, no. 8, pp. 681–690, 1984.

[35] C. Taylor and R. Schwarz, "The anatomy and mechanics of the human hand," *Artificial Limbs*, vol. 2, pp. 22–35, 1955.

[36] T. Iberall, "The nature of human prehension: Three dextrous hands in one," in *Proceedings of IEEE International Conference on Robotics and Automation*, Mar. 1987, pp. 396–401.

[37] M. R. Cutkosky, "On grasp choice, grasp models, and the design of hands for manufacturing tasks," *IEEE Transactions on Robotics and Automation*, vol. 5, no. 3, Jun. 1989.

[38] A. Bicchi and V. Kumar, "Robotic grasping and contact: a review," in *Proceedings of IEEE International Conference on Robotics and Automation*, Apr. 2000, pp. 348–353.

[39] ——, "Robotic grasping and manipulation," in *Ramsete*, ser. Lecture Notes in Control and Information Sciences, S. Nicosia, B. Siciliano, A. Bicchi, and P. Valigi, Eds. Springer Berlin / Heidelberg, 2001, vol. 270, pp. 55–74.

[40] M. R. Cutkosky and I. Kao, "Computing and controlling the compliance of a robotic hand," *IEEE Transactions on Robotics and Automation*, vol. 5, no. 2, pp. 151–165, Apr. 1989.

[41] D. J. Montana, "The condition for contact grasp stability," in *Proceedings of IEEE International Conference on Robotics and Automation*, vol. 1, Apr. 1991, pp. 412–417.

[42] W. S. Howard and V. Kumar, "On the stability of grasped objects," *IEEE Transactions on Robotics and Automation*, vol. 12, no. 6, pp. 904–917, 1996.

[43] I. Kao, M. R. Cutkosky, and R. S. Johansson, "Robotic stiffness control and calibration as applied to human grasping tasks," *IEEE Transactions on Robotics and Automation*, vol. 13, no. 4, pp. 557–566, Aug. 1997.

[44] J. K. Salisbury, "Active stiffness control of a manipulator in cartesian coordinates," in *Proceedings of IEEE Conference on Decision and Control including the Symposium on Adaptive Processes*, vol. 19, Dec. 1980, pp. 95–100.

[45] N. Hogan, "Impedance control: An approach to manipulation: Part I-Theory," *ASME Journal of Dynamic Systems, Measurement and Control*, vol. 107, pp. 1–7, Mar. 1985.

[46] ——, "Stable execution of contact tasks using impedance control," in *Proceedings of IEEE International Conference on Robotics and Automation*, Mar. 1987, pp. 1047–1054.

[47] S. Stramigioli, C. Melchiorri, and S. Andreotti, "A passivity-based control scheme for robotic grasping and manipulation," in *Proceedings of 38th IEEE Conference on Decision and Control*, Dec. 1999, pp. 2951–2956.

[48] K. F. Laurin-Kovitz, J. E. Colgate, and S. D. R. Carnes, "Design of components for programmable passive impedance," in *Proceedings of IEEE International Conference on Robotics and Automation*, Apr. 1991.

[49] A. Bicchi and G. Tonietti, "Fast and "soft-arm" tactics [robot arm design]," *Robotics and Automation Magazine, IEEE*, vol. 11, no. 2, pp. 22–33, Jun. 2004.

[50] T. Wimbock, C. Ott, A. Albu-Schaeffer, A. Kugi, and G. Hirzinger, "Impedance control for variable stiffness mechanisms with nonlinear joint coupling," in *Proceedings of IEEE/RSJ International Conference on Intelligent Robots and Systems*. IEEE, Sep. 2008, pp. 3796–3803.

[51] S. Wolf and G. Hirzinger, "A new variable stiffness design: Matching requirements of the next robot generation," in *Proceedings of IEEE International Conference on Robotics and Automation*, May 2008.

[52] M. Grebenstein and P. van der Smagt, "Antagonism for a highly anthropomorphic hand-arm system," *Advanced Robotics*, vol. 22, no. 1, pp. 39–55, 2008.

[53] A. D. Price, A. Jnifene, and H. E. Naguib, "Design and control of a shape memory alloy based dexterous robot hand," *Smart Materials and Structures*, vol. 16, no. 4, pp. 1401–1414, Jul. 2007.

[54] F. Rothling, R. Haschke, J. J. Steil, and H. Ritter, "Platform portable anthropomorphic grasping with the bielefeld 20-DOF Shadow and 9-DOF TUM hand," in *Proceedings of IEEE/RSJ International Conference on Intelligent Robots and Systems*, Nov. 2007, pp. 2951–2956.

[55] B. Massa, S. Roccella, M. C. Carrozza, and P. Dario, "Design and development of an underactuated prosthetic hand," in *Proceedings of IEEE International Conference on Robotics and Automation*, vol. 4, May 2002, pp. 3374–3379.

[56] A. M. Dollar, "Design principles for robust grasping in unstructured environments," Ph.D. dissertation, Harvard University, Cambridge, Massachusetts, 2006.

[57] D. Prattichizzo, M. Malvezzi, and A. Bicchi, "On motion and force controllability of grasping hands with postural synergies," in *Proceedings of Robotics: Science and Systems*, Jun. 2010.

[58] C. Y. Brown and H. H. Asada, "Inter-finger coordination and postural synergies in robot hands via mechanical implementation of principal components," in *Proceedings of IEEE/RSJ International Conference on Intelligent Robots and Systems*, Nov. 2007, pp. 2877–2882.

[59] M. Santello and J. F. Soechting, "Force synergies for multifingered grasping," *Experimental Brain Research*, vol. 133, pp. 457 – 467, 2000.

[60] M. Santello, M. Flanders, and J. F. Soechting, "Postural hand synergies for tool use," *The Journal of Neuroscience*, vol. 18, no. 23, pp. 10 105–10 115, Dec. 1998.

[61] E. Todorov and Z. Ghahramani, "Analysis of the synergies underlying complex hand manipulation," in *Proceedings of 26th Annual International Conference of the IEEE EMBS*, Sep. 2004, pp. 4637 – 4640.

[62] L. Birglen, T. Laliberte, and C. Gosselin, *Underactuated Robotic Hands*, ser. Springer Tracts in Advanced Robotics. Springer Berlin / Heidelberg, 2008.

[63] V. Duindam, "Port-based modeling and control for efficient bipedal walking robots," Ph.D. dissertation, University of Twente, The Netherlands, 2006.

[64] V. Duindam, A. Macchelli, S. Stramigioli, and H. Bruyninckx, Eds., *Modeling and Control of Complex Physical Systems - The Port-Hamiltonian Approach*. Springer-Verlag Berlin Heidelberg, 2009.

[65] D. Prattichizzo and J. C. Trinkle, *Springer Handbook of Robotics*. Springer Berlin Heidelberg, 2008, ch. Grasping, pp. 671–700.

[66] D. M. Brouwer, J. Bennik, J. Leideman, H. M. J. R. Soemers, and S. Stramigioli, "Mechatronic design of a fast and long range 4 degrees of freedom humanoid neck," in *Proceedings of IEEE International Conference on Robotics and Automation*, May 2009, pp. 574–579.

[67] V. Duindam and S. Stramigioli, "Modeling the kinematics and dynamics of compliant contact," in *Proceedings of IEEE International Conference on Robotics and Automation*, Sep. 2003, pp. 4029–4034.

[68] H. Bruyninckx, S. Demey, and V. Kumar, "Generalized stability of compliant grasps," in *Proceedings of IEEE International Conference on Robotics and Automation*, May 1998, pp. 2396–2401.

[69] A. Ben-Israel and T. N. E. Greville, *Generalized Inverses: Theory and Applications*, 2nd ed. New York: Springer-Verlag New York Inc., 2003.

[70] J. Duffy, "The fallacy of modern hybrid control theory that is based on "orthogonal complements" of twist and wrench spaces," *Journal of Robotic Systems*, vol. 7, no. 2, pp. 139–144, 1990.

[71] K. L. Doty, C. Melchiorri, and C. Bonivento, "A theory of generalized inverses applied to robotics," *The International Journal of Robotics Research*, vol. 12, no. 1, 1993.

[72] Y. Nakamura, *Advanced Robotics: Redundancy and Optimization*. Boston, MA, USA: Addison-Wesley Longman Publishing Co., Inc., 1990, no. 0201151987.

[73] G. Basile and G. Marro, *Controlled and Conditioned Invariants in Linear Systems Theory*. Englewood Cliffs, NJ: Prentice Hall, 1992.

[74] H. Nijmeijer and A. van der Schaft, *Nonlinear Dynamical Control Systems*. New York: Springer-Verlag New York Inc, 1990.

[75] J. Joh and H. Lipkin, "Lagrangian wrench distribution for cooperating robotic mechanisms," in *Proceedings of IEEE International Conference on Robotics and Automation*, Apr. 1991.

[76] A. Bicchi, "On the problem of decomposing grasp and manipulation forces in multiple whole-limb manipulation," *Robotics and Autonomous Systems*, vol. 13, no. 2, pp. 127 – 147, 1994.

[77] F. Bullo and A. D. Lewis, *Geometric Control of Mechanical Systems*, ser. Texts in Applied Mathematics. New York: Springer Science & Business Media, Inc., 2004.

[78] D. Williams and O. Khatib, "The virtual linkage: A model for internal forces in multi-grasp manipulation," in *Proceedings of IEEE International Conference on Robotics and Automation*, 1993.

[79] R. M. Murray, Z. Li, and S. S. Sastry, *A Mathematical Introduction to Robotic Manipulation*. Boca Raton, FL, USA: CRC Press, 1994.

[80] V. Kumar and K. J. Waldron, "Force distribution in closed kinematic chains," *IEEE Journal of Robotics and Automation*, vol. 4, no. 6, Dec. 1988.

[81] I. D. Walker, R. A. Freeman, and S. I. Marcus, "Analysis of motion and internal loading of objects grasped by multiple cooperating manipulators," *The International Journal of Robotics Research*, vol. 10, no. 4, pp. 396–409, Aug. 1991.

[82] R. G. Bonitz and T. C. Hsia, "Force decomposition in cooperating manipulators using the theory of metric spaces and generalized inverses," in *Proceedings of IEEE International Conference on Robotics and Automation*, vol. 2, 1994, pp. 1521–1527.

[83] ——, "Internal force-based impedance control for cooperating manipulators," *IEEE Transactions on Robotics and Automation*, vol. 12, no. 1, Feb. 1996.

[84] H. Lipkin, "Invariant properties of the pseudoinverse in robotics," in *Proceedings of NSF Design and Manufacturing Systems Conference*, Jan. 1990.

[85] M. Wassink, R. Carloni, and S. Stramigioli, "Port-hamiltonian analysis of a novel robotic finger concept for minimal actuation variable impedance grasping," in *Proceedings of IEEE International Conference on Robotics and Automation*, May 2010.

[86] ——, "Compliance analysis of an under-actuated robotic finger," in *Proceedings of IEEE RAS & EMBS International Conference on Biomedical Robotics and Biomechatronics*, Sep. 2010.

[87] N. Pavlovic, R. Keimer, and H.-J. Franke, "Adaptronic revolute joints for parallel robots based on simultaneous quasi-statical axial and radial clearance adjustment," in *Proceedings of ASME International Design Engineering Technical Conferences and Computers and Information in Engineering Conference*, Aug. 2008.

[88] S. Stramigioli, *Modeling and IPC Control of Interactive Mechanical Systems, A Coordinate-Free Approach*, 1st ed. London: Springer-Verlag, 2001.

[89] H. Kobayashi, K. Hyodo, and D. Ogane, "On tendon-driven robotic mechanisms with redundant tendons," *The International Journal of Robotics Research*, vol. 17, no. 5, pp. 561–571, May 1998.

[90] T. Pigoski, M. Griffis, and J. Duffy, "Stiffness mappings employing different frames of reference," *Mech. Mach. Theory*, vol. 33, no. 6, pp. 825–838, 1998.

[91] G. Tonietti, R. Schiavi, and A. Bicchi, "Design and control of a variable stiffness actuator for safe and fast physical human/robot interaction," in *Proceedings of IEEE International Conference on Robotics and Automation*, Apr. 2005.

[92] P. C. Breedveld, "The context-dependent trade-off between conceptual and computational complexity illustrated by the modeling and simulation of colliding objects," in *Proceedings of Computational Engineering in Systems Applications 96 IMACS/IEEE-SMC Multiconf.*, 1996, pp. 48–54.

[93] D. W. Marhefka and D. E. Orin, "A compliant contact model with nonlinear damping for simulating of robotics systems," in *Proceedings of IEEE Transactions on systems, Man, and Cybernetics - Part A: Systems and Humans*, vol. 29, no. 6, 1999, pp. 566–572.

[94] L. C. Visser, R. Carloni, R. Ünal, and S. Stramigioli, "Modeling and design of energy efficient variable stiffness actuators," in *Proceedings of IEEE International Conference on Robotics and Automation*, May 2010, pp. 3273–3278.

[95] G. Pulcini, "Design of a miniaturized joint lock for an under actuated robotic finger," Master's thesis, Control Engineering, University of Twente, 2010. [Online]. Available: http://www.ce.utwente.nl/rtweb/publications/MSc2010/pdf-files/005CE2010_Pulcini.pdf

[96] T. Mennink, "Virtualization of the Falcon humanoid finger into a direct drive system," Control Engineering, University of Twente, Tech. Rep., Apr. 2010. [Online]. Available: http://www.ce.utwente.nl/rtweb/publications/MSc2010/pdf-files/009CE2010_Mennink.pdf

[97] H. Differ, "Design and implementation of an impedance controller for prosthetic grasping," Master's thesis, Control Engineering, University of Twente, Aug. 2010. [Online]. Available: http://www.ce.utwente.nl/rtweb/publications/MSc2010/pdf-files/021CE2010_Differ.pdf

[98] M. Wassink, R. Carloni, P. Poulakis, and S. Stramigioli, "Digital elevation map reconstruction for port-based dynamic simulation of contacts on irregular surfaces," in *Proceedings of IEEE/RSJ International Conference on Intelligent Robots and Systems*, 2009, pp. 5179 – 5184.

[99] R. Giaccotto, "Smooth surface fitting by patches, a new method of interpolation for contact modeling," Master's thesis, Control Engineering, University of Twente, Dec. 2008. [Online]. Available: http://www.ce.utwente.nl/rtweb/publications/MSc2008/pdf-files/037CE2008_Giaccotto.pdf

[100] M. Wassink and S. Stramigioli, "Towards a novel safety norm for domestic robotics," in *Proceedings of IEEE/RSJ International Conference on Intelligent Robots and Systems*, 2007, pp. 3354 – 3359.

Dankwoord (Acknowledgements)

Luctor et Emergo; Hoewel ik geenszins Zeeuw[2] ben, noch mijn voorvaderen dat waren, leen ik, telg uit Twentse ouders, geboren Noord-Hollander en getogen Gelderlander, dankbaar deze wapenspreuk en vreugdekreet van de Zeeuwen. Het vat voor mij kort, bondig en recht door zee samen hoe ik de afgelopen vier jaar heb beleefd. Met gepaste trots stel ik vast dat dit proefschrift het bewijs vormt van de zege na de worsteling en de euforie na de inspanning. Velen hebben aan dit succes op verschillende wijze bijgedragen. Ik ben iedereen hiervoor zeer dankbaar. Slechts enkelen van hen zal ik hier in het bijzonder bedanken.

Allereerst bedank ik mijn eerste begeleider en promotor: Stefano, je staat van dienst en kennis spreekt tot de verbeelding en het was telkens weer een groot plezier om daar kennis van te mogen nemen. Het begon tijdens jouw colleges. Later, tijdens mijn stage in de VS, bezocht je me binnen vier dagen zelfs twee keer. Zo veel inspiratie en enthousiasme werkte aanstekelijk. Ook je persoonlijke begeleiding, motiverende woorden, openheid, steun en je vertrouwen in mij heb ik altijd zeer gewaardeerd. Grote dank daarvoor. Ik hoop dat wij elkaar in de toekomst nog vaak zullen treffen.

Big thanks also to my second supervisor and assistant promotor: Raffaella, thanks for letting me disturb you all the time. You were always ready to discuss, ask me difficult questions and give me feedback and new input to help me straighten out ideas and thoughts. I enjoyed and appreciated our many formal and informal discussions very much. You always encouraged me and helped me in difficult times! You are such a generous and fun person. Marlies and I still laugh when we think about the dinner at your place, when we missed the train and you let us borrow your car. Grazie mille!

En ook Dannis bedankt! Wel of geen begeleider, ik weet het niet precies. Hoe dan ook, ik vond onze samenwerking erg prettig, leerzaam en vooral ook leuk. Zeker ook onze levendige beschouwingen over verschillende samenwerkingsvormen. Bedankt voor al je tijd, adviezen en de begeleiding van 'onze' werktuigbouw studenten.

Graag bedank ik de organisatoren van het Falcon project, waaronder het Embedded Systems Institute en Vanderlande Industries B.V. Ik vind het zeer lovenswaardig dat Vanderlande Industries, een Nederlandse onderneming, zo'n groot en ambitieus project financieel mogelijk maakt. Evenzo belangrijk zijn de mensen die het doen: Jan, Jacques en Roelof (Embedded Systems Institute) en ook Toine, Frank, Bruno, Evert en Cor (Vanderlande Industries), bedankt voor alle leerzame discussies en brainstorm sessies. Ook bedank ik alle andere project partners en in het bijzonder Gert. Gert, ik heb genoten van onze discussies en fijne gesprekken, zowel vakinhoudelijk als privé. Het waren er eigenlijk nog te weinig! En niet te vergeten, onze trip naar Engeland. Bovendien, je hebt me kennis laten maken met 'underactuated grasping'.

Ook ben ik zeer dankbaar voor de ondersteuning vanuit Demcon B.V. Onze samenwerking herinner ik mij als een uitdagende en leerzame zoektocht. Dennis, HenkJan, Rini, Jan en Hernes, bedankt voor jullie gedreven inzet, hulp, gastvrijheid, openheid en flexibele beschik-

[2]Officiële wapenspreuk onder het wapen van Zeeland, een provincie van Nederland.

baarheid. Hernes en Robert, bedankt voor de realisatie van de 'Falcon robotic grasp test-setup', welke nog jaren vruchtbaar dienst zal doen als test platform in het CE-lab. Ook Pieter bedankt voor de vele gezellige ritjes naar en van Demcon in de zomer van 2008.

Dankbaar heb ik gebruik gemaakt van 20-sim en 4C; twee geweldige tools van Controllab Products B.V.! Christian, Paul, Frank en Peter, bedankt voor jullie continue hulp en beschikbaarheid tijdens mijn onderzoek en in het bijzonder tijdens de realisatie van de software voor de 'Falcon robotic grasp test-setup'. Jullie software leverde een first-time-right run. Ook Noord- en Midden-Nederland Maxon Motor Benelux B.V., dhr. Geukes, bedankt voor de donatie van de Maxon motoren in de 'Falcon robotic grasp test-setup'.

Marcel, l-u-nch? Marcel, jouw inzet en geleverde werk voor de 'Falcon robotic grasp test-setup' verdienen een dikke pluim: ook al heb je liever een 'tientje', toch bedankt en excuses voor de stress! Ook Gerben en Alfred bedankt voor het altijd weer klaarstaan, zodat ik bij tijd en wijle van jullie kennis en kunde gebruik kon maken. En ook Carla en Jolanda bedankt voor jullie hulp (hopelijk was ik niet te lastig?) en het af en toe eens even gezellig bijkletsen.

Gijs, bedankt voor alle '3 minuutjes', waarin ik jou als klankbord mocht gebruiken. Marcel Groothuis, ook jou mocht ik veelvuldig succesvol raadplegen. Niet alleen voor de 'Falcon robotic grasp test-setup', maar ook voor vele andere software zaken, al dan niet voor hobby doeleinden. En natuurlijk mijn altijd opgewekte en gezellig spraakzame kamergenoot, Michel. Bedankt voor je steun, gezelligheid en gastvrijheid. Met plezier heb ik beschuitjes met je gegeten! Sorrie dat ik bij voorkeur zonder muziek werk. Met muziek stond ik regelmatig met Ludo op de spinning-bike, 'kom op, kom op!' En ook Ludo had regelmatig een bed klaar staan voor de keren dat ik 's nachts werkte. Van onze trip naar St. Louis herinner ik mij o.a. de (verloren) fietswedstrijd en de roadtrip naar Indianapolis. Dank ook voor de vele leuke discussies die wij hadden. Job, bedankt voor je goede adviezen. Pantelis, thanks for our enjoyable collaboration and pleasant chats, which resulted in a.o. a publication, drinking beer in blues bars in St. Louis and in an impressive tour at ESA ESTEC. Also thanks to all students with whom I had the pleasure to work with and who let me try to develop some coaching skills.

Ook buiten het werk zijn er veel vrienden en familie die mij hebben gesteund en zo minstens een even zo grote bijdrage aan dit werk hebben geleverd. Ik noem er slechts een paar: Gunnar en Koen, ik ben trots op ons succes met TeamWebs, maar bovenal vereerd dat ik jullie vriend mag zijn. Ik geniet van alles wat we doen en voel me enorm door jullie gesteund. Mark, 'Battus', altijd beschikbaar en altijd lol, lekker sporten, 'chillen' en gezelligheid, goed voor afleiding en een hart onder mijn riem, bedankt! Daan, hoewel je bijna altijd ver weg bent, stond je klaar wanneer ik je nodig had. Ik koester onze bijzondere momenten en wereldse gesprekken, any-place-any-time: Brazilië, Portugal, Amerika, Nederland of ergens on-the-road. Jaap en George, 'jongûh's', sorrie dat ik er niet altijd bij kon zijn, maar als ik er wel was, genoot ik dubbel: altijd gezelligheid! Hotel Meijerink, alias Roland, ook bij jou stond een lekker bedje klaar, zelfs nadat je al naar Hoofddorp was verhuisd. Swa's, ofwel Seb en Stef, hoewel onze momenten (te) spaarzaam zijn, altijd fun. Reinout, bedankt voor je cruciale adviezen.

Het belangrijkste heb ik voor het eind bewaard, mijn familie: papa en mama, het is ongelofelijk hoe veel jullie voor mij betekend hebben (en altijd zullen betekenen) en mij ook in dit traject weer onvoorwaardelijk hebben gesteund. Ik hou van jullie. En ook van mijn lieve broertjes, van Marjon en van Ineke en Theo, enorm bedankt voor jullie begrip, steun en het delen in de zorgen en de vreugde. En dan mijn lieve, lieve, lieve Marlies. Wat heb ik het jou soms zwaar gemaakt en wat heb je mij met liefde, daad en raad bijgestaan, gesteund, vertroeteld en de ruimte gegeven. Ik geniet van ons samenzijn, ik ben je super dankbaar, ik hou van je, je bent mijn alles!

- *Martin*, 3 januari 2011, Amersfoort

About the Author

Martin Wassink was born in Alkmaar (The Netherlands) on September 5, 1981. He obtained his high school degree (VWO diploma) from Grammar School 'Stedelijk Gymnasium, Johan van Oldenbarnevelt' (Amersfoort, The Netherlands) in 1999. Subsequently, Martin started studying Electrical Engineering at the University of Twente and received his first year's diploma (propaedeutics) *cum laude* in 2000.

From April to June 2001, he collaborated with a fellow student to investigate adaptive rate protocols in ADSL access networks at Lucent Technologies (Bell Labs Innovations, Enschede, The Netherlands). For his Bachelor's thesis, he worked on the modeling and implementation of a haptic interaction control scheme on a Fokker flight-stick setup (2004). During his Bachelor's studies, Martin followed a minor on business administration and was also involved in several extra-curricular activities. From 2001 to 2002, he acted as treasurer of the board of student sports association T.C. Ludica. From 2003 to 2005, he co-organized the Shouraizou studytour project to Japan. Martin's main responsibility was to raise funds by bringing in contract research assignments for each of the 28 student participants.

During his Master's program, Martin performed an internship at Philips Applied Technologies North-America (Pittsburgh, PA, USA), where he worked on modeling and control of a 6 DOF magnetic levitation stage (September 2005 - January 2006). In 2006 he investigated safety issues for domestic robotics and performed an exploration on design requirements for a robotic household arm at Philips Applied Technologies (Eindhoven, The Netherlands). He wrote his M.Sc. thesis on these topics and published some of the results in [100]. Martin received his M.Sc. degree and graduated *cum laude* in 2006. Also in 2006, his entrepreneurial interests inspired him to found TeamWebs together with two companions. As product manager, his main responsibilities are to lead the development of a social community website, which supports people active in team sports (www.teamwebs.nl).

In February 2007, he started as Ph.D. student at the control engineering group of the University of Twente, under supervision of Prof. dr. ir S. Stramigioli and dr. R. Carloni. His research was part of the FALCON project and is described in this Ph.D. thesis. In February 2011, he continued his career as strategy consultant at Roland Berger Strategy Consultants, Amsterdam (The Netherlands).

Technology changes the world. Robots are moving from structured manufacturing tasks to unstructured professional and personal service applications. These trends inspired to investigate versatile human-like robotic fingers to create robotic hands for service applications. Several advantages of using variable compliant and underactuated actuation methods for such robotic fingers are discussed. These ideas are combined into a novel robotic finger concept. This Ph.D. thesis presents a study on this concept, the control thereof and an accompanying theoretic treaty on natural pseudo-inverses.

ISBN 978-90-365-3154-2
DOI 10.3990/1.9789036531542